UNIVERSITY OF COPENHAGEN
FACULTY OF HEALTH AND MEDICAL SCIENCES

Exploring nicotinic receptors and histone deacetylases through neuroimaging

PhD thesis

Janus Houe Magnussen, MSc.

This thesis has been submitted to the Graduate School of Health and Medical Sciences, University of Copenhagen on 12 June 2024

“*It is more fun to talk with someone who doesn't use long, difficult words but rather short, easy words like 'what about lunch?*”
— Winnie-the-Pooh, in A.A. Milne's *Winnie-the-Pooh*

PhD thesis

Exploring nicotinic receptors and histone deacetylases through neuroimaging

Janus Houe Magnussen, M.Sc.

Title:	Exploring nicotinic receptors and histone deacetylases through neuroimaging
Author:	Janus Houe Magnussen, M.Sc.
Department:	Neurobiology Research Unit, Rigshospitalet, Denmark
Institution:	Graduate School of Health and Medical Sciences, University of Copenhagen, Denmark
Date of submission:	12 June 2024
Date of defense:	6 September 2024
Principal supervisor:	Professor Gitte Moos Knudsen, Neurobiology Research Unit, Rigshospitalet, Denmark
Assessment committee:	Associate professor Birgitte Rahbek Kornum (chairperson) Department of Neuroscience, University of Copenhagen, Denmark Associate professor Anne M. Landau Department of Clinical Medicine - Translational Neuropsychiatry Unit, Aarhus University, Denmark Dr. Francisco Lopez Picon Preclinical Imaging Unit of the Turku PET Centre University of Turku, Finland

Preface

The research presented in this thesis was conducted at the Neurobiology Research Unit, Copenhagen University Hospital Rigshospitalet, from September 2014 to June 2024 under the supervision of Professor Gitte Moos Knudsen. During this period, I have held various scientific positions in the pharmaceutical industry. Therefore, I applied to the Graduate School to combine this research into a PhD thesis without enrolment, in accordance with the Ministerial Order on the PhD programme, section 15(2). This application was approved by the Head of the Graduate School in June 2023.

The thesis has two parts: an introductory section covering key concepts, impact, and perspectives of the research, followed by the included research papers listed on the next page.

Janus Houe Magnussen,
— London, June 2024

Publications

The following is a list of the publications that are included in the thesis. Throughout the text, they will be referred to by their roman numerals, as listed below.

I. **Magnussen, J. H.**, Ettrup, A., Donat, C. K., Peters, D., Pedersen, M. H. F., Knudsen, G. M., & Mikkelsen, J. D. (2015). Radiosynthesis and in vitro validation of (3)H-NS14492 as a novel high affinity alpha7 nicotinic receptor radioligand. *European Journal of Pharmacology*, *762*, 35-41, doi:10.1016/j.ejphar.2015.04.036

II. Donovan, L. L., **Magnussen, J. H.**, Dyssegaard, A., Lehel, S., Hooker, J. M., Knudsen, G. M., & Hansen, H. D. (2020). Imaging HDACs in vivo: Cross-validation of the [11 C]Martinostat radioligand in the pig brain. *Molecular Imaging and Biology*, *22*, 569-577, doi:10.1007/s11307-019-01403-9

III. **Magnussen, J. H.,** Ettrup, A., Lehel, S., Peters, D., Dyssegaard, A., Thomsen, M. S., Mikkelsen, J.D., & Knudsen, G. M. (2024). Characterizing the binding of TC-5619 and encenicline on the alpha7 nicotinic acetylcholine receptor using PET imaging in the pig. *Frontiers in Neuroimaging*. vol. 3 1358221. 27 Mar. 2024, doi:10.3389/fnimg.2024.1358221

The following publications are not included in the thesis but are related to the research outlined and are cited as normal references:

A. Hansen, H. D., Andersen, V. L., Lehel, S., **Magnussen, J. H.**, Dyssegaard, A., Stroth, N., Kristensen, J. L., Knudsen, G. M., & Herth, M. M. (2015). Labeling and preliminary in vivo evaluation of the 5-HT7 receptor selective agonist [11C] E-55888. *Bioorganic & Medicinal Chemistry Letters*, 25(9), 1901-1904. doi:10.1016/j.bmcl.2015.03.039

B. Hansen, H. D., Constantinescu, C. C., Barret, O., Herth, M. M., **Magnussen, J. H.**, Lehel, S., Dyssegaard, A., Colomb, J., Billard, T., Zimmer, L., Tamagnan, G., & Knudsen, G. M. (2019). Evaluation of [18F]2FP3 in pigs and non-human primates. *Journal of Labelled Compounds and Radiopharmaceuticals*, 62(1), 34-42. doi:10.1002/jlcr.3692

Acknowledgments

The research included in this thesis would not have been possible without the great collaborations, guidance, and invaluable support from colleagues, friends, and family, to whom I owe a tremendous thanks. A special thanks to Hanne Demant Hansen and Anders Ettrup for invaluable support and guidance during our time at NRU.

My greatest thanks go to Gitte Moos Knudsen. After graduating in 2014, I pursued a PhD under your supervision. Although we did not secure funding immediately, a few months later, we obtained full three-year funding. By then, I was working in the industry and decided not to return to NRU, despite your encouragement. In hindsight, I regretted that decision and have since sought ways to pursue the PhD. Fortunately, I found an alternative path: a PhD without enrollment. You supported this idea, and here we are. Thank you for this incredible opportunity!

I am sure you have been praised numerous times for your great academic and supervisor skills, your incredibly knowledge in the field of neuroscience and your kind human being. What I would like to highlight is that you believe in people and do not give up on them easily, even though they might not choose the straight path. I am so thankful for your continuous support, which has been crucial for me to reach this point.

Lastly, I want to thank my wife, Amalie. Throughout this entire you have kept pushing me to pursue it, encouraged me to give it yet another shot, and always supported this crazy project. I could not have done it without you.

Abstract

The neuronal nicotinic acetylcholine receptor (nAChR), particularly the α7 subtype, is widely distributed throughout the central nervous system (CNS) and plays an essential role in synaptic transmission, neural network dynamics, and cognitive function, contributing to both physiological processes and pathological conditions such as Alzheimer's disease (AD) and schizophrenia. In AD, the α7 nAChR exhibits a dual role, with evidence suggesting both neuroprotective and disease-exacerbating effects. Similarly, in schizophrenia, the involvement of α7 nAChRs has gained attention for its potential in the cognitive impairments associated with the disease. However, clinical trials targeting α7 nAChRs for cognitive symptoms in both AD and schizophrenia have so far been unsuccessful, reflecting issues such as the translational validity of animal models and the complex dose-response relationships. Moreover, epigenetic mechanisms, particularly histone acetylation and deacetylation, have emerged as crucial regulators of gene expression implicated in AD pathogenesis. Positron emission tomography (PET) imaging offers a promising non-invasive approach for real-time visualization of histone deacetylase (HDAC) dynamics in vivo. Furthermore, in the context of drug discovery, particularly for CNS disorders, PET molecular imaging plays a crucial role in assessing critical drug attributes such as tissue accessibility and target engagement, which are essential for the success of development programs, and crucial for potential compounds targeting neuronal α7 nAChR and HDACs. By interrogating these parameters, PET imaging enhances our understanding of CNS drug pharmacology and aids in mitigating the high failure rates and long development timelines associated with CNS drug development.

The aims of the research presented here are threefold: 1) To assess the suitability of ^{3}H-NS14492 as a radioligand for the α7 nAChR; 2) To validate the newly developed radioligand, ^{11}C-Martinostat, in the pig brain; 3) To evaluate the binding of prior clinical drug candidates, bradanicline (TC-5619) and encenicline (EVP-6124), to the α7 nAChR in the pig brain using PET imaging with ^{11}C-NS14492;

In Paper I, we evaluated the in vitro properties of ^{3}H-NS14492, revealing saturable binding in pig brain sections and homogenate with favorable nanomolar affinity. The radioligand displayed specificity in displacement studies with α7 nAChR agonists and positive allosteric modulators, suggesting its utility for studying

pharmacological properties of these compounds. Paper II focused on the in vivo properties and validation of ^{11}C-Martinostat for measuring HDAC1–3 levels. PET imaging demonstrated excellent signal-to-noise ratio and substantial brain uptake with widespread distribution, confirming specificity through blocking experiments. This highlights the potential of ^{11}C-Martinostat for investigating epigenetic changes in vivo. In Paper III, we investigated α7 nAChR agonist engagement using ^{11}C-NS14492, revealing distinct occupancies for previous clinically tested partial and full agonists, encenicline and bradanicline, respectively. These findings emphasize PET's role in CNS drug development, necessitating comprehensive evaluations before initiating large-scale clinical trials, particularly for challenging therapeutic targets like α7 nAChRs.

In conclusion, this research highlights PET imaging's versatility and significance in studying α7 nAChRs, HDAC levels, and α7 nAChR ligand engagement, offering valuable insights into radioligands' in vitro and in vivo properties and their potential as tools in drug development.

Dansk resumé

Den neurale nikotinerge acetylcholinreceptor (nAChR), især α7, er bredt fordelt i hele det centrale nervesystem (CNS) og spiller en afgørende rolle i synaptisk transmission, neurale netværk og kognitive funktioner, hvilket bidrager til både fysiologiske processer og patologiske tilstande såsom Alzheimers sygdom (engelsk forkortelse, AD) og skizofreni. I AD har α7 nAChR en dobbelt rolle, hvor der er evidens for både neurobeskyttende og sygdomsfremkaldende virkninger. På samme måde har α7 nAChR fået opmærksomhed i skizofreni på grund af receptorens rolle i de kognitive forstyrrelser forbundet med sygdommen. Indtil nu har kliniske forsøg rettet mod α7 nAChR for kognitive symptomer ved både AD og skizofreni været mislykkede, hvilket afspejler udfordringer med translationel validitet af dyremodeller og komplekse dosis-responsforhold. Desuden er epigenetiske mekanismer, især histonacetylering og deacetylering, foreslået som afgørende regulatorer af genekspression, der er impliceret i AD sygdomsudvikling. Positronemissionstomografi (PET) er en lovende ikke-invasiv metode til visualisering af histondeacetylase (HDAC) dynamikken in vivo i realtid. Derudover spiller PET billeddannelse en afgørende rolle i vurderingen af lægemiddelegenskaber såsom vævsadgang og receptor- eller molekyleokkupans, hvilket er afgørende for succesen af tidlige kliniske udviklingsprogrammer og essentielt for lægemidler rettet mod neurale α7 nAChR og HDAC. Ved at undersøge disse parametre forbedrer PET billeddannelse vores forståelse af CNS-lægemidlers farmakologi og hjælper med at mindske de høje fejlrater og lange udviklingsprogrammer der ses ved CNS-lægemiddeludvikling.

Formålene med den præsenterede forskning er trefoldige: 1) At vurdere ^{3}H-NS14492 som en radioligand for α7 nAChR; 2) At validere den nyudviklede radioligand, ^{11}C-Martinostat, i grisehjerner; 3) At evaluere bindingen af tidligere kliniske lægemiddelkandidater, bradanicline (TC-5619) og encenicline (EVP-6124), til α7 nAChR i grisehjerner ved hjælp af PET-billeddannelse med ^{11}C-NS14492.

I Publikation I blev in vitro egenskaberne af ^{3}H-NS14492 evalueret, hvilket viste mætning af bindingssteder i sektioner af grisehjernen og i homogenat med nanomolær affinitet. Radioliganden viste specificitet i bindingsstudier med α7 nAChR agonister og positive allosteriske modulatorer, hvilket viser radioligandens

anvendelighed til at studere farmakologiske egenskaber for disse stoffer. Publikation II fokuserede på in vivo egenskaber og validering af ^{11}C-Martinostat til måling af HDAC1–3 niveauer. PET-billeddannelse viste et godt signal-støj-forhold og betydelig hjerneoptagelse med en bred distribution. Specificiteten blev bekræftet ved blokeringsforsøg. Dette understreger potentialet af ^{11}C-Martinostat til at undersøge epigenetiske ændringer in vivo. Publikation III undersøgte α7 nAChR agonist binding ved brug af ^{11}C-NS14492, hvilket afslørede forskellige niveauer af binding for tidligere klinisk testede delvise og fulde agonister, henholdsvis encenicline og bradanicline. Disse resultater understreger PET's rolle i CNS-lægemiddeludvikling og understreger nødvendigheden af grundige evalueringer før større kliniske forsøg igangsættes, især for vanskelige terapeutiske mål som α7 nAChR.

Afslutningsvis fremhæver disse publikationer PET-billeddannelses alsidighed og betydning i studiet af α7 nAChR'er, HDAC niveauer og α7 nAChR ligand binding, idet de bidrager med indsigter i radioligandernes in vitro og in vivo egenskaber og deres potentiale som relevante værktøjer i lægemiddeludviklingen.

Abbreviations

1TCM	One tissue compartment model
2TCM	Two tissue compartment model
ACh	Acetylcholine
AD	Alzheimer's disease
AIC	Akaike information criterion
Aβ	Amyloid beta
BBB	Blood-Brain Barrier
B_{max}	Maximum binding capacity
BP	Binding potential
CNS	Central nervous system
eV	Electronvolt
f_P	Free fraction of radiotracer in plasma
FDA	U.S. Food and Drug Administration
GABA	Gamma-aminobutyric acid
HAT	Histone acetyl transferase
HDAC	Histone deacetylase
HRRT	High-resolution research tomograph
IC_{50}	Half maximal inhibitory concentration
IP	Imaging plate
IV	Intravenous
K_d	Dissociation constant
K_i	Inhibition constant
LOR	Line of response
LTP	Long-term potentiation
MA1	Multilinear analysis-1
MRI	Magnetic resonance imaging
nAChR	Nicotinic acetylcholine receptor
NAM	Negative allosteric modulator
ND	Non-displaceable
NSB	Non-specific binding
PAM	Positive Allosteric Modulator
PD	Pharmacodynamics
PET	Positron emission tomography
PK	Pharmacokinetics

ROI	Region of interest
SAM	Silent allosteric modulator
SB	Specific binding
STP	Short-term potentiation
SUV	Standardized uptake values
SUVR	Standardized uptake value ratio
TAC	Time-activity curve
TB	Total binding
TE	Tissue equivalent
VOI	Volume of interest
V_T	Volume of distribution
α-Btx	Alpha-bungarotoxin

Table of contents

Chapter 1

Introduction and background

The nicotinic acetylcholine receptor

The earliest evidence of the nicotinic acetylcholine receptor (nAChR) can be traced back to the work of Otto Loewi, who discovered the neurotransmitter acetylcholine in 1921 (Valenstein, 2002). He jointly won the 1936 Nobel Prize in Physiology or Medicine with Henry Dale for demonstrating the chemical transmission of nerve impulses, a discovery supposedly inspired by two dreams (McCoy & Tan, 2014):

"*The night before Easter Sunday of [1920] I awoke, turned on the light and jotted down a few notes on a tiny slip of thin paper. Then I fell asleep again. It occurred to me at 6.00 o'clock in the morning that during the night I had written down something important, but I was unable to decipher the scrawl. The next night, at 3.00 o'clock, the idea returned. It was the design of an experiment to determine whether or not the hypothesis of chemical transmission that I had uttered 17 years ago was correct. I got up immediately, went to the laboratory, and performed a simple experiment on a frog heart according to the nocturnal design*."

Loewi conducted experiments on two frog hearts, isolating one with a connected vagus nerve and the other without, housed in separate perfusion chambers (Loewi, 1921). Stimulating the vagus nerve in the first heart led to a significant slowdown in its pulse and when the fluid from the first heart was transferred to the second, the

second heart similarly slowed down, mimicking the effects of direct nerve stimulation. He named the inhibitory substance *vagusstoff*, now known as acetylcholine (ACh). This experiment highlighted that nerve cells primarily communicate through chemical signals, not electrical impulses. Building on Loewi's work, Henry Dale conducted further research on ACh and revealed its role as a neurotransmitter. Dale demonstrated that ACh transmitted impulses from the vagus nerve to the heart muscle—experiments that provided concrete evidence of chemical neurotransmission, leading to a paradigm shift in neuroscience. Together, their work paved the way for the identification of the ACh receptor (Tansey, 2006).

In the 1950s and 60s, Bernard Katz and Ricardo Miledi used microelectrode techniques to study muscle cell electrical activity, discovering that ACh caused transient depolarization by opening ion channels (Katz & Miledi, 1965, 1967, 1968). Bernard Katz received the Nobel Prize in 1970 for this work (Bennett, 2003). Around the same time, Victor Nachmansohn showed that nAChR was present in the electric organ of the electric eel, and that it was responsible for the production of the electric discharge (Nachmansohn, 1964, 1966, 1972). In the following years, several researchers worked to purify and characterize the nAChR protein: Chen-Yuan Lee made a significant discovery regarding alpha-bungarotoxin (α-Btx), a snake venom from the many-banded krait (*Bungarus multicinctus)* which specifically blocked neuromuscular transmission without affecting acetylcholinesterase (Chang, 1999). Lee, along with Jean-Pierre Changeux and Michiki Kasai, demonstrated α-Btx's ability to block the electric eel's electrical response and ion flux response to nicotinic agonists, highlighting its use in neuromuscular and nicotinic receptor studies (Changeux, Kasai, Huchet, et al., 1970; Changeux, Kasai, & Lee, 1970). In 1971, Miledi and colleagues isolated nAChR from the torpedo fish, revealing it as a protein complex consisting of five polypeptide subunits arranged around a central pore that, upon binding ACh, undergo a conformational change allowing ion passage and membrane depolarization (Miledi et al., 1971). Fast-forwarding to this century, studies on the structure of the receptor has been made with purification and crystallization leading to the first full X-ray structures for a pentameric ligand-gated ion channel in a closed-channel state (Hilf & Dutzler, 2008) and in an open-channel state (Bocquet et al., 2009; Hilf & Dutzler, 2009) as well as more recent high-resolution structures of human α7 nAChR (Prevost et al., 2023). nAChRs are part of the ligand-gated ion channel superfamily of receptors, which also includes $GABA_A$, glycine, and $5\text{-}HT_3$ receptors (Betz, 1990).

Different combinations of subunits create various nAChR subtypes, broadly classified into three functional groups based on their evolutionary, pharmacological, and physiological characteristics:

1) The muscle subunits (α1, β1, δ, ε, γ), which are outside the scope of this thesis.
2) The neuronal subunits (α2-α6, α10, and β2-β4) combine to form nAChRs in αβ configurations.
3) Neuronal subunits (α7-α9) can form homomeric nAChRs, which are sensitive to inhibition by α-Btx.

Notably, the α7 subunit is distributed across the mammalian central nervous system (CNS). The α10 subunit can combine with α9, while the α8 subunit is present in avian tissue only. The functional diversity of α7 nAChR subunits is evident as they predominantly form homopentameric receptors but can also assemble with β-subunits into heteromeric receptors in both expression systems and the brain (Azam et al., 2003; Khiroug et al., 2002; Moretti et al., 2014). These α7β heteromers display unique pharmacological properties different from homomeric receptors and are likely vital for cholinergic neurotransmission (Thomsen et al., 2015), and reviewed in Wu et al. (2016).

The combination of the five subunits have a significant role in determining the channel kinetics, ion conductance, and selectivity, and determines both the pharmacological characteristics of the ligand binding sites and the channel's preference for cations (Albuquerque et al., 2009). For the α4β2 nAChR, ACh binds within a small pocket between the α4 and β2 subunits, with both subunits influencing the pharmacology of the heteromeric binding site. In contrast, for homopentameric receptors like the α7 nAChR, the ligand-binding site is located between adjacent α7 subunits. This also explains why heteropentameric receptors have two binding sites, while homopentameric receptors have five (Gotti et al., 2006) (Figure 1).

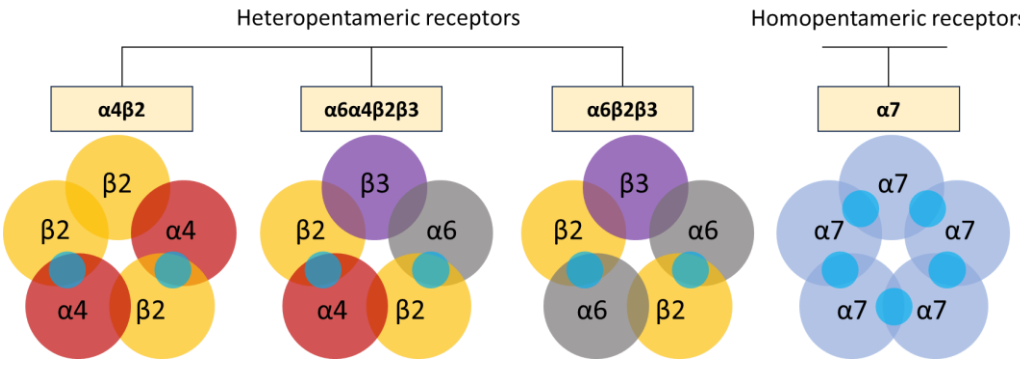

Fig. 1 | The organization and structure of nAChRs involve heteropentameric and homopentameric configurations. Both subtypes feature a pentameric arrangement with distinct ACh-binding sites. The heteropentameric α4β2 and α6β2β3 receptors have two identical binding sites (small blue circle) located between α4/α6 and β2 subunits, respectively, while the heteropentameric α6α4β2β3 subtype has two different binding sites at the interfaces of α4β2 and α6β2. The homomeric α7 subtype features five identical ACh-binding sites. Figure redrawn with permission (CC BY 4.0) from Taly et al. (2009), doi:10.1038/nrd2927.

The endogenous neurotransmitter for nAChRs, ACh, along with the well-known agonist nicotine, binds in the extracellular domain of the receptor between two subunits, at what is commonly known as the orthosteric binding site (Picciotto et al., 2000). In addition to this primary site, nAChRs also have binding sites within the channel lumen for compounds like local anesthetics and some antiepileptic drugs (Bouzat & Sine, 2018). Additionally, there are allosteric modulatory sites on the nAChR. Compounds that bind to these sites are called allosteric modulators and are categorized based on their effects: positive allosteric modulators (PAMs) enhance, negative allosteric modulators (NAMs) reduce, and silent allosteric modulators (SAMs) compete with PAMs and NAMs, effectively blocking their effects and diminishing any impact. PAMs are thought to facilitate agonist binding through minor conformational changes in the receptor, lowering the energy barrier to transition from a closed to an open state, or raising the barrier from an open to a desensitized state, thereby modulating the receptor's activity (Bertrand & Gopalakrishnan, 2007; Hogg et al., 2005).

Function of the neuronal nicotinic acetylcholine receptor

All mammalian neuronal nAChR subtypes share a key functional characteristic: they are permeable to small monovalent and divalent cations, primarily sodium (Na^+), potassium (K^+), and calcium (Ca^{2+}). When an agonist, such as ACh or

exogenous nicotine, binds to the receptor, it induces a tertiary conformational change that stabilizes the nAChR channel in its open state. This change temporarily allows the channel to permit the passage of cations before it either returns to its resting state or transitions into a desensitized state, becoming unresponsive to further activation (Figure 2).

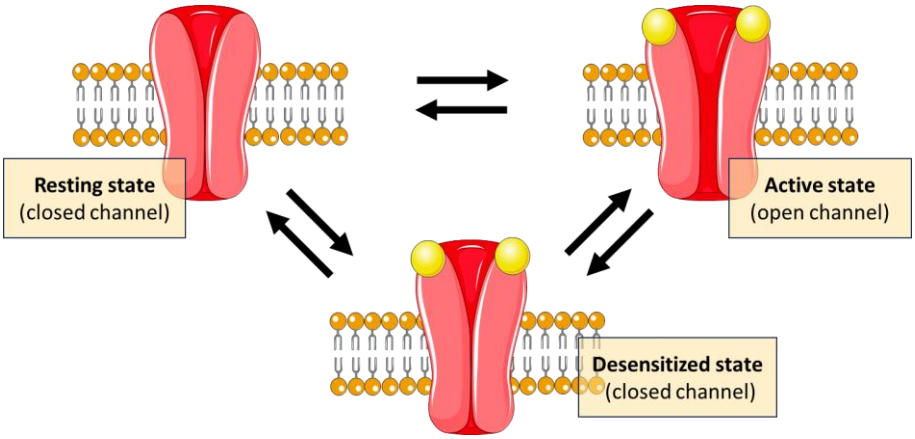

Fig. 2 | The nAChR has three main functional states: resting, open, and desensitized. In the resting state, ACh (yellow ball) binding sites are empty, and the pore is closed. When activated, the channel opens, allowing cations to pass. In the desensitized state, ACh, nicotine, or other ligands bind but the pore remains closed. Figure redrawn with permission conveyed through Copyright Clearance Center license number 5815340172776 from Wittenberg et al. (2020), doi: 10.1016/j.neuropharm.2020.108256.

At a synaptic cleft, short exposure to high concentrations of ACh leads to synchronous opening of the nAChRs' pores whereas prolonged exposure to low concentrations of nicotine from tobacco use results in partial activation of the receptors but also significant desensitization, leading to the closed state where they are unresponsive to further activation (Dani, 2015; Papke & Lindstrom, 2020). This mechanism is important when evaluating the therapeutic potential of the receptor. Just as brief exposure to the native neurotransmitter ACh activates receptors, prolonged exposure leads to desensitization, inhibiting further responses. This implies that extended treatment with an α7 nAChR agonist might not result in a sustained receptor response. Thus, in clinical settings, it is important to assess the effects of longer and cumulative exposures to avoid tachyphylaxis—the reduction in medication effectiveness over time.

Receptors composed of α7 subunits rapidly desensitize and have a high Ca^{2+} to Na^{+} permeability ratio. Consequently, activating α7 nAChRs can significantly elevate

intracellular Ca^{2+} concentrations. This increase is partly due to the activation of second messengers that trigger the release of calcium from intracellular stores and voltage-gated Ca^{2+} channels (Dajas-Bailador et al., 2002; Mulle et al., 1992). The influx of ions through α7 nAChR channels results in the depolarization of the postsynaptic membrane, which activates downstream signaling pathways. The α7 nAChR plays a pivotal role in numerous physiological and pathological processes within the CNS (Terry et al., 2023). Its activation influences several key functions, including the modulation of neurotransmitter release (Albuquerque et al., 2009; Gray et al., 1996), enhancement of cognitive functions (Bloem et al., 2014; Levin, 2013; Wallace & Bertrand, 2013), and regulation of neuronal development and survival (Ji et al., 2001), as will be discussed later.

Distribution of the α7 nicotinic acetylcholine receptor

The α7 nAChRs are widely distributed across the CNS, playing a significant role in various physiological and pathological processes. Their distribution has been mapped through radioligand binding of ^{125}I-α-Btx and in situ hybridization of mRNA specific to the receptor. In the brain, α7 nAChRs are highly expressed in areas linked to cognitive and sensory functions, memory, and attention. Key regions with high expression include the hippocampus, cerebral cortex, thalamus, and amygdala (Figure 3) (Gotti et al., 2006). This widespread distribution highlights their crucial role in neural functioning. The hippocampus, especially in the CA1, CA3, and dentate gyrus areas, has a dense concentration of α7 nAChRs, which play a crucial role in learning, memory, and synaptic plasticity (Frazier et al., 1998). Additionally, the cerebral cortex, particularly layers I and VI, which are involved in higher cognitive functions, has significant expression of α7 nAChRs (Clarke et al., 1985; Seguela et al., 1993; Tribollet et al., 2004). Apart from their presence in regions associated with higher cognitive functions, α7 nAChRs are also found in sensory processing areas. In the thalamus, which relays sensory information to the cortex, α7 nAChRs modulate synaptic transmission and contribute to sensory gating processes (Zoli et al., 2015). Similarly, α7 nAChRs are expressed in the amygdala, an area involved in emotional processing, potentially playing a role in emotional regulation and fear conditioning (Klein & Yakel, 2006; Pidoplichko et al., 2013). Finally, the presence of α7 nAChRs in the substantia nigra and ventral tegmental area, regions abundant with dopaminergic neurons, highlights their involvement in modulating the dopaminergic system and reward processing (Mansvelder & McGehee, 2000).

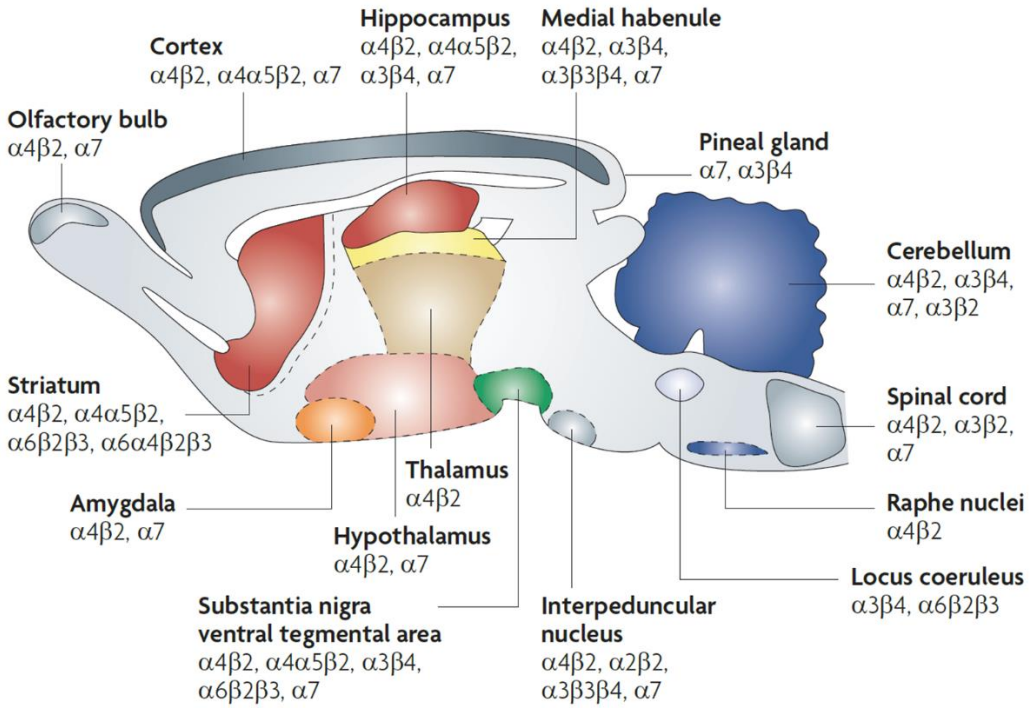

Fig. 3 | Regional distribution of primary nicotinic receptor subtypes in the rodent CNS. Figure reprinted from Taly et al. (2009), doi:10.1038/nrd2927. © 2009, Nature Publishing Group, distributed under a Creative Commons Attribution 4.0 International License.

While neuronal nAChRs are found in both pre- and post-synaptic locations, α7 nAChRs are predominantly pre-synaptic. When activated by ACh or nicotine, they modulate the release of neurotransmitters such as dopamine, glutamate, and gamma-aminobutyric acid (GABA), influencing synaptic transmission. Although α7 nAChRs can also be located post-synaptically and mediate postsynaptic responses, their primary recognition comes from their pre-synaptic roles (Dajas-Bailador & Wonnacott, 2004; Dani & Bertrand, 2007; Jones et al., 1999). Finally, the α7 nAChR is also distributed perisynaptically where it mediates modulating effects of non-synaptically released ACh (Kasa et al., 1995; Shen & Yakel, 2009).

The widespread distribution of α7 nAChRs in the CNS highlights their involvement in a wide array of physiological processes and functions. Their activation can lead to changes in synaptic transmission, neural network dynamics, and cognitive processing. However, dysregulation of α7 nAChRs has been linked to various neurological and neuropsychiatric disorders, including Alzheimer's disease and schizophrenia, making them a potential target for therapeutic interventions (Papke & Horenstein, 2021).

Nicotinic receptor's role in memory and cognition

The hippocampus, a seahorse-shaped structure located in the medial temporal lobe of the brain, plays a key role in learning, cognition, and in the formation, consolidation, and retrieval of memories (Lisman et al., 2017). Also, spatial navigation and the formation of cognitive maps rely heavily on the proper functioning of the hippocampus, which is, as described above, widely populated with nAChRs in all layers. The α7 nAChRs are primarily located in the granule and pyramidal cells of the hippocampus (Dominguez del Toro et al., 1994; Fabian-Fine et al., 2001). Here, activation of the α7 nAChR exerts effects on the network through various mechanisms: firstly, it directly depolarizes neurons, particularly interneurons, as the receptor is highly expressed in their somatic regions (Khiroug et al., 2003). Secondly, its activation regulates both glutamatergic and GABAergic transmission through pre- and postsynaptic mechanisms and thirdly, the timing of α7 nAChR activation in relation to glutamatergic transmission plays a crucial role in modulating plasticity associated with glutamatergic transmission (Ge & Dani, 2005; Gu & Yakel, 2011). For instance, the activation of α7 nAChR leads to an increase in presynaptic release of both glutamate and GABA, facilitating the induction of long-term potentiation (LTP). However, the specific outcome in primary excitatory cells is dependent on the location and timing of α7 nAChR activation. As an example, in CA1 interneurons, α7 nAChR activation can dampen the induction of short-term potentiation in nearby connected pyramidal neurons and conversely; activation of α7 nAChRs located on CA1 dendrites in pyramidal neurons can enhance short-term potentiation (STP) or LTP (Cheng & Yakel, 2015; Radcliffe et al., 1999). The effects of α7 nAChR activation in different cellular compartments highlight its complex regulatory role in hippocampal synaptic plasticity and ultimately in learning and memory formation and cognition (Hasselmo, 2006; Letsinger et al., 2022). Several studies in animal models and humans also suggest that extrinsic activation of α7 nAChRs enhances synaptic plasticity, facilitates LTP, and improves memory formation (Buccafusco et al., 2005; Levin et al., 2006) and conversely, receptor antagonists have been shown to impair cognitive function (Leiser et al., 2009).

The α7 nicotinic receptor in Alzheimer's disease

Alzheimer's disease (AD) is a complex neurodegenerative disorder characterized by progressive cognitive decline, memory impairment, and synaptic dysfunction (Scheltens et al., 2016). AD is the primary cause of cognitive impairment and

dementia in older individuals globally, significantly affecting those living with the condition, their relatives, and imposing a substantial economic burden on society (Tahami Monfared et al., 2022). For these reasons, AD has been named a European and global priority to tackle and prevent (Cahill, 2020; Winblad et al., 2016). The role of the α7 nAChR in AD has received significant attention due to its complex dual function in the disease's pathogenesis.

Evidence indicates that α7 nAChRs, present on neurons and glial cells and engaged in neuroprotective signaling pathways, may contribute to neuroprotection in AD. Activation of these receptors can release neurotrophic factors such as brain-derived neurotrophic factor, which supports neuronal survival and plasticity (Cai et al., 2022; Wei et al., 2022). Additionally, α7 nAChRs have anti-inflammatory properties, modulating microglial activation and cytokine production, which may protect against neuroinflammation in AD (Dineley et al., 2015). Further, α7 nAChRs are essential for regulating inflammation by modulating macrophage cytokine release both outside the CNS (Wang et al., 2003), and within it (Shytle et al., 2004). In the study by Shytle and colleagues, α7 nAChRs were shown to be expressed in primary cultured microglial cells and brain slices. When pre-treated with ACh and nicotine, these receptors inhibited lipopolysaccharide-induced cytokine release, an effect that was impaired by the addition of α-Btx. Additionally, α7 nAChRs have been implicated in the clearance of amyloid beta (Aβ), a key process in AD. In AD, microglial cells, the primary immune cells of the CNS, phagocytize and degrade Aβ, thereby facilitating its removal from the brain and potentially mitigating disease progression (Hansen et al., 2018). However, aging can cause microglia to enter a pro-inflammatory state, diminishing their phagocytic capabilities (Harry, 2013). Nonetheless, studies have demonstrated that activating α7 nAChRs on microglia induces a phenotypic shift, enhancing their ability to phagocytize and metabolize Aβ (Kwon & Koh, 2020; Takata et al., 2010).

Based on these findings, it is reasonable to suggest that nicotine intake and cholinesterase inhibitors, which prevent the breakdown of acetylcholine in the synaptic cleft, could reduce Aβ burden and thereby improve symptoms of AD. Studies in rat microglia (Takata et al., 2010) and transgenic mice (Hernandez et al., 2010; Medeiros et al., 2014) showed beneficial effects of nicotine or cholinesterase inhibitors, while the knock-out of α7 nAChR, competitive antagonists or antibodies targeting the receptor masked their effects or even worsened the pathology. However, in patients with AD, cholinesterase inhibitors have demonstrated limited cognitive benefits early in the disease course (Kaduszkiewicz et al., 2005) and the effects are often constrained by cholinergic adverse effects (Haake et al., 2020).

Regarding nicotine and its effect on AD, the picture is less clear: a meta-analysis of prospective cohort studies indicated that smoking increases the risk of cognitive impairment and AD in individuals aged 65 to 75. However, this increased risk was not observed in smokers under the age of 65 (Zhong et al., 2015). In their review, Parri et al. (2011) suggest that the age-related variability in risk might stem from the interaction between Aβ and α7 nAChRs. Aβ has been found to bind to α7 nAChRs, and the finding has been confirmed in numerous studies, but the consequences of this interaction are still unclear. That is, whether Aβ binding inhibits or activates the receptor, and whether agonists or antagonists can effectively reverse these effects. Also, the finding that cholinergic neurons in the basal forebrain express the α7β2 isoform presents another complication relevant to the pathophysiology of AD (Liu et al., 2009; Thomsen et al., 2015). It has been reported that the α7β2 receptor appears especially sensitive to Aβ, leading to inhibition of functional responses to ACh even at very low concentrations (nanomolar range). The neurotoxic effects of α7β2 receptor blockade on cholinergic neurons are not fully understood, nor is it clear if microglia cells in the basal forebrain express this specific nicotinic receptor. However, an interplay of factors may contribute to a positive feedback loop in AD pathophysiology: 1) the aging brain pushes microglia towards a less effective phagocytic phenotype, resulting in impaired Aβ clearance. 2) Accumulation of extracellular Aβ can then block the α7β2 nAChR on basal forebrain cholinergic neurons, leading to their degeneration. 3) Reduced ACh levels result in decreased stimulation of microglia's α7 nAChRs, further compromising their phagocytic function. This result in a diminished clearance of Aβ leading to extracellular precipitates, triggering microglial recruitment, inflammatory processes, and additional toxicity to cholinergic neurons. Early intervention with nicotine, as well as cholinesterase inhibitors, and α7 nAChR agonists may delay the onset of this detrimental feedback loop. However, when Aβ accumulates as an effect of disease progression, the availability of α7 nAChRs is reduced due to negative interactions with oligomeric Aβ which could explain why the toxic effects of smoking outweigh the neuroprotective effects in later stages of AD. Collectively, these findings suggest that α7 nAChRs may play a crucial role in mitigating Aβ accumulation and neuroinflammation, thereby contributing to neuroprotection in the early stages of AD.

Despite its neuroprotective potential, the involvement of α7 nAChRs in AD is complex, and chronic dysregulation of these receptors can also contribute to disease progression. More than four decades ago the cholinergic hypothesis of the cognitive deficits in AD was suggested. This hypothesis was initially proposed by Raymond Bartus (Bartus et al., 1982) and was based on the observation of reduced choline

acetyltransferase activity in the brains of patients with AD and the connection between ACh and memory processes (historic review, Contestabile (2011)). The hypothesis suggest that the loss of cholinergic neurons and the subsequent decline in ACh release impair cognitive function, specifically memory and learning, in patients with AD which was further supported by the finding that nicotine and ACh binding sites in AD postmortem brain tissue were lost (Nordberg & Winblad, 1986). These findings have been investigated at the cholinergic receptor level: for nAChRs, numerous studies using a combination of autoradiographic, immunochemical, and radioligand binding methods have consistently demonstrated extensive and substantial reductions in α4β2 nAChR levels within the AD affected brain (Court et al., 2001; Kendziorra et al., 2011), while it is less clear for the muscarinic AChRs, since their levels seems to be intact (Aubert et al., 1992). Specifically, for the α7 nAChR, this remain an area of ongoing research since the findings are not entirely consistent across studies. While the majority of studies seems to suggest that α7 nAChR levels may remain relatively stable or even increased (Counts et al., 2007; Dineley et al., 2015; Mufson et al., 2008), some studies have reported decreased α7 nAChR levels in certain brain regions affected by AD (Teaktong et al., 2004). Of note, the contradicting evidence could stem from an increased α7nAChR levels in astrocytes and decreased levels in neurons as recently reviewed in Fontana et al. (2023). For this reason, and for its apparent role in cognition, the α7 nAChR was found to be an appealing pharmaceutical target for the cognitive impairments associated with AD.

The α7 nicotinic receptor in Schizophrenia

Schizophrenia is a complex psychiatric condition characterized by positive symptoms such as hallucinations and delusions, negative symptoms including blunted affect and social withdrawal, and cognitive deficits involving impaired executive functions, memory, and mental processing speed (McCutcheon et al., 2020). Schizophrenia is believed to affect approximately 1% of the global population (Marder & Cannon, 2019) and is ranked among the top 15 global causes of disability (Vos et al., 2017). Additionally, individuals with schizophrenia have a significantly reduced life expectancy, with higher mortality rates across all age groups, resulting in a lifespan approximately 20 years shorter than the general population (Laursen et al., 2014). Cognitive impairment is a key symptom of schizophrenia, that often appears before psychotic symptoms and persists throughout the illness, significantly affecting long-term outcomes (Kahn, 2019).

Antipsychotics are the primary treatment for schizophrenia and are effective in reducing positive symptoms in some patients; however, they do not consistently improve cognitive function (Hill et al., 2010). This unmet need has been a central focus in drug discovery efforts for several decades. However, as of today, no pro-cognitive compounds have been approved for clinical use in the treatment of schizophrenia (McCutcheon et al., 2023). The complex and incompletely understood etiology and pathophysiology of schizophrenia presents a major challenge in developing drug candidates. The disease involves multiple neurotransmitter systems, including dopaminergic, serotonergic, glutamatergic, adrenergic, and cholinergic pathways (Steeds et al., 2015). Over the last two decades, the role of the α7 nAChR in the underlying biology of schizophrenia has gained significant interest, providing insights into the disease mechanisms and opening up possibilities for new treatments (Tregellas & Wylie, 2019). This connection is supported by 1) behavioral, 2) neurobiological, and 3) genetic evidence. Firstly, individuals with schizophrenia show significantly higher rates of tobacco product use, ranging from 70–85%, which starkly contrasts with the ~20% prevalence in the general population and is higher than rates observed in any other mental illness (Ziedonis et al., 2008). Also, individuals with schizophrenia who smoke extract more nicotine per cigarette and smoke a greater number of cigarettes per day than the general population (Donde et al., 2020). This increased nicotine consumption is believed to be a self-medicating behavior, particularly targeting cognitive symptoms (Leonard et al., 2007). Secondly, postmortem studies of brains from individuals with schizophrenia have shown reduction in α7 nAChR expression and function, particularly in brain regions associated with cognitive processing and sensory gating (Guan et al., 1999; Martin & Freedman, 2007). Thirdly, genetic studies have identified single-nucleotide polymorphisms in the CHRNA7 gene, encoding α7 nAChR subunits, that are associated with an increased risk of schizophrenia (Sinkus et al., 2015). These findings, taken together, suggest that α7 nAChR dysregulation contribute to the cognitive deficits of schizophrenia.

Therapeutic targeting of α7 nAChRs in AD and schizophrenia

Based on the evidence discussed in the previous sections, the α7 nAChR has been pursued as a pharmaceutical target for cognitive symptoms of both AD and schizophrenia for over 20 years (Burns et al., 2023; Crestini et al., 2024), (Table 1).

A significant number of partial agonists have been tested: Encenicline (EVP-6124) is the compound that advanced the furthest in clinical development. A proof-of-concept, randomized trial in patients with schizophrenia showed promising results (Preskorn et al., 2014), and a subsequent, phase 2 placebo controlled clinical trial spanning 6-month in patients with mild-to-moderate AD demonstrated significant improvements in cognitive and functional parameters (Deardorff et al., 2015). Similarly, a phase 2 placebo-controlled trial in participants with schizophrenia showed significant and clinically meaningful improvements in cognition (Keefe et al., 2015). Despite these promising results, in 2015, the U.S. Food and Drug Administration (FDA) suspended two large phase 3 clinical trials in patients with mild-to-moderate AD due to significant gastrointestinal side effects (Alzforum, 2015), and the phase 3 trials in schizophrenia failed to meet primary endpoints (Brannan, 2019). No further development of this compound in AD or schizophrenia has been initiated.

Six other partial agonists have been developed and tested in various stages, but they have all either failed to meet primary endpoints or have been discontinued for other reasons: **1)** GTS-21 was the first compound to be evaluated in clinical trials (Kem, 2000), where it enhanced cognitive performance in healthy subjects (Kitagawa et al., 2003). In a later randomized phase 2 clinical trial, four doses of GTS-21 or a placebo were administered over 28 days to patients with probable AD, but no significant treatment benefits were observed. It is worth noting that while GTS-21 did not demonstrate cognitive enhancement in schizophrenia, it did improve negative symptoms in a separate phase 2 study (Freedman et al., 2008). **2)** SSR180711, which elevated extracellular ACh levels and enhanced LTP in hippocampal slices of rats and mice in a dose-dependent manner (Biton et al., 2007), was evaluated in a four-week, placebo-controlled phase 2 trial in patients with mild AD. However, the trial was prematurely terminated due to an insufficient expected risk-benefit ratio and results have not been published. **3)** AZD0328 was found to improve operant responding acquisition and novel object recognition in mice (Sydserff et al., 2009), but failed to meet the primary endpoint of improved cognition or show significant improvement in secondary endpoints in a 14-day phase 2 clinical trial with 100 patients with schizophrenia (results not published). AZD0328 has not been formally evaluated in AD, except for a small phase 1 pharmacokinetic (PK) trial in healthy elderly subjects. **4)** ABT-126 was evaluated in a 12-week phase 2 clinical trial, showing a non-significant trend in cognitive performance improvements compared to placebo in 274 patients with mild-to-moderate AD (Gault et al., 2015). However, a later phase 2 trial with 438 patients with mild-to-moderate AD showed no significant improvements over the course of

24 weeks (Florian et al., 2016; Gault et al., 2016). Additionally, a phase 2 clinical trial in patients with schizophrenia showed no significant cognitive improvements (Haig et al., 2016). **5)** RG3487 demonstrated positive results in a phase 2 clinical trial involving 80 patients with mild-to-moderate AD (Alzforum, 2007; Rezvani et al., 2009). Later, a 6-month placebo-controlled phase 2 trial with 389 patients with mild-to-moderate AD was conducted, but the results were never published. Moreover, RG3487 did not meet the primary endpoint of cognitive improvement in a phase 2 trial with 215 patients with schizophrenia (Umbricht et al., 2014). **6)** AQW051 was evaluated in a four-week randomized phase 2 clinical trial with 54 patients with mild AD or amnestic mild cognitive impairment. After an inconclusive task-related functional magnetic resonance imaging trial in patients with schizophrenia (Barch et al., 2016), a larger trial involving patients with schizophrenia was conducted, but the results have not yet been published. AQW051 was also tested in 74 patients with moderate to severe L-Dopa-induced dyskinesia, showing no significant improvements (Trenkwalder et al., 2016).

Considering the many α7 nAChR partial agonists evaluated in clinical trials, only one full agonist has been assessed: bradanicline (TC-5619) (Mazurov et al., 2012). The compound was evaluated in a 12-week placebo-controlled phase 2 clinical trial involving 184 patients with schizophrenia, assessing cognitive enhancement. The results were encouraging, with the primary efficacy measure showing statistically significant improvements (Lieberman et al., 2013). Subsequently, TC-5619 was evaluated in 603 patients with schizophrenia with cognitive dysfunction (Walling et al., 2016), 250 patients with ADHD, and in a phase 1 placebo-controlled trial involving healthy elderly and patients with AD. However, the drug did not meet efficacy goals in any of these studies and further development was discontinued.

Another treatment strategy explored involves using PAMs for the α7 nAChR, which enhance receptor function without direct activation, allowing for precise and controlled modulation of receptor activity. This method provides the potential to fine-tune receptor responses, making PAMs an attractive therapeutic option (Manetti et al., 2023; Sanders & Millar, 2023; Williams et al., 2011). Despite this apparent advantage, only two compounds have advanced to clinical testing: AVL-3288 and JNJ-39393406. AVL-3288 was tested in a first-in-human phase 1 clinical trial in 12 healthy participants and the results indicated possible cognitive improvements (Gee et al., 2017). It was later evaluated in a phase 1 clinical trial in 24 patients with schizophrenia but failed to show any improvements (Kantrowitz et al., 2020). JNJ-39393406 was evaluated in two phase 2 clinical trials for smoking cessation and for treating cognitive or depressive symptoms in patients with

unipolar depression. It was also investigated in a placebo-controlled phase 1 trial in 47 patients with schizophrenia for the improvement of sensory gating deficits (Winterer et al., 2013). However, due to unfavorable outcomes across all trials, further development of the drug was discontinued (Davidson et al., 2021; Perkins et al., 2018).

Table 1 | List of compounds developed targeting the α7 nAChR in AD and schizophrenia that progressed to clinical trials and reasons for their discontinuation. Type: (A) = Agonist, (PA) = Partial agonist, (PAM) = Positive allosteric modulator. Table compiled from Bertrand et al. (2015); Papke and Horenstein (2021); Tregellas and Wylie (2019); Burns et al. (2023); Crestini et al. (2024) and available data on clinicaltrials.gov.

Name, (type)	Indication	Clinical phase reached	Result/reason discontinued	Clinicaltrials.gov identifier (NCT)	Reference
ABT-126 (PA)	AD	2	Trend in cognitive performance improvements	00948909	Gault et al., 2015
ABT-126 (PA)	AD	2	No significant effects	01527916	Florian et al., 2016
ABT-126 (PA)	Schizophrenia	2	No significant effects	01678755	Haig et al. 2016
AQW051 (PA)	Mild cognitive impairment	2	Terminated; unknown reason	00582855	None found
AQW051 (PA)	Schizophrenia	2	None reported	01730768	Barch et al., 2016
AQW051 (PA)	L-DOPA-induced dyskinesia	2	No significant effects	01474421	Trenkwalder et al., 2016
AVL-3288 (PAM)	First-in-human	1	Trend on cognitive improvement	01851603	Gee et al., 2017
AVL-3288 (PAM)	Schizophrenia	1	No significant effects	02978599	Kantrowitz et al., 2020

AZD0328 (PA)	PK study	1	Company decision	00687141	Sydserff et al., 2009
AZD0328 (PA)	Schizophrenia	2	Company decision	00669903	Sydserff et al., 2009
EVP-6124 (PA)	Schizophrenia	1	Positive effects in performance on cognitive tests	01556763	Preskorn et al., 2014
EVP-6124 (PA)	Schizophrenia	2	Cognitive improvements	00968851	Keefe et al., 2015
EVP-6124 (PA)	AD	2	Cognitive improvements	01073228	Deardorff et al., 2015
EVP-6124 (PA)	AD	3	Clinical hold due to adverse events	01969123, 01969136	None found
EVP-6124 (PA)	Schizophrenia	3	No significant effects	01714661, 01716975	Brannan, 2019
GTS-21 (PA)	Probable AD	2	No significant effects	00414622	Kem, 2000
GTS-21 (PA)	Schizophrenia	2	No significant effects	01400477, 00100165	Freedman et al., 2008
JNJ-39393406 (PAM)	Smoking cessation in patients with schizophrenia	2	No treatment benefit	02230384	Perkins et al., 2018
JNJ-39393406 (PAM)	Cognition in patients with unipolar depression	2	No treatment benefit	02677207	Davidson et al., 2021
JNJ-39393406 (PAM)	Schizophrenia	1	No treatment benefit	01137799	Winterer et al., 2013
RG3487 (PA)	AD	2	Not reported	00884507	None found

RG3487 (PA)	Schizophrenia	2	No cognitive improvement	00604760	Umbricht et al., 2014
SSR18071 (PA)	Mild AD	2	Early terminated	00602680	Biton et al., 2007
TC-5619 (A)	PK in healthy elderly and AD	1	Not reported	01254448	Mazurov et al., 2012
TC-5619 (A)	Schizophrenia	2	Cognitive improvements	01003379	Lieberman et al., 2013
TC-5619 (A)	ADHD	2	Not reported	01472991	None found
TC-5619 (A)	Schizophrenia	2	No significant effects	01488929	Walling et al., 2016

Antagonists of the α7 nAChR are less impactful than agonists and partial agonists in practical applications. Memantine, a compound approved for treating AD, is primarily known as a potent NMDA receptor antagonist but also acts as an α7 nAChR antagonist (Aracava et al., 2005). While some studies suggest that this antagonistic action may be beneficial in treating AD (Banerjee et al., 2005), the usefulness is still unclear. Other well-known antagonists are the natural toxins from two groups of proteins: conotoxins and α-Btx. Conotoxins are peptides from the cone snails that target ion channels, with α-conotoxins specifically targeting the α7 nAChR in a selective and reversible manner (Azam & McIntosh, 2009). In contrast, α-Btx binds irreversibly to nAChRs. Due to their molecular size and properties, conotoxins do not cross the blood-brain barrier (BBB) and primarily act in the peripheral nervous system limiting their practical use (Blanchfield et al., 2007).

Translational challenges in α7 nAChR drug development

The disappointing results of clinical trials for pro-cognitive drugs targeting the α7 nAChR in schizophrenia and AD raise questions about the translational validity of

animal models used in preclinical development (Lewis et al., 2017). The translational elements in animal models for neuropsychiatric and neurological disorders like schizophrenia and AD is a major challenge and can be a roadblock in drug discovery and several factors contribute to this complexity: the subjective nature of symptoms associated with these disorders, the absence of reliable biomarkers and objective diagnostic tests, and our limited understanding of the neurobiology and pathophysiology of neuropsychiatric and neurological disorders in general (Bale et al., 2019; Nestler & Hyman, 2010). When considering translational validity, rodent models undoubtedly play a crucial role in basic research for testing disease-related hypotheses and the initial assessment of new therapeutic agents. However, an overreliance on these models, particularly in the later preclinical stages of neuropsychiatric drug development, is problematic (Markou et al., 2009). This reliance is questionable due to the considerable limitations in the behavioral repertoire of rodents compared to humans as well as substantial anatomical differences, particularly in the development of cortical regions of the forebrain, which is involved in cognitive processes such as working memory, sustained attention, decision-making, and executive function. In addition, differences in α7 nAChRs, such as genetic and pharmacological difference between rodents and humans might also contribute to the contradictory outcomes observed in preclinical and clinical trials. In a study, participants with 15q13.3 microdeletion syndrome, which involves the CHRNA7 gene, showed behaviors commonly associated with schizophrenia, but interestingly, in a knockout mouse model of the same gene, no similarities to this phenotype was observed (Yin et al., 2017).

PK studies reveal further differences between rodent and human receptors: in vitro, GTS-21 stimulates the rat α7 nAChR to achieve more than double the maximal response compared to the human α7 nAChR. Additionally, the inhibition constant (K_i) value at the rat receptor is approximately ten times lower than that at the human receptor (Meyer et al., 1998). This difference suggests that similar serum levels might yield different effects across species. Furthermore, although the general organization of brain structures is similar between rodents and humans, a study by Hodge et al. (2019) highlights significant differences in gene expression among comparable cell types in mouse and human brains: the study used single-cell transcriptomics to analyze various cell types in the mouse cortex and the human middle temporal gyrus. By comparing the gene expression in homologous cell types, significant variations were found across species in neurotransmitter receptors, ion channels, extracellular matrix elements, and cell-adhesion molecules among similar cell types. These differences could play a crucial role in explaining the limited success of translating pharmacological treatments for CNS disorders

between rodents and humans. Since we are still far from developing robust tissue models like brain organoids and in silico models that accurately mimic brain functions and diseases, the need for animal models still exists (Homberg et al., 2021).

Taken together, these findings highlight the need in neuropsychiatry and drug discovery research for the use of more appropriate species, that resemble humans more closely both in terms their behavioral repertoire and their brain anatomy (please refer to the Section 'The pig as a model animal in neurobiology', page 55).

Clinical trial design and dosing strategies

Another limitation to the clinical studies is linked to decisions regarding dosage, administration frequency, and treatment duration. Unlike animal studies that frequently show robust cognitive effects with acute or subacute dosing of α7 nAChR ligands, as reviewed in Thomsen et al. (2010), many clinical trials have used much longer durations, spanning weeks and months. Prolonged exposure to an agonist, such as the dosing in most of the clinical trials, leads to temporary inactivity in α7 nAChRs as described earlier, potentially resulting in receptor desensitization or even functional antagonism (Quick & Lester, 2002). A recent theory suggests that α7 nAChR ligands could be more effective at lower concentrations, as higher concentrations may desensitize the receptors, leading to an inverted-U shaped dose-response curve (Tregellas & Wylie, 2019). Animal studies support this idea, revealing that optimal responses to α7 nAChR agonists often occur with lower doses, and in contrast, increasing the dose tends to produce diminishing effects, attributable to receptor desensitization. As an example, a study in non-human primates demonstrated that low doses of PHA543613, an α7 nAChR agonist, improved cognitive performance and enhanced neuronal activity in the prefrontal cortex, but treatment with higher doses were ineffective (Yang et al., 2013). For TC-5619, the investigators speculate about the selected dosing strategy and treatment duration in relation to the primary outcome of the phase 2 clinical trial: "*It is possible that relatively low doses (e.g., 1mg) are sufficient to initiate CNS processes that produce clinically observable benefits, and that higher starting doses (e.g., 5mg, 50mg) do not invoke or desensitize these processes, as may a longer treatment duration*" (Walling et al., 2016).

The ability to select a suitable dose of an α7 nAChR ligand for optimal target engagement could be improved if non-invasive neuroimaging methods such as positron emission tomography (PET) was used in both preclinical and clinical studies. Finally, the possibility of coadministration of a PAM with an agonist or partial agonist could also be an interesting strategy, but not something that has been tested in clinical trials yet. This could potentially overcome dosing strategy challenges and desensitization, allowing for lower doses, and possibly avoiding side effects seen in clinical trials.

Decades of preclinical and clinical research support the idea that α7 nAChRs represent a promising therapeutic target for cognitive disorders in AD and schizophrenia (Pastor & Medina, 2024). Several drugs targeting the receptor have demonstrated pro-cognitive effects in animal studies, with some showcasing positive effects in both preclinical investigations and early clinical trials. Despite this, the field has not yet seen a large-scale phase 3 clinical trial in AD or schizophrenia where a compound specifically targeting the α7 nAChR has shown clear pro-cognitive effectiveness without significant adverse effects. This lack of conclusive success has diminished enthusiasm among many pharmaceutical companies, leading several to abandon their activities in this area. As this section makes clear, several factors—including the translational value of animal models, complex dose-effect relationships, and their combination—have contributed to the failure of compounds targeting this otherwise interesting target. Therefore, the apparent clinical failures may not necessarily reflect the true potential of the compounds or the receptor in terms of cognitive improvement. Overcoming these hurdles through refined research strategies, innovative clinical trial designs, and the utilization of PET imaging could still reveal the benefits of targeting α7 nAChRs, reigniting interest and progress in this area of cognitive disorder treatment.

Epigenetic principles and neurodegenerative connections

Epigenetics is the research field that investigates heritable changes in gene expression that occur without modifications to the DNA sequence itself. The DNA code remains highly stable and consistent across all cell types, enduring through cell divisions. In contrast, epigenetic marks, or modifications, are reversible, varying between cell types, and responsive to both internal and external stimuli, including environmental signals. Evidence suggests that these epigenetic marks act as a cellular memory of early-life exposure to adverse environments, potentially leading to long-term changes in gene transcription and the onset of diseases later in life (Petronis, 2010) (Figure 4).

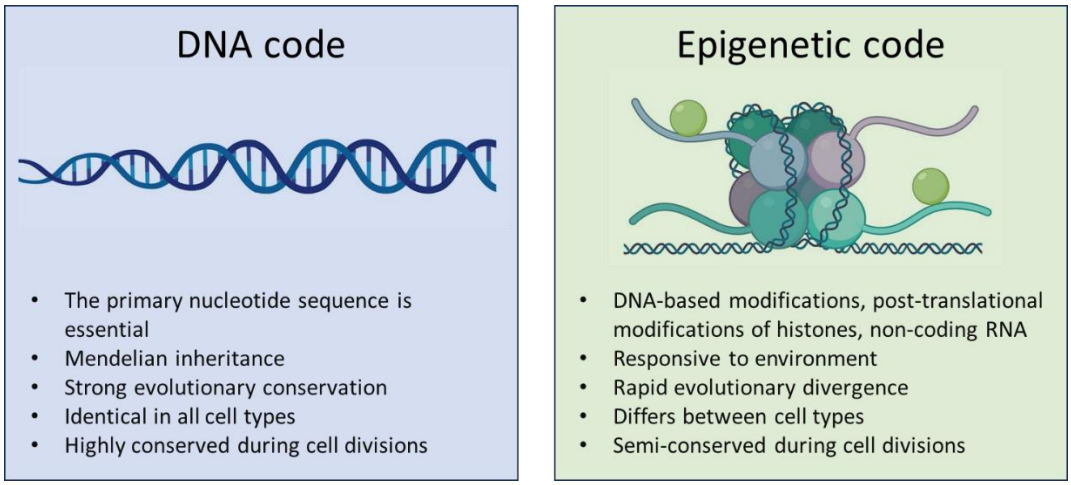

Fig. 4 | Schematic comparison of the static DNA code with the dynamic epigenetic code. Figure redrawn with permission conveyed through Copyright Clearance Center license number 5815340498889 from Webster et al. (2013), doi:10.1016/j.cjca.2012.10.023.

Principles of epigenetics

Some of the earliest scientific support for epigenetic principles came from Waddington's 1940s experiments with fruit flies (Murray et al., 2022). He demonstrated that environmental stress, like heat shock, could induce a heritable phenotype—specifically a cross-veinless pattern in the wings. Selective breeding of these affected flies showed that the phenotype could persist in subsequent

generations without further stress. This led Waddington to propose the 'epigenetic landscape,' a concept illustrating how genes interact with the environment to shape development. The term 'epigenetics' comes from the Greek prefix 'epi', meaning 'above' or 'beyond', combined with 'genetics', referring to the study of genes (Waddington, 2012). In short, his work expanded the genetic idea that 'phenotype = genotype + environment' into a developmental concept where 'phenotype = genotype + epigenetics + environment' (Gilbert, 2012). Further evidence for the role of epigenetic processes in gene regulation came from studies on X chromosome inactivation in female mammals. In 1961, Mary Frances Lyon proposed the 'random X inactivation' hypothesis to explain how female cells balance the expression of genes on the two X chromosomes (Lyon, 1961), a key discovery that has had profound implications for genetics and developmental biology (Rastan, 2015). Later work showed that X inactivation is controlled by epigenetic modifications, including DNA methylation and histone modification (Fang et al., 2019). It is the presence of this epigenetic code that enables cells with identical genetic makeup to show diverse gene expression patterns. There are three main classes of epigenetic regulation (Al Aboud et al., 2018), (Figure 5): **1) DNA methylation.** One of the best-known modifications is DNA methylation, which involves the addition of methyl groups to the DNA molecule. DNA methylation can silence genes by blocking the binding of transcription factors or by recruiting proteins that modify chromatin structure (Smith & Meissner, 2013). **2) Histone modifications.** This modification, which involves the addition or removal of chemical groups from histone proteins that package DNA, can also affect gene expression by altering the accessibility of DNA to the transcriptional machinery (Kouzarides, 2007; Strahl & Allis, 2000). **3) Non-coding RNA actions.** Other epigenetic mechanisms that have been studied include non-coding RNA molecules that regulate gene expression by interacting with DNA or other RNA molecules, and chromatin remodeling complexes that can physically reposition nucleosomes to activate or silence genes (Mattick & Makunin, 2006; Statello et al., 2021).

While these modifications can function independently, they often work synergistically, particularly in the case of methylation and histone modifications by acetylation (Cedar & Bergman, 2009).

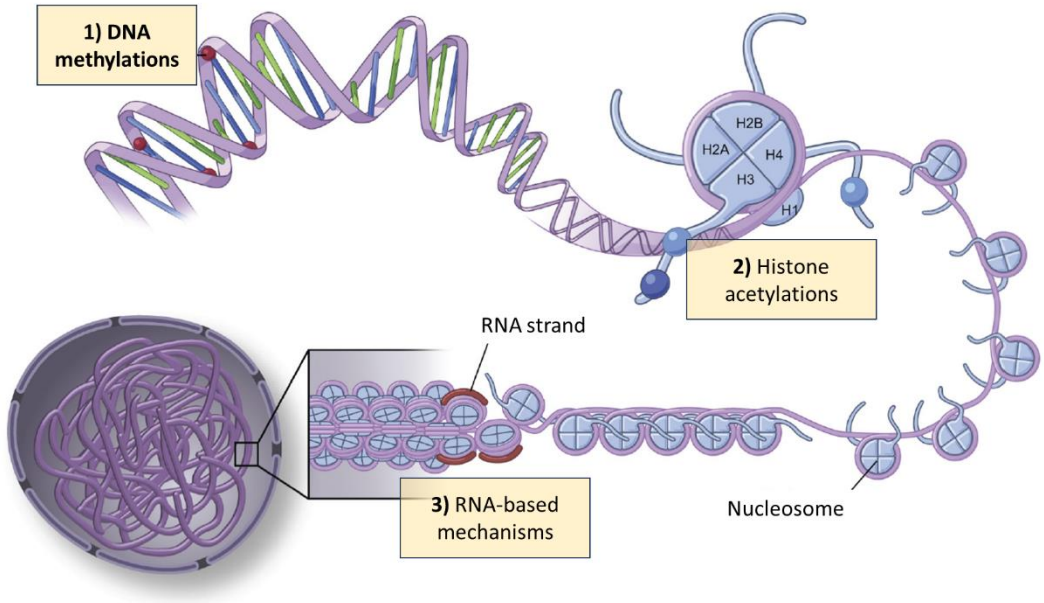

Fig. 5 | The relationship between DNA and epigenetic mechanisms—1) DNA methylation, 2) histone modifications like acetylation, and 3) RNA-based mechanisms—plays a crucial role in encoding the blueprint for the body's structural and functional proteins. Figure modified from Yan et al. (2010), doi:10.1152/japplphysiol.00131.2010. © 2010, the American Physiological Society, permission conveyed through Copyright Clearance Center license number 501915297.

In an early landmark study by Allfrey et al. (1964), they discovered histone acetylation, showing that adding acetyl groups to histones enhances transcriptional activity, a key mechanism in gene regulation. This understanding enabled further research using twin studies to examine how genetic and environmental factors influence traits and diseases. One such study, by Fraga et al. (2005), investigated monozygotic twins and found that although their epigenetic profiles were nearly identical during infancy, notable differences in DNA methylation and histone acetylation patterns emerged as they aged. These differences, which correlated with changes in gene expression, were attributed to variances in environmental exposures and lifestyle choices over time, illustrating the interplay between genetics and environment.

The role of histone modifications in gene regulation

The concept of histone modifications extends beyond acetylation to include a diverse array of chemical alterations, such as methylation, phosphorylation, ubiquitination, and more (Bannister & Kouzarides, 2011). Together, these modifications form the 'histone code,' a complex and dynamic system that serves as a regulatory platform for gene expression. Specifically focusing on acetylation, this process is mediated by two groups of enzymes: histone acetyltransferases (HATs), which add acetyl groups to protein lysine residues in the N-terminal extensions of core histones, and histone deacetylases (HDACs), which remove these acetyl groups. Collectively, this affects gene expression through its influence on chromatin conformation. The condensed nucleosome structure is primarily formed through ionic interactions between positively charged histones and the negatively charged DNA backbone. This conformation limits the access of the transcriptional machinery but can be relaxed when acetylation neutralizes the positive charge of lysine residues on the histone surface. This modification enhances RNA polymerase II accessibility, leading to increased gene expression, and vice versa, HDAC action restores a positive charge on lysine side chains of histones, resulting in a compact chromatin structure making access by RNA polymerase challenging, ultimately reducing gene repression (Gallinari et al., 2007) (Figure 6).

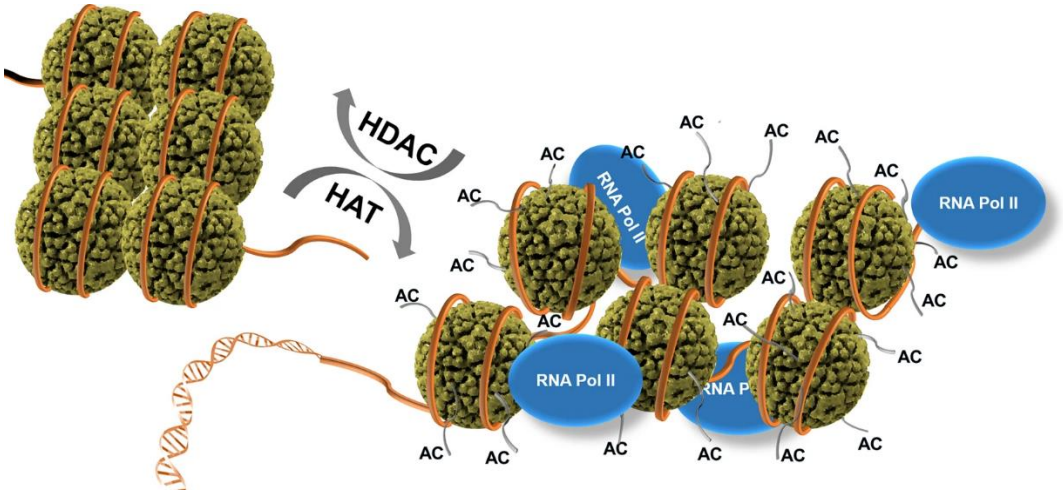

Fig. 6 | Histone acetylation (AC) by HAT opens the chromatin structure, facilitating RNA polymerase II (RNA Pol II) binding. Conversely, histone deacetylation by HDAC results in a closed chromatin conformation. Histones are shown as dark green spheres with DNA wound around them in orange, and histone lysine residues are depicted as short gray tails on the spheres. Figure reprinted from Park and Kim (2020), doi:10.1038/s12276-020-0382-4. © 2020, The Authors, distributed under a Creative Commons Attribution 4.0 International License.

Accordingly, the upregulation of DNA transcription can be accomplished through the stimulation of HAT or the inhibition of HDAC activities, while the downregulation of transcription can be achieved through the opposite actions. Consequently, an imbalance in the activities of HAT and HDAC can cause abnormal expression of a particular gene, resulting in chromatin structure instability and the onset of epigenetic diseases (Egger et al., 2004). Therefore, targeting HDACs with selective HDAC inhibitors has been pursued for the development of treatments for several cancer forms (West & Johnstone, 2014) as well as neurological disorders (Chuang et al., 2009) including AD (Kazantsev & Thompson, 2008). To date, 18 mammalian HDACs have been identified and grouped into the below different HDAC classes I-IV (Haberland et al., 2009):

I. This class includes HDAC1, HDAC2, HDAC3, and HDAC8. They are primarily localized in the nucleus and are associated with transcriptional regulation. HDAC3 can also be found in the cytoplasm. These HDACs, except for muscle specific HDAC8, are widely expressed in the brain including areas associated with memory formation.

II. This class is further divided into two subclasses (all of which can be found expressed in the brain):
    a) Class IIa: HDAC4, HDAC5, HDAC7, and HDAC9. These HDACs shuttle between the nucleus and the cytoplasm, and their activity is often associated with signal-dependent processes.
    b) Class IIb: HDAC6 and HDAC10. These HDACs are primarily found in the cytoplasm and are involved in the deacetylation of non-histone proteins.

III. Also called sirtuins, this class includes SIRT1-7. Unlike Class I and II HDACs, Class III HDACs require NAD^+ as a cofactor for their enzymatic activity. Sirtuins are involved in various cellular processes, including metabolism, DNA repair, and aging.

IV. This class includes only HDAC11, which shares a catalytic domain with class I and class II HDACs. HDAC11 is a new and less studied member of the HDAC family, reviewed in Liu et al. (2020).

Epigenetic involvement in Alzheimer's disease

The exact cause of AD is still unknown, but recent evidence shows that epigenetic modifications significantly influence its development (Pereira et al., 2024). Here are key insights from three areas impacting histone modifications:

1. Several studies have identified specific environmental exposures capable of inducing alterations in the epigenetic code relevant for AD. While most of these investigations have centered on DNA methylation, there is increasing evidence suggesting impacts on histone modifications as well. The environmental factors that have the biggest impact on the epigenome are heavy metals and metalloids (such as lead, arsenic, cadmium, and mercury), air pollution, persistent organic pollutants, and certain lifestyle factors including tobacco smoke, alcohol consumption, and certain drug therapies. Also, findings from cellular and animal models suggest that many of these environmental agents can change levels of AD-related biomarkers and pathway activity via epigenetic mechanisms (Migliore & Coppede, 2022) (Figure 7).

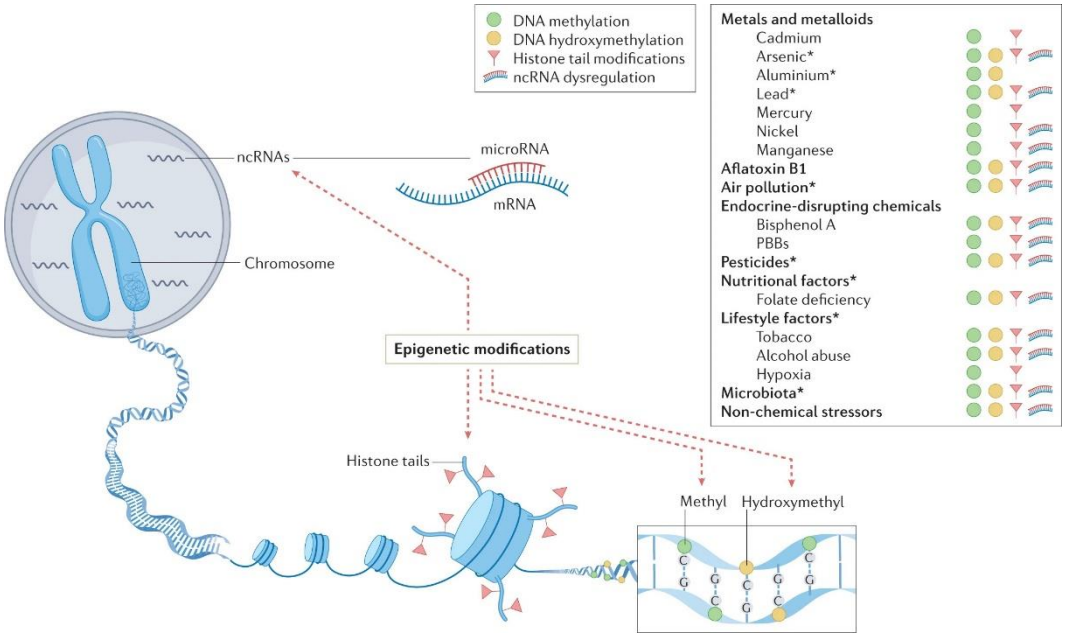

Fig. 7 | Schematic overview of environmental factors and their proposed epigenetic modifications. *= environmental factors deemed especially relevant to AD. ncRNA; non-coding RNA, and PBBs; polybrominated biphenyls. Figure reprinted from Migliore and Coppede (2022), doi:10.1038/s41582-022-00714-w. © 2022, Springer Nature Ltd., permission conveyed through Copyright Clearance Center license number 5813600621861.

2. Class I HDACs, particularly HDAC2 and HDAC3, are found in high levels in brain regions associated with memory and have a major impact on cognitive functions. Studies in mouse models of AD have demonstrated the essential role of HDACs in AD pathology. As an example, deletion of HDAC1 and HDAC2 genes in microglial cells resulted in decreased Aβ load and improved cognitive impairment by enhancing microglial Aβ phagocytosis (Datta et al., 2018). Conversely, elevated HDAC2 levels were found to suppress the expression of neuroplasticity genes crucial for learning and memory in AD mouse models (Graff et al., 2012). Moreover, HDAC2 overexpression in neurons led to reduced dendritic spine density, synapse number, synaptic plasticity, and impaired memory formation in a study by Guan et al. (2009). These effects were found to be a result of the association of HDAC2 with the promoter regions of memory-related genes, such as brain-derived neurotrophic factor and early growth response protein 1. Finally, HDAC3 is also modulating long-term memory formation, as evidenced by enhanced memory upon its deletion in the dorsal hippocampus, also in a mouse model (McQuown et al., 2011).

3. One hallmark of AD is the accumulation of extracellular Aβ plaques in the brain and the subsequent loss of dendritic spines and synapses. Recent research indicates that HDACs may influence the production and clearance of Aβ peptides (Atluri et al., 2019) and dysregulation of HDAC activity has been linked to increased Aβ production, contributing to the formation of neurotoxic aggregates and the initiation of neurodegenerative inflammatory processes (Karisetty et al., 2020). A study by Panikker et al. (2018) demonstrated that decreased levels of the HAT Tip60 (KAT5) lead to repression of key neuroplasticity genes and disruptions in Tip60-mediated epigenetic regulation, caused by amyloid precursor protein or Aβ pathology, lead to the repression of genes essential for synaptic function.

These findings emphasize the significance of the epigenetic dimension to AD. However, there are significant gaps in our understanding regarding the precise impact. As an example, it remains unclear whether these changes are consequences of pathophysiological processes like exposure to Aβ or neuroinflammation, or if they play a primary role upstream in disease progression. Currently, evidence leans towards the latter as studies have shown that epigenetic changes appear before the onset of clinical symptoms in patients with AD (Nikolac Perkovic et al., 2021). This suggests that these epigenetic modifications are not merely consequences of pathophysiological processes but may actively contribute to disease progression.

Methods for investigating HDACs

Various analytical methods are used to study HDACs, each having its own set of strengths and limitations:

- Enzymatic assays are used to assess HDAC activity in vitro using synthetic substrates that fluoresce or emit luminescence upon deacetylation, providing quantitative data. They are valuable for screening and comparing the inhibitory effects of compounds on HDAC activity (Marks & Breslow, 2007).

- Western blotting is a widely used to assess the expression levels of specific HDAC isoforms with high specificity aiding in the understanding of their roles in cellular processes and changes in disease (Xu et al., 2007).

- Chromatin immunoprecipitation followed by sequencing (ChIP-Seq) and RNA sequencing (RNA-Seq) offer insights into HDAC genomic and transcriptomic regulation. ChIP-Seq identifies HDAC binding sites on chromatin, while RNA-Seq quantifies gene expression levels, revealing HDAC impact on the transcriptome. These methods are valuable for understanding HDACs' broader functional consequences in cellular processes.(Wilson et al., 2008).

- More indirect methods such as epigenome-wide association studies can provide insights into HDAC activity by identifying changes in DNA methylation patterns associated with disease states. While this method primarily focuses on DNA methylation, it can highlight regions of altered chromatin structure and histone modifications, indirectly reflecting HDAC regulation. Integration with other omics data, such as transcriptomics and proteomics, can further clarify HDAC-related mechanisms (Rakyan et al., 2011).

While these methods are crucial for studying HDACs, they have limitations. Primarily operating in vitro, these methods may not fully capture the in vivo microenvironment's influence on HDAC activity, and using cultured cells or tissue lysates may not accurately reflect HDAC behavior in living organisms, and some rely on post-mortem tissue samples, limiting the capture of dynamic HDAC activity in disease progression. In contrast, PET imaging offers a promising complement by providing real-time, non-invasive visualization of HDAC activity within living organisms, overcoming many limitations of in vitro approaches.

Fundamentals of PET imaging

PET is an imaging technique that has revolutionized our understanding of the human brain. It is a non-invasive method that allows us to visualize and quantify molecular processes in the living brain, such as metabolism, neurotransmitter release, and receptor binding. The history of PET imaging began in the early 1950s, when Benedict Cassen began using radioactive isotopes and a detector to produce nuclear images of various organs (Rich, 1997). In the 1970s, the first PET scanner was developed by Michel Ter-Pogossian and Mike Phelps. This early scanner used only a few detectors and had limited resolution, but nevertheless provided proof-of-concept for the use of PET in medical imaging (Phelps, Hoffman, Huang, et al., 1975; Phelps, Hoffman, Mullani, et al., 1975; Ter-Pogossian et al., 1975). The principle of PET imaging is the detection of positron-emitting isotopes such as carbon-11, nitrogen-13, oxygen-15, fluorine-18—all pure positron emitters—and bromine-76 (Table 2). These isotopes are introduced into the body through intravenous (IV) injection of a tracer molecule, referred to as a radioligand when targeting a receptor, and are carried to the target organ via the bloodstream. The radioligand is administered in low mass amounts to image the function of targets without altering them pharmacologically. As the isotopes decay, they emit positrons that travel a short distance before colliding with electrons in the surrounding tissue (Bailey et al., 2005).

Table 2 | Physical properties of commonly used positron-emitting radionuclides used in PET imaging. Modified from Conti and Eriksson (2016), doi:10.1186/s40658-016-0144-5.

Radionuclide	Half-life (minutes)	Max β+ energy (MeV)	Max β+ range in tissue (mm)	Mean β+ range in tissue (mm)
Carbon-11 (^{11}C)	20.4	0.96	4.2	1.2
Nitrogen-13 (^{13}N)	9.96	1.2	5.5	1.8
Oxygen-15 (^{15}O)	2.1	1.73	8.4	3.0
Fluorine-18 (^{18}F)	109.8	0.64	2.4	0.6
Bromine-76 (^{76}Br)	16.2	3.38	17.4	7.1

The interaction between the positron and the electron, called annihilation, produces two gamma rays of 511 kilo electronvolts (keV) each that are emitted in opposite directions. These gamma rays are captured by a ring of detectors surrounding the subject. When the rays reach a scintillator in the scanner, they create a burst of light, which is then picked up by photomultiplier tubes. It is the phenomenon where they are emitted in nearly perfect opposite 180-degree directions that allow for the localization of the positron and its target. The line of response (LOR) in PET imaging is the line connecting the detectors, representing the path along which radioactive decay is assumed to have occurred. Using the relative delay in activating the detectors, the position can be calculated (Zanzonico, 2004), (Figure 8).

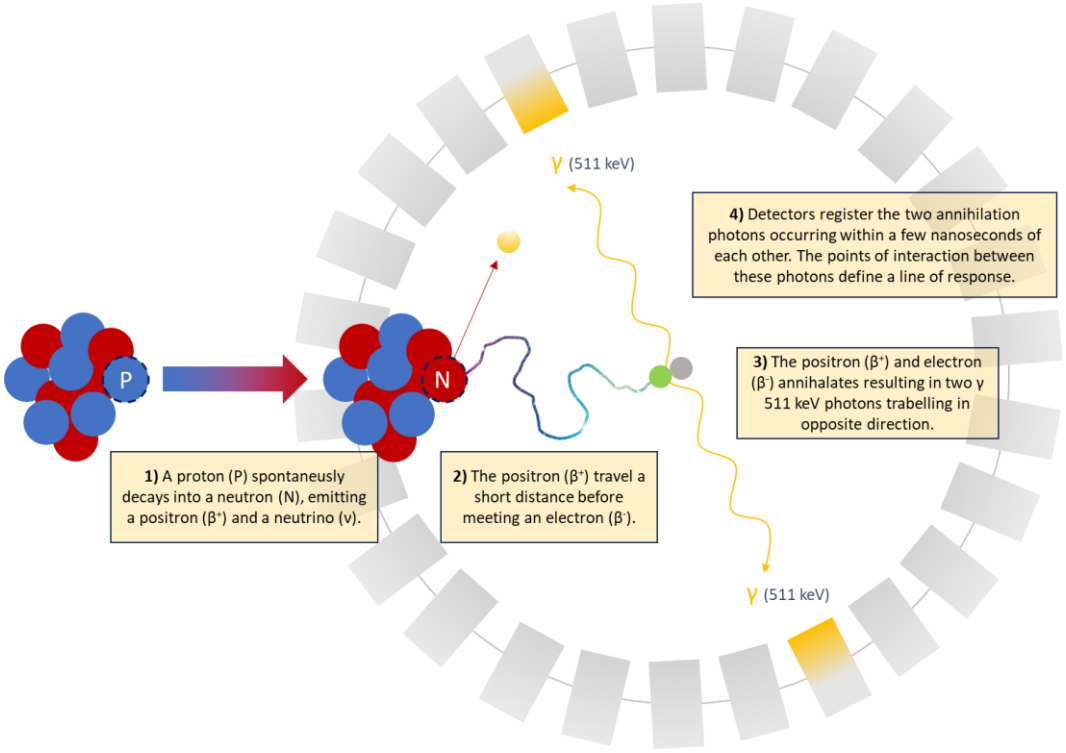

Fig. 8 | Schematics of principles in a PET scan: 1) A proton (blue ball) undergoes radioactive decay into a neutron (red ball), resulting in the emission of a positron (green ball) and an electron neutrino (yellow ball). 2) After undergoing random scattering and losing kinetic energy over a short distance, the positron encounters its antiparticle, the electron (gray ball). 3) The subsequent annihilation of both particles produces two 511 keV annihilation photons traveling in opposite directions. 4) During a PET scan, the subject is positioned within the scanner, surrounded by a ring of detectors. The detectors register the detection of two annihilation photons occurring within a few nanoseconds of each other. The points of interaction between these photons define a LOR. Figure redrawn with permission conveyed through Copyright Clearance Center license number 1497505 from Vaquero and Kinahan (2015), doi:10.1146/annurev-bioeng-071114-040723.

During a scan, multiple LORs are generated, and the data are reconstructed using computer algorithms to produce a time-dependent three-dimensional and quantitative distribution of the radioactive tracer in the tissue after correcting for absorption, scatter, and random coincidence (Vaquero & Kinahan, 2015).

Despite the many advantages of the technique, there are also limitations. One of the main limitations is the cost and availability of PET scanners and radiotracers, which can be expensive and difficult to obtain, as well as logistical challenges around the setup (Keppler & Conti, 2001). The second limitation is the low spatial resolution of PET imaging. The image resolution ranges from 4–5 mm for most clinical whole-body PET scanners to ~2.5 mm for the brain-specific high-resolution research tomograph (HRRT) (de Jong et al., 2007). The determination of this is influenced by the variability in estimating the interaction point of the photon within the scintillator. This, in turn, is impacted by the optics of the scintillator, the quantity of emitted photons, and the accuracy of the photomultiplier tubes. These factors contribute to the noise and resolution characteristics of the PET image (Vaquero & Kinahan, 2015). Due to the relatively low spatial resolution of PET images, the technique is often combined with high resolution methods such as magnetic resonance imaging (MRI) (Ehman et al., 2017), or X-ray computed tomography to merge anatomical and biological information (Pichler et al., 2008). Encouragingly, new ultra-high performance human brain PET imaging systems are being developed with ~1 mm resolution (Carson et al., 2023), close to the theoretical limit of 0.67 mm resolution (Moses, 2011).

PET imaging applications in drug development

Over the last several decades, scientific progress has led to the development of tools enhancing drug discovery. Despite this progress and increased funding, the industry struggles with low productivity, long timelines, and exorbitant costs for delivering new medicines (DiMasi et al., 2016). The picture is even more discouraging when looking at new treatments targeting the CNS (Gribkoff & Kaczmarek, 2017). Here, the rate of unsuccessful outcomes is notably higher and average development times substantially longer (Kesselheim et al., 2015; Pangalos et al., 2007). Considerable efforts have been made to analyze failures in clinical development to pinpoint significant risks (Cook et al., 2014; Morgan et al., 2012; Owens et al., 2015). From their analysis, Morgan et al. (2012) introduce a framework outlining three critical drug attributes named the ‘three pillars of survival’ that should reduce the risk of program failure when characterized: **1)** tissue accessibility, **2)** target engagement,

and **3)** demonstration of downstream pharmacology. Specifically for drugs targeting the CNS, tissue exposure and target engagement are essential in early drug development programs, where PET serves as a highly valuable imaging tool to interrogate these parameters as described in the following three sections (Ghosh et al., 2022; Gunn & Rabiner, 2017).

Measuring tissue accessibility through PET imaging

PET enables the assessment of drug access by providing real-time imaging of the spatial distribution, concentration, and kinetics of radiolabeled compounds within the brain (Bergstrom et al., 2003). This is important in 'privileged' tissue such as the CNS, where assessing a compound's ability to cross the BBB is crucial and often represents a major roadblock and a key factor limiting success (Abbott, 2013). The distribution within the brain of a drug candidate can be assessed by radiolabeling the compound with a positron emitting isotope as described in the previous section. This type of approach is referred to as microdosing, or the Phase 0 stage (Burt et al., 2020), because it consists of the administration of a negligible amount of the compound in a radiolabeled form, typically less than 10 μg, or less than 5% receptor occupancy without any pharmacological effect. However, this approach has some inherent challenges, as it requires the isotope to be incorporated into the molecule late in its synthesis. For ^{18}F, this is further challenging because fluorine is not a part of many drug molecules—although an increasing number of compounds are being fluorinated (Clayden, 2019; Shah & Westwell, 2007). If these hurdles can be overcome, the radiolabeled drug candidate can be used in animal and humans for both PK and distribution studies. This approach is typically used in pre-clinical development in experimental animals, such as rats and non-human primates, when a PET radioligand for the target receptor or protein is not available for direct assessment of target occupancy. Under the assumption that the in vitro and in vivo K_i are the same, the microdosing approach can also be used to estimate the occupancy of the drug to the target. A modification to the microdosing studies is where a pharmacological dose of 'cold' (i.e., non-radiolabeled) compound is administered together with the radiolabeled compound. In this way it can be investigated if the uptake of the radiolabeled compound is influenced by the cold dose e.g., by increased activity of transporters located on the BBB. This approach is also done to make sure that only the non-displaceable (ND) signal of the radiolabeled compound is used for measuring the ratio of brain to plasma.

PET imaging for evaluating target engagement

PET imaging can facilitate the evaluation of target engagement by visualizing in vivo interactions between a drug and its molecular target, such as in competition binding studies. This strategy provides important information for determining dosage in clinical trials (Takano et al., 2016). Once brain accessibility is confirmed, the next step is to assess the compound's interaction with its target, known as target or receptor occupancy. This is crucial for understanding the link between target engagement and downstream pharmacological effects in vivo. PET occupancy studies become feasible when a radioligand is available for imaging the target of interest, and while well-established tracers exist for several targets in the CNS as reviewed in George et al. (2015); McCluskey et al. (2020), the discovery of radioligands often constitutes an initial phase in drug development programs. This approach offers an advantage over radiolabeling the drug compound itself, as it eliminates the need to radiolabel each drug individually and consequently, multiple drug candidates can be tested using the same radioligand for a given target. As examples of our contributions to this approach, please refer to Papers A (Hansen et al., 2015), and B (Hansen et al., 2019).

Occupancy (O%) is calculated by measuring the decrease in radioligand uptake from a baseline to a challenge scan. This decrease reflects how much of the receptor or target sites the drug occupies. This process involves two PET scans: a baseline scan to measure selective radioligand uptake, followed by a second scan after administering the investigated drug. Of note, efforts are made, also within our group, to make kinetic models for estimating occupancy from single-scan PET displacement studies (Laurell et al., 2023). Commonly, occupancy is calculated based on the reduction in radioligand uptake observed in the second scan compared to the baseline. This calculation incorporates the measure of binding potential (*BP*), (Equation 1) (Passchier et al., 2002):

$$O(\%) = \frac{BP_{baseline} - BP_{drug}}{BP_{baseline}} x100 \quad (1)$$

BP is a ratio consisting of the maximum density of a receptor (B_{max}) and the affinity of a ligand to its receptor (K_D, dissociation constant), (Mintun et al., 1984). In PET imaging, *BP* is calculated as the ratio of specifically bound ligand concentration (C_S) to free ligand concentration (C_F) under the assumption of equilibrium and when C_F is low relative to K_D (Innis et al., 2007) (Equation 2):

$$BP = \frac{B_{max}}{K_D} = \frac{C_S}{C_F}$$

(2)

Distinguishing C_S and C_F within the same region is challenging. However, it is assumed that at equilibrium, C_F equals C_P times the fraction of free radioligand in plasma (f_P), assuming passive diffusion of the radioligand (Equation 3):

$$BP = \frac{B_{max}}{K_D} = \frac{C_S}{C_F} = \frac{C_S}{C_P f_P}$$

(3)

Direct measurement of C_P involves collecting radioligand from arterial blood samples during the scan and correcting for its metabolism. This is considered the gold-standard, but the invasiveness of the procedure is a limitation, and new methods and approaches are being considered (Volpi et al., 2023). C_S is determined as the radioactivity within the brain, expressed as the total radioactivity concentration in brain tissue (C_T) at time t and measured within a specific region of interest (ROI) between the intervals of t_1 and t_2, typically in units of microcurie per cubic centimeter (μCi/cm³). In any brain region, C_T is the sum of C_F, non-specifically bound (C_{NS}), and C_S compartments (Equation 4):

$$C_T = C_F + C_{NS} + C_S$$

(4)

When equilibrium is achieved between the free and non-specifically bound compartments, the equation can be simplified (Equation 5):

$$C_T = C_{F+NS} + C_S$$

(5)

In this context, a test drug selectively displaces only the C_S compartment, leaving the combined compartment C_{F+NS} unaffected and constant throughout the brain as the ND fraction (C_{ND}). Regions without the target receptor can serve as a reference, with their concentration representing the ND fraction. The radioligand freely exchanges between compartments until equilibrium is reached and the rates of movement and binding are linearly related (Equation 6) (Watabe et al., 2006):

$$\frac{dC_{F+NS}(t)}{dt} = K_1 C_P(t) - (k_2 + k_3) C_{F+NS}(t) + k_4 C_S(t),$$

$$\frac{dC_S(t)}{dt} = k_3 C_{F+NS}(t) - k_4 C_S(t)$$

(6)

Here, K_1 is the transportation rate (perfusion), and k_2, k_3, and k_4 are rate constants of the radiotracer between the different compartments at time t in min^{-1} in a two-tissue compartment model (2TCM) (Figure 9).

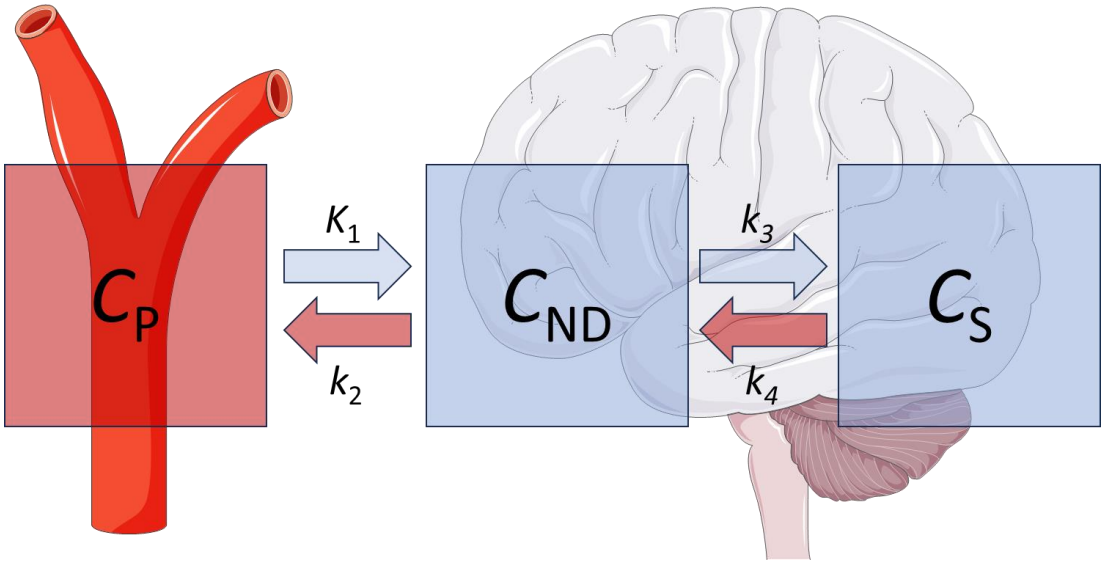

Fig. 9 | Illustration of the 2TCM. The model consists of three compartments but two different tissues, hence the name. First compartment is for the input function, the concentration of radiotracer in plasma, C_P. The following two compartments are for the two distinct kinetic compartments in the brain tissue, representing the free and non-specifically bound i.e., the ND compartment, C_{ND}, and specific bound radiotracer concentrations, C_S. Compartments are connected by four rate constants, K_1, k_2, k_3, and k_4. Figure redrawn with permission as per Sage Publications guidelines from Innis et al. (2007), doi:10.1038/sj.jcbfm.9600493.

From these equations, BP_F can be calculated as a combination of kinetic parameters and measurements of f_P, (Equation 7), (Ichise et al., 2001; Mintun et al., 1984; Watabe et al., 2006):

$$BP_F = \frac{K_1 k_3}{k_2 k_4 f_P} \quad (7)$$

Or as BP_P if not corrected for f_P, (Equation 8):

$$BP_P = \frac{K_1 k_3}{k_2 k_4} \quad (8)$$

Or simply as BP_{ND} in case there is a reference region in the brain (Equation 9):

$$BP_{ND} = \frac{k_3}{k_4} \quad (9)$$

Using the metabolite-corrected plasma time-activity curve (TAC) as an input function, the kinetic parameters (K_1, k_2, k_3, and k_4) of receptor-rich areas can be derived through nonlinear regression. In cases without a true reference region for BP_{ND} estimation, the revised Lassen plot is used to derive an occupancy measure, where apparent tissue volume (V_T, in units of mL/cm^3) is the outcome (Cunningham et al., 2010; Lassen et al., 1995). The difference between estimates of V_T post-drug and V_T at baseline across multiple regions is plotted against V_T baseline using linear regression, with the slope providing an estimate of occupancy and the intercept on the x-axis yielding an estimate of V_{ND}.

Utilizing PET imaging in downstream pharmacology

To assess the last of the three 'pillars of survival', PET allows for the observation of downstream pharmacology, offering insights into how drugs affect physiological processes and molecular pathways over time i.e., the pharmacodynamic (PD) properties. The essence of using PET imaging to interrogate downstream pharmacology lies in understanding how a drug's initial interaction with a molecular target leads to broader physiological effects and alters radioligand binding. One area where PET imaging has made significant contributions is in the field of psychotropic medication research. As an example, studies using PET radioligands targeting the dopamine system have provided key insights into the downstream

effects of antipsychotic medications and various radioligands can be used to investigate dopamine synthesis capacity, baseline D2 and D3 subtype receptor *BP*, and dopamine release in response to pharmacological intervention (Kilbourn, 2021; Laruelle, 2000). Beyond neurotransmitter systems, PET imaging is used in the study of downstream events at the molecular level including the exploration of signal transduction pathways (Holland et al., 2013), gene expression patterns (Blasberg, 2002; Yu et al., 2000), and alterations in protein function (Phelps, 2000). Also, PET imaging played a crucial role in the development of aducanumab, a monoclonal antibody for AD, which received FDA approval in 2021 (Dhillon, 2021). This has been the first new drug to be approved for the treatment of AD since 2003 and the first drug to ever be approved for modification of the course of AD. In this instance, the radioligand ^{18}F-florbetapir, designed to bind Aβ plaques, was developed alongside the monoclonal antibodies targeting Aβ (van Waarde et al., 2021). The radioligand showed dose- and time-dependent decreases in the Aβ PET binding (Chiao et al., 2019; Sabri et al., 2015) thereby confirming that aducanumab reduce cerebral Aβ deposits (Sevigny et al., 2016). While this might seem like the poster story for PET in assessing downstream pharmacology, it needs mentioning that the approval of aducanumab has been very controversial. First, because it was done against the recommendation of the FDAs advisory panel (Mahase, 2021), second, as there has been a lack of evidence that the therapy improves cognitive outcomes (Alexander et al., 2021; Schneider, 2022) and third, due to the controversy of deeming Aβ plaque reductions an approvable surrogate endpoint that is "*reasonably likely to predict a clinical benefit*" (Mullard, 2021) and finally, since the diagnostic value of Aβ PET imaging has been challenged and it has been argued that there are significant limitations as a marker of efficacy (Hoilund-Carlsen & Alavi, 2021; Hoilund-Carlsen et al., 2022; Kepp et al., 2023). This example shows the role of PET imaging as an essential tool for PD interrogation, but also emphasizes the need for a multimodal approach: incorporating other read-outs, biomarkers and endpoints alongside PET imaging can enhance the robustness and reliability of neuroimaging data in drug development (Liu & Howard, 2021).

PET imaging of the α7 nicotinic acetylcholine receptor

PET radioligands targeting α7 nAChRs have been developed and used to investigate the distribution, density, and occupancy of these receptors in vivo, and offers a valuable approach for investigating the development and progression of CNS diseases associated with α7 nAChR (Zhang et al., 2023), (Table 3). However,

the development has been challenging due to the low density of the receptor in the brain (Marutle et al., 2001), and therefore, a suitable radioligand must have high specificity, low nano- or picomolar binding affinity, good brain penetration, and appropriate PK properties for PET imaging (Halldin et al., 2001). The following section looks at current radioligands targeting α7 nAChRs, highlighting their strengths and limitations.

^{11}C-GTS-21 was the first PET radioligand tested in vivo, acting as a partial agonist for α7 nAChR (Figure 10). It was radiolabeled in two different positions as well as radiolabeling of two metabolites for PK PET studies in baboons and mice but showed only modest specificity (Kim et al., 2007).

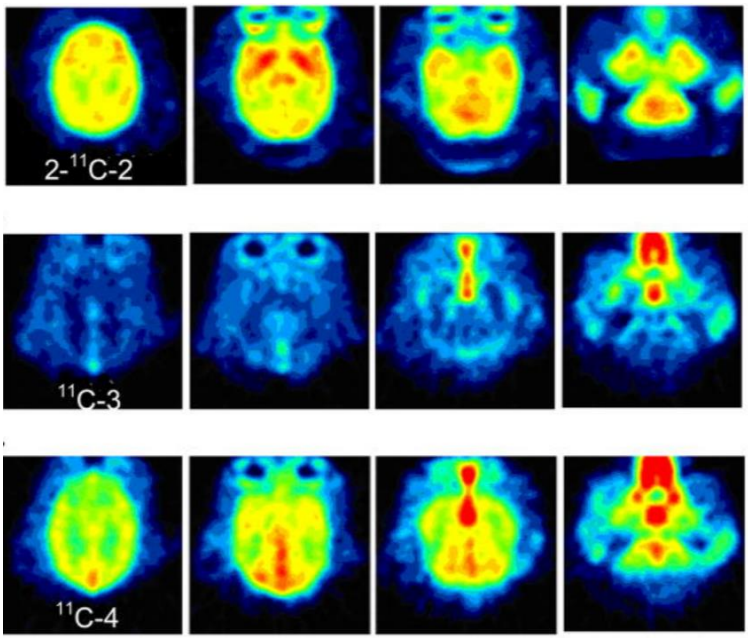

Fig. 10 | The first α7 nAChR PET in vivo images in baboon with three ^{11}C labeled versions of GTS-21. Figure reprinted from Kim et al. (2007), doi:10.1016/j.nucmedbio.2007.04.005. © 2007, Elsevier Inc., permission conveyed through Copyright Clearance Center license number 5813610561679.

SSR180711, was shown to have good binding affinity for rat and human α7 nAChRs and was radiolabeled with ^{76}Br and ^{11}C to yield ^{76}Br-SSR180711 and ^{11}C-SSR180711, respectively. Further, a ^{76}Br-SSR180711 analogue, where ^{76}Br was replaced with $^{11}CH_3$ was also developed (^{11}C-CHIBA-1001) (Hashimoto et al., 2008). ^{76}Br-SSR180711 and ^{11}C-CHIBA-1001 were tested in rhesus monkeys, showing a heterogeneous distribution pattern and good region-specific brain uptake and specificity was demonstrated with competition binding studies. These results

led to ^{11}C-CHIBA-1001 being the first α7 nAChRs specific radioligand to be tested in humans in vivo (Toyohara et al., 2009) (Figure 11).

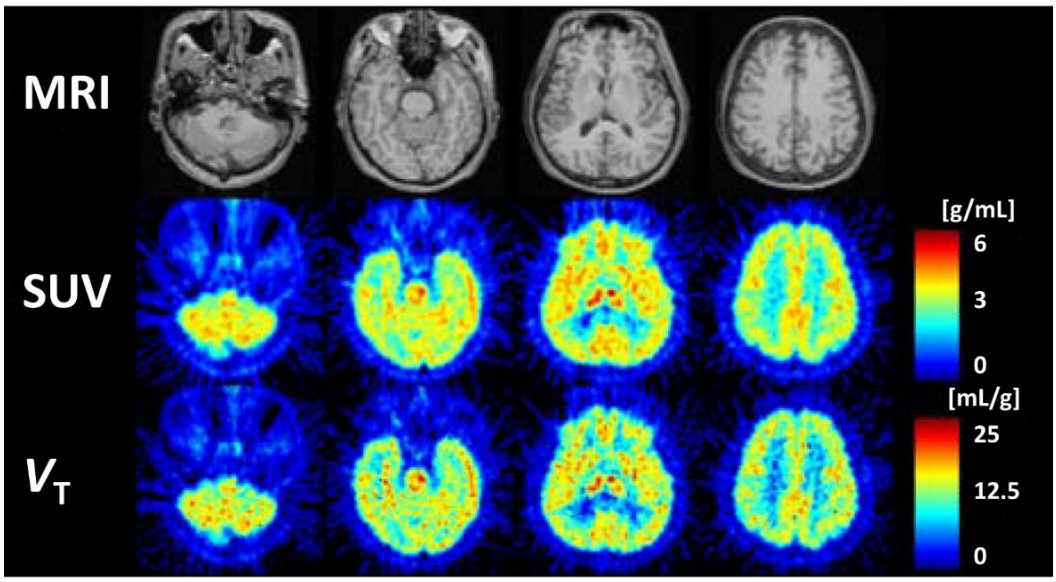

Fig. 11 | The first α7 nAChR PET in vivo images in humans with ^{11}C-CHIBA-1001. Top panel: MRI of the corresponding slices. Middle panel: static images from 0 to 90 min post ^{11}C-CHIBA-1001 injection, shown as SUV. Lower panel: total distribution volume of ^{11}C-CHIBA-1001 via Logan graphical analysis (30 to 90 min data). Figure modified from Toyohara et al. (2009), doi:10.1007/s12149-009-0240-x. © 2009, The Japanese Society of Nuclear Medicine, permission conveyed through Copyright Clearance Center license number 5813610854886.

This study revealed a heterogeneous brain uptake with the highest uptake found in the thalamus. However, the human data showed comparable radioligand uptake in the cerebellum to that in the cerebral cortex, in contrast to the monkey data, which might be due to low receptor affinity (Ding et al., 2012). For this reason, no further development of the radioligand has been reported.

Three α7 nAChRs specific compounds, 1,4-diazabicyclo[3.2.2]nonane derivatives, were radiolabeled as potential PET radioligands: **1)** ^{18}F-NS10743 was developed with good binding affinity toward α7 nAChRs and ex vivo studies in mice indicated good BBB permeability as well as target specificity (Deuther-Conrad et al., 2009). However, later in vivo PET studies in pigs revealed modest specificity as shown by a low decrease of SB in competition binding studies (Deuther-Conrad et al., 2011). **2)** ^{11}C-NS14492 is a selective α7 nAChR partial agonist that was evaluated in our group using in vivo PET imaging in pigs (Ettrup et al., 2011). The radioligand showed good BBB penetration, with high binding in the thalamus and

cerebral cortex, moderate binding in the striatum, and low cerebellar binding, in accordance with known distribution of α7 nAChR in the human brain. Selectivity was demonstrated by dose-dependent signal blocking, with pre-dosing of cold NS14492 and SSR180711. Taken together, these results demonstrate that ^{11}C-NS14492 is a promising radioligand for α7 nAChRs brain imaging and used as part of the work in this thesis. **3)** ^{18}F-NS14490 was developed as a radioligand with high binding affinity and selectivity, but PET studies in mice and pigs revealed limited brain uptake (Rotering et al., 2013). Recently, Reid et al. (2023) used tritiated ^{3}H-NS14490 as an imaging marker to study cardiac repair after myocardial infarction, supporting α7 nAChR's involvement in key repair processes.

^{18}F-ASEM and its isomer ^{18}F-DBT10T are two potent α7 nAChR antagonists with very high binding affinity and good selectivity (Horti, 2015). Biodistribution studies in mice revealed a higher uptake in the brain of ^{18}F-ASEM compared to ^{18}F-DBT10 and given their structural similarity, further investigations of ^{18}F-ASEM were pursued. These studies revealed heterogeneous binding: high in the hippocampus and frontal cerebral cortex, intermediate in the striatum, and low in the cerebellum, consistent with known α7 nAChR distribution in the mouse brain. Similar results, including in vivo dose-dependent blocking in competition binding studies, were obtained in baboons (Horti et al., 2014) and pigs, as investigated in our group (Donat et al., 2020). These results let to the first human in vivo PET study with ^{18}F-ASEM, making it only the second radioligand to be tested in humans (Wong et al., 2014). This study showed good brain uptake and regional binding matching postmortem human and non-human primate results with high levels in parietal cortex, putamen, thalamus, temporal lobes, cingulate, frontal lobes, and hippocampus. This led to a series of human studies: **1)** Coughlin, Du, Rosenthal, et al. (2018) investigated the potential relationship between α7 nAChR distribution and ageing using ^{18}F-ASEM in 25 healthy volunteers aged 21-86 years. Here, they found that V_T's of six brain regions, including the striatum and five cortical regions, were negatively correlated with age. **2)** Coughlin, Du, Crawford, et al. (2018) used ^{18}F-ASEM to study α7 nAChR distribution in 11 participants with recent-onset psychosis compared to 15 healthy controls and found lower binding in hippocampus in the patient group. **3)** Further, ^{18}F-ASEM was used to study α7 nAChR distribution in 14 participants with mild cognitive impairment and 17 controls, revealing higher binding across all brain regions in the cognitively impaired group, suggesting increased receptor density (Coughlin et al., 2020). Finally, these recent studies are worth mentioning: **4)** Vetel et al. (2020) used ^{18}F-ASEM to study the evolution of the α7 nAChR using in vivo PET in an early-stage Parkinson's disease rat model. They found an early and transient rise in receptor expression in the

lesioned striatum and substantia nigra. **5)** Yang et al. (2021) investigated α7 nAChR expression in the vasculature in two animal models of atherosclerotic plaques and found that ^{18}F-ASEM made it feasible to locate atherosclerotic plaques and to evaluate the vulnerability of plaques toward rupture. **6)** Kim et al. (2024) showed that α7 nAChR imaging has potential as a noninvasive diagnostic method for peripheral nervous system disorders. **7)** Nag et al. (2022) used in silico modelling to produce ASEM analogues with improved radioligand properties and tested six of these lead compounds with in vitro autoradiography in post-mortem human tissue and in in vivo PET imaging in non-human primates. **8)** Finally, two recent abstracts have been presented indicating higher availability of the α7 nAChR in the brains of older, cognitively normal subjects (Woolsey et al., 2024), and low hippocampal levels of α7 nAChRs in patients with recent-onset psychosis (Wong et al., 2024).

^{11}C-(*R*)-MeQAA was developed with reasonable binding affinity and biodistribution and in vivo receptor blocking studies in mice demonstrated high initial brain uptake, and a heterogeneous distribution with high binding in the hippocampus and low binding in the cerebellum. Further, pretreatment with α7 nAChR antagonist MLA resulted in a significant blocking of signals in the hippocampus. Later, PET imaging studies in rhesus monkeys showed regional brain uptake with high levels in the thalamus, moderate levels in the cerebral cortex, and low levels in the cerebellum (Ogawa et al., 2010). ^{11}C-(*R*)-MeQAA was assessed in twenty human patients with AD and ten healthy age-matched controls in combination with Aβ deposition evaluation with ^{11}C-Pittsburg compound B (Nakaizumi et al., 2018). This study showed significantly lower ^{11}C-(*R*)-MeQAA binding in the temporal and prefrontal cholinergic projection regions in patients with AD, and the binding levels of ^{11}C-(*R*)-MeQAA showed significant correlation with memory function scores in patients with AD. Finally, from a pilot study in patients with schizophrenia, significantly lower levels of ^{11}C-(*R*)-MeQAA BP_{ND} were found in the middle frontal cortex. There was also a trend toward decreased BP_{ND} levels in the temporal and parietal cortex. No difference was observed in the superior frontal cortex (Wakuda et al., 2018). Despite the promising results, no further development of the radioligand has been reported.

Table 3 | List of radioligands targeting the α7 nAChR. Type: (A) = Agonist, (PA) = Partial agonist, (AN) = Antagonist. n.s. = not specified.

Name (type)	Affinity	Animals tested in	Study highlights	Reference
^{11}C-2 (A)	n.s.	Rats	Reasonable uptake in several brain regions	Dolle et al., 2001
^{11}C-3 (n.s.)	K_d = 0.54 nM	Mice	High binding affinity, no in vivo studies conducted	Pomper et al., 2005
^{11}C-4 (n.s.)	K_d = 5.8 nM	Mice	High binding affinity, no in vivo studies conducted	Pomper et al., 2005
^{18}F-6 (A)	K_i = 1.3 nM	Baboons	Poor signal in the baboon brain	Kim et al., 2008
^{18}F-7 (A)	K_i = 18 nM	Rats	Showed low and homogeneous distribution	Pin et al., 2014
^{11}C-A-582941 (A)	K_i = 10.8 - 17 nM	Mice, monkeys	Good BBB penetration but lacked sufficient regional specificity	Toyohara et al., 2010
^{11}C-A-752274 (A)	K_d = 0.092 nM	Mice, baboons	Ultra-high binding affinity but low brain uptake	Horti et al., 2013
^{11}C-A-833834 (A)	K_d = 1.53 nM	Mice, baboons	High binding affinity but low brain uptake	Horti et al., 2013
^{11}C-A-844606 (A)	IC_{50}=11 nM (rat)	Mice, monkeys	Good BBB penetration but lacked sufficient regional specificity	Toyohara et al., 2010
^{18}F-ASEM (AN)	K_i = 0.37 nM	Mice, baboons, pigs, humans	Second human in vivo PET study. Good brain uptake and regional binding. Widely used.	Wong et al., 2014
^{18}F-AZ11637326 (A)	K_d = 0.2 nM	Mice, monkeys	Limited brain uptake	Ravert et al., 2013

^{11}C-CHIBA-1001 (PA)	K_d = 120-180 nM	Monkeys, humans	First α7 nAChR specific radioligand tested in humans with heterogeneous brain uptake	Toyohara et al., 2009
^{18}F-DBT10 (AN)	K_i = 1.32 nM	Mice	Similar uptake and binding as 18F-ASEM	Wong et al., 2014
^{11}C-GTS-21 (PA)	Low (n.s.)	Baboons, mice	First 11C-labeled PET radioligand tested in vivo	Kim et al., 2007
^{11}C-(*R*)-MeQAA (PA)	K_i = 41 nM	Mice, monkeys, humans	Good brain uptake, useful in AD and schizophrenia studies	Ogawa et al., 2010
^{18}F-NS10743 (A)	K_d = 8.99 nM	Mice, pigs	Good BBB permeability, but limited specificity	Deuther-Conrad et al., 2009
^{18}F-NS14490 (A)	K_i = 2.5 nM	Mice, pigs	Limited brain uptake	Rotering et al., 2013
^{11}C-NS14492 (PA)	K_i = 2.2 nM	Pigs	Dose-dependent signal blocking. Good BBB penetration, promising for α7 nAChR imaging	Ettrup et al., 2011
^{76}Br-SSR180711 (PA)	K_i = 14 - 22 nM	Monkeys	Good specificity in competition binding studies	Hashimoto et al., 2008
^{18}F-YLF-DW (A)	K_i = 2.98 nM	Mice	Promising brain uptake, used for atherosclerotic plaques identification	Wang et al., 2018

In the interest of conciseness, the following nine α7 nAChR radioligands deserve brief mention, although they all failed for various reasons: **1)** ^{11}C-2 showed no specific accumulation and low specific binding (SB), (Dolle et al., 2001); **2)** ^{11}C-3 and ^{11}C-4 showed low brain uptake and homogeneous distribution (Pomper et al., 2005); **3)** ^{18}F-6 showed poor binding signal (Kim et al., 2008); **4)** ^{18}F-7 showed low and homogeneous distribution and poor SB (Pin et al., 2014); **5)** ^{18}F-AZ11637326

showed limited brain uptake and low SB (Ravert et al., 2013); **6)** ^{11}C-A-582941 and **7)** ^{11}C-A-844606 both penetrated the BBB in mice and monkeys but lacked sufficient regional selectivity and specificity (Toyohara et al., 2010); **8)** ^{11}C-A-752274 and **9)** ^{11}C-A-833834, showed very high binding affinity but had low brain uptake (Horti et al., 2013).

Finally, Wang et al. (2018) developed ^{18}F-YLF-DW and initial mouse studies revealed promising brain uptake and it was subsequently used for identifying vulnerable atherosclerotic plaques in carotid arteries (Wang et al., 2021). The last example shows that the emergence of whole-body PET targeting α7 nAChRs in the periphery could complement CNS studies and identify new potential treatment targets.

The pursuit for PET radioligands targeting the α7 nAChR has been long and challenging, marked by numerous setbacks and failures in preclinical stages. Most often the failure is due to limited specificity or inability to penetrate the BBB. However, amidst these challenges, some promising radioligands such as ^{11}C-(*R*)-MeQAA and ^{18}F-ASEM have been developed and we will continue to further develop ^{11}C-NS14492 as we believe that the application of α7 nAChR-targeted PET radioligands are positioned to impact the diagnosis, treatment, and management of α7 nAChR-related disorders.

PET imaging of HDACs

Similar to its use in studying the α7 nAChR, PET imaging offers significant advantages for investigating HDACs. Its non-invasive nature allows real-time visualization and quantification of HDAC activity, providing insights into gene regulation processes in the living human brain. A key benefit of PET in studying HDACs is its ability to assess the effectiveness of novel therapeutic interventions. By visualizing HDAC occupancy and enzymatic activity over time, it becomes possible to monitor drug response, optimize dosages, and evaluate the efficacy of potential HDAC-targeted therapies (Wang, Schroeder, & Hooker, 2014). This is crucial for advancing drug development and precision medicine strategies for conditions affected by HDAC dysregulation. Additionally, PET facilitates the examination of early disease stages associated with HDAC dysfunction, providing information about the development of conditions such as AD.

The following radioligands have been developed and tested, but only one has been reported in human studies.

The first HDAC specific radioligand, ^{18}F-FAHA, was developed by Mukhopadhyay et al. (2006). Studies in rats examined the in vivo characteristics of the compound, showing brain uptake and decreased binding in a competition assay with the HDAC inhibitor SAHA (suberoylanilide hydroxamic acid, generic name vorinostat) (Yeh et al., 2013). However, studies in baboons showed rapid metabolism of the compound, with the main radiometabolite penetrating the BBB, complicating data analysis. (Reid et al., 2009). Bonomi et al. (2015) introduced ^{18}F-DFAHA and ^{18}F-TFAHA, with improved selectivity towards class IIa HDACs and PET/CT imaging in rats demonstrated high accumulation of both compounds in brain regions such as the cerebellum, nucleus accumbens, and hippocampus, where class IIa HDACs are expressed. Subsequently, ^{18}F-TFAHA has been used in various rodent models to investigate HDAC class IIa expression in intracerebral glioma (Laws et al., 2019), mild traumatic brain injury (Kamal et al., 2022), low- and high-cocaine intake (Perrine et al., 2022), and finally in a transgenic mouse model of AD (Chen et al., 2021). As of today, ^{18}F-TFAHA has not been used in humans, but studies are currently underway (personal communication, Juri Gelovani). Four other SAHA-based compounds were evaluated, but none had suitable properties for further development: ^{18}F-FESAHA (Zeglis et al., 2011), *p*-^{18}F-SAHA (Hendricks et al., 2011), and two ^{11}C-labeled analogues (Seo et al., 2013).

Wang, Schroeder, Wey, et al. (2014) developed the first adamantane-conjugated HDAC imaging radioligand, ^{11}C-Martinostat at the Athinoula A. Martinos Center for Biomedical Imaging at Massachusetts General Hospital, hence the name. The adamantane group is often used to improve a compound's BBB permeability (Wanka et al., 2013), and here it was linked to a potent HDAC inhibitor. From their initial validation, low IC_{50} values were seen for HDAC1, 2, 3, and 6 (between 0.3 and 4.1 nM), and more modest levels for HDAC4, and 5 (between 0.4 and 2.0 μM), with high values for HDAC7, 8, and 9 (between 15 and 20 μM). Specificity was confirmed using in vitro autoradiography in rat brain sections and competition binding with SAHA. In vivo PET imaging in rats and baboons showed brain accumulation of ^{11}C-Martinostat, which decreased dose-dependently with cold compound pre-treatment (Figure 12). These results suggested ^{11}C-Martinostat is a suitable radioligand for HDAC imaging, prompting further PET studies.

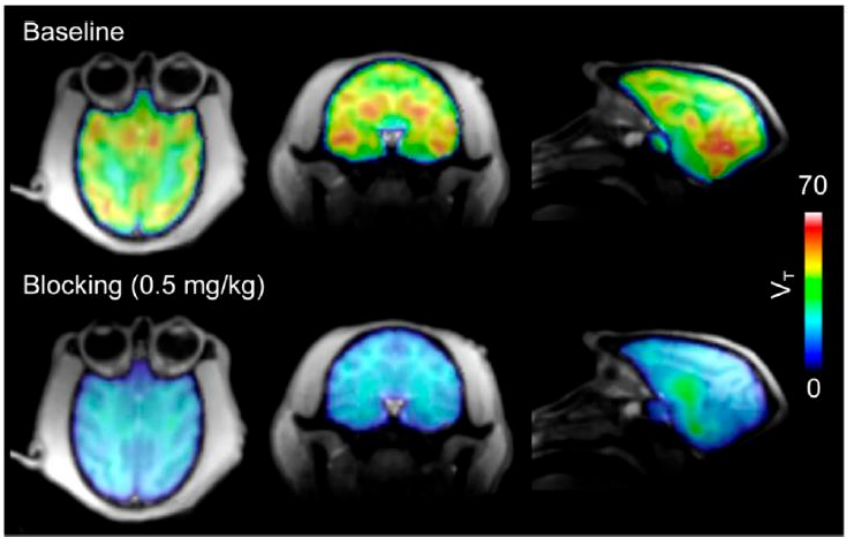

Fig. 12 | V_T images of ^{11}C-Martionstat in a baboon brain. Top panel is baseline and lower panel shows decreased signal by pre-treatment with unlabeled Martinostat. Figure reprinted from Wang, Schroeder, Wey, et al. (2014), doi:10.1021/jm500872p. © 2014, American Chemical Society, distributed under a Creative Commons Attribution 4.0 International License.

Schroeder et al. (2014) conducted PET studies in rats using a subset of HDAC inhibitors to assess the relationship between HDAC target engagement and in vivo effect. Later, the first human PET study with ^{11}C-Martinostat was performed in eight healthy volunteers (Wey et al., 2016). Here, high HDAC expression was found in cortical gray matter regions, with conserved regional distribution patterns between test subjects, while lowest expression was found in the hippocampus and amygdala. (Figure 13).

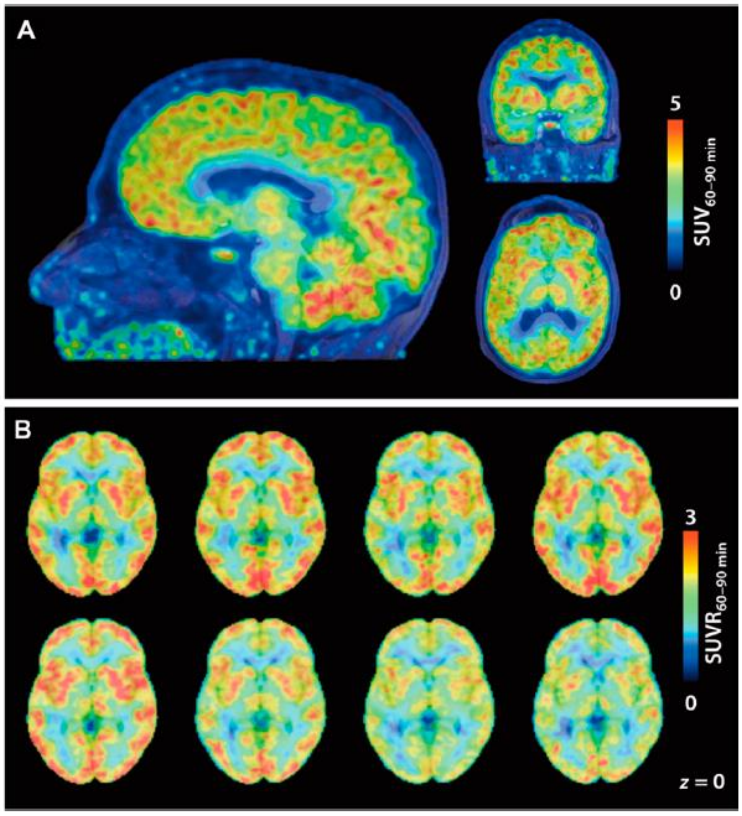

Fig. 13 | ^{11}C-Martinostat PET scans from a first-in-human trial. Top panel (A) average SUV brain images from 60 to 90min following injection with PET images overlaid on MRI. (B) ^{11}C-Martinostat SUVR images of eight individual participants. Figure reprinted from Wey et al. (2016), doi:10.1126/scitranslmed.aaf7551. © 2016, American Association for the Advancement of Science, reprinted with permission from AAAS.

Following this pivotal study, ^{11}C-Martinostat has been used extensively to investigate the role of HDACs in the following clinical settings: **1) Schizophrenia**: Gilbert, Zurcher, Wu, et al. (2019) compared uptake between 14 patients with schizophrenia or schizoaffective disorder and 17 healthy controls, showing lower HDAC expression in the dorsolateral prefrontal cortex of patients, correlating with cognitive performance. **2) Amyotrophic lateral sclerosis**: Dios et al. (2019) investigated altered HDAC levels but found no significant differences between patients and healthy controls, indicating it is not a pathological hallmark of amyotrophic lateral sclerosis. **3) Age and sex differences**: Gilbert, Zurcher, Catanese, et al. (2019) examined age- and sex-related alterations in gene transcription, finding HDAC expression increases with age in cerebral white matter and sex-specific differences in brain regions associated with emotion and memory, including the amygdala and hippocampus. **4) Bipolar disorder**: Tseng et al. (2020)

compared in vivo brain expression of HDACs in 11 participants with bipolar disorder, finding lower binding in the right amygdala compared to healthy controls, with no changes in the dorsolateral prefrontal cortex in contrast to the previous finding in participants with schizophrenia. **5) AD**: Pascoal et al. (2022) studied epigenetic dysregulations and their role in neurodegeneration and cognitive impairment in 94 participants ranging from cognitively unimpaired young participants, cognitively unimpaired elderly, mild cognitive impaired individuals, and participants with AD dementia. This study showed a high correlation of HDAC I reduction with elevated Aβ and tau in patients with AD, in contrast with previous studies that predicted HDAC I increase. This finding is critical, as the use of HDAC inhibitors in treating AD has been suggested, but these results indicate it may be counterproductive. Furthermore, the authors found that HDAC I reduction predicted longitudinal neurodegeneration and cognitive decline, suggesting that HDAC I reduction is an important element associated with both AD pathophysiology and cognitive impairment in general. **6) Dementia with Lewy bodies**: Goodheart et al. (2023) studied HDAC expression in participants with dementia with Lewy bodies, finding increased binding in regions with Lewy body pathology (brainstem, medial temporal lobe, anterior cingulate) compared to healthy subjects. Increased uptake was also observed in motor function areas (striatum, motor cortex, cerebellum), while ^{11}C-Martinostat uptake decreased in the parietal cortex, indicating abnormal class I HDAC expression in these regions.

Recently, Tago et al. (2021) developed the HDAC6 specific radioligand ^{18}F-FSW-100, which showed good brain penetration and moderate stability in mice but was rapidly metabolized. Blocking studies with the unlabeled compound and HDAC6 inhibitors demonstrated its selectivity. Subsequent preclinical validation in non-human primates confirmed good brain penetration and specificity (Tago et al., 2024).

In summary, recognizing epigenetic abnormalities in the brain as therapeutic target for neurodegenerative diseases has led to a focus on PET imaging to quantify the activity of HDAC enzymes non-invasively and support the development of new treatments. Notably, PET imaging ligands for HDACs are well-developed, with the adamantane-conjugated radioligand ^{11}C-Martinostat emerging as a promising tool for imaging HDACs.

Chapter 2

Aims

Due to the challenges and limitations highlighted in the introduction, there remains a gap in the field of effective radioligands for neuronal nAChRs and HDACs. Therefore, with this thesis, I aim to investigate the following:

1. **To assess the suitability of ^{3}H-NS14492 as an in vitro radioligand for the α7 nAChR (Paper I):** Targeting neuronal nAChRs, particularly the α7 subtype, still holds promise for addressing cognitive impairments in conditions like AD and schizophrenia. Our investigation aims to evaluate the binding properties of ^{3}H-NS14492 to the α7 nAChR.

2. **To validate the newly developed radioligand, ^{11}C-Martinostat, in the pig brain (Paper II):** HDACs are crucial enzymes in epigenetic modifications, and their dysregulation is implicated in neurological and psychiatric disorders, including AD. This aim supports the exploration of HDACs as therapeutic targets and diagnostic tools.

3. **To evaluate the binding of previous clinical drug candidates, bradanicline (TC-5619) and encenicline (EVP-6124), to the α7 nAChR in the pig brain using PET imaging with ^{11}C-NS14492 (Paper III):** This study aims to understand the interaction of these drug candidates with the α7 nAChR, which may offer insights into their potential therapeutic efficacy.

Chapter 3

Materials and methods

The methods used in the studies are covered here, with specific experimental details provided in the methodology sections of the relevant publications.

In vitro receptor autoradiography

Autoradiography is an imaging technique used to visualize the location and distribution of radiolabeled molecules within a solid biological sample, typically a thin tissue section. It relies on the radioactive isotope in the molecule, such as tritium (^{3}H), carbon-14 (^{14}C), or iodine-125 (^{125}I), emitting radiation that can be detected by photosensitive film or phosphor imaging plates (Solon, 2007). Tritium labeling is often preferred since substituting hydrogen with tritium does not alter the chemistry of the ligand. Additionally, tritium's long half-life of 12.32 years and low β^--decay energy (18.6 keV) allows for long-term storage and use. The resulting autoradiograms display excellent spatial resolution, used for visual interpretation of radioligand binding and distribution in distinct anatomical structures. For this reason, autoradiography has been used to study the localization of macromolecules within cells, tissues, and organs, as well as to map the distribution of neurotransmitters and their receptors in the brain. Furthermore, quantification by comparing binding levels with a standard allows for the characterization of ligand affinity measurements K_d, K_i, and B_{max} (Davenport, 2008; Manuel et al., 2015).

The autoradiographic procedures used in Papers I and III involve two main steps: pre-incubation and incubation. The conditions for these steps are specifically adjusted to differentiate between total binding (TB) and non-specific binding (NSB), with each binding type having distinct protocols for pre-incubation and incubation. A subsequent washing step is identical for both TB and NSB. In in vitro binding assays, TB includes SB to the targeted receptor and NSB to tissue and other receptors. SB is determined by subtracting NSB from TB, where NSB is measured in the presence of an excess of a cold competitor that also binds to the target

receptor. This method is applicable to both autoradiography and homogenate binding assays (discussed later). During pre-incubation, tissue sections are treated with assay buffer alone, with the addition of a cold competitor for NSB to prevent nonspecific interactions. Following this, sections undergo incubation in assay buffers containing the radioactive ligand, differing only in the addition of the cold competitor for NSB measurements.

Autoradiograms and image analysis

In Papers I and III, we used phosphor imaging plates (IP) to detect radioactive decay and measure receptor binding. The IP captures radiation energy, emitting photo-stimulated luminescence upon stimulation (Amemiya & Miyahara, 1988). Tritium radiation-sensitive IPs were used in Paper I (Griem-Krey et al., 2019). Photo-stimulated luminescence, directly proportional to emitted radiation, enables quantification of in vitro receptor binding through densitometric measurements.

In Paper I, ImageJ software was used for image analysis, with manually drawn ROIs for each brain region. Mean pixel density was converted to ligand binding using standard ^{3}H-microscales. Calibration was performed using a 3rd-degree polynomial function to relate densitometric measurements to decay-corrected ^{3}H-microscale activity levels, and ImageJ computed the results as binding (in nCi/mg tissue equivalent (TE)) using this calibration function. We calculated TB, NSB, and SB in fmol/mg TE for each ROI using decay-corrected specific activity to convert from nCi to fmol. The difference between binding in adjacent sections determined SB for all measured sections.

Homogenate binding assays

The homogenate binding assay is a technique used to measure the binding affinity of ligands to specific receptors or proteins in a crude homogenate of cells or tissue. The method involves the preparation of a homogenate by disrupting the cells or tissues of interest, followed by the addition of a radioligand to the homogenate. The ligand binds to the receptor or protein of interest, and the bound ligand is separated from the unbound ligand using various separation techniques, such as filtration. The amount of bound ligand is then measured using scintillation counting and is proportional to the amount of receptor or protein present in the homogenate. K_d of

the ligand-receptor or ligand-protein interaction can be determined using saturation binding assays, where the concentration of the radioligand is varied while keeping the amount of homogenate constant. This is also the main strength of the assay: its ability to measure the binding affinity of ligands to specific receptors or proteins, without the need for purification of the target protein. One major limitation is the potential for NSB of the radioligand to other proteins or components in the homogenate, which can result in inaccurate measurements of SB (Maguire et al., 2012). In Paper I, brain tissue homogenate binding assays were used. Key parameters, including buffer composition, temperature, and the radioligand-to-membrane concentration ratio, was optimized to enhance TB while minimizing NSB. Saturation binding assay was conducted with serial dilutions of ^{3}H-NS14492, and NSB was determined in the presence of excess SSR180711 as a competitor. Homogenate was added to the assay buffer and incubated and bound radioligand-receptor were collected on glass microfiber filters. After washing with buffer, filters were stored overnight before being quantified in a liquid scintillation counter. For competition binding assays assessing K_i's of various α7 nAChR agonists, inhibition curves were generated. SB was plotted against the logarithm of the competing ligand concentration, and a one-site binding model was applied to determine K_i, using the ^{3}H-NS14492 concentration and K_d.

Positron emission tomography protocol

In Papers II and III, we performed PET scans on young female Danish Landrace pigs using a HRRT scanner at the PET and Cyclotron Unit, Rigshospitalet. List mode data acquisition began at radioligand injection, administered as a bolus in the milk vein catheter. Femoral artery catheterization allowed for arterial blood sampling during PET scanning, used for determining radioactive concentrations in plasma and whole blood, and we quantified radiometabolites with a HPLC system using a radiodetector. Continuous whole blood radioactivity measurement occurred in the first 30 minutes.

In Paper II, ^{11}C-Martinostat synthesis followed Wang, Schroeder, Wey, et al. (2014), while Paper III used ^{11}C-NS14492 synthesized as per Ettrup et al. (2011), with both processes conducted at the PET and Cyclotron Unit, Rigshospitalet. The short half-life of ^{11}C makes it possible to conduct receptor blocking studies within a single experiment, allowing repeat scans as soon as two hours post-baseline in the same animal.

In Paper II, in vivo selectivity of ^{11}C-Martinostat was tested through self-blocking with unlabeled compound. For Paper III occupancy studies, we administered bradanicline (TC-5619) or encenicline (EVP-6124) as bolus injections. Re-scans were done with the same PET protocol. Finally, PET images were reconstructed into 38 dynamic frames of increasing length using an iterative method, as reported by Sureau et al. (2008).

PET image analysis

PET images obtained during dynamic scans provide a quantitative assessment of radioligand concentration in each volume of interest (VOI) over time. The relationship is often depicted as a TAC, with the outcome expressed as the concentration of the radioligand in the VOI (measured in kBq/ml), adjusted for the injected dose and corrected for the animal's weight, resulting in standardized uptake values (SUV) expressed in g/ml. This normalization allows for the merging of regional activity data from different animals and injected doses on the same graph, assuming a consistent fraction of injected radioligand uptake by a given region. Kinetic modeling uses this data to calculate the distribution volume (V_T) of the radioligand in each VOI, serving as a measure of receptor concentration. Accurate measurement of radioactivity in each VOI is crucial for both TACs and kinetic modeling. In Paper II, brain parcellation was achieved through an automated PET/MRI method developed in our group by Villadsen et al. (2018), defining 178 brain regions, with only selected regions used for the study. In Paper III, co-registration to a standardized MRI atlas of the Danish Landrace pig brain was done, and discrete points on the PET image were co-registered to this atlas using the Register software as described by Kornum et al. (2009). After co-registration, radioactive concentrations in VOIs were extracted from the dynamic PET scans.

Several kinetic models exist, with compartmental analyses often considered the gold standard for receptor binding quantification, using parent-compound corrected arterial concentration as an input function (Innis et al., 2007). In Paper II, V_T was computed using 1TCM, 2TCM, Ichise Multilinear Analysis (MA1), and Logan invasive. In Paper III, V_T for selected regions was calculated using a Logan graphical analysis with arterial input function (Logan et al., 1990).

The pig as a model animal in neurobiology

As discussed in the section ‘Translational challenges in α7 nAChR drug development’, the limitations of rodent models in neurobiological research highlight the need for alternative animals. While non-human primates are often considered the gold standard, their use is constrained for various reasons, as reviewed in Capitanio and Emborg (2008). Pigs are increasingly being used as an alternative animal model in biomedical research due to their anatomical, physiological, and genetic similarities to humans (Netzley & Pelled, 2023). They have been effectively used in studies on various diseases, including neurological and psychiatric disorders, and developmental processes. Pigs are particularly valuable in neurobiology due to their large brain size and complex behavior, which provide a closer approximation to human brain function compared to traditional rodent models (Lunney et al., 2021). Like humans, pigs have a gyrencephalic brain structure, facilitating complex cognitive functions compared to the lissencephalic structure of rodent brains without cortical folds (Lind et al., 2007). Moreover, pig brains surpass rodents in size, weighing approximately 180 g compared to the rodent's ~10 g, though still notably smaller than the human brain, averaging ~1,300 g. Additionally, the white matter composition in humans and pigs is similar, with a 60:40 ratio of white to gray matter (Platt et al., 2014; Simchick et al., 2019). Finally, the size of the pig and its brain makes it suitable for use in human imaging equipment such as a PET scanner which has been done extensively in our group, thereby eliminating the need for specialized animal imaging equipment. In the studies detailed in Papers II and III, a total of thirteen female pigs were used weighing between 20–22 kg. All pigs were sourced from local farms and allowed to acclimatize for 7–9 days in an enriched environment prior to PET scans. For procedures, anesthesia was initially induced by midazolam, followed by a zoletil mixture, maintained with propofol, with endotracheal intubation for ventilation and venous and arterial access established for monitoring and blood sampling. Vital parameters were continuously monitored throughout the experiments, which concluded with euthanasia using a pentobarbital IV injection. Ethical approval for both studies was granted by the Danish Council for Animal Ethics (journal no. 2012-15-2934-00156).

Chapter 4

Results and discussions

In vitro validation of ^{3}H-NS14492

In Paper I, we have evaluated the in vitro properties of ^{3}H-NS14402. Autoradiographic binding in pig brain sections proved to be saturable, with a K_d of 2.1 ± 0.7 nM and a B_{max} of 15.7 ± 2.0 fmol/mg TE (Figure 14).

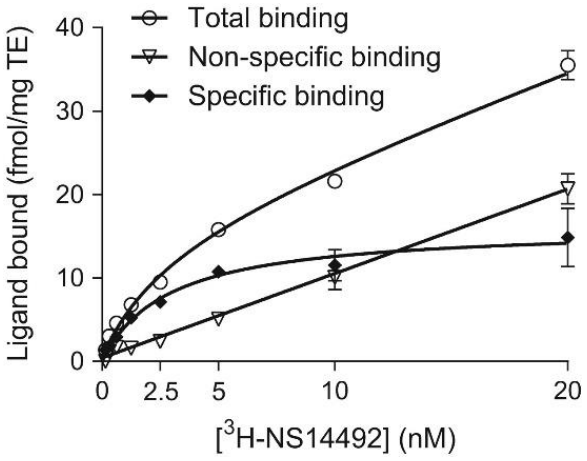

Fig. 14 | Saturation binding of ^{3}H-NS14492 on 12 µm pig frontal cerebral cortex sections included determination of NSB in the presence of 10 µM SSR180711. Data points represent mean ± S.D. Figure reprinted from Paper I, Magnussen et al. (2015), doi:10.1016/j.ejphar.2015.04.036. © 2015, Elsevier B.V., reprinted with permission as per publisher's copyright policy.

The autoradiograms of ^{3}H-NS14492 displayed laminar distribution in gray matter, with the highest density in superficial cortical layers (Figure 15). The structural distribution of ^{3}H-NS14492 binding closely resembled that of ^{125}I-Btx, though a more detailed structural distribution was observed with the former.

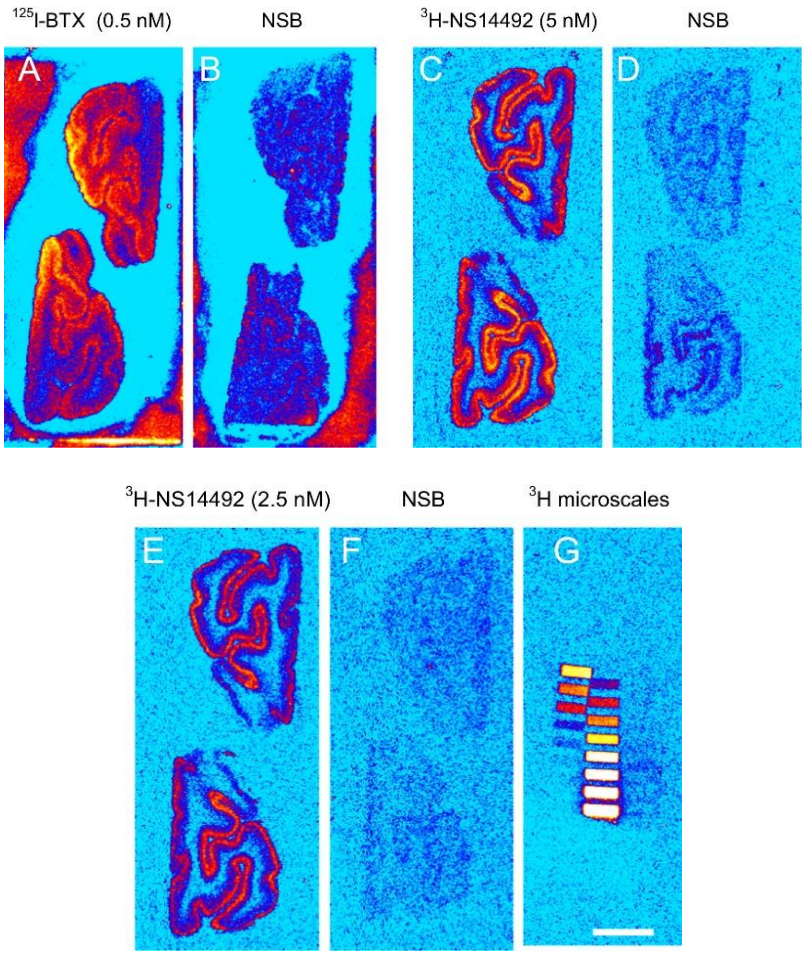

Fig. 15 | Representative autoradiograms depict the distribution of TB and NSB in pig frontal cerebral cortex sections for ^{125}I-Btx (A and B) and ^{3}H-NS14492 (C – E). NSB was determined in the presence of 1 mM (−)-nicotine (B) and 10 µM SSR180711 (D and F). Additionally, ^{3}H microscales are shown (G). Figure modified from Paper I, Magnussen et al. (2015), doi:10.1016/j.ejphar.2015.04.036. © 2015, Elsevier B.V., reprinted with permission as per publisher's copyright policy.

The displacement of 0.5 nM ^{125}I-Btx by unlabeled NS14492 was assessed on similar sections, revealing a K_i of 23 nM (^{125}I-Btx K_d = 0.45 nM). At the highest concentration of unlabeled NS14492 (1 µM), 81% of ^{125}I-Btx was displaced compared to NSB with 1 mM (−)-nicotine (Figure 16). This observation may suggest a potential lack of reversibility in α-Btx binding to the α7 nAChR, as previously suggested (Young et al., 2003).

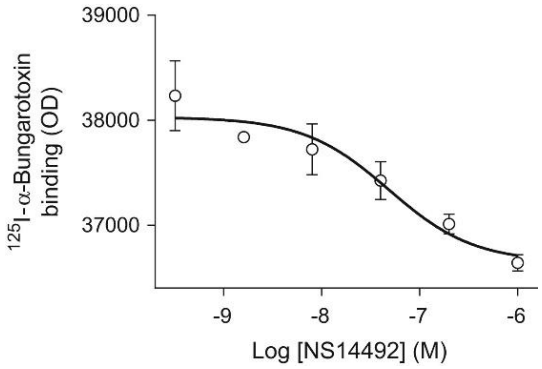

Fig. 16 | Inhibition curve for displacement of ^{125}I-α-Btx with cold NS14492 with fitted K_i value = 23 nM. Points represent mean value ± S.D. from an experiment in duplicate. Figure reprinted from Paper I, Magnussen et al. (2015), doi:10.1016/j.ejphar.2015.04.036. © 2015, Elsevier B.V., reprinted with permission as per publisher's copyright policy.

With an optimized protocol in pig frontal cerebral cortex homogenate, ^{3}H-NS14492 showed saturable binding with a K_d of 0.8 ± 0.3 nM and a B_{max} of 30.2 ± 11.6 fmol/mg protein (Figure 17). The difference in K_d values between the two experimental methods could be attributed to differences in incubation temperature: room temperature for autoradiography versus 4°C for homogenate binding assay. Lower temperature is known to decrease dissociation (k_{off}) more than association (k_{on}) rate constants thereby lowering the K_d (Hulme & Trevethick, 2010). The calculated B_{max} values, 15.7 ± 2.0 fmol/mg TE in autoradiography and 30.2 ± 11.6 fmol/mg protein in the homogenate binding assay, align with values found in macaque monkeys (Kulak et al., 2006), humans (Anderson et al., 2008; Falk et al., 2003), and pigs (Hoffmeister et al., 2011). However, it is important to consider species-specific differences in receptor structure that may influence binding, complicating direct B_{max} comparisons. The difference in B_{max} between the two assays is due to methodological variations, as greater variation in B_{max} was observed in homogenized samples compared to autoradiography.

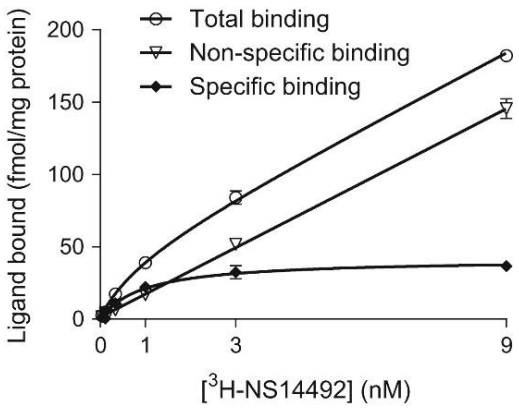

Fig. 17 | Saturation binding of ^{3}H-NS14492 in homogenized tissue from pig frontal cerebral cortex. NSB determined in the presence of 10 µM SSR180711. Points represent mean value ± S.D. Figure reprinted from Paper I, Magnussen et al. (2015), doi:10.1016/j.ejphar.2015.04.036. © 2015, Elsevier B.V., reprinted with permission as per publisher's copyright policy.

We assessed the binding properties of ^{3}H-NS14492 by displacement with α7 nAChR agonists and PAMs in pig brain homogenate (Figure 18). TC-5619, EVP-6124, SSR180711, and the unlabeled NS14492 displaced ^{3}H-NS14492 binding with a similar nanomolar affinity rank order, with K_i values of 0.06 nM (95% CI: 0.039−0.104 nM), 0.19 nM (95% CI: 0.095−0.396 nM), 0.26 nM (95% CI: 0.169−0.406 nM), and 1.44 nM (95% CI: 1.128−1.844 nM), respectively. In contrast, (−)-nicotine displaced ^{3}H-NS14492 binding with 2–3 orders of magnitude lower affinity, having a K_i value of 123 nM (95% CI: 30.64−494.4 nM). The α7 nAChR PAMs, AVL-3288 and PNU-120592, were incapable of displacing ^{3}H-NS14492 binding in the tested range, as expected, given their binding to a site different from the orthosteric agonist site.

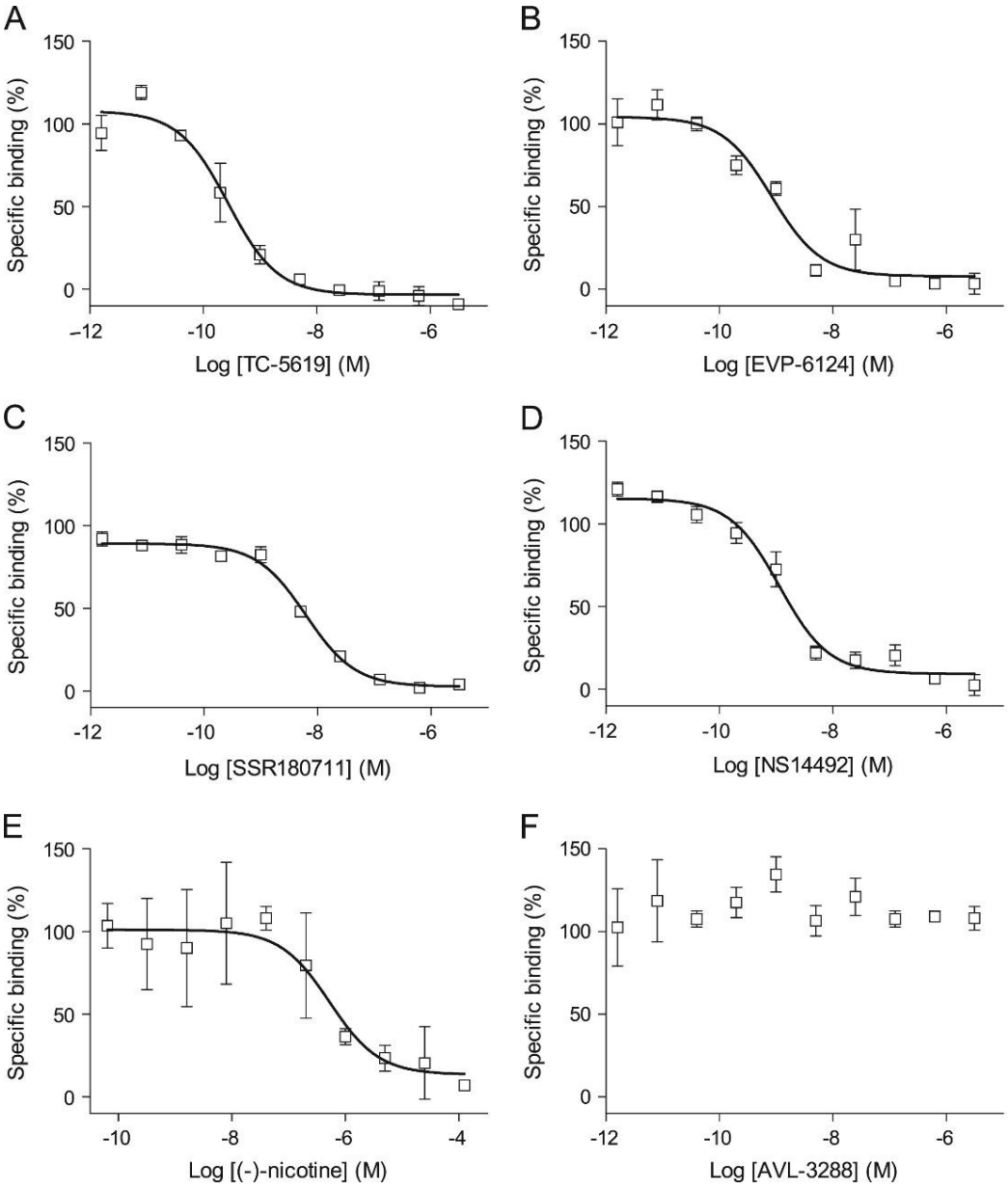

Fig. 18 | Inhibition curves for displacing 2.5 nM ^{3}H-NS14492 in pig brain homogenate, presented as percent SB: (A) TC-5619, (B) EVP-6124, (C) SSR180711, (D) NS14492, (E) (−)-nicotine, and (F) AVL-3288. Compounds ((A)–(D) and (F)) were tested in concentrations from 40 pM to 3.125 µM, while (−)-nicotine (E) was tested in concentrations from 1.6 nM to 125 µM. Points represent mean ± S.D. from a representative duplicate experiment. K_i values were determined by fitting a one-site function to TB with defined ^{3}H-NS14492 concentration and K_d. Figure reprinted from Paper I, Magnussen et al. (2015), doi:10.1016/j.ejphar.2015.04.036.

PNU-120596 appears to display an inhibition curve (Figure 19A), but even at the highest tested concentration (10 µM), SB remained at 95 ± 4% of baseline. Lower concentrations exceeded baseline SB, e.g., 25 pM PNU-120596 resulted in 136 ± 7% SB, indicating a potential increase in ^{3}H-NS14492 binding to pig α7 nAChR. Another experiment (Figure 19B), conducted in triplicate, showed no displacement but a significant increase of 169 ± 2% SB at 100 pM PNU-120596. These results underscore the utility of ^{3}H-NS14492 for evaluating both partial and full agonists and functionally diverse molecules like type II PAMs. Szabo et al. (2014) suggests that PNU-120596 decreases the k_{off} rate, increasing ^{3}H-NS14492 binding and favoring the bound state. Conversely, AVL-3288 did not increase maximal 3H-NS14492 binding (data not shown).

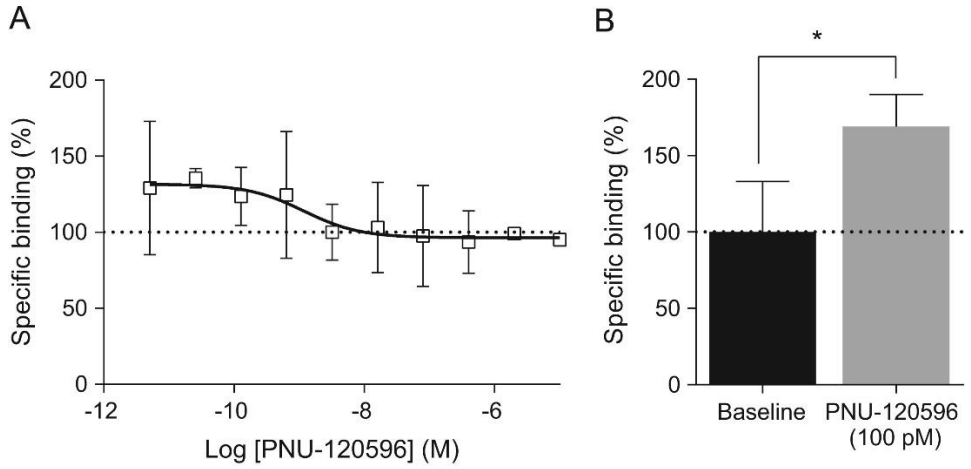

Fig. 19 | Percent SB of 2.5 nM ^{3}H-NS14492 to homogenized pig frontal cerebral cortex tissue co-incubated with PNU-120596: (A) Across concentrations from 5 pM to 10 µM, and (B) in the presence of 100 pM PNU-120596. NSB was determined in the presence of 10 µM SSR180711. Points in (A) represent mean ± S.D. from a representative duplicate experiment, while bars in (B) represent mean ± S.D. from an experiment in triplicate. *P<0.05 indicates a significant difference from baseline in an unpaired t-test. Figure reprinted from Paper I, Magnussen et al. (2015), doi:10.1016/j.ejphar.2015.04.036. © 2015, Elsevier B.V., reprinted with permission as per publisher's copyright policy.

Taken together, ^{3}H-NS14402 demonstrated high specificity and affinity for α7 nAChRs with strong binding in pig brain sections and homogenates. Autoradiography showed cortical layer binding and displacement studies confirmed nanomolar affinity for α7 nAChR agonists and PAMs. Notably, PNU-120596 increased binding, indicating its utility for evaluating partial and full agonists, as well as type II PAMs. Overall, these findings suggest ^{3}H-NS14402 is a promising tool for α7 nAChR neurobiological and pharmacological research.

Evaluation of ^{11}C-Martinostat in the pig brain

In Paper II, we investigated the in vivo properties of ^{11}C-Martinostat in the pig brain and its potential to measure HDAC1–3 levels. Following the administration of ^{11}C-Martinostat, we observed substantial brain uptake, reaching a peak SUV of 4 in the cerebellum vermis. ^{11}C-Martinostat showed slow kinetics with no apparent wash-out observed across any brain region during the 121-minute acquisition period (Figure 20a), aligning with findings in non-human primates (Wang, Schroeder, Wey, et al., 2014; Wey et al., 2015) and humans (Wey et al., 2016). ^{11}C-Martinostat showed a widespread uptake pattern (Figure 20d), with the highest levels observed in the cerebellum vermis and cortical regions, while the lowest levels were found in the olfactory bulbs and subcortical regions. Notably, both white and gray matter regions showed significant uptake, emphasizing the conserved nature of the HDACs as reviewed in Seto and Yoshida (2014).

To assess ^{11}C-Martinostat specificity, we coadministered 0.5 mg/kg unlabeled Martinostat, significantly reducing the signal (Figure 20e) and leading to accelerated radioligand kinetics (Figure 20b). Blocking decreased regional V_T values, as shown by the Lassen plot (Figure 20c), revealing 89% Martinostat occupancy and a V_{ND} of 2.87 ml/cm³. This V_{ND}, approximately 6% of V_T in high-binding regions and below 16% in low-binding regions, highlighted ^{11}C-Martinostat's excellent signal-to-noise ratio

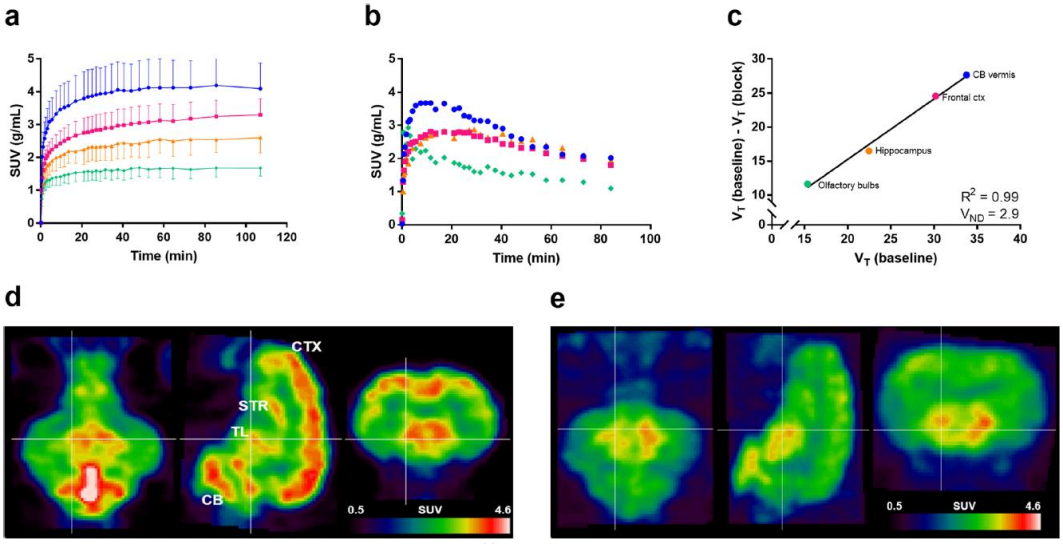

Fig. 20 | Regional distribution and PK in the pig brain of ^{11}C-Martinostat. (a) Regional TACs at baseline (mean ± SD, n = 13). (b) TACs after 0.5 mg/kg unlabeled Martinostat administration. (c) Lassen plot illustrating regional V_T differences of ^{11}C-Martinostat before and after 0.5 mg/kg Martinostat administration (R^2 = 0.99, n = 1). (d) Representative PET image (0–121 min) showing radioactivity in the pig brain after ^{11}C-Martinostat injection. (e) PET image (0–121 min) after 0.5 mg/kg unlabeled Martinostat injection (symbols denote regions: ● = cerebellum vermis, ■ = frontal cerebral cortex, ▲ = hippocampus, ♦ = olfactory bulbs). SUV: Standardized Uptake Values, V_T: Total Distribution Volume. CB: Cerebellum, TL: Thalamus, STR: Striatum, CTX: Cortex. Figure reprinted from Paper II, Donovan, Magnussen, et al. (2020), doi:10.1007/s11307-019-01403-9. © 2019, World Molecular Imaging Society, permission conveyed through Copyright Clearance Center license number 5816970762368.

The olfactory bulbs had the lowest baseline binding, although the V_T value was still approximately five times higher than the V_{ND}. This highlights the absence of an ideal reference region in the pig brain for non-invasive reference tissue modeling. Evaluation of the standardized uptake value ratio (SUVR) measure as an alternative to full kinetic modeling, following the approach described in humans by Wey et al. (2016), revealed positive correlations with V_T values for the three pig brain regions investigated. We quantified ^{11}C-Martinostat using various kinetic models: 1TCM, 2TCM, Logan invasive, and MA1. The 1TCM showed poor fit and underestimated binding, while 2TCM and MA1 provided satisfactory fits. The MA1 model, with individual t* for each ROI, had the lowest Akaike information criterion (AIC) scores, making it the preferred model. AIC is a measure used to compare different statistical models, taking into account the goodness of fit and the number of parameters used (Akaike, 1998). Lower AIC scores indicate a model that better balances fit and complexity. Comparisons with previous studies in non-human

primates and humans suggested that the MA1-calculated V_T's from pig brain aligned with 2TCM-calculated V_T's from nonhuman primates, whereas human V_Ts were notably lower, though V_{ND} in humans remains to be measured. Due to the absence of an ideal reference region in the pig brain, reference tissue models could not be applied. Instead, we explored the use of SUVR as a BP_{ND} surrogate, using the olfactory bulb as a reference due to its relative low binding. The TACs remained constant over time, with varying timepoints for different brain regions. The BP_{ND}s, calculated based on MA1-generated V_Ts and self-blocking-derived V_{ND} ($BP_{ND} = (V_T - V_{ND})/V_{ND}$), showed robust correlations with the SUVRs (Table 4).

Table 4 | Total volumes of distribution (V_T) from four different kinetic models, ND BPs (BP_{ND}), and SUVR. All values are expressed as mean ± SD (except for AIC values, expressed as mean value). Table modified from Paper II, Donovan, Magnussen, et al. (2020), doi:10.1007/s11307-019-01403-9. © 2019, World Molecular Imaging Society, permission conveyed through Copyright Clearance Center license number 5816970762368.

	V_T (mL/cm3)				BP_{ND}	
	1TCM	2TCM	Logan	MA1	MA1	SUVRx-121
Cerebellum vermis	42.6 ± 10.2	49.6 ± 12.5	45.5 ± 10	47.4 ± 10.6	15.5 ± 3.7	2.5 ± 0.3
AIC	17.4	-19.3	147	-11.5	-	-
Frontal cerebral cortex	36.9 ± 9.6	44.6 ± 10.6	40.7 ± 9	41.7 ± 9.1	13.5 ± 3.2	2 ± 0.2
AIC	4.4	-34.4	124	-16.1	-	-
Hippocampus	26.6 ± 5.3	34.6 ± 9.1	28.9 ± 6.2	30.8 ± 6.8	9.7 ± 2.4	1.5 ± 0.1
AIC	49.6	41.7	146	5.6	-	-
Olfactory bulbs	16.5 ± 3.7	20.9 ± 5	17.9 ± 3.3	18.9 ± 3.7	5.6 ± 1.3	-
AIC	61.3	46.2	142	2.4	-	-

To assess test-retest variability, four pigs were scanned twice. Three showed V_T differences of 7–12% in the frontal cerebral cortex, while the fourth had a larger difference of 39%. However, concerning SUVRs, all four pigs displayed differences of less than 9% between scans in the frontal cerebral cortex.

Taken together, ^{11}C-Martinostat showed substantial brain uptake in the pig brain, with the highest levels in the cerebellum vermis and cortical regions. Specificity was confirmed through coadministration of unlabeled Martinostat, significantly reducing the signal. Various kinetic models were evaluated, with the MA1 model preferred due to the lowest AIC scores. These findings demonstrate ^{11}C-Martinostat's promise for measuring HDAC levels and its applicability in neurobiological research.

^{11}C-NS14492 PET imaging of bradanicline and encenicline binding

In Paper III, we investigated the target engagement for two α7 nAChR specific compounds that have failed in clinical trials: bradanicline (TC-5619) and encenicline (EVP-6124), using ^{11}C-NS14492. This study involved both in vitro autoradiography and in vivo PET imaging in the pig brain. Results from in vitro autoradiography on coronal pig sections revealed laminar binding in cortical layers and reduced binding in white matter, aligning with findings obtained with ^{3}H-NS14492. Additionally, a near-complete blocking effect was observed with 10 µM concentrations of both bradanicline and encenicline. As a control, SSR180711 was included, showing robust blocking effects for comparison (Figure 21).

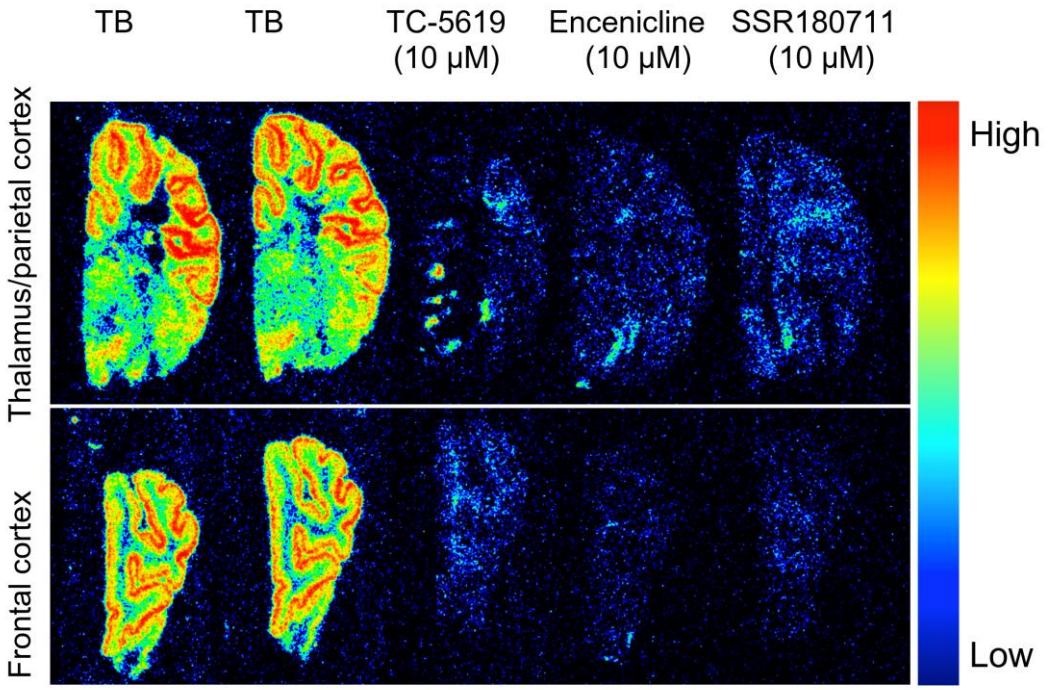

Fig. 21 | In vitro autoradiography in coronal pig brain sections. TB was determined with 10 nM ^{11}C-NS14492. Blocking shown with bradanicline (TC-5619), (10 µM), encenicline (10 µM), and SSR180711 (10 µM). Figure reprinted from Paper III, Magnussen et al. (2024), doi:10.3389/fnimg.2024.1358221.

In vivo PET imaging revealed a distinctive brain uptake pattern of ^{11}C-NS14492, with the highest uptake observed in the thalamus and cortical areas, intermediate striatal uptake, and low cerebellar uptake (Figure 22). For occupancy studies, pre-treatment with 3 mg/kg of either bradanicline or encenicline was correlated with a lower V_T in all assessed brain regions (Figure 23a). Specifically, pre-treatment with 3 mg/kg bradanicline resulted in an occupancy ranging from 38% to 42% (Figure 23c – d), while pre-treatment with 3 mg/kg encenicline yielded an average occupancy of less than 10% (Figure 23e – f). The average V_{ND} was determined to be 5.3 ± 1.7 mL/cm^3 based on a sample size of n = 3. After IV injection, the parent fraction of ^{11}C-NS14492 declined rapidly, with about 50% of plasma radioactivity attributable to the parent compound after 7 minutes (Figure 23b). No radiolabeled lipophilic metabolites were detected, as indicated by the absence of distinct peaks in the lipophilic range on radiochromatograms. (data not shown).

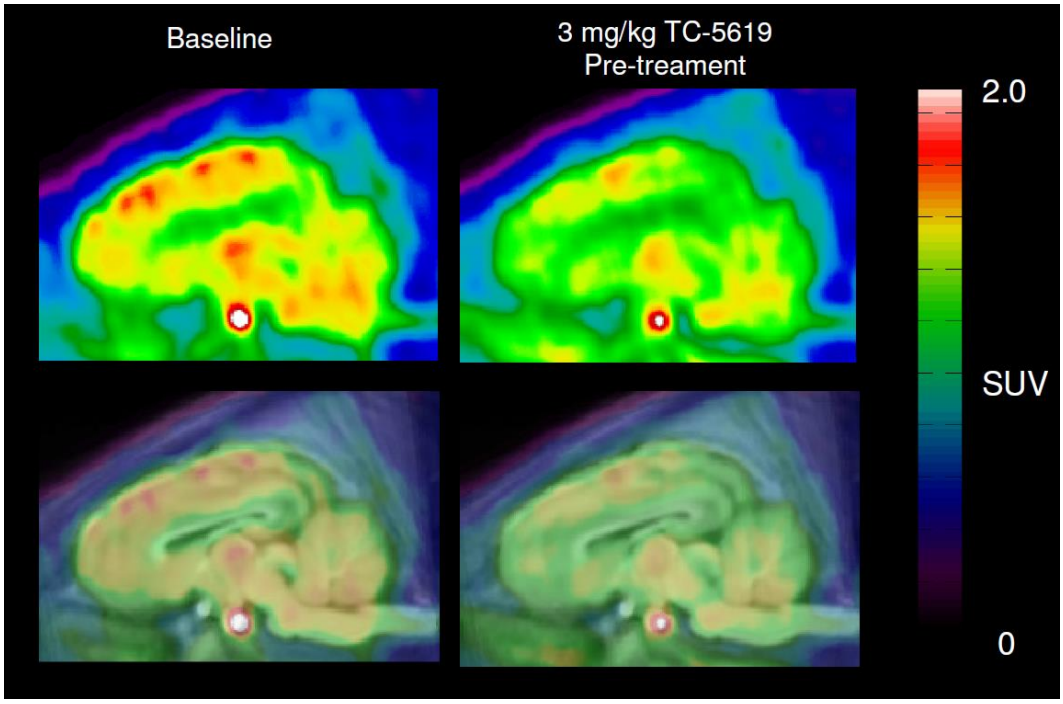

Fig. 22 | Regional distribution of ^{11}C-NS14492 in the pig brain. Representative sagittal PET images pre and post bradanicline challenge. PET images summed and averaged over 0–90 minutes (top panel) overlaid MRI-based pig brain atlas (lower panel). Figure reprinted from Paper III, Magnussen et al. (2024), doi:10.3389/fnimg.2024.1358221.

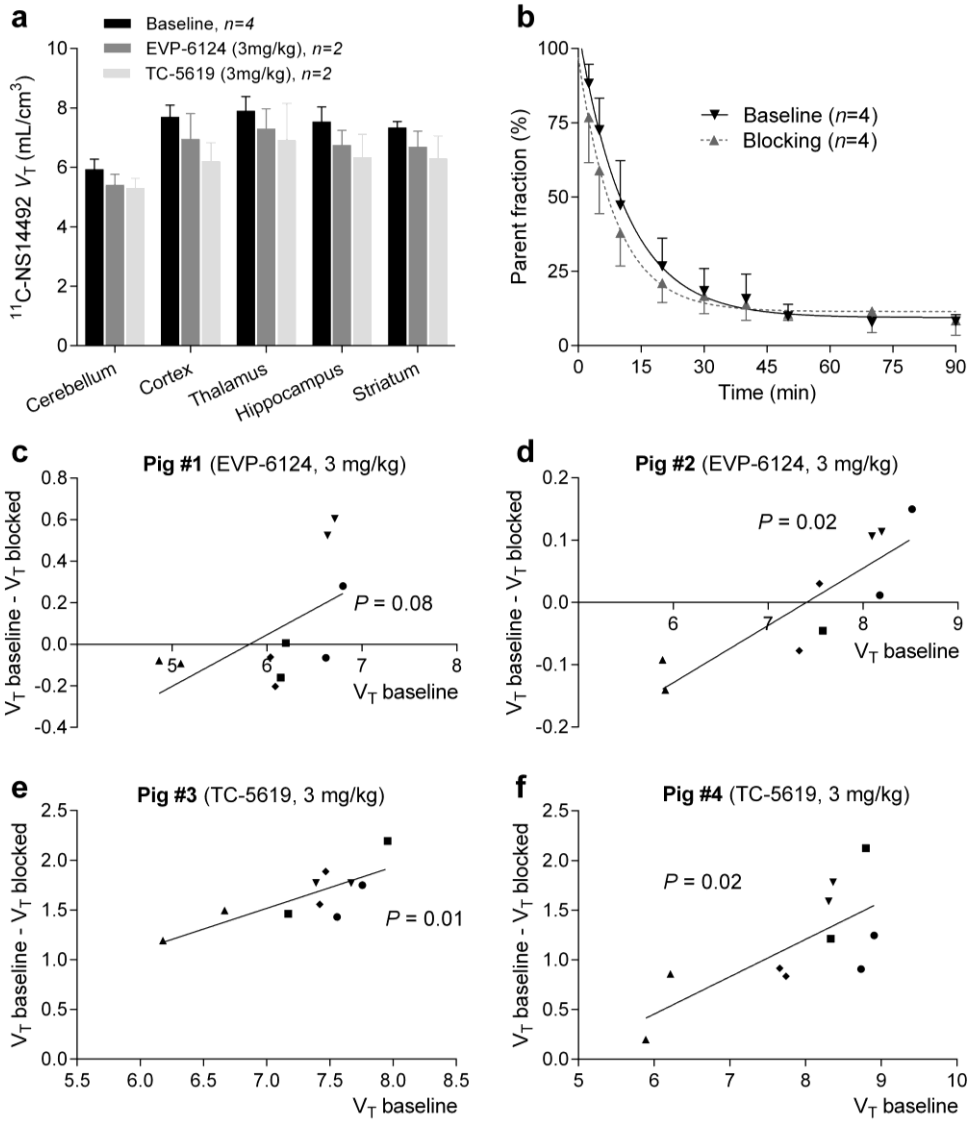

Fig. 23 | (a) Logan plot V_T's of ^{11}C-NS14492 in different brain regions at baseline and with encenicline (EVP-6124) or bradanicline (TC-5619) (both given IV at 3 mg/kg 30 minutes prior to second scan). Bars indicate mean ± SEM. (b) Relative radioactive parent compound in pig plasma as a function of time after IV injection of ^{11}C-NS14492. Data from 8 PET scans were averaged: 4 baseline scans (black) and 4 challenge scans (gray) with 3 mg/kg Encenicline (n = 2) or 3 mg/kg TC-5619 (n = 2). Solid black and gray lines represent a single exponential decay function fitted to the data. (c-f) Occupancy plots of ^{11}C-NS14492 V_T's at baseline and pharmacological challenge for individual pigs. Statistical test results (*P*-values) for slope not equal to zero is shown for the individual fits. ▼ = cerebral cortex; ● = thalamus; ▲ = cerebellum; ■ = hippocampus; ♦ = striatum. Figure reprinted from Paper III, Magnussen et al. (2024), doi:10.3389/fnimg.2024.1358221. © 2024, Magnussen, Ettrup, Lehel, Peters, Dyssegaard, Thomsen, Mikkelsen and Knudsen, distributed under a Creative Commons Attribution 4.0 International License.

We found two plausible explanations for the low receptor occupancy of encenicline:

1. If encenicline is rapidly cleared after IV dosing, it may not have sufficient time for uptake by the brain initially. Evidence from rat studies shows that following oral administration, brain-to-plasma ratios of encenicline reach approximately 2 between 1 and 4 hours and 5 at 8 hours (Prickaerts et al., 2012). This suggests that while encenicline eventually accumulates in the brain, the initial plasma clearance rate may impact its early availability for receptor binding. The increasing brain-to-plasma ratio over time indicates that the drug's uptake in the brain and equilibration with receptors improve significantly at later time points. In contrast, the plasma half-life in humans is much longer, 50–65 hours after oral administration of encenicline (Barbier et al., 2015). However, potential PK differences between humans and pigs, along with variations between oral and IV administration, could influence the observed differences. These factors should be considered when evaluating the drug's kinetics and its potential impact on brain uptake, especially in the context of varying routes of administration and inter-species variations.

2. An alternative explanation may be found in the well-documented species variation in BBB permeability, observed among rats, pigs, and humans (Deo et al., 2013; Stanimirovic et al., 2015; Syvanen et al., 2009). This variability could, in part, contribute to the failure of encenicline in clinical trials. Moreover, a thorough examination of the available literature has yielded no documented evidence supporting that encenicline can effectively cross the BBB in humans.

In contrast, bradanicline demonstrates the ability to pass the BBB in pigs with high occupancy at the α7 nAChR. Despite these promising characteristics, no studies have yet determined the optimal α7 nAChR occupancy range for treatment effects. It is therefore possible that the lack of significant pro-cognitive effects observed in the clinical trials of bradanicline could be attributed to the selection of a suboptimal dose. Previous research indicates that the pro-cognitive effects of certain α7 nAChR agonists, including encenicline (Keefe et al., 2015), bradanicline (Hauser et al., 2009), AZD0328 (Castner et al., 2011), DMXB-A (Olincy et al., 2006), and PHA543613 (Yang et al., 2013), tend to be more pronounced at lower doses. This suggests the possibility that the cognitive enhancement effect for at least some α7 nAChR agonists follows an inverted U-shaped dose-response curve, with peak efficacy occurring at lower doses. This observation underscores the complexity of

dosing decisions in human clinical trials and emphasizes the need for robust pre-clinical tools such as PET for dose finding.

Overall, ^{11}C-NS14492 effectively assessed the target engagement of bradanicline and encenicline in the pig brain. In vitro autoradiography showed significant cortical binding and robust blocking effects. In vivo PET imaging indicated distinct uptake patterns, with bradanicline achieving 38-42% occupancy and encenicline less than 10%. The low occupancy of encenicline is likely due to rapid plasma clearance or species differences in BBB permeability.

Chapter 5

Conclusions and future perspectives

The research projects presented in this thesis are all concerned with the exploration and characterization of new radioligands and their applications in studying critical targets within the CNS. The studies focus on the α7 nAChRs and HDACs. α7 nAChRs are involved in cognitive functions and have been implicated in several neuropsychiatric conditions, including schizophrenia and AD. HDACs, on the other hand, play a crucial role in the regulation of gene expression through epigenetic mechanisms and are linked to various neurological and psychiatric disorders as well as other diseases outside the CNS. Using advanced imaging techniques and comprehensive in vitro and in vivo methodologies, we aim to enhance our understanding of these molecular targets, which hold potential for therapeutic intervention in neurological and psychiatric disorders and potentially to bridge the gap between molecular pharmacology and clinical application. The following sections summarize the key findings from the three papers included in this thesis. Additionally, they discuss future perspectives and potential directions for continued research.

In Paper I we established that ^{3}H-NS14492 demonstrates favorable binding properties for studying α7 nAChRs. The radioligand demonstrate saturable binding, consistent nanomolar affinity across methods, and good binding characteristics. These findings underscore its suitability as a valuable tool for investigating α7 nAChR interactions in neuroscientific research. The findings from Paper I suggest several areas for future exploration: continued investigation into the applicability of ^{3}H-NS14492 in various experimental settings and other animal models, as well as in human brain samples, could enhance our understanding of its utility. Additionally, an exciting area for future use involves a more in-depth examination of the properties of PAMs, such as the clinically testes AVL-3288 and JNJ-39393406, to enhance binding with ^{3}H-NS14492 in tissue as we saw with the addition of PNU-120596. This, coupled with the in vivo PET imaging approach discussed in Paper III for dose-finding, presents an exciting area for investigation.

Exploring microdosing of both compounds, a PAM and a conventional agonist or partial agonist, holds promise for addressing potential dose-related side effects and may broaden our understanding of the therapeutic window, especially in the context of the hypothesized inverted U-shaped dose-response curve for some α7 nAChR agonists.

In Paper II, we explored the in vivo properties of ^{11}C-Martinostat in the pig brain for measuring HDAC1–3 levels. The radioligand showed substantial brain uptake with slow kinetics, displaying a widespread distribution pattern and an excellent signal-to-noise ratio. Coadministration experiments with unlabeled Martinostat confirmed the specificity of binding. Together, the results highlight the potential of ^{11}C-Martinostat for investigating epigenetic changes in vivo. Further exploration of ^{11}C-Martinostat in various animal models and human disease contexts could broaden our understanding of the potential implication of epigenetic changes in a broad range of diseases, both neurological and psychiatric, as well as diseases outside the CNS. Investigating the epigenetic status and longitudinal changes in early diagnosed patients with e.g., AD could also pose a way to monitor and guide early treatment interventions. Caution should be applied to avoid a repetition of the single-sided use of just one biomarker as was seen with the approval of aducanumab as discussed elsewhere in this thesis. In such a case, a multimodal approach involving many biomarkers and efficacy output measures should be combined. Finally, ^{11}C-Martinostat should be used to validate potential treatments targeting HDAC1–3, guide dosing, and aid in early clinical decision-making processes.

In Paper III, target engagement for α7 nAChR agonists bradanicline and encenicline was investigated using ^{11}C-NS14492 in the pig using both in vitro and in vivo methods. Occupancy studies revealed distinct in vivo α7 nAChR occupancies for the two compounds, with bradanicline demonstrating robust occupancy in contrast to the modest binding observed with encenicline. These findings underscore the significance of PET as an indispensable pre-clinical tool in CNS drug development, highlighting the necessity for comprehensive evaluations before starting up large-scale clinical trials. This is particularly crucial for the α7 nAChR as a therapeutic target, given its potentially challenging pharmacology and the history of numerous failed clinical trials in the field.

Collectively, these papers highlight the versatility and significance of PET imaging, here in the context of α7 nAChRs, HDAC1–3 levels, and target engagement of α7 nAChR ligands. The studies provide insights into the in vitro and in vivo properties of radioligands, demonstrating their potential as essential tools in drug development.

Paper I

Magnussen, J. H., Ettrup, A., Donat, C. K., Peters, D., Pedersen, M. H. F., Knudsen, G. M., & Mikkelsen, J. D. (2015). Radiosynthesis and in vitro validation of (3)H-NS14492 as a novel high affinity alpha7 nicotinic receptor radioligand. *European Journal of Pharmacology*, *762*, 35-41, doi:10.1016/j.ejphar.2015.04.036

European Journal of Pharmacology 762 (2015) 35–41

Contents lists available at ScienceDirect

European Journal of Pharmacology

journal homepage: www.elsevier.com/locate/ejphar

Molecular and cellular pharmacology

Radiosynthesis and in vitro validation of ^{3}H-NS14492 as a novel high affinity alpha7 nicotinic receptor radioligand

Janus H. Magnussen [a], Anders Ettrup [a], Cornelius K. Donat [a], Dan Peters [b], Martin H.F. Pedersen [c], Gitte M. Knudsen [a], Jens D. Mikkelsen [a,*]

[a] Neurobiology Research Unit, Copenhagen University Hospital, Rigshospitalet, Copenhagen, Denmark
[b] DanPET AB, Malmö, Sweden
[c] The Hevesy Laboratory, DTU Nutech, The Technical University of Denmark, Denmark

ARTICLE INFO

Article history:
Received 17 September 2014
Received in revised form
22 April 2015
Accepted 23 April 2015
Available online 1 May 2015

Keywords:
alpha7
Radioligand
Autoradiography
Binding assay
PET ligand

ABSTRACT

The neuronal α7 nicotinic acetylcholine receptor is a homo-pentameric ligand-gated ion channel that is a promising drug target for cognitive deficits in Alzheimer's disease and schizophrenia. We have previously described ^{11}C-NS14492 as a suitable agonist radioligand for in vivo positron emission tomography (PET) occupancy studies of the α7 nicotinic receptor in the pig brain. In order to investigate the utility of the same compound for in vitro studies, ^{3}H-NS14492 was synthesized and its binding properties were characterized using in vitro autoradiography and homogenate binding assays in pig frontal cortex. ^{3}H-NS14492 showed specific binding to α7 nicotinic receptors in autoradiography, revealing a dissociation constant (K_d) of 2.1 ± 0.7 nM and a maximum number of binding sites (B_{max}) of 15.7 ± 2.0 fmol/mg tissue equivalent. Binding distribution was similar to that of another selective ligand ^{125}I-α-bungarotoxin (^{125}I-BTX) in autoradiography, and unlabeled NS14492 displaced ^{125}I-BTX with an inhibition constant (K_i) of 23 nM. ^{3}H-NS14492 bound to α7 nicotinic receptors in homogenized pig frontal cortex with a K_d of 0.8 ± 0.3 nM and a B_{max} of 30.2 ± 11.6 fmol/mg protein. This binding assay further revealed the K_i rank order for a number of α7 nicotinic receptor agonists, and positive allosteric modulators (PAMs). Further, we saw increased binding of ^{3}H-NS14492 to pig frontal cortex membranes when co-incubated with PNU-120596, a type II PAM. Taken together, these findings show that ^{3}H-NS14492 is a useful new in vitro radioligand for the pig α7 nicotinic receptor.

1. Introduction

Neuronal nicotinic acetylcholine receptors are a class of pentameric ligand-gated ion channels composed of α and β subunits that can assemble in a number of combinations. In the brain the heteromeric α4β2 and the homomeric α7 are the most common nicotinic receptors (Gotti et al., 2006). The α7 nicotinic receptors are widely distributed in the mammalian brain, with highest receptor density in hippocampus, hypothalamus, amygdala and the cerebral cortex, and lowest receptor density in cerebellum (Baddick and Marks, 2011). Maximum density (B_{max}) for neuronal α7 nicotinic receptors is 32–73 fmol/mg protein in rodents (Anderson et al., 2008; Whiteaker et al., 1999, 2008), 6 fmol/mg protein in macaque monkeys (Kulak et al., 2006) and 2–20 fmol/mg protein in humans (Anderson et al., 2008; Falk et al., 2003). Several lines of evidence suggest that the α7 nicotinic receptor is a promising drug target for cognitive impairments in brain diseases such as Alzheimer's disease and schizophrenia (Olincy and Freedman, 2012). These diseases are representing a large medical unmet need and much attention is paid on novel treatment opportunities, and in particular α7 nicotinic receptor agonists (Citrome, 2014; Citron, 2010).

In the search for novel α7 nicotinic receptor agonists in the treatment of CNS disorders, the ability to define receptor binding sites in the human brain in vivo is of major importance. Changes in binding density in a pathological setting and receptor occupancy of selective compounds in humans is investigated with positron emission tomography (PET) (Lee and Farde, 2006). We have previously demonstrated that ^{11}C-NS14492 is a selective α7 nicotinic acetylcholine receptor agonist PET radioligand (Ettrup et al., 2011). In order to compare PET data from in vivo studies with in vitro binding studies, we have tritiated NS14492 and charaterized the binding properties of this novel ligand. There are a few available α7 nicotinic acetylcholine receptor specific radioligands such as ^{125}I-α-bungarotoxin (^{125}I-BTX) but these have some disadvantages as radioligands. ^{125}I-BTX is a

Abbreviations: B_{max}, maximum density; ^{125}I-BTX, ^{125}I-α-bungarotoxin; K_d, dissociation constant; K_i, inhibition constant; NSB, non-specific binding; OD, optical density; PAM, positive allosteric modulator; SB, specific binding; TB, total binding; TE, tissue equivalent

* Correspondence to: Neurobiology Research Unit, Rigshospitalet, Blegdamsvej 9, DK-2100 Copenhagen, Denmark. Tel.: +45 3545 6701; fax: +45 3545 6713.
E-mail address: jens_mikkelsen@dadlnet.dk (J.D. Mikkelsen).

http://dx.doi.org/10.1016/j.ejphar.2015.04.036
0014-2999/

peptide antagonist that seems to display pseudo-reversible binding with slow kinetics, and it also binds with high affinity to muscle-type nicotinic receptor, to α8 and α9α10 containing receptors (Arias, 2000; Elgoyhen et al., 2001). [^{3}H]AZ11637326 was recently described (Gordon et al., 2010; Maier et al., 2011) and showed good binding properties in rat brain tissue with a dissociation constant (K_d) of 0.2 nM, but the ^{18}F fluorinated PET version of the same compound did not reveal specific binding in non-human primates (Ravert et al., 2013). Finally, [^{3}H]A-585,539 with sub-nanomolar K_ds in rat and human brain homogenate displayed good binding properties with low non-specific binding, but it has not been developed as a PET radioligand (Anderson et al., 2008).

In this study, we describe the radiosynthesis and binding characteristics for ^{3}H-NS14492 in the pig brain using autoradiography and homogenate binding assays.

2. Materials and methods

2.1. Synthesis of ^{3}H-NS14492

^{3}H-NS14492 was produced in a radiochemical reaction between desmethyl-NS14492 and tritiated methyl-iodide (Fig. 1). A reaction vial with a volume of 0.4 ml was charged with desmethyl-NS14492 (1.5 mg, 5.8 μmol) and then added acetone (0.3 ml). After dissolution of material, tetrabutylammonium hydroxide (20 μl, 1 M in methanol) was added followed by the addition of [H-3]methyl iodide (20 μl, 2.37 mCi). The vial was capped and heated to 50 °C for 2 h. After reaction the solution was evaporated by a flow of helium and the remaining solids re-dissolved in 10% ethanol in 0.l% phosphoric acid. High-performance liquid chromatography (HPLC) methods were used for purification. The solution was injected onto a Princeton Spher C30 200 Å (250 mm × 10.0 mm, 5 μm) column at a flow of 2.0 ml/min. Sample was eluted with 10% B: 0–50 min, 10–100% B: 50–51 min, 100% B: 51–56 min, 100–10% B: 56–57 min, 10% B: 57–60 min. A=0.1% phosphoric acid, B=96% ethanol. The excess of desmethyl-NS14492 was eluted between 14 and 20 min and the product was collected in two fractions from 24 to 30 min (10.6 MBq/ml) and 30–34 min (3.6 MBq/ml). The purified ^{3}H-NS14492 and the cold standard were analyzed on the same RP–HPLC system with 100 μl and 25 μl injection volumes using a separate column and injection port. Detection was performed using radiodetection (Bioscan Triathler equipped with CaF_2 Solid Scintillant 100 μl Flow Cell) and UV detection at 250 nm and 290 nm (Waters 2487). A Phenomenex Luna C18(2) (250 mm × 4.6 mm, 5 μm) column with a guard front was used with a flow of 1 ml/min. Samples were eluted with 10% B: 0–15 min, 10–100% B: 15–16 min, 100% B: 16–18 min, 100–10% B: 18–19 min and 10% B: 19–22 min. A=0.1% phosphoric acid, B=96% ethanol. The total yield of labeled compound was calculated to 2.25 mCi (yield: 95.0%) with a specific activity of 70 mCi/mmol.

2.2. Compounds

^{125}I-BTX ([^{125}I]-Tyr54) with high specific activity (2200 Ci/mmol) was purchased from Perkin-Elmer (Skovlunde, Denmark). EVP-6124 (Prickaerts et al., 2012), PNU-120596 (Hurst et al., 2005), SSR180711 (Biton et al., 2007; Pichat et al., 2007), TC-5619 (Hauser et al., 2009), AVL-3288 (also known as XY4083 and CCMI) (Ng et al., 2007), NS14492 and desmethyl-NS14492 were synthesized at NeuroSearch A/S, Denmark and received as a gift. (−)-nicotine hydrogen tartrate salt was purchased from Sigma-Aldrich (Brøndby, Denmark). All other reagents used were from Sigma-Aldrich and of analytical grade.

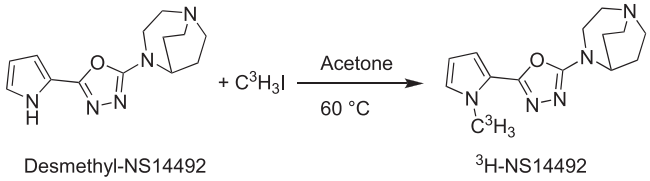

Fig. 1. Radiosynthesis of ^{3}H-NS14492.

2.3. Tissue sectioning

Brain tissue from three 2-month-old female Danish Landrace pigs was used for autoradiography and homogenate binding assay. Rapidly after euthanasia (intravenous injection of pentobarbital), brains were excised, separated sagitally in two hemispheres and frozen on dry ice, before being stored at −80 °C. Coronal serial sections of 12 μm containing frontal cortex were cut on a HM500OM Cryostat (Microm Intl GmbH, Walldorf, Germany) at −20 °C, thaw mounted on SuperFrost Plus glass slides (Thermo Scientific, Hvidovre, Denmark) with two sections per slide, air dried and stored at −80 °C until use.

2.4. Autoradiography

Slides were allowed to reach room temperature, and then pre-incubated in buffer (50 mM Tris–HCl, 4 mM $CaCl_2$, 0.1% bovine serum albumin (BSA), 120 mM NaCl, 5 mM KCl, pH 7.4) under constant gentle shaking for 25 min. Slides were then incubated for 2 h under constant gentle shaking in buffer with ^{3}H-NS14492 in serial dilutions (0.15 − 20 nM) in duplicate. Non-specific binding (NSB) was determined in the presence of 10 μM SSR180711 in both incubation steps. Slides were washed for 2 min × 2 min in ice cold buffer followed by a quick dip in ice cold distilled water, dried and placed overnight in paraformaldehyde vapor at 4 °C. Slides were left to dry for 2 h in a dessicator at room temperature before being exposed to a BAS TR2040 tritium sensitive imaging plate (IP) (Fujifilm, Tokyo, Japan) in a BAS-2040 cassette for 14 days at 4 °C along with a set of high and low activity tritium standards (^{3}H-microscales: equivalent to 0.07 − 33.4 nCi/mg tissue; GE Healthcare, Little Chalfont, UK). The IP was scanned in a BAS-2500 (Fujifilm) scanner. A number of steps in this procedure were optimized: This included testing of different buffers, incubation temperature, washing procedure and pH in the buffer.

It was investigated whether unlabeled NS14492 (0.32 nM − 1 μM) could displace 0.5 nM ^{125}I-BTX, the antagonist reference ligand used for α7 nicotinic receptor autoradiography. NSB was determined in the presence of 1 mM (−)-nicotine. The procedure was similar to ^{3}H-NS14492 autoradiography with some exceptions: 30 min pre-incubation in buffer (50 mM Tris–HCl, 0.1% BSA, pH 7.4), followed by 2 h of incubation in buffer. Slides were washed 2 min × 30 min in ice cold buffer followed by a quick dip in distilled water, and left to dry overnight. Slides were exposed for 6 h to a BAS-MS IP.

Receptor binding was quantified by measuring the optical density (OD) in a hand-drawn region of interest (ROI) on the autoradiogram in a prominent dorsal sulcus. The images were analyzed using Quantity One version 6.4.9 (Bio-Rad, CA, USA). Mean OD was converted to ligand binding using an equation derived from fitting the OD of the measured microscales to the decay-corrected tissue equivalent (TE) values. ^{125}I-BTX binding was measured with OD as main outcome measure. Specific binding (SB) was calculated as total binding (TB) minus NSB for the same region in adjacent sections.

2.5. Membrane preparation

A part of the pig frontal cortex containing white and gray matter was dissected and homogenized with a Polytron homogenizer for 10 s in 10 volumes of buffer (50 mM Tris–HCl, 150 mM

NaCl, 20 mM EDTA, pH 7.4) until a uniform texture was reached. Brain homogenates were centrifuged at 33,000 × g for 10 min. The pellet was homogenized in lysis buffer (5 mM Tris–HCl, 5 mM EDTA) and left to stand for 10 min. After centrifugation at 1000 × g for 1 min, supernatant was collected and this procedure was repeated once. The collected supernatant was centrifuged at 33,000 × g for 10 min and the final membrane fraction pellet was resuspended in assay buffer (50 mM Tris–HCl). Samples and buffers were kept on ice, and centrifugation was performed at 0–2 °C. Protein concentration was measured using a Bio-Rad Protein Assay with a BSA standard dilution.

2.6. Homogenate binding assay

Initial optimization of assay conditions was performed to maximize TB and minimize NSB. Parameters examined included buffer composition and temperature and ratio of radioligand to membrane concentration. In this optimized setup saturation binding assay was conducted with serial dilutions of ^{3}H-NS14492 (0.037 − 9 nM) in duplicate. NSB was determined in the presence of 10 μM SSR180711. Homogenate containing ~200 μg total protein was added to assay buffer (100 mM Tris–HCl, 4 mM $CaCl_2$, 120 mM NaCl, 5 mM KCl, 0.3% BSA, pH 7.4) to a final volume of 1 ml. Samples were incubated at 4 °C for 2 h under constant gentle shaking. A 24 well harvester (Brandel, MD, USA) was cooled down by pumping ice cold water through the system and just before end of incubation ice cold buffer was perfused. Bound radioligand was collected in Whatman GF/B glass microfiber filter (GE Healthcare, Little Chalfont, UK) pre-moistened with 1% polyethylenimine by vacuum filtration. Filters were washed with buffer (4 ml × 10 ml), placed in scintillation vials with 2 ml Ultima Gold scintillation solution (Perkin-Elmer) and stored overnight at 4 °C before being counted in a Tri-Carb 2900TR Liquid Scintillation analyzer (Packard, CT, USA), counting efficiency = 60%. Competition binding assays were performed to determine inhibition constants (K_i) for a number of α7 nicotinic receptor agonists; SSR180711, EVP-6124, TC-5619, unlabeled NS14492 and (−)-nicotine and the positive allosteric modulators (PAM) AVL-3288 and PNU-120596. All compounds were tested in concentrations of serial dilutions in duplicate against 2.5 nM ^{3}H-NS14492. (−)-Nicotine was tested in a concentration range of 1.6 nM–125 μM, whereas all other compounds were tested in a range of 40 pM–3.125 μM. NSB were determined in the presence of 10 μM SSR180711 or 10 μM EVP-6124 for K_i determination of SSR180711. Inhibition curves were generated by plotting specific binding against the logarithm to competing ligand concentration and a one-site function was applied fitting K_i directly based on ^{3}H-NS14492 concentration and K_d. An additional binding assay was conducted with 100 pM PNU-120596 in triplicate with 2.5 nM ^{3}H-NS14492 and compared to specific binding in a baseline setting without PNU-120596 but with NSB determined in the presence of 10 μM SSR180711.

2.7. Data analysis

All curve fitting (competition, saturation, and kinetic data) was performed using interactive, nonlinear, least-squares curve-fitting programs of GraphPad Prism version 6.0 (GraphPad Software, San Diego, CA). All statistical tests were performed using Prism version 6.0 (GraphPad software). *P*-values below 0.05 were considered statistically significant. Results are expressed as mean ± standard deviation (S.D.) unless otherwise stated.

3. Results

3.1. Autoradiography

Binding of ^{3}H-NS14492 in pig brain sections was saturable and nonlinear regression analysis of SB revealed a K_d of 2.1 ± 0.7 nM and a B_{max} of 15.7 ± 2.0 fmol/mg TE (n = 5) (Fig. 2 and Table 1). ^{3}H-NS14492 binding showed laminar distribution in gray matter with highest density in the superficial cortical layers, and in particular laterally and dorsally (Fig. 3C and E). The ability of unlabeled NS14492 to displace 0.5 nM ^{125}I-BTX was tested on similar sections with increasing concentrations of NS14492. In this setup K_i was determined to be 23 nM (^{125}I-BTX K_d = 0.45 nM), and at the highest concentration of unlabeled NS14492 (1 μM), 81% of ^{125}I-BTX was displaced compared to NSB (1 mM (−)-nicotine) (Fig. 4). Autoradiography revealed a structural distribution of ^{3}H-NS14492 binding comparable to that of ^{125}I-BTX (Fig. 3A), which also bound with a laminar pattern and with the ability to distinguish gray and white matter.

3.2. Homogenate binding assays

Binding of ^{3}H-NS14492 was measured using an optimized protocol in pig frontal cortex homogenate. Here, SB was saturable and nonlinear regression analysis revealed a K_d of 0.8 ± 0.3 nM and a B_{max} of 30.2 ± 11.6 fmol/mg protein at 4 °C (n = 8) (Fig. 5 and Table 1).

Binding properties of ^{3}H-NS14492 were assessed by examining its displacement by other α7 nicotinic receptor agonists and PAMs from pig brain homogenate. The α7 nicotinic receptor agonists TC-5619 (Fig. 6A), EVP-6124 (Fig. 6B), SSR180711 (Fig. 6C), and the cold ligand NS14492 (Fig. 6D) were found to displace ^{3}H-NS14492 binding with similar rank order of affinity in the nanomolar range. By contrast, (−)-nicotine (Fig. 6E) displaced ^{3}H-NS14492 binding with 2–3 orders of magnitude lower affinity (see Table 2). The two α7 nicotinic receptor PAMs, AVL-3288 (Fig. 6F) and PNU-120592 (Fig. 7A), were unable to displace ^{3}H-NS14492 binding at the full concentration range up to 0.1 mM.

PNU-120596 does seem to display an inhibition curve (Fig. 7A), but in fact the lowest specific binding reached at 10 μM PNU-120596 was still 95 ± 4% of baseline, whereas lower concentrations of PNU-120596 generally achieved more than 100% specific binding compared to baseline. As an example, 25 pM PNU-120596 resulted in 136 ± 7% specific binding, and could indicate a

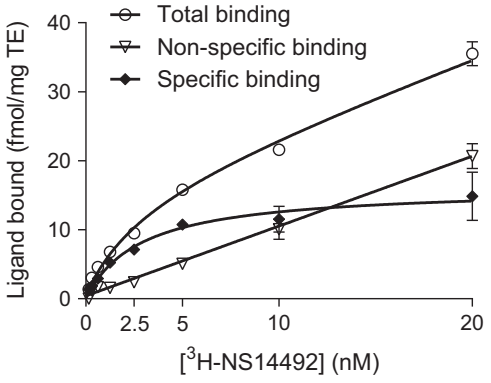

Fig. 2. Saturation binding of ^{3}H-NS14492. Binding of ^{3}H-NS14492 (0.15–20 nM) to 12 μm thick sections from pig frontal cortex. Non-specific binding (NSB) determined in the presence of 10 μM SSR180711. Specific binding (SB) (total binding (TB) minus NSB). Optical density of the autoradiograms was converted into ligand binding (fmol/mg tissue equivalent (TE)) using decay-corrected tritium microscales. Points represent mean value ± S.D. from a representative experiment in duplicate out of five independent experiments. Data from saturation binding experiments were analyzed by nonlinear regression. K_d and B_{max} values are shown in Table 1.

Table 1
K_d and B_{max} values from ^{3}H-NS14492 saturation binding analysis. TE; tissue equivalent.

Tissue	Method	K_d (nM)	B_{max}	n
Pig frontal cortex	Autoradiography	2.1 ± 0.7	15.7 ± 2.0 fmol/mg TE	5
Pig frontal cortex	Homogenate binding assays	0.8 ± 0.3	30.2 ± 11.6 fmol/mg protein	8

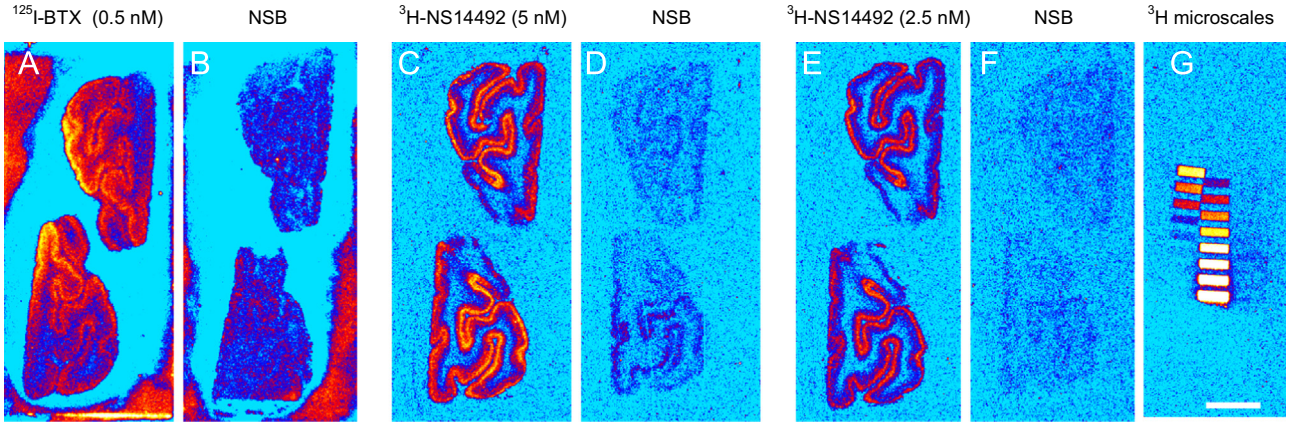

Fig. 3. Representative autoradiograms showing distribution of TB and NSB in sections of pig frontal cortex for 0.5 nM ^{125}I-BTX (A and B) and ^{3}H-NS14492 at concentrations 5 nM (C) and 2.5 nM (E). NSB determined in the presence of 1 mM (−)-nicotine (B) and 10 μM SSR180711 (D and F). ^{3}H microscales (G). Figures shown are from a representative experiment in duplicate out of five independent experiments for ^{3}H-NS14492 and from a single experiment in duplicate with ^{125}I-BTX. Scale bar = 1 cm.

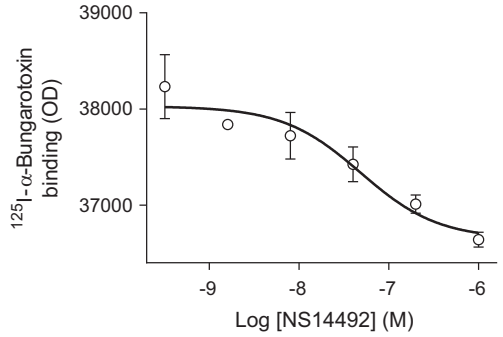

Fig. 4. Inhibition curve for displacement of ^{125}I-BTX with unlabeled NS14492 with fitted K_i value = 23 nM. Points represent mean value ± S.D. from an experiment in duplicate.

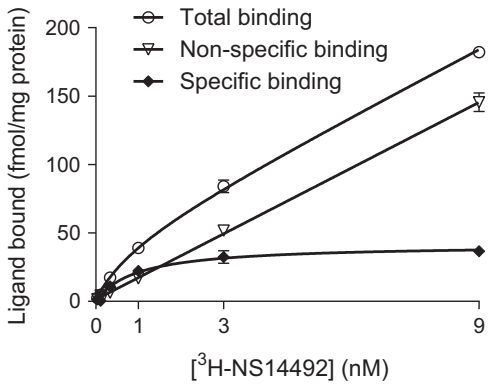

Fig. 5. Saturation binding of ^{3}H-NS14492 in homogenates. Binding of ^{3}H-NS14492 (0.037–9 nM) to homogenized tissue from pig frontal cortex at 4 °C. NSB determined in the presence of 10 μM SSR180711. SB (TB minus NSB). Points represent mean value ± S.D. from a representative experiment in duplicate out of eight independent experiments. Data from saturation binding experiments were analyzed by nonlinear regression. K_d and B_{max} values are shown in Table 1.

tendency toward enhancing ^{3}H-NS14492 binding to pig α7 nicotinic receptor. This experiment was repeated in triplicate (Fig. 7B). Again we saw no displacement, but a significant increase (169 ± 21% specific binding compared to baseline) at 100 pM PNU-120596 (Fig. 7B). AVL-3288 did not increase maximal binding (not shown).

4. Discussion

Here, we examined binding properties of ^{3}H-NS14492 in pig brain tissue to determine the utility of this radioligand for in vitro assessment of α7 nicotinic acetylcholine receptor occupancy. ^{3}H-NS14492 showed high-affinity and specific binding to α7 nicotinic receptors in the pig brain both in autoradiography and in homogenate binding assays. We have previously described the α7 nicotinic acetylcholine receptor selectivity of NS14492 (Ettrup et al., 2011), and this study further supports this finding. Saturation binding experiments revealed nanomolar K_d values: 2.1 ± 0.7 nM in autoradiography and 0.8 ± 0.3 nM in homogenate binding assays. There are small differences in K_d values between the two experimental methods used in this study. Notably, the optimal temperatures for the two methods were not the same as the incubation in autoradiography was conducted at room temperature versus 4 °C for homogenate binding assays. Lowering the temperature is known to decrease dissociation (k_{off}) more than association (k_{on}) rate constants and so lowering the K_d ($K_d = k_{off}/k_{on}$) (Hulme and Trevethick, 2010). A single autoradiography experiment assessing incubation temperature revealed a more than threefold lower K_d at 4 °C (K_d = 5.0 nM at room temperature versus K_d = 1.4 nM at 4 °C incubation) (data not shown) suggesting that the difference in incubation temperatures could indeed explain the differences in K_d values. The calculated B_{max} values, 15.7 ± 2.0 fmol/mg TE found in autoradiography and 30.2 ± 11.6 fmol/mg protein in the homogenate binding assay correlates to values found in macaque monkeys (Kulak et al., 2006), human (Anderson et al., 2008; Falk et al., 2003)

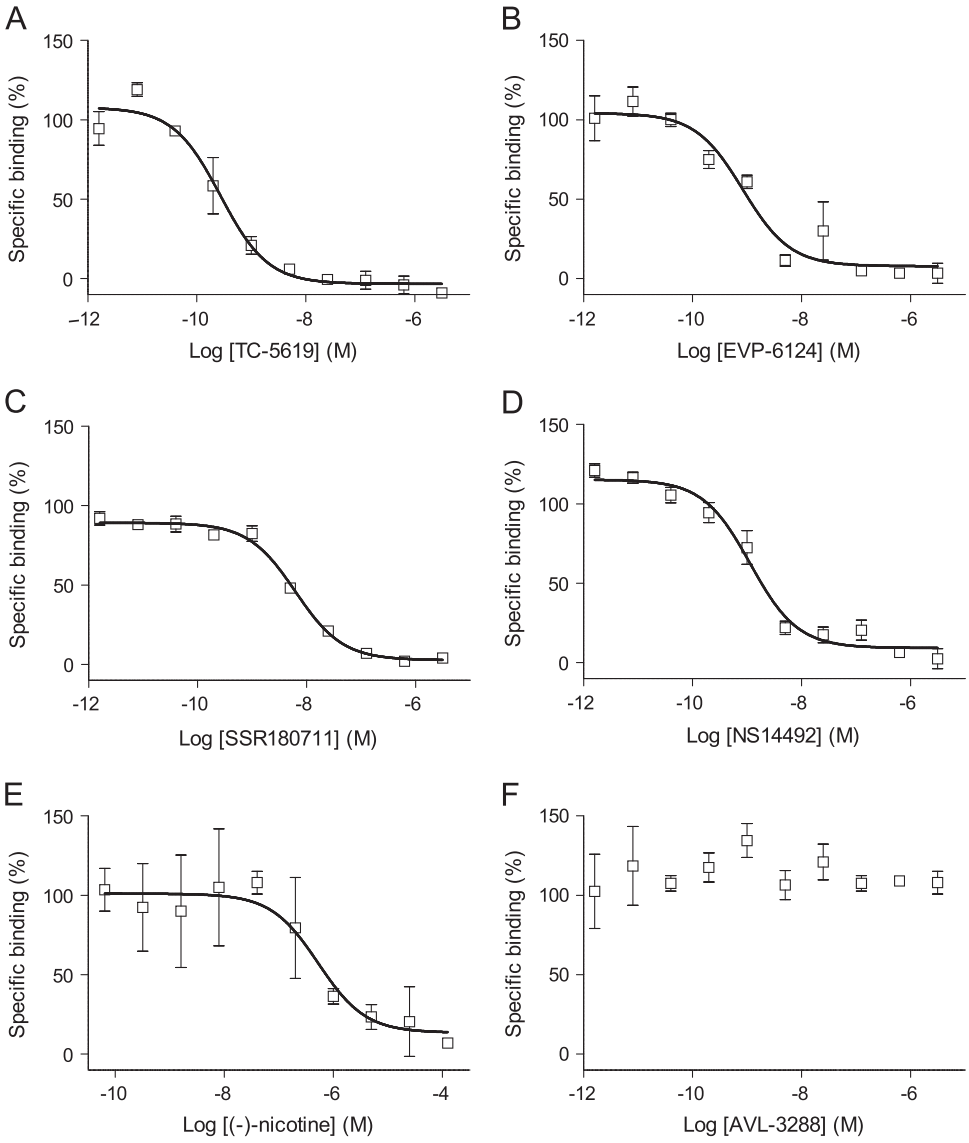

Fig. 6. Inhibition curves for displacement of 2.5 nM ^{3}H-NS14492 in pig brain cortical membranes shown as percent specific binding. (A) TC-5619, (B) EVP-6124, (C) SSR180711, (D) NS14492, (E) (−)-nicotine and (F) AVL-3288. Compounds ((A)–(D) and (F)) were tested in concentrations from 40 pM to 3.125 μM. (−)-nicotine (E) was tested in concentrations from 1.6 nM to 125 μM. Points represent mean value ± S.D. from a representative experiment in duplicate. K_i values were determined by fitting a one-site function to TB with defined ^{3}H-NS14492 concentration and K_d.

Table 2
Displacement of ^{3}H-NS14492 binding in pig brain homogenate. CI; 95% confidence interval.

Compound	K_i (nM)	95% CI
TC-5619	0.06	0.039 – 0.104
EVP-6124	0.19	0.095 – 0.396
NS14492	0.26	0.169 – 0.406
SSR180711	1.44	1.128 – 1.844
(−)-nicotine	123	30.64 – 494.4
AVL-3288	–	–
PNU-120596	–	–

and pig (Hoffmeister et al., 2011). However, it is important to keep in mind that species specific differences in the receptor structure may exist that could influence binding, and so complicating direct comparison of B_{max} values between species and between radioligands. The observed difference in B_{max} in the two assays is most likely due to the methodological differences as greater variation in B_{max} in the homogenized samples as compared to autoradiography was observed. The non-specific binding at concentrations near the K_d was less than 50% of TB in both assays and produced a robust signal at this concentration. When comparing this result to that reported for another in vitro radioligand [^{3}H]A-585539 tested in rat brain homogenate under comparable conditions (Anderson et al., 2008), we do observe more non-specific binding with ^{3}H-NS14492. Unlabeled NS14492 displaced 0.5 nM ^{125}I-BTX with a K_i=23 nM. However, even at 1 μM, NS14492 was only able to displace 81% of ^{125}I-BTX when compared to NSB (1 mM (−)-nicotine). This could indicate a lack of reversibility in BTX binding to the α7 nicotinic receptor, which has earlier been suggested (Gill et al., 2011). From this comparison it is also evident that ^{3}H-NS14492 offers a higher discriminative resolution and a more clearly defined laminar binding distribution than ^{125}I-BTX.

Displacement of ^{3}H-NS14492 binding in pig frontal cortex homogenate with structurally different α7 nicotinic acetylcholine receptor selective modulators revealed a binding potency rank order of the orthosteric compounds with TC-5619, EVP-6124, NS14492 and SSR180711 displaying affinities in the nanomolar range and (−)-nicotine in the lower micromolar range. As

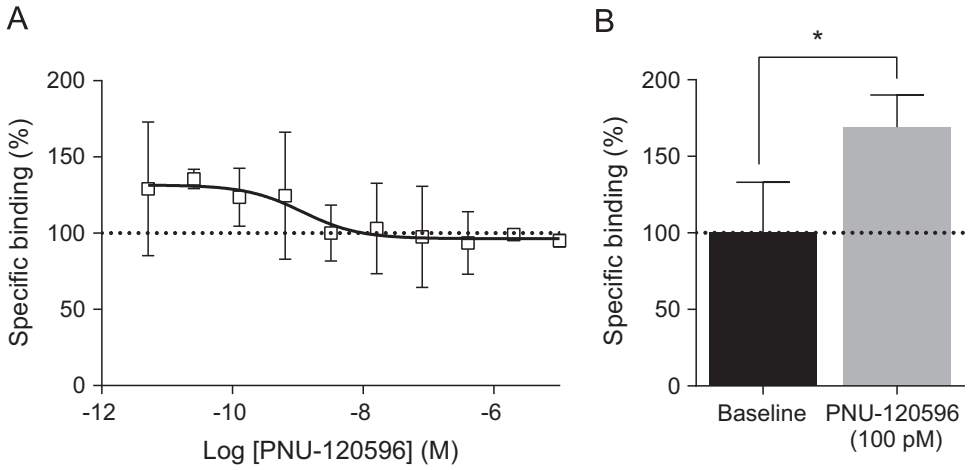

Fig. 7. Percent specific binding of 2.5 nM ^{3}H-NS14492 to homogenized tissue from pig frontal cortex co-incubated with PNU-120596. (A) Percent specific binding with PNU-120596 at concentrations from 5 pM to 10 μM. (B) Percent specific binding with the presence of 100 pM PNU-120596. NSB determined in the presence of 10 μM SSR180711. Points (A) represent mean value ± S.D. from a representative experiment in duplicate. Bars (B) represent mean value ± S.D. from an experiment in triplicate. $^{*}P < 0.05$ indicate significant difference from baseline in an unpaired *t*-test.

expected, the different allosteric modulators AVL-3288 and PNU-120596, were unable to displace the binding of ^{3}H-NS14492, as these compounds bind to a site different from the orthosteric agonist site. Interestingly, we found that the addition of PNU-120596 increased the maximal binding compared to a baseline setting. This greatly adds to the usability of ^{3}H-NS14492 as a tool for assessing pharmacological properties of both classical agonists but also functionally different compounds such as type II PAMs. It has recently been suggested that PNU-120596 works by decreasing the k_{off} rate in the equilibrium process (Szabo et al., 2014). This hypothesis may well fit with the observed increase in ^{3}H-NS14492 binding which could be explained by a shift in equilibrium favouring the bound state by lowering the rate of radioligand leaving the receptor-radioligand complex. In conclusion, we have here demonstrated that ^{3}H-NS14492 is a suitable radioligand for detection and quantification of amount and distribution of α7 nicotinic receptors in pig brain tissue.

Conflict of interest

DanPET AB (100% owned by Dan Peters, CEO) is the registered owner of the patent application WO/2011/058002 including ^{11}C-NS14492.

Acknowledgments

The authors thank Jonni Heberg for technical assistance. This work is supported by the Danish Strategic Research Council (COGNITO), Denmark, CCJobs and FBÖ TransTechTrans.

References

Anderson, D.J., Bunnelle, W., Surber, B., Du, J., Surowy, C., Tribollet, E., Marguerat, A., Bertrand, D., Gopalakrishnan, M., 2008. [^{3}H]A-585539 [(1S,4S)-2,2-dimethyl-5-(6-phenylpyridazin-3-yl)-5-aza-2-azoniabicyclo[2.2.1]heptane], a novel high-affinity alpha7 neuronal nicotinic receptor agonist: radioligand binding characterization to rat and human brain. J. Pharm. Exp. Ther. 324, 179–187.

Arias, H.R., 2000. Localization of agonist and competitive antagonist binding sites on nicotinic acetylcholine receptors. Neurochem. Int. 36, 595–645.

Baddick, C.G., Marks, M.J., 2011. An autoradiographic survey of mouse brain nicotinic acetylcholine receptors defined by null mutants. Biochem. Pharmacol. 82, 828–841.

Biton, B., Bergis, O.E., Galli, F., Nedelec, A., Lochead, A.W., Jegham, S., Godet, D., Lanneau, C., Santamaria, R., Chesney, F., Leonardon, J., Granger, P., Debono, M. W., Bohme, G.A., Sgard, F., Besnard, F., Graham, D., Coste, A., Oblin, A., Curet, O., Vige, R., Voltz, C., Rouquier, L., Souilhac, J., Santucci, V., Gueudet, C., Francon, D., Steinberg, R., Griebel, G., Oury-Donat, F., George, P., Avenet, P., Scatton, B., 2007. SSR180711, a novel selective alpha7 nicotinic receptor partial agonist: (1) binding and functional profile. Neuropsychopharmacology 32, 1–16.

Citrome, L., 2014. Unmet needs in the treatment of schizophrenia: new targets to help different symptom domains. J. Clin. Psychiatry 75 (Suppl 1), 21–26.

Citron, M., 2010. Alzheimer's disease: strategies for disease modification. Nat. Rev. Drug Discov. 9, 387–398.

Elgoyhen, A.B., Vetter, D.E., Katz, E., Rothlin, C.V., Heinemann, S.F., Boulter, J., 2001. alpha10: a determinant of nicotinic cholinergic receptor function in mammalian vestibular and cochlear mechanosensory hair cells. Proc. Natl. Acad. Sci. 98, 3501–3506.

Ettrup, A., Mikkelsen, J.D., Lehel, S., Madsen, J., Nielsen, E.O., Palner, M., Timmermann, D.B., Peters, D., Knudsen, G.M., 2011. ^{11}C-NS14492 as a novel PET radioligand for imaging cerebral alpha7 nicotinic acetylcholine receptors: in vivo evaluation and drug occupancy measurements. J. Nucl. Med. 52, 1449–1456.

Falk, L., Nordberg, A., Seiger, A., Kjaeldgaard, A., Hellstrom-Lindahl, E., 2003. Higher expression of alpha7 nicotinic acetylcholine receptors in human fetal compared to adult brain. Brain Res. Dev. Brain Res. 142, 151–160.

Gill, J.K., Savolainen, M., Young, G.T., Zwart, R., Sher, E., Millar, N.S., 2011. Agonist activation of alpha7 nicotinic acetylcholine receptors via an allosteric transmembrane site. Proc. Natl. Acad. Sci. 108, 5867–5872.

Gordon, J.C., Phillips, E., Gurley, D.A., Heys, J.R., Lazor, L.A., Barthlow, H.G., Mallamaci, M.A., Keith, R.A., 2010. In vitro binding characteristics of [^{3}H] AZ11637326, a novel alpha7-selective neuronal nicotinic receptor agonist radioligand. Eur. J. Pharmacol. 645, 63–69.

Gotti, C., Zoli, M., Clementi, F., 2006. Brain nicotinic acetylcholine receptors: native subtypes and their relevance. Trends Pharmacol. Sci. 27, 482–491.

Hauser, T.A., Kucinski, A., Jordan, K.G., Gatto, G.J., Wersinger, S.R., Hesse, R.A., Stachowiak, E.K., Stachowiak, M.K., Papke, R.L., Lippiello, P.M., Bencherif, M., 2009. TC-5619: an alpha7 neuronal nicotinic receptor-selective agonist that demonstrates efficacy in animal models of the positive and negative symptoms and cognitive dysfunction of schizophrenia. Biochem. Pharmacol. 78, 803–812.

Hoffmeister, P.G., Donat, C.K., Schuhmann, M.U., Voigt, C., Walter, B., Nieber, K., Meixensberger, J., Bauer, R., Brust, P., 2011. Traumatic brain injury elicits similar alterations in alpha7 nicotinic receptor density in two different experimental models. Neuromol. Med. 13, 44–53.

Hulme, E.C., Trevethick, M.A., 2010. Ligand binding assays at equilibrium: validation and interpretation. Br. J. Pharmacol. 161, 1219–1237.

Hurst, R.S., Hajos, M., Raggenbass, M., Wall, T.M., Higdon, N.R., Lawson, J.A., Rutherford-Root, K.L., Berkenpas, M.B., Hoffmann, W.E., Piotrowski, D.W., Groppi, V.E., Allaman, G., Ogier, R., Bertrand, S., Bertrand, D., Arneric, S.P., 2005. A novel positive allosteric modulator of the alpha7 neuronal nicotinic acetylcholine receptor: in vitro and in vivo characterization. J. Neurosci. 25, 4396–4405.

Kulak, J.M., Carroll, F.I., Schneider, J.S., 2006. [^{125}I]Iodomethyllycaconitine binds to alpha7 nicotinic acetylcholine receptors in monkey brain. Eur. J. Neurosci. 23, 2604–2610.

Lee, C.M., Farde, L., 2006. Using positron emission tomography to facilitate CNS drug development. Trends Pharmacol. Sci. 27, 310–316.

Maier, D.L., Hill, G., Ding, M., Tuke, D., Einstein, E., Gurley, D., Gordon, J.C., Bock, M.J., Smith, J.S., Bialecki, R., Eisman, M., Elmore, C.S., Werkheiser, J.L., 2011. Preclinical validation of a novel alpha-7 nicotinic receptor radiotracer, [(^{3})H] AZ11637326: target localization, biodistribution and ligand occupancy in the rat brain. Neuropharmacology 61, 161–171.

Ng, H.J., Whittemore, E.R., Tran, M.B., Hogenkamp, D.J., Broide, R.S., Johnstone, T.B., Zheng, L., Stevens, K.E., Gee, K.W., 2007. Nootropic alpha7 nicotinic receptor allosteric modulator derived from GABAA receptor modulators. Proc. Natl. Acad. Sci. 104, 8059–8064.

Olincy, A., Freedman, R., 2012. Nicotinic mechanisms in the treatment of psychotic disorders: a focus on the alpha7 nicotinic receptor. Handb. Exp. Pharmacol. 213, 211–232.

Pichat, P., Bergis, O.E., Terranova, J.P., Urani, A., Duarte, C., Santucci, V., Gueudet, C., Voltz, C., Steinberg, R., Stemmelin, J., Oury-Donat, F., Avenet, P., Griebel, G., Scatton, B., 2007. SSR180711, a novel selective alpha7 nicotinic receptor partial agonist: (II) efficacy in experimental models predictive of activity against cognitive symptoms of schizophrenia. Neuropsychopharmacology 32, 17–34.

Prickaerts, J., van Goethem, N.P., Chesworth, R., Shapiro, G., Boess, F.G., Methfessel, C., Reneerkens, O.A., Flood, D.G., Hilt, D., Gawryl, M., Bertrand, S., Bertrand, D., Konig, G., 2012. EVP-6124, a novel and selective alpha7 nicotinic acetylcholine receptor partial agonist, improves memory performance by potentiating the acetylcholine response of alpha7 nicotinic acetylcholine receptors. Neuropharmacology 62, 1099–1110.

Ravert, H.T., Dorff, P., Foss, C.A., Mease, R.C., Fan, H., Holmquist, C.R., Phillips, E., McCarthy, D.J., Heys, J.R., Holt, D.P., Wang, Y., Endres, C.J., Dannals, R.F., Pomper, M.G., 2013. Radiochemical synthesis and in vivo evaluation of [^{18}F]AZ11637326: an agonist probe for the alpha7 nicotinic acetylcholine receptor. Nucl. Med. Biol. 40, 731–739.

Szabo, A.K., Pesti, K., Mike, A., Vizi, E.S., 2014. Mode of action of the positive modulator PNU-120596 on alpha7 nicotinic acetylcholine receptors. Neuropharmacology 81, 42–54.

Whiteaker, P., Davies, A.R., Marks, M.J., Blagbrough, I.S., Potter, B.V., Wolstenholme, A.J., Collins, A.C., Wonnacott, S., 1999. An autoradiographic study of the distribution of binding sites for the novel alpha7-selective nicotinic radioligand [^{3}H]-methyllycaconitine in the mouse brain. Eur. J. Neurosci. 11, 2689–2696.

Whiteaker, P., Marks, M.J., Christensen, S., Dowell, C., Collins, A.C., McIntosh, J.M., 2008. Synthesis and characterization of ^{125}I-alpha-conotoxin ArIB[V11L;V16A], a selective alpha7 nicotinic acetylcholine receptor antagonist. J. Exp. Pharmacol. Ther. 325, 910–919.

Paper II

Donovan, L. L., **Magnussen, J. H.**, Dyssegaard, A., Lehel, S., Hooker, J. M., Knudsen, G. M., & Hansen, H. D. (2020). Imaging HDACs in vivo: Cross-validation of the [11 C]Martinostat radioligand in the pig brain.
Molecular Imaging and Biology, *22*, 569-577,
doi:10.1007/s11307-019-01403-9

MOLECULAR IMAGING AND BIOLOGY

Mol Imaging Biol (2020) 22:569–577
DOI: 10.1007/s11307-019-01403-9

Published Online: 9 July 2019

WMIS World Molecular Imaging Society
esmi European Society for Molecular Imaging

Check for updates

RESEARCH ARTICLE

Imaging HDACs *In Vivo*: Cross-Validation of the [^{11}C]Martinostat Radioligand in the Pig Brain

L. L. Donovan,[1,2] J. H. Magnussen,[1] A. Dyssegaard,[1] S. Lehel,[3] J. M. Hooker,[4] G. M. Knudsen,[1,2] H. D. Hansen[1]

[1]*Neurobiology Research Unit and Center for NeuroPharm, Copenhagen University Hospital Rigshospitalet, 9 Blegdamsvej, 2100, Copenhagen O, Denmark*
[2]*Faculty of Health and Medical Sciences, University of Copenhagen, 2200, Copenhagen N, Denmark*
[3]*PET and Cyclotron Unit, Copenhagen University Hospital Rigshospitalet, 2100, Copenhagen O, Denmark*
[4]*MGH/HST A. A. Martinos Center for Biomedical Imaging, Massachusetts General Hospital, Charlestown, MA, 02129, USA*

Abstract

Purpose: With the emerging knowledge about the impact of epigenetic alterations on behavior and brain disorders, the ability to measure epigenetic alterations in brain tissue *in vivo* has become critically important. We present the first *in vivo*/*in vitro* cross-validation of the novel positron emission tomography (PET) radioligand [^{11}C]Martinostat in the pig brain with regard to its ability to measure histone deacetylase 1–3 (HDAC1–3) levels *in vivo.*

Procedures: Nine female Danish landrace pigs underwent 121-min dynamic PET scans with [^{11}C]Martinostat. We quantified [^{11}C]Martinostat uptake using both a simple ratio method and kinetic models with arterial input function. By the end of the scan, the animals were euthanized and the brains were extracted. We measured HDAC1–3 protein levels in frontal cortex, cerebellum vermis, and hippocampus and compared the protein levels and regional outcome values to the [^{11}C]Martinostat PET quantification.

Results: [^{11}C]Martinostat distributed widely across brain regions, with the highest uptake in the cerebellum vermis and the lowest in the olfactory bulbs. Based on the Akaike information criterion, the quantification was most reliably performed by Ichise MA1 kinetic modeling, but since the radioligand displayed very slow kinetics, we also calculated standard uptake value (SUV) ratios which correlated well with V_T. The western blots revealed higher brain tissue protein levels of HDAC1/2 compared to HDAC3, and HDAC1 and HDAC2 levels were highly correlated in all three investigated brain regions. The *in vivo* SUV ratio measure correlated well with the *in vitro* HDAC1–3 levels, whereas no correlation was found between V_T values and HDAC levels.

Conclusions: We found good correlation between *in vivo* measured SUV ratios and *in vitro* measures of HDAC 1–3 proteins, supporting that [^{11}C]Martinostat provides a good *in vivo* measure of the cerebral HDAC1–3 protein levels.

Key words: Positron emission tomography, Martinostat, Epigenetics, Histone deacetylase, Pig, Western blot, HDAC1, HDAC2, HDAC3, Brain

Electronic supplementary material The online version of this article (https://doi.org/10.1007/s11307-019-01403-9) contains supplementary material, which is available to authorized users.

Correspondence to: H. Hansen; *e-mail:* hanne.d.hansen@nru.dk

Introduction

Epigenetic modifying enzymes, such as histone deacetylase (HDAC), have received increasing attention over the last decades, since they have been recognized as part of the pathophysiology of multiple neurological and psychiatric pathologies, such as Parkinson's disease, Alzheimer's disease, and depression (for review, see [1, 2]), and are therefore potential diagnostic and therapeutic targets [3]. HDAC proteins are epigenetic modifiers which deacetylate histone tails, resulting in decreased gene transcription. Until the development of the positron emission tomography (PET) radioligand [^{11}C]Martinostat in 2014 [4], however, molecular investigations of cerebral epigenetic alterations had been confined to animal studies or postmortem human brain examinations.

[^{11}C]Martinostat is an adamantane-based hydroxamic acid, which is able to image HDAC paralogs 1, 2, and 3, and has very minimal off-target binding [4]. *In vitro* assays determined a partition coefficient (log D) of 2.03 for [^{11}C]Martinostat, and IC_{50} values in the nanomolar range for all three targets: HDAC1 = 0.3 nM, HDAC2 = 2.0 nM, and HDAC3 = 0.6 nM [4]. The radioligand has good brain penetrance, with a peak brain concentration after 20 min in non-human primates [5]. [^{11}C]Martinostat has been tested in rodents, non-human primates, and humans [3–7]; however, we report the first direct comparison of *in vitro* and *in vivo* measures of HDAC1–3. We chose to perform this cross-validation of [^{11}C]Martinostat in pigs, because the pig offers several advantages as an animal model compared to rodents: The brain is gyrencephalic like the human brain, and the size is substantially larger than that of mice and rats, which provides a better match to the spatial resolution of PET scans and a tremendous amount of postmortem tissue for further molecular investigations. Being a large animal, the pig also allows for acquiring an arterial input function during the PET scan, and this is a requirement to calculate the total distribution volume (V_T). Therefore, the increased housing cost and handling difficulties, compared to rodents, are made up for in data quality. Finally, studies in pigs are cheaper and the use of pigs is not considered as ethically challenging as in non-human primates. The use of pigs thus does not necessitate that they are reused for many different experiments, and this rules out concerns about carry-over effects from previous experiments. However, the Danish Landrace pigs used in this study is bred to grow fast, so longitudinal studies require a different breed of pigs, *e.g.*, Göttingen minipigs.

Materials and Methods

Radiochemistry

[^{11}C]Martinostat was prepared at the Copenhagen University Hospital Rigshospitalet using carbon-11 methyl iodide in a modified procedure, as described earlier by Wang et al. [4]. [^{11}C]Martinostat yields ranged from 235 to 730 MBq and molar radioactivity ranged from 30 to 709 GBq/μmol at end-of-synthesis.

Animals

Nine female pigs (crossbreed of Landrace × Yorkshire × Duroc) weighing 20–22 kg (approx. 9 weeks old) were used in the present study. Animals were sourced from a local farm and acclimatized for 7–9 days in an enriched environment prior to experiments. For PET scanning, anesthesia was induced approx. 3 h prior to scanning by i.m. injection of 0.13 ml/kg zoletil veterinary mixture (11.36 mg/mL xylazine, 11.36 mg/ml ketamine, 1.82 mg/ml butorphanol, 1.82 mg/ml methadone) and maintained by 15 mg/kg/h propofol infusion i.v. Femoral arteries and mammary veins were used for i.v. access. Endotracheal intubation allowed for ventilation with 20 % oxygen in air at 10 ml/kg. Urine catheter was placed to avoid discomfort and stress. The animals were closely monitored throughout the experiment, with peripheral O_2 and end-tidal CO_2 saturation, heart rate, blood pressure, and temperature. The animals were terminated by 15 ml pentobarbital/lidocaine i.v. injection. After euthanasia, the brains were swiftly removed, snap frozen on dry-ice, and stored at −80 °C until use. All animal procedures were performed in accordance with the European Commission's Directive 2010/63/EU, approved by the Danish Council of Animal Ethics (Journal no. 2012-15-2934-00156), and were in compliance with the ARRIVE guidelines.

PET Scanning Protocol

The pigs were PET-scanned with a high-resolution research tomograph (HRRT) scanner (CPS Innovations/Siemens, USA). Data acquisition lasted 121 min after a bolus injection of [^{11}C]Martinostat. Injected dose was 334.3 ± 99.1 MBq (mean ± SD) while injected mass was 0.87 ± 0.94 μg (mean ± SD). In one pig, we performed a self-blocking study with a bolus injection of 0.5 mg/kg cold Martinostat, administered immediately prior to injection of [^{11}C]Martinostat. The unlabeled Martinostat was dissolved in DMSO and diluted in sterile water to reach a 10 % DMSO solution.

Blood Sampling and Analyses

Manual arterial blood samples were drawn at 2.5, 5, 10, 20, 30, 45, 60, 90, and 121 min after injection, while an ABSS autosampler (Allogg Technology, Sweden) continuously measured arterial whole blood radioactivity during the first 30 min. Manual blood samples were collected for measurements of total radioactivity in whole blood and plasma using a gamma well counter (Cobra 5003; Packard Instruments, Meriden, USA). Radiolabeled parent and metabolite

fractions were determined in plasma using an automatic column-switching radio-HPLC (high-performance liquid chromatography) as previously described [8], but with some modifications. Up to 4 ml of filtered but otherwise unadulterated plasma was loaded onto a Shimadzu Shimpack MAYI-ODS column (30 × 4.6 mm, 50 µm, Holm&Halby, Denmark) to trap lipophilic component of the plasma sample using a mixture of 20 mM disodium hydrogen phosphate, 2 mM sodium 1-decane sulfonate, and 2 % 2-propanol. The mobile phase was adjusted to pH 7.2 with phosphoric acid. After a 4-min extraction phase, the trapping column was eluted, by reversed direction of flow, with analysis eluent consisting of 24 % acetonitrile in 100 mM sodium dihydrogen phosphate (pH 2.6) containing 5 mM sodium 1-decane sulfonate. The analysis eluent was then passed through an analytical column (Onyx Monolithic C-18, 50 × 4.6 mm, Phenomenex Aps, Denmark) to separate the retained components. Flow rate was adjusted to 5 ml/min and the total analysis time was 8.5 min. To increase sensitivity in samples with low levels of radioactivity, eluents (10 ml) from the HPLC were collected with a fraction collector (Foxy Jr FC144; Teledyne, Lincoln, NE, USA), and fractions were counted offline in a gamma well counter (2480 Wizard2 Automatic Gamma Counter, Wallac Oy, Turku, Finland).

PET Quantification

The PET emission data was reconstructed into time frames of increasing lengths: 6 × 10, 6 × 20, 4 × 30, 9 × 60, 8 × 120, 4 × 180, 2 × 240, 1 × 300, 1 × 360, 1 × 420, 1 × 600, 1 × 900, 1 × 1680 s. The reconstruction used an ordinary Poisson three-dimensional ordered-subset expectation maximization with point spread function modeling (OP-3D-OSEM-PSF), 16 subsets and 10 iterations [9, 10] with all standard corrections. Attenuation correction was done using the HRRT maximum *a posteriori* transmission reconstruction method (MAP-TR) µ-map [11]. Images consist of 207 planes of 256 × 256 voxels of 1.22 × 1.22 × 1.22 mm in size.

Brain parcellation was performed according to the newly developed PET-MRI (magnetic resonance imaging) pig brain atlas method [12]. The input for the methodology was frame-length weighted, summed PET images of the total scan time (0–121 min). The extracted regional radioactive concentration (kBq/ml) was normalized to injected dose (MBq) and corrected for animal weight (kg) to give standardized uptake values (SUV, g/ml). The atlas contains 178 regions [13], but for the present study, only the cerebellum vermis, frontal cortex, hippocampus, and olfactory bulbs were compared to *in vitro* data. All graphical presentations were created using GraphPad Prism 7 (GraphPad, USA).

PMOD 3.7 (PMOD Technologies, Switzerland) was used for kinetic modeling. V_T values were calculated using the 1 tissue compartment (1TC), 2 tissue compartment (2TC), Ichise Multilinear Analysis 1 (MA1), and Logan invasive models. For the MA1 and Logan models, all model fits were visually inspected with regard to the residuals to determine an optimal threshold time (t*) for each region of interest (ROI), so to avoid frame-inclusion bias between scans. For each ROI and across all scans, we chose the earliest frame in which the residuals of the fit appeared normally distributed and in homoscedatic manner. For Logan modeling, t* was 28 in frontal cortex, hippocampus, and olfactory bulbs and 24 for cerebellum vermis. In MA1 modeling cerebellum vermis and frontal cortex, t* was 33, hippocampus 26, and olfactory bulbs 28.

For the self-block study, we calculated the occupancy and non-displaceable volume of distribution (V_{ND}) using the V_T values from the MA1 model in a Lassen plot [14]. Non-displaceable binding potentials (BP_{ND}) were determined by reverse calculations from MA1 V_Ts using the formula:

$$BP_{ND} = (V_T - V_{ND})/V_{ND}.$$

It has previously been suggested to use the SUV ratio (SUVR) as a simplified quantification method [5]; here, we used linear regression to find the time (x) where a plateau of the time-activity curve was reached (slope of line = 0). For each scan and each ROI, an average $SUV_{X\text{-}121}$ was calculated from timepoint x to the end of the scan (121 min). For the olfactory bulbs, which is here used as pseudo-reference region, the plateau was reached at 33 min. SUVRs are consequently calculated by dividing the ROI-$SUV_{X\text{-}121}$ by the corresponding olfactory bulbs $SUV_{33–121}$, providing a $SUVR_{X\text{-}121}$.

Nuclear Protein Extraction

Tissue samples from frontal cortex (605 mg ± 82), cerebellum vermis (424 mg ± 120), and hippocampus (537 mg ± 120) (n = 9/region) were used for nuclear protein extraction. Tissue was homogenized in 10 ml ice-cold lysis buffer containing 0.4 M sucrose, 10 mM HEPES (pH 8), 5 mM β-mercaptoethanol, protease inhibitor cocktail (P8340, Sigma-Aldrich) using a Polytron PT1200 (Kinematica, Switzerland). Volume was adjusted to 30 ml with ice-cold lysis buffer, followed by centrifugation (20 min 3000 *g* 4 °C). The pellet was resuspended in 1 ml ice-cold buffer 2 containing 0.25 M sucrose, 10 mM HEPES (pH 8), 1 % Triton X-100, 10 mM $MgCl_2$, 5 mM β-mercaptoethanol, protease inhibitor cocktail (P8340, Sigma-Aldrich), transferred to low-bind protein microtubes (Sarstedt, Germany), and centrifuged (10 min 12,000 *g* 4 °C). The pelleted nuclei were lysed by 30 min ice-incubation in RIPA buffer (150 mM NaCl, 1 % Triton X-100, 0.5 % sodiumdeoxycholate, 1 % sodium dodecyl sulfate, 50 mM Tris–HCl, protease inhibitor cocktail (P8340, Sigma-

Aldrich)), followed by centrifugation (20 min 20,800 *g* 4 °C). Protein concentrations of the supernatants were determined using the *DC*™ Protein Assay (BioRad, USA) according to the manufacturer's protocol, including a serial dilution of known BSA concentration, and absorbance was measured by iMark Microplate Absorbance Reader (BioRad, USA).

Western Blotting

All reagents and equipment were from BioRad (USA), unless otherwise stated.

Nine micrograms nuclear protein was denatured in the presence of 4× Laemmli buffer supplemented with 10 % β-mercaptoethanol at 95 °C for 5 min. The samples were subjected to sodium dodecyl sulfate–polyacrylamide gel electrophoresis (SDS–PAGE) in Criterion™ TGX Stain-Free™ Precast Gels at 200 V, and followingly blotted onto Immun-Blot® low fluorescence polyvinylidene difluoride (PVDF) membranes using the Trans-Blot® Turbo™ 7 min standard program. After membrane washing 4× 5 min in TBS-T (10 % TBS pH 7.5, 0.1 % Tween-20), the membranes were blocked by 5 % Blotting-Grade Blocker in TBS for 1 h at RT. The membranes were incubated overnight at 4 °C in primary antibody solution with the following dilutions: HDAC1 1:10,000 (PA1–860, Thermo Scientific, USA), HDAC2 1:20,000 (PA1–861, Thermo Scientific, USA), HDAC3 1:1000 (PA1–862, Thermo Scientific, USA). Following 4× 5 min washing in TBS-T, the membranes were incubated in 1:2000 polyclonal goat anti-rabbit horseradish peroxidase (HRP)-conjugated secondary antibody (P0448, Dako, Denmark) for 1 h at RT. After washing the membrane 1× 15 min and 4× 5 min in TBS-T, Western Lightning ECL Pro (NEL121001EA, Perkin Elmer, USA) was used for visualization by 1 min incubation immediately before imaging by ChemiDoc XRS+.

Recombinant HDAC1–3 protein was kindly provided by Prof. Christian Olsen (Center for Biopharmaceuticals, University of Copenhagen). Calibration rows of known HDAC protein amounts were included in the workflow described above: HDAC1 5-250 ng (50,051, bpsbioscience, USA), HDAC2 5-250 ng (50,002, bpsbioscience, USA), and HDAC3 2.5-60 ng for frontal cortex and cerebellum vermis samples, and 1.25-40 ng for hippocampal samples (50,003, bpsbioscience, USA).

Image Lab 6.1 (BioRad, USA) was used for image analysis, with rolling disc (70 mm) background subtraction and total loaded protein normalization. Statistical tests were performed in GraphPad Prism 7 (GraphPad, USA). Quantified HDAC isoforms (X ng/µg nuclear protein) were directly correlated to one another. In order to compare the *in vitro* measured HDAC1–3 to the *in vivo* PET measure, the tissue volume and yield from protein extraction was corrected. Total HDAC per ml fresh brain tissue were determined as

$$\left(\frac{X\ nmol\ HDAC1{-}3}{9\ \mu g\ protein}\right) * \left(\frac{total\ mg\ protein\ extracted}{total\ mL\ tissue\ used\ for\ extraction}\right).$$

Results

Regional Distribution of HDAC Proteins

After injection of [^{11}C]Martinostat, we observed high brain uptake of the radioligand with a peak SUV of 4 in the cerebellum vermis. The kinetics of the radioligand was very slow, with no observable wash-out from any brain region during the 121 min acquisition time (Fig. 1a). [^{11}C]Martinostat showed a widespread regional distribution (Fig. 1d), with the highest uptake in cerebellum vermis and cortical areas and lowest uptake in olfactory bulbs and subcortical areas.

Self-Block Experiment

To investigate the specificity of [^{11}C]Martinostat, we co-administrated the radioligand with 0.5 mg/kg unlabeled Martinostat in a single pig. Co-administration reduced the radioactive signal substantially (Fig. 1e) and induced markedly faster radioligand kinetics (Fig. 1b), and all three regional time activity curves (TACs) approached that of the olfactory bulbs. As expected, blocking was associated with lower regional V_T values. The quantitative effect of co-administration of unlabeled Martinostat (0.5 mg/kg) was determined from the Lassen plot (Fig. 1c). We found 89 % occupancy of the administered Martinostat, and a V_{ND} of 2.87 ml/cm^3.

Parent Compound Data

[^{11}C]Martinostat administration caused a rapid peak in plasma radioactivity (Fig. 2c), which plateaued around 20 min after injection and with a slight increase occurring at around 60 min. A representative [^{11}C]Martinostat radiochromatogram at 30 min after radiotracer injection is shown in Fig. 2a. The plasma parent fraction of [^{11}C]Martinostat decreased during the acquisition time, with approx. 60 % intact radioligand left after 30 min and 20 % at 121 min (Fig. 2b). The parent fraction was fitted to a 1-exponential curve, for quantification.

Quantification

Quantification of [^{11}C]Martinostat was performed with the 1-tissue compartment (TC), 2TC, Logan invasive, and MA1 kinetic models. Visual inspection of the fits revealed a general poor fit of the 1TC model whereas the 2TC model

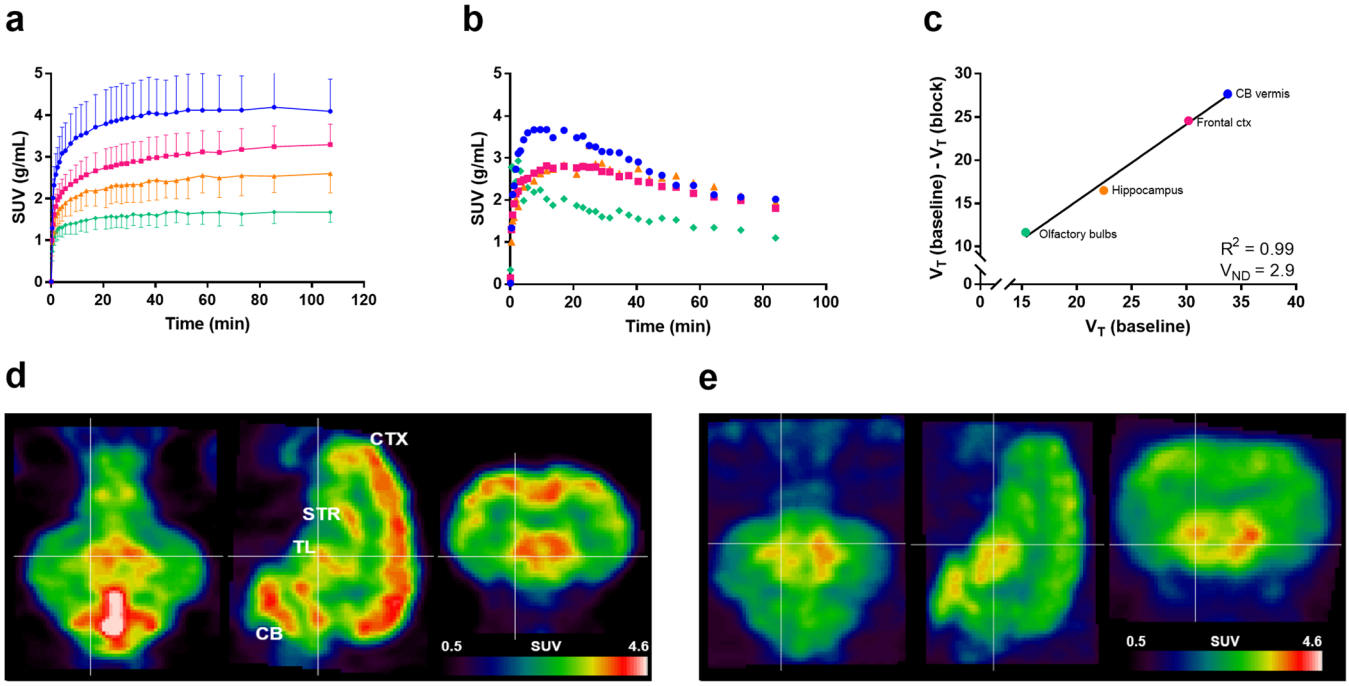

Fig. 1. Regional distribution and pharmacokinetics of [^{11}C]Martinostat in the pig brain. **a** Regional time-activity curves for [^{11}C]Martinostat at baseline (mean ± SD, $n = 13$). **b** Regional time-activity curves for [^{11}C]Martinostat after administration of 0.5 mg/kg unlabeled Martinostat. **c** Lassen plot showing regional differences in total distribution volumes (V_T) of [^{11}C]Martinostat before and after administration of 0.5 mg/kg Martinostat ($R^2 = 0.99$, $n = 1$). **d** A representative summed frame-length weighted PET image (0–121 min) of radioactivity in the pig brain following [^{11}C]Martinostat injection. **e** Summed frame-length weighted PET image (0–121 min) with 3 mm filter of radioactivity in the pig brain following 0.5 mg/kg unlabeled Martinostat injection circle cerebellum vermis, square frontal cortex, triangle Hippocampus, diamond olfactory bulbs. SUV standardized uptake values, V_T total distribution volume. CB cerebellum, TL thalamus, STR striatum, CTX cortex.

fitted the data well (Suppl. Fig. 1, see Electronic Supplementary Material (ESM)). The MA1 model also fitted the data well using individual t* for each ROI (see method section for t* determination). Similar to MA1 quantification, a ROI-specific t* was used for the Logan invasive model and the resulting V_Ts were similar to those from MA1 modeling (Table 1). Of all four models (Table 1), the MA1 model had the lowest Akaike information criterion (AIC) scores and therefore MA1 is considered the best model choice.

To evaluate test-retest variability within animals, four pigs were scanned twice. In three animals, the difference in V_T was in the order of 7–12 % in frontal cortex, but the fourth animal had a 39 % difference in V_T. However, in regard to the SUVRs, all four pigs had < 9 % difference between scans in frontal cortex.

Simplified Quantification

In the absence of an ideal reference region in the pig brain, we could not apply any reference tissue models to the data but Wey et al. [7] described the use of SUVR as an alternative and simplified quantification method. We found a relatively low V_{ND} in the pig brain, so we proceeded by investigating the use of SUVR as a BP_{ND} surrogate (Table 1). Whereas in the human brain, a white matter region was used a pseudo-reference region, we here chose to use the olfactory bulb, as this region had the lowest binding in the pig brain. For the SUVR method to be valid, the TACs need to remain relatively constant over time, and this was achieved at timepoints that differed between brain regions: olfactory bulbs = 33 min, cerebellum vermis = 39 min, hippocampus = 50 min, and frontal cortex = 68 min. Note, the radioligand kinetics in the frontal cortex was so slow, we only had three frames for calculating the SUVR in this region.

The BP_{ND}s calculated on the basis of MA1 generated V_Ts and self-blocking derived V_{ND} ($BP_{ND} = (V_T - V_{ND})/V_{ND}$), correlated well with the SUVRs (Suppl. Fig. 2a, see ESM).

Brain Tissue HDAC Determination

In vitro western blotting revealed substantial differences in protein amounts between the three HDAC subtypes: HDAC1 5 ± 1.5 ng/μg, HDAC2 18.7 ± 4.9 ng/μg, and HDAC3 1.7 ± 0.4 ng/μg nuclear protein (Fig. 3b). To examine if the large amount of HDAC2 was the major determinant of the *in vivo–in vitro* correlations, we also investigated the relationship between the HDACs themselves. We found strong positive correlation

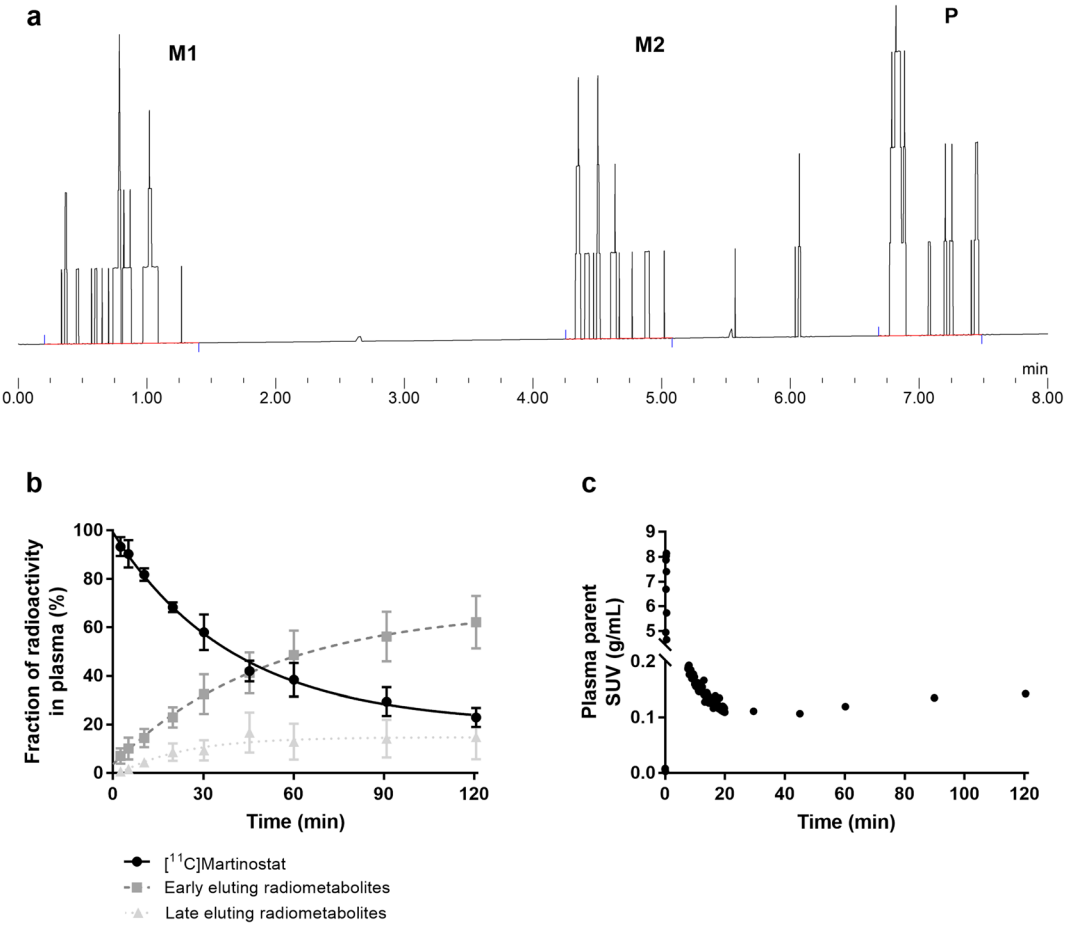

Fig. 2. [^{11}C]Martinostat parent compound. **a** Representative radiochromatogram 30 min after injection indicating the elution times of early (M1) and late (M2) eluting radiometabolites, and the parent compound [^{11}C]Martinostat (P) ($n = 1$). **b** Time course of the percentage of [^{11}C]Martinostat and metabolites measured in pig arterial plasma ($n = 10$). **c** Representative metabolite-corrected arterial input as a function of time after [^{11}C]Martinostat administration ($n = 1$).

between HDAC1 and HDAC2 in all three investigated brain regions ($R^2 = 0.78$ $p < 0.0001$, Fig. 3b). HDAC2 and HDAC3 levels were also correlated ($R^2 = 0.28$ $p = 0.004$, Fig. 3b), although the HDAC3 protein levels only differed slightly between regions.

We found a good correlation between *in vitro* HDAC levels, corrected for tissue volume and protein extraction yield, and the *in vivo* SUVR measure ($R^2 = 0.36$, $p = 0.001$, Fig. 3c), whereas the HDAC1–3 protein

Table 1. Regional total volumes of distribution (V_T) data resulting from four different arterial input models, non-displaceable binding potentials (BP_{ND}), and standardized uptake value ratio (SUVR)

		V_T (ml/cm^3)				BP_{ND}	
		1TC	2TC	Logan	MA1	MA1	$SUVR_{X-121}$
Frontal cortex	mean ± SD	36.9 ± 9.6	44.6 ± 10.6	40.7 ± 9	41.7 ± 9.1	13.5 ± 3.2	2 ± 0.2
	AIC	*4.4*	*− 34.4*	*124*	*− 16.1*	–	–
Hippocampus	mean ± SD	26.6 ± 5.3	34.6 ± 9.1	28.9 ± 6.2	30.8 ± 6.8	9.7 ± 2.4	1.5 ± 0.1
	AIC	*49.6*	*41.7*	*146*	*5.6*	–	–
Olfactory bulbs	mean ± SD	16.5 ± 3.7	20.9 ± 5	17.9 ± 3.3	18.9 ± 3.7	5.6 ± 1.3	–
	AIC	*61.3*	*46.2*	*142*	*2.4*	–	–
Cerebellum vermis	mean ± SD	42.6 ± 10.2	49.6 ± 12.5	45.5 ± 10	47.4 ± 10.6	15.5 ± 3.7	2.5 ± 0.3
	AIC	*17.4*	*− 19.3*	*147*	*− 11.5*	–	–

Data is presented as mean ± SD with the mean Akaike information criteria (AIC) below in italic. BP_{ND} was calculated by the formula $(V_T(ROI)-V_{ND})/V_{ND}$, using the MA1 determined V_T values. For SUVR calculations, an average SUV of time intervals described in the method section was used and the olfactory bulbs were used as pseudo-reference region

1TC 1 tissue compartment model, *2TC* 2 tissue compartment model, *MA1* Ichise multilinear analysis 1

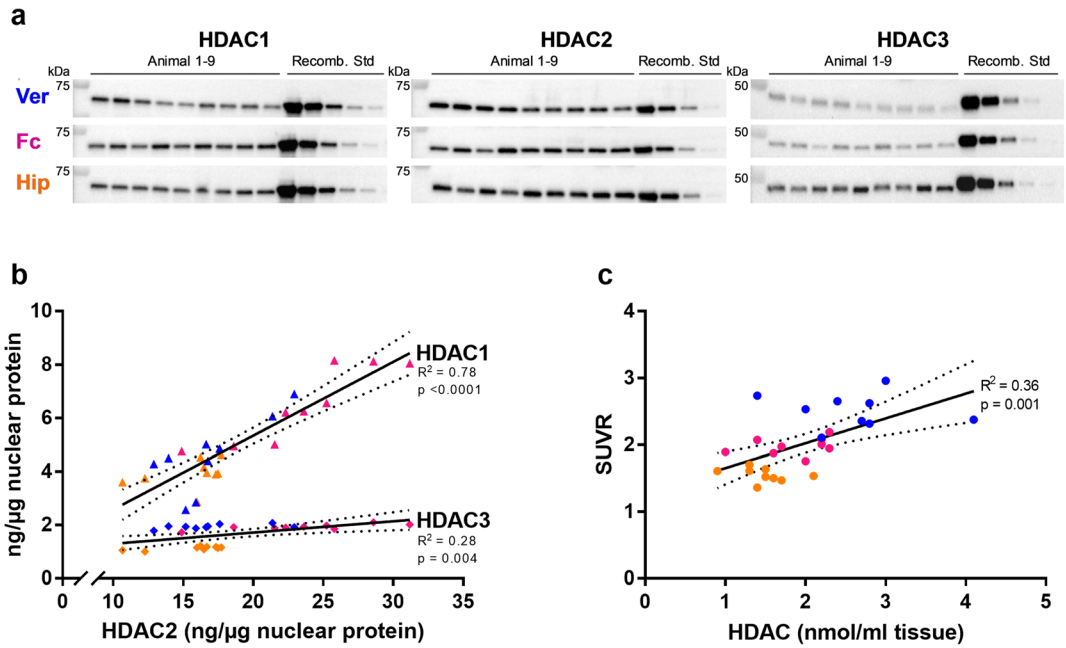

Fig. 3. Correlation between *in vivo* and *in vitro* measures of HDACs. **a** Equal amounts of nuclear protein from [^{11}C]Martinostat scanned pigs were quantified by human recombinant standards of HDAC1–3 through western blotting ($n = 9$, 3 brain regions). **b** Linear correlation between HDAC2 and either HDAC1 (triangle $R^2 = 0.78$ $p < 0.0001$) or HDAC3 (diamond $R^2 = 0.28$ $p = 0.0042$) in the three investigated brain regions ($n = 9$). **c** Linear correlation between the summed amounts of HDAC1–3, measured by western blotting and corrected for tissue volume and protein extraction yield, and the individual pig's corresponding SUVR, measured by [^{11}C]Martinostat PET imaging ($R^2 = 0.36$ $p = 0.001$ $n = 9$ pigs, three brain regions). ver cerebellum vermis (blue), fc frontal cortex (magenta), hip hippocampus (orange).

concentrations did not correlate with the V_T values ($p = 0.16$, Suppl. Fig. 3, see ESM).

Discussion

Here, we present for the first time an *in vivo–in vitro* cross-validation of the [^{11}C]Martinostat PET radioligand in pigs. We found a good correlation between HDAC1–3 proteins and the [^{11}C]Martinostat binding quantified with SUVR, supporting the use of [^{11}C]Martinostat PET for *in vivo* neuroimaging of HDAC1–3 .

The [^{11}C]Martinostat PET experiments in pigs revealed high brain uptake and slow radioligand kinetics, similar to what has been described in non-human primates [4, 5] and in humans [7]. We found uptake in both white and gray matter regions, which underscores the conserved nature of the proteins [15]. The highest brain uptake was found in the cerebellum vermis and the lowest in the olfactory bulbs.

Quantification of PET data was performed with four different arterial input kinetic models: 1TC, 2TC, Logan invasive, and MA1. All models produced similar V_T values, although the 1TC underestimated the binding slightly, which is evident by the model fit (Suppl. Fig. 3, see ESM). Given that the MA1 generated the lowest AIC values, we suggest this model to be the most appropriate kinetic model for quantification of [^{11}C]Martinostat in the pig brain. Previous studies in non-human primates and humans used the 2TC model to compute V_T values based on model fits assessed by AIC values and model selection criterion [4, 5, 7]. Furthermore, V_Ts from the Logan invasive model have shown good correlation with those from the 2TC model in non-human primates [5]. Our MA1 calculated V_Ts from the pig brain are in line with 2TC calculated V_Ts from the non-human primate brain, whereas the V_Ts from the human brain are in the order of 3–4 times lower, but V_{ND} in humans remains to be measured.

The self-block experiment revealed that 0.5 mg Martinostat/kg resulted in 89 % occupancy and that V_{ND} constitutes only about 6 % of V_T in high-binding regions and less than 16 % of V_T in low-binding regions, which means that [^{11}C]Martinostat has an excellent signal-to-noise ratio. The ROI with the lowest baseline binding, the olfactory bulbs, had a V_T value ~5 times higher than the V_{ND}, meaning that the pig brain has no ideal reference region that can be used for non-invasive reference tissue modeling. We also evaluated if the SUVR measure provides a good alternative to full kinetic modeling, as has been described in humans [7]. Indeed, SUVRs correlated well with the V_T values for the three pig brain regions investigated here (Suppl. Fig. 1b, see ESM), but for brain regions with particularly high [^{11}C]Martinostat binding, such as the frontal cortex, SUVR may be biased. This also indicates that long acquisition time is necessary, if SUVR is to be used as surrogate for BP_{ND}. Importantly, however,

SUVR may not be a suitable quantification method if the experimental setting involves interventions that alter radioligand kinetics. For a quantification model that would be compatible with altered kinetics of the radioligand, full arterial input modeling is necessary.

Using specific antibodies for HDAC1–3 and dilution rows of recombinant protein, we quantified the protein levels in three different brain regions: cerebellum vermis, frontal cortex, and hippocampus. We found 3–4 times higher levels of HDAC2 than HDAC1 and 2–3 times higher levels of HDAC1 than HDAC3 (HDAC2 > HDAC1 > HDAC3). The literature on brain tissue HDAC subtype quantification is sparse and results are inconsistent. In line with our results, Anderson et al. found HDAC1,2 >> HDAC3 in whole mouse brain lysate [16], whereas Wang et al. found protein levels to be HDAC3 > HDAC2 > HDAC1 in various mouse brain regions [17], and Chen et al. found HDAC2 > HDAC3 > HDAC1 in mouse cortex [18]. Generally, it seems that HDAC3 levels vary quite a lot between species and brain regions [7, 17].

We found a strong correlation between HDAC1 and HDAC2 protein levels, which is in line with previous reports [19, 20]. The reports found stronger correlation between HDAC1/2 and HDAC3, than what we found, but our samples had limited variability of HDAC3 levels, with similar levels in two out of three regions. Needless to say, had we included more than three regions, we would be able to make better conclusions regarding the inter-relationships, but that was not the scope of our validation study. Regardless of the described differences, there is a general agreement of the interplay and possible redundancy between the HDAC isoforms: Several reports show that knock-out of HDAC1 increases the levels of HDAC2, and *vice versa* [21, 22]. However, distinct roles have also been described, such as the necessity of HDAC2 for HDAC1 recruitment [23].

In our study, we conducted the correlation analysis between the PET measures and the summed concentration of the three HDAC subtypes. Since [^{11}C]Martinostat binds to the HDAC 1–3 with different affinities [4], we also tested if weighing the HDAC 1–3 protein concentration with their individual affinities would improve the association between [^{11}C]Martinostat PET and *in vitro* measures but that did not result in substantial improvements of the fit.

The *in vitro* measures of HDAC1–3 levels correlated well with the *in vivo* SUVR; however, we did not see a similar correlation with the V_T. Although the SUVR and V_Ts showed good correlation, the variation in the V_T values was much larger than in the SUVR. The SUVRs had test–retest variations < 9 % in the frontal cortex in all four scans, consistent with the previous report from Wey et al. on SUVRs of [^{11}C]Martinostat in the human brain [7].

In order to ensure that we examined the exact same brain regions in our *in vivo* and *in vitro* comparisons, we chose three anatomically well-defined and easily distinguishable regions that represented a good range of expected HDAC protein concentrations. Inclusion of more regions might have helped to establish an even firmer relationship, but three were deemed sufficient for our purpose. Also, we do recognize that our comparison assumes that the section used for *in vitro* western blotting are representative for the regions used for the PET quantification, *i.e.*, that HDAC protein concentrations only show small variations within the defined PET volume.

Anesthesia may potentially have confounding effect on experimental outcomes, but to the best of our knowledge, no one has reported an effect of propofol on the HDAC proteins. Isoflurane, on the other hand, has been shown to induce neurotoxicity in the developing hippocampus of rats, with HDACs playing an important role [24]. Further studies are needed to ensure that propofol does not affect the epigenetic machinery. In this study, however, all animals have received the same anesthetic regime and have been under anesthesia for the same duration of time. Therefore, we have no reason to believe that the anesthesia is affecting the comparison of data across animals. Also, the *in vitro* cross-validation was performed on the PET-scanned pigs, so a potential effect of anesthesia would not influence the correlations.

It may be seen as a limitation that we only investigated the blocking effect on the PET data of one dose (0.5 mg/kg) of Martinostat limiting us to just one estimate of V_{ND}. A better estimation of V_{ND} might have improved our estimate of BP_{ND}s, and this is also based on the assumption that the non-displaceable binding is similar across the animals.

The sample size in this study is relatively small; however, we are confident in the results given that the correlations are made across multiple brain regions, and we have performed technical replicates of the *in vitro* work. The olfactory bulbs are difficult to extract from the pig skull and are often lost during whole-brain extraction and accordingly, we were unfortunately unable to validate the olfactory bulbs *in vitro* as pseudo-reference region. In the absence of available porcine recombinant HDAC1–3 proteins, we used human recombinant protein to generate the calibration curves for the western blot. Because the proteins are well conserved across eukaryotes [25], we found it safe to assume similar affinity of the antibodies between species. Finally, for practical reasons, only adolescent females were used in this study but we find it reasonable to assume that our findings can be generalized to the fully developed adult brain as well as in both sexes.

The NCBI HomoloGene database reveals that the HDAC1–3 proteins are conserved across evolution, from fungi to plants and animals (HomoloGene ref no. 68426, 68187, and 48250 for HDAC 1, 2, and 3 respectively). More specifically, the NCBI protein BLAST function reveals the sequence similarity between pig and human is 99 %, 100 %, and 100 % for HDAC1, 2, and 3 respectively. Therefore, we believe that the function of the proteins is preserved through evolution, and our results is translatable and validates [^{11}C]Martinostat as a PET radioligand in pigs as well as humans.

Conclusions

We performed the first direct *in vivo*/*in vitro* cross-validation of the PET-radioligand [^{11}C]Martinostat. We found good correlation between *in vitro* quantified HDAC1–3 levels and *in vivo* measured SUVRs. We recommend to use SUVR as a good proxy for HDAC1–3 levels. We find that the changed kinetics after blocking of HDACs calls for a different quantification method, of which the MA1 model provides the best solution.

Acknowledgments. The authors would like to give thanks to C.A. Olsen for kindly providing recombinant HDAC proteins and the staff of Department of Experimental Medicine at University of Copenhagen for excellent assistance.

Funding information. This study was funded by The Lundbeck Foundation (grant no. R180-2014-3171 and R233-2016-3416).

Compliance with Ethical Standards

Conflict of Interest

LLD, GMK, and HDH report grants from The Lundbeck Foundation. JHM, AD, SL declare no conflict of interest. JMH reports grants from NIH, Brain and Behavior Foundation, CureAlz Foundation; non-financial support and other from MGH; personal fees from Rodin Therapeutics, Psy Therapeutics, Merck, NIMH, Evelop Biosciences, Treventis, American Chemical Society, SV Life Sciences, Sunovian, Vertex, Therapeutics; grants and personal fees from Alzheimer's Drug Discovery Foundation; and other from Eikonizo. In addition, Dr. Hooker has a patent PCT/US2O14/061179 with royalties paid to NucMedCor and Rodin Therapeutics (Previously).

References

1. Abel T, Zukin S (2008) Epigenetic targets of HDAC inhibitition in neurodegenerative and psychiartic disorders. Curr Opin Pharmacol 8:57–64
2. Penney J, Tsai L-H (2014) Histone deacetylases in memory and cognition. Neuroscience 7:3–10
3. Gilbert TM, Zürcher NR, Wu CJ, Bhanot A, Hightower BG, Kim M, Albrecht DS, Wey HY, Schroeder FA, Rodriguez-Thompson A, Morin TM, Hart KL, Pellegrini AM, Riley MM, Wang C, Stufflebeam SM, Haggarty SJ, Holt DJ, Loggia ML, Perlis RH, Brown HE, Roffman JL, Hooker JM (2018) PET neuroimaging reveals histone deacetylase dysregulation in schizophrenia. J Clin Invest 129:364–372. https://doi.org/10.1172/JCI123743
4. Wang C, Schroeder FA, Wey HY, Borra R, Wagner FF, Reis S, Kim SW, Holson EB, Haggarty SJ, Hooker JM (2014) In vivo imaging of histone deacetylases (HDACs) in the central nervous system and major peripheral organs. J Med Chem 57:7999–8009
5. Wey H-Y, Wang C, Schroeder FA, Schroeder FA, Logan J, Price JC, Hooker JM (2015) Kinetic analysis and quantification of [^{11}C]Martinostat for in vivo HDAC imaging of the brain. ACS Chem Neurosci 6:708–715
6. Schroeder FA, Wang C, Van De Bittner GC et al (2014) PET imaging demonstrates histone deacetylase target engagement and clarifies brain penetrance of known and novel small molecule inhibitors in rat. ACS Chem Neurosci 5:1055–1062
7. Wey H-Y, Gilbert TM, Zurcher NR et al (2016) Insights into neuroepigenetics through human histone deacetylase PET imaging. Sci Transl Med 8:351ra106. https://doi.org/10.1126/scitranslmed.aaf7551
8. Gillings N (2009) A restricted access material for rapid analysis of [11C]-labeled radiopharmaceuticals and their metabolites in plasma. Nucl Med Biol 36:961–965
9. Hong IK, Chung ST, Kim HK et al (2007) Ultra fast symmetry and SIMD-based projection-backprojection (SSP) algorithm for 3-D PET image reconstruction. IEEE Trans Med Imaging 6:789–803
10. Sureau FC, Reader AJ, Comtat C, Leroy C, Ribeiro MJ, Buvat I, Trebossen R (2008) Impact of image-space resolution modeling for studies with the high-resolution research tomograph. J Nucl Med 49:1000–1008
11. Keller SH, Svarer C, Sibomana M (2013) Attenuation correction for the HRRT PET-scanner using transmission scatter correction and total variation regularization. IEEE Trans Med Imaging 32:1611–1621
12. Villadsen J, Hansen HD, Jørgensen LM et al (2017) Automatic delineation of brain regions on MRI and PET images from the pig. J Neurosci Methods 294:51–58
13. Saikali S, Meurice P, Sauleau P, Eliat PA, Bellaud P, Randuineau G, Vérin M, Malbert CH (2010) A three-dimensional digital segmented and deformable brain atlas of the domestic pig. J Neurosci Methods 192:102–109
14. Cunningham VJ, E a R, Slifstein M et al (2010) Measuring drug occupancy in the absence of a reference region: the Lassen plot re-visited. J Cereb Blood Flow Metab 30:46–50
15. Seto E, Yoshida M (2014) Erasers of histone acetylation: the histone deacetylase enzymes. Cold Spring Harb Perspect Biol 6. https://doi.org/10.1101/cshperspect.a018713
16. Anderson KW, Chen J, Wang M, Mast N, Pikuleva IA, Turko IV (2015) Quantification of histone deacetylase isoforms in human frontal cortex, human retina, and mouse brain. PLoS One 10:e0126592. https://doi.org/10.1371/journal.pone.0126592
17. Wang Y, Zhang YL, Hennig K, Gale JP, Hong Y, Cha A, Riley M, Wagner F, Haggarty SJ, Holson E, Hooker J (2013) Class I HDAC imaging using [3H]CI-994 autoradiography. Epigenetics 8:756–764
18. Chen YT, Zang XF, Pan J, Zhu XL, Chen F, Chen ZB, Xu Y (2012) Expression patterns of histone deacetylases in experimental stroke and potential targets for neuroprotection. Clin Exp Pharmacol Physiol 39:751–758
19. Gu Y, Yang P, Shao Q et al (2013) Investigation of the expression patterns and correlation of DNA methyltransferases and class I histone deacetylases in ovarian cancer tissues. Oncol Lett 5:452–458
20. Quint K, Agaimy A, Di Fazio P et al (2011) Clinical significance of histone deacetylases 1, 2, 3, and 7: HDAC2 is an independent predictor of survival in HCC. Virchows Arch 459:129–139
21. Jurkin J, Zupkovitz G, Lagger S, Grausenburger R, Hagelkruys A, Kenner L, Seiser C (2011) Distinct and redundant functions of histone deacetylases HDAC1 and HDAC2 in proliferation and tumorigenesis. Cell Cycle 10:406–412
22. Wilting RH, Yanover E, Heideman MR, Jacobs H, Horner J, van der Torre J, DePinho RA, Dannenberg JH (2010) Overlapping functions of Hdac1 and Hdac2 in cell cycle regulation and haematopoiesis. EMBO J 29:2586–2597
23. Somanath P, Herndon Klein R, Knoepfler PS (2017) CRISPR-mediated HDAC2 disruption identifies two distinct classes of target genes in human cells. PLoS One 12:1–21
24. Joksimovic SM, Osuru HP, Oklopcic A et al (2018) Histone deacetylase inhibitor entinostat (MS-275) restores anesthesia-induced alteration of inhibitory synaptic transmission in the developing rat hippocampus. Mol Neurobiol 55:22–228
25. Gregoretti IV, Lee YM, Goodson HV (2004) Molecular evolution of the histone deacetylase family: functional implications of phylogenetic analysis. J Mol Biol 338:17–31

Paper III

Magnussen, J. H., Ettrup, A., Lehel, S., Peters, D., Dyssegaard, A., Thomsen, M. S., Mikkelsen, J.D., & Knudsen, G. M. (2024). Characterizing the binding of TC-5619 and encenicline on the alpha7 nicotinic acetylcholine receptor using PET imaging in the pig.
Frontiers in Neuroimaging. vol. 3. 27 Mar. 2024,
doi:10.3389/fnimg.2024.1358221

frontiers | Frontiers in Neuroimaging

TYPE Brief Research Report
PUBLISHED 27 March 2024
DOI 10.3389/fnimg.2024.1358221

OPEN ACCESS

EDITED BY
Khalil Hajiasgharzadeh,
Tabriz University of Medical Sciences, Iran

REVIEWED BY
Narges Dastmalchi,
University College of Nabi Akram, Iran
William Kem,
University of Florida, United States

*CORRESPONDENCE
Gitte M. Knudsen
✉ gmk@nru.dk

RECEIVED 19 December 2023
ACCEPTED 11 March 2024
PUBLISHED 27 March 2024

CITATION
Magnussen JH, Ettrup A, Lehel S, Peters D, Dyssegaard A, Thomsen MS, Mikkelsen JD and Knudsen GM (2024) Characterizing the binding of TC-5619 and encenicline on the alpha7 nicotinic acetylcholine receptor using PET imaging in the pig.
Front. Neuroimaging 3:1358221.
doi: 10.3389/fnimg.2024.1358221

Characterizing the binding of TC-5619 and encenicline on the alpha7 nicotinic acetylcholine receptor using PET imaging in the pig

Janus H. Magnussen[1,2], Anders Ettrup[1], Szabolcs Lehel[3], Dan Peters[4], Agnete Dyssegaard[1], Morten S. Thomsen[1,5], Jens D. Mikkelsen[1,6] and Gitte M. Knudsen[1,7]*

[1]Neurobiology Research Unit, Rigshospitalet, Copenhagen, Denmark, [2]Faculty of Health and Medical Sciences, University of Copenhagen, Copenhagen, Denmark, [3]PET and Cyclotron Unit, Rigshospitalet, Copenhagen, Denmark, [4]DanPET AB, Malmö, Sweden, [5]Department of Drug Design and Pharmacology, Faculty of Health and Medical Sciences, University of Copenhagen, Copenhagen, Denmark, [6]Institute of Neuroscience, University of Copenhagen, Copenhagen, Denmark, [7]Department of Clinical Medicine, University of Copenhagen, Copenhagen, Denmark

The alpha7 nicotinic acetylcholine receptor (α7-nAChR) has has long been considered a promising therapeutic target for addressing cognitive impairments associated with a spectrum of neurological and psychiatric disorders, including Alzheimer's disease and schizophrenia. However, despite this potential, clinical trials employing α7-nAChR (partial) agonists such as TC-5619 and encenicline (EVP-6124) have fallen short in demonstrating sufficient efficacy. We here investigate the target engagement of TC-5619 and encenicline in the pig brain by use of the α7-nAChR radioligand ^{11}C-NS14492 to characterize binding both with *in vitro* autoradiography and *in vivo* occupancy using positron emission tomography (PET). *In vitro* autoradiography demonstrates significant concentration-dependent binding of ^{11}C-NS14492, and both TC-5619 and encenicline can block this binding. Of particular significance, our *in vivo* investigations demonstrate that TC-5619 achieves substantial α7-nAChR occupancy, effectively blocking approximately 40% of α7-nAChR binding, whereas encenicline exhibits more limited α7-nAChR occupancy. This study underscores the importance of preclinical PET imaging and target engagement analysis in informing clinical trial strategies, including dosing decisions.

KEYWORDS

positron emission tomography (PET), alpha7, nicotinic acetylcholine receptors, autoradiography, occupancy study, cognitive impairment

Introduction

The alpha7 nicotinic acetylcholine receptor (α7-nAChR) is a homopentameric ligand-gated ion channel that is involved in the regulation of cognitive processes in normal conditions as well as is in the pathophysiology of some brain disorders. The receptor is composed of five identical α7 subunits, yielding an equal number of binding sites (Dani and Bertrand, 2007; Li et al., 2011). This receptor is widely distributed in the central nervous systems (CNS) and found with high densities in regions associated with cognitive functions (Tribollet et al., 2004; Wessler and Kirkpatrick, 2008). Of note, there is substantial evidence

for the presence of heteromeric α7-nAChRs in mammalian CNS, where α7 subunits co-assemble with β2 subunits to form functional α7β2-nAChR (Wu et al., 2016). The exact implications of the existence of this receptor are unknown. The homopentameric α7-nAChR has been investigated as a potential therapeutic target for addressing cognitive impairments associated with neurological and psychiatric diseases, including Alzheimer's disease and schizophrenia (Wallace and Porter, 2011). Over the past 20 years, several compounds have been developed to selectively target the α7-nAChR, demonstrating promising effects in enhancing cognitive functions in animal models (Thomsen et al., 2010). However, a significant translational challenge persists, as these encouraging preclinical outcomes have not translated into corresponding benefits in human clinical trials (Lewis et al., 2017). Some notable examples are TC-5619 from Targacept (Figure 1A), encenicline (EVP-6124) from Forum Pharmaceuticals (Figure 1B), and SSR180711 from Sanofi (Figure 1C). *In vitro*, TC-5619 is a full and potent α7-nAChR agonist reported to be effective in rodent models of schizophrenia (Hauser et al., 2009). Initially, in an exploratory 12-week randomized clinical phase 2 trial involving 185 subjects with schizophrenia, TC-5619 showed promising effects on cognitive endpoints and negative symptoms compared to placebo (Lieberman et al., 2013). However, in a clinical phase 2 trial lasting 24 weeks, TC-5619 failed to meet the primary outcome measure of change from baseline on the Scale for the Assessment of Negative Symptoms (SANS) compared to placebo (Walling et al., 2016). Additionally, TC-5619 did not demonstrate improvement in the key secondary measures of cognitive function (ClinicalTrials.gov identifier: NCT01488929) and further development was stopped (Targacept, 2013). SSR180711 is a partial α7-nAChR agonist (Biton et al., 2007) that has been shown to improve long-term and short-term episodic memory and spatial working memory in rodents (Pichat et al., 2007). The compound was tested in a placebo-controlled phase 2 clinical trial, spanning 4 weeks and three different dosage regimens, in patients with mild Alzheimer's disease (NCT00602680). However, the trial was prematurely terminated in 2008 due to an inadequate risk-benefit ratio, as documented on clinicaltrials.gov. Encenicline is a partial α7-nAChR agonist *in vitro* and it reverses a scopolamine-induced memory deficit *in vivo* in rats (Prickaerts et al., 2012). Despite encenicline showing effects in a proof-of-concept, randomized trial in patients with schizophrenia (Preskorn et al., 2014) and in mild-to-moderate Alzheimer's disease patients on functional and cognitive skills compared to placebo (Deardorff et al., 2015), this outcome was not confirmed in two larger global clinical phase 3 trials as the trials were put on hold due to severe gastrointestinal adverse effects (Alzforum, 2016). Further, encenicline is so far the only compound targeting the α7-nAChR that has been evaluated in a large-scale clinical phase 3 trial in schizophrenia patients, but no effect could be seen (Brannon, 2019) [see review by Terry and Callahan (2020)]. The lack of success in clinical trials involving α7-nAChR ligands in Alzheimer's disease or schizophrenia has reduced the enthusiasm for this target and consequently, many pharmaceutical companies have discontinued their research efforts in this field (Bertrand and Terry, 2018).

However, before discarding α7-nAChR as a viable target, it is worth noting that despite several large clinical trials, little information regarding the compounds' blood-brain barrier permeability, target involvement and the level of α7-nAChR occupancy has been published. For these purposes, molecular brain imaging emerges as a powerful tool capable of providing invaluable insights into target engagement and occupancy. Several α7-nAChR positron emission tomography (PET) radioligands have so far been tested: ^{18}F-ASEM was developed as an α7-nAChR antagonist with suitable binding properties (Horti et al., 2014) and tested in 21 healthy non-smoking volunteers and in 6 males with schizophrenia (Wong et al., 2014, 2018). We have also validated ^{11}C-NS14492 (Figure 1D) as a selective α7-nAChR agonist PET radioligand capable of measuring α7-nAChR occupancy of SSR180711 and unlabelled NS14492 in the pig brain (Ettrup et al., 2011b). This compound has been further described and validated as a tritiated *in vitro* radioligand (Magnussen et al., 2015). In our study, we chose pigs as experimental animal due to their physiological and anatomical similarities to humans, facilitating translational relevance. Furthermore, the presence of the nAChR in the pig brain has been well-documented, particularly validated through numerous PET experiments, including a recent study employing ^{18}F-ASEM, confirming the comparability of nAChR expression patterns between humans and pigs (Donat et al., 2020). Here, we report the effect of TC-5619 and encenicline on ^{11}C-NS14492 binding in the pig brain using both *in vitro* autoradiography and *in vivo* PET imaging to elucidate the target occupancy for these molecules.

Methods

Compounds

^{11}C-NS14492 was produced as described previously (Ettrup et al., 2011b). Briefly, the radioligand was produced by transferring ^{11}C-methyl triflate in a stream of helium to a vial containing desmethyl-NS14492 fumarate dissolved in 300 μL of acetone and 10 μL of 1 M tetrabutylammonium hydroxide in methanol before being heated to 60°C for 3 min prior to high-performance liquid chromatography purification. The specific radioactivity of the radioligand was in the range of 84–152 GBq/μmol, calculated at the end of synthesis, and the radiochemical purity was >99% (n = 8). Encenicline, TC-5619, SSR180711, desmethyl-NS14492, and NS14492 were synthesized at NeuroSearch A/S, (Ballerup, Denmark). All other reagents were purchased from Sigma-Aldrich (Brøndby, Denmark) and were of analytical grade.

Animal procedures

All animal procedures were approved by the Danish Council for Animal Ethics (journal no. 2012-15-2934-00156). For this study, four female Danish Landrace pigs (*Sus scrofa*) (mean weight ± SD, 19 ± 3 kg) were used. The animals were sourced from a local farm, placed in standard housing conditions, and given a minimum acclimatization period of 1 week in the veterinary facilities. At the day of the experiment, but before scanning, the pigs were treated with midazolam [0.5 mg/kg intramuscular (i.m.)] and anesthesia was subsequently induced with an i.m. injection of 1 mL/kg

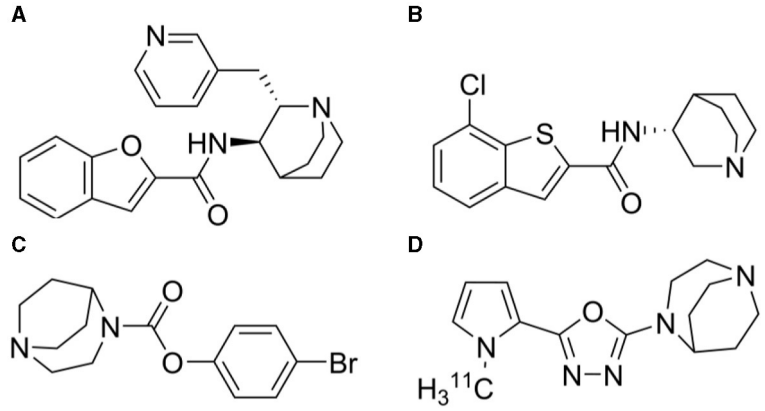

FIGURE 1
Chemical structures of **(A)** TC-5619 (*N*-((2*S*,3*R*)-2-(pyridin-3-ylmethyl)quinuclidin-3-yl)benzofuran-2-carboxamide) **(B)** Encenicline [(*R*)-7-chloro-*N*-(quinuclidin-3-yl)benzo[*b*]thiophene-2-carboxamide] **(C)** SSR180711 (4-bromophenyl 1,4-diazabicyclo[3.2.2]nonane-4-carboxylate) and **(D)** ^{11}C-NS14492 [2-(1,4-diazabicyclo[3.2.2]nonan-4-yl)-5-(1-(methyl-^{11}C)-1*H*-pyrrol-2-yl)-1,3,4-oxadiazole].

Zoletil veterinary mixture [6.25 Pt. xylazine (20 mg/mL) + 1.25 Pt. ketamine (100 mg/mL) + 2 Pt. butorphanol (10 mg/mL) + 2 Pt. methadone (10 mg/mL); Virbac, Kolding, Denmark]. Hereafter, anesthesia was maintained with a constant propofol infusion [10 mg/kg/h intravenous (i.v.); B. Braun, Melsungen, Germany]. During anesthesia, animals were endotracheally intubated and ventilated. Venous access was granted through the peripheral milk veins, and an arterial line for blood sampling was inserted in the femoral artery after a minor incision. Vital parameters (heart rate, body temperature, blood pressure, oxygen saturation, and end-tidal pCO_2) were continuously monitored during the scans. The pigs were euthanized immediately after scanning with an i.v. injection of pentobarbital.

In vitro autoradiography

In vitro autoradiography was performed on post-mortem brain tissue from pigs. Coronal 12 µm sections of pig frontal cortex and thalamus/parietal cortex were cut on a HM500OM Cryostat (Microm Intl GmbH, Walldorf, Germany) at −20°C, thaw-mounted on SuperFrost Plus glass slides (Thermo Scientific, Hvidovre, Denmark), air-dried, and stored at −80°C until use. Autoradiography was conducted at room temperature with 10 nM ^{11}C-NS14492 for total binding, and non-specific binding was determined in the presence of either TC-5619 or encenicline or SSR180711 (10 µM) used in pre-incubation buffer (50 mM tris–HCl, 4 mM $CaCl_2$, 0.1% bovine serum albumin (BSA), 120 mM NaCl, 5 mM KCl, pH 7.4). Sections were then incubated for 30 min in 50 mM tris-HCl buffer (pH 7.4) containing 120 mM NaCl, 5 mM KCl, 1 mM $MgCl_2$, 2.5 mM $CaCl_2$, 0.1% BSA, and 10 nM ^{11}C-NS14492 and washed 2 × 2 min in ice-cold buffer followed by 20 seconds in ice-cold distilled water. Sections were exposed to an imaging plate (IP) (Fujifilm, Tokyo, Japan) in a BAS-2040 cassette overnight. The IP was scanned in a BAS-2500 (Fujifilm) image reader. Image analysis was done with ImageJ analysis software (http://rsb.info.nih.gov/ij/).

In vivo PET imaging

PET experiments were performed with a high-resolution research tomography (HRRT) scanner (Siemens Medical Solutions, Munich, Germany) as previously described (Ettrup et al., 2011b). Briefly, ^{11}C-NS14492 was given as an i.v. bolus injection (injected dose, 458 ± 93 MBq; injected cold mass, 0.8 ± 0.4 µg, $n = 8$), and the pigs were scanned at baseline for 90 min in list mode. After a baseline scan, the animals were given a bolus injection of either TC-5619 (3 mg/kg i.v., $n = 2$) or encenicline (3 mg/kg i.v., $n = 2$) dissolved in 10 mL saline and rescanned 30 min later using the same PET protocol. Whole blood radioactivity was continuously measured for the first 30 min after radioligand injection using an ABSS autosampler (Allogg Technology, Strängnäs, Sweden). Additionally, manual sampling of arterial whole blood (8–13 mL) occurred at intervals of 2.5, 5, 10, 20, 30, 50, 70, and 90 min after injection. Subsequently, radioactivity levels in both whole blood and plasma were quantified using a Cobra 5,003 well counter (Packard Instruments).

The PET data was reconstructed as previously reported (Ettrup et al., 2011a), and the individual summed images of all counts during the 90-min scan time were co-registered to a standardized MRI atlas of the Danish Landrace pig brain using the software Register, as previously described (Kornum et al., 2009). Radioactive concentrations (Bq/mL) were extracted from specific brain regions of both hemispheres [cerebellum, cortex, hippocampus, thalamus (average of lateral and medial), and striatum (average of caudate and putamen)]. Time-activity curves of radioactive concentrations in volumes of interest were normalized to the injected dose and adjusted for body weight. ^{11}C-NS14492 metabolism was measured with HPLC analysis with online radioactivity detection, as previously described (Gillings, 2009). For kinetic modeling purposes, an average metabolite curve for all 8 scans was generated and used to correct plasma activity in the individual scans for the parent compound fraction, thereby obtaining the ^{11}C-NS14492 arterial input function. Volumes of distribution (V_T) for selected regions were calculated using PMOD software (version 3.0; PMOD

Technologies Inc.) applying a Logan graphical analysis with arterial input function (Logan et al., 1990). Because there is no suitable brain reference region devoid of α7-nAChRs, occupancy was measured using the revisited Lassen plot (Cunningham et al., 2010). In the four blocking scans, occupancies of the receptor by encenicline or TC-5619 were calculated as the slope of the occupancy plot visualizing V_T(baseline) – V_T(blocking) as a linear function of V_T(baseline) in the specific brain regions (cortex, thalamus, striatum, cerebellum, and hippocampus). The non-displaceable distribution volume (V_{ND}) was determined by the x-intercept of the regression line.

Statistical analyses

All statistical tests were performed using GraphPad Prism version 6.0 (GraphPad Software, San Diego, USA). *P*-values below 0.05 were considered statistically significant. Results are presented as mean ± standard error of the mean (SEM) unless stated otherwise.

Results

Regional binding and blocking effects of TC-5619, encenicline, and SSR180711 in cortical pig sections

To investigate the binding properties of TC-5619, encenicline and SSR180711 we performed *in vitro* autoradiography in coronal pig sections using 10 nM ^{11}C-NS14492 (Figure 2). We observed laminar binding in cortical layers and less binding in white matter. Further, we observed an almost complete blocking with 10 μM of all three compounds: TC-5619, encenicline, and SSR180711.

Imaging *in vivo* binding profiles and blocking effects of TC-5619 and encenicline

After a bolus injection of ^{11}C-NS14492, we observed heterogeneous brain uptake of radioactivity (Figure 3) with the highest uptake in thalamus and cortical areas, intermediate uptake in the striatum and the lowest uptake in the cerebellum. Pre-treatment with 3 mg/kg TC-5619 or 3 mg/kg encenicline was associated with a lower V_T in all measured regions (Figure 4A). Whereas pre-treatment with 3 mg/kg TC-5619 resulted in an occupancy of 38%—42% (Figures 4C, D), pre-treatment with 3 mg/kg encenicline resulted in less than in average 10% occupancy. In one pig, the slope of the linear regression was not significantly different from zero (Figures 4E, F). The average V_{ND} was 5.3 ± 1.7 mL/cm^3 ($n = 3$).

After i.v. injection, the parent fraction of ^{11}C-NS14492 declined rapidly, and after 7 min, approximately 50% of radioactivity in plasma was attributable to parent ^{11}C-NS14492 (Figure 4B). We detected no radiolabelled lipophilic metabolites of ^{11}C-NS14492 in the plasma, as indicated by lack of distinct peaks in the lipophilic range on the radiochromatograms (data not shown).

Discussion and conclusion

Here, we present *in vitro* receptor autoradiography and *in vivo* ^{11}C-NS14492 PET data on α7-nAChR ligands in the pig brain. The *in vitro* autoradiography revealed laminar binding in cortical layers with a clear discrimination between gray and white matter binding, consistent with previous studies (Gotti et al., 2006). The three α7-nAChR ligands TC-5619, encenicline, and SSR180711 were all able to block ^{11}C-NS14492 binding *in vitro*, supporting their effectiveness as competitive ligands for the α7-nAChR orthosteric site.

With *in vivo* PET imaging we find that 3 mg/kg TC-5619 given i.v. results in 40% occupancy at the α7-nAChR whereas the same dose of encenicline results in negligible occupancy. By using an *in vitro* homogenate binding assay with ^{3}H-NS14492, we previously found K_i values for TC-5619 and encenicline of 0.063 nM and 0.194 nM respectively (Magnussen et al., 2015). That is, given the observed occupancy of TC-5619, one could expect to find that a dose of 3 mg/kg encenicline would result in 16% α7-nAChR occupancy.

Several factors could explain the low *in vivo* occupancy of encenicline in the pig brain. If encenicline displayed a very rapid drug clearance it may have insufficient time to be taken up by the brain. We know from rats that encenicline has good brain penetration after oral administration (0.3 mg/kg), with brain-to-plasma ratios of approximately 2 between 1 and 4 h and 5 at 8 h (Prickaerts et al., 2012), indicating that the plasma clearance of encenicline is considerably faster than the brain uptake and receptor equilibration. In humans, and after oral administration, encenicline has a long plasma half-life of 50–65 h (Barbier et al., 2015), but pharmacokinetic differences between humans and pigs could be a factor as well as differences between oral and intravenous administration. Another explanation could lie with the known interspecies differences in blood-brain barrier permeability for compounds like encenicline and TC-5619 among rats, pigs, and potentially humans (Syvanen et al., 2009; Deo et al., 2013; Stanimirovic et al., 2015). This theory could partially explain the reason for encenicline's clinical trial failure. Furthermore, an extensive review of the existing literature and public domain resources has revealed no documented evidence demonstrating the ability of encenicline to cross the blood-brain barrier in humans.

Our investigation in the pig model reveals that TC-5619 effectively penetrates the blood-brain barrier and exhibits significant binding to the α7-nAChR with a reasonable occupancy. However, it is noteworthy that no prior studies have definitively established an optimal range of α7-nAChR occupancy necessary for eliciting therapeutic effects. This lack of established benchmarks raises the possibility that the failure of TC-5619 to produce significant pro-cognitive effects in clinical trials may stem from the selection of suboptimal dosages. Interestingly, previous research on selective α7-nAChR agonists, including encenicline (Keefe et al., 2015), TC-5619 (Hauser et al., 2009), as well as other compounds such as AZD0328 (Castner et al., 2011), DMXB-A (Olincy et al., 2006), and PHA543613 (Yang et al., 2013) has indicated a trend

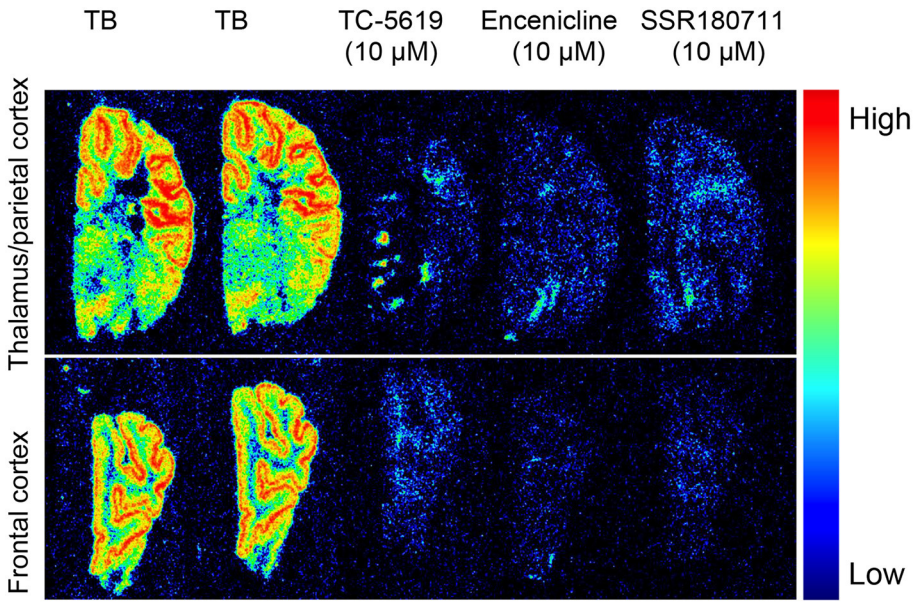

FIGURE 2
In vitro autoradiography with ^{11}C-NS14492 in 12 μm coronal pig sections containing thalamus **(upper panel)** and frontal cortex **(lower panel)**. Total binding (TB) was measured with 10 nM ^{11}C-NS14492. Non-specific binding shown with TC-5619 (10 μM), Encenicline (10 μM) and SSR180711 (10 μM).

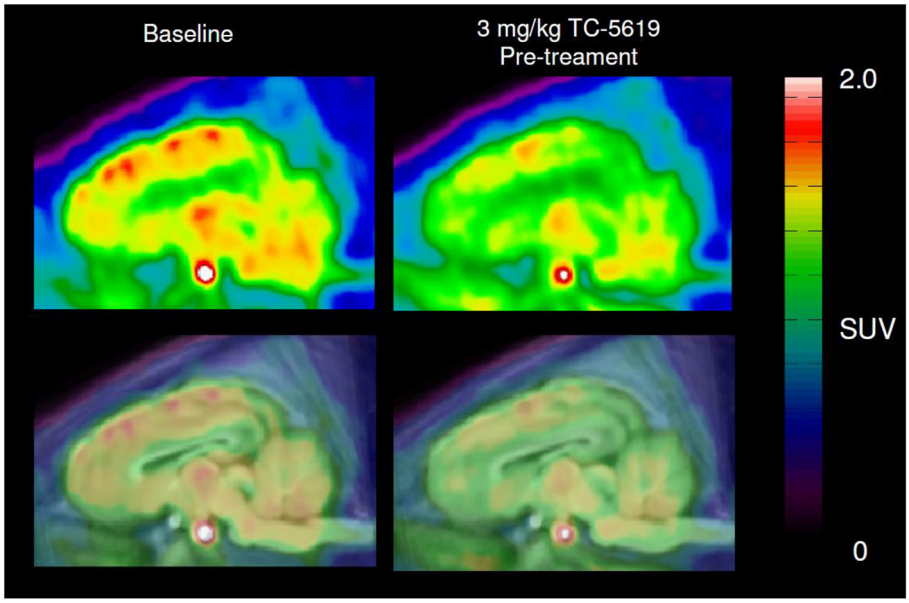

FIGURE 3
Representative sagittal PET images of ^{11}C-NS14492 PET scans before and after TC-5619 pre-treatment. Summed and averaged over 0–90 min PET image **(top panel)** overlaid MRI-based pig brain atlas **(bottom panel)**. SUV; standardized uptake value.

where the pro-cognitive effects peak at lower doses, following an inverted U-shaped dose-response curve. This phenomenon suggests that while lower doses may elicit optimal cognitive enhancement, escalating doses beyond this threshold could lead to diminishing effect or even receptor desensitization, thereby limiting further cognitive improvement. The implications of this dose-response pattern are profound, particularly in the context of human clinical trials. The absence of a clear understanding of optimal dosing presents a considerable challenge, underscoring the need for robust pre-clinical tools for dose finding.

Our study is not without limitations. First, it was not possible to measure drug concentrations during the PET studies so an eventual ultra-fast drug metabolism of encenicline cannot be excluded. As discussed above, this could potentially result in an underestimation

10.3389/fnimg.2024.1358221

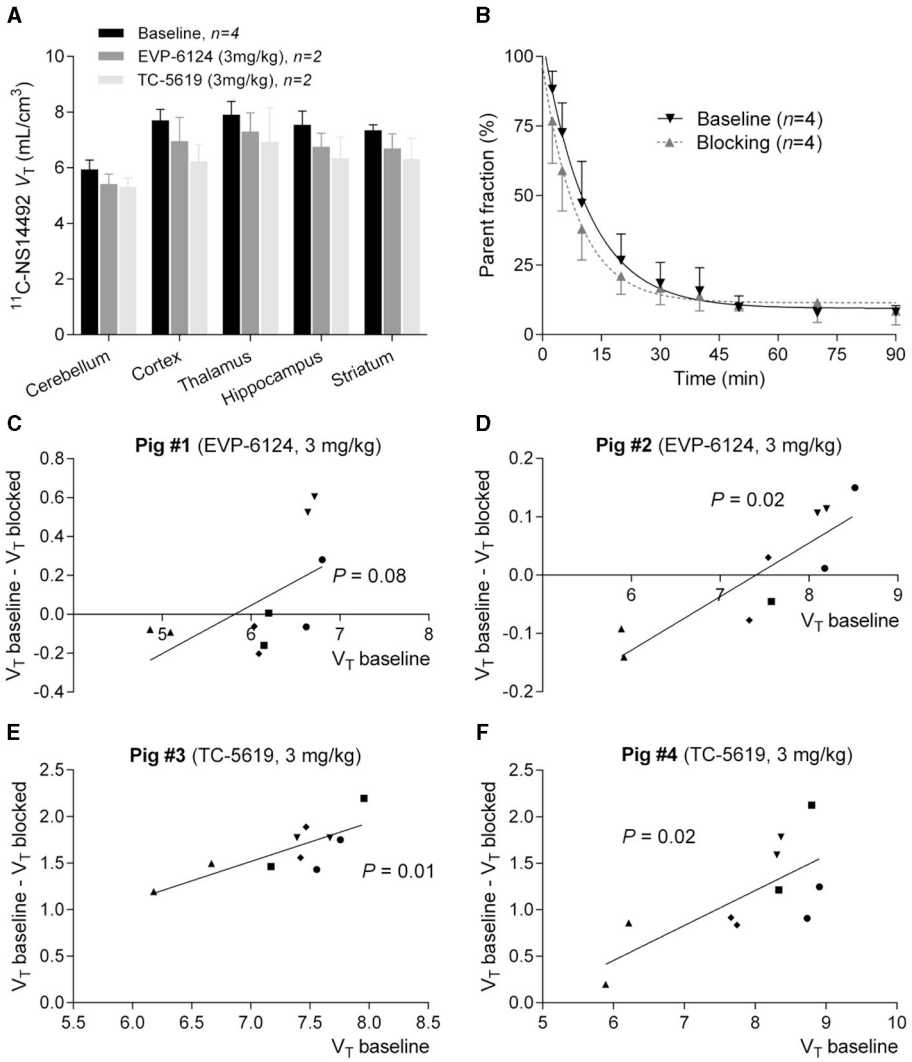

FIGURE 4
(A) Logan plot V_T's of ^{11}C-NS14492 in five brain regions are shown at baseline and after intervention with EVP-6124 (Encenicline) (3 mg/kg i.v. administered 30 minutes before second scan) or TC-5619 (3 mg/kg i.v. administered 30 min before second scan). Bars indicate mean ± SEM. **(B)** Relative radioactive parent compound in pig plasma as a function of time after i.v. injection of ^{11}C-NS14492. Average of measurements from 8 PET scans is shown. Baseline scans (black, $n = 4$) and challenge scans (gray, $n = 4$) with 3 mg/kg Encenicline ($n = 2$) or 3 mg/kg TC-5619 ($n = 2$) is shown. Solid lines (black and gray) correspond to a single exponential decay function fitted to the data. **(C–F)** Occupancy plots of ^{11}C-NS14492 regional left and right V_T's at baseline and in intervention scan for individual pigs. Receptor occupancy by EVP-6124 (Encenicline) **(C, D)** or TC-5619 **(E, F)** is measured as slope of regression line. ^{11}C-NS14492 V_{ND} is found as x-axis intercept. Statistical test results (*P*-values) for slope not equal to zero is shown for the individual regression lines. ▼ = cortex; ● = thalamus; ▲ = cerebellum; ■ = hippocampus; ◆ = striatum.

of its occupancy. Secondly, only 4 animals were used in total limiting the statistical power of the study. However, each animal served as its own control, and we measured five distinct occupancy regions in each animal. Thirdly, we administered both TC-5619 and encenicline at 3 mg/kg but cannot exclude that an even higher dose of encenicline could have returned a larger occupancy.

In conclusion, we find that the two α7-nAChR ligands TC-5619 and encenicline, when given at equal doses, display different α7-nAChR occupancy *in vivo* in the pig brain. Our findings underscore the significance of utilizing PET radiotracers in CNS pre-clinical drug development in assessing crucial factors such as blood-brain barrier permeability and target engagement, as well as in aiding dose finding for potential therapeutic agents. By proposing the establishment of target occupancy through PET experiments prior to embarking on clinical trials, we advocate for a more precise dosing strategy for emerging α7-nAChR selective drug candidates. This proactive approach has the potential to mitigate uncertainties surrounding dosing regimens, thereby enhancing the likelihood of therapeutic success while minimizing adverse effects.

Data availability statement

The raw data supporting the conclusions of this article will be made available by the authors, without undue reservation.

Ethics statement

The animal studies were approved by the Danish Council for Animal Ethics. The studies were conducted in accordance with the local legislation and institutional requirements. Written informed consent was obtained from the owners for the participation of their animals in this study.

Author contributions

JHM: Conceptualization, Data curation, Formal analysis, Investigation, Methodology, Visualization, Writing – original draft, Writing – review & editing. AE: Formal analysis, Methodology, Writing – review & editing. SL: Formal analysis, Software, Writing – review & editing. DP: Writing – review & editing. AD: Data curation, Formal Analysis, Writing – review & editing. MT: Methodology, Writing – review & editing. JDM: Conceptualization, Data curation, Formal analysis, Funding acquisition, Methodology, Resources, Supervision, Writing – review & editing. GK: Conceptualization, Data curation, Formal analysis, Funding acquisition, Methodology, Resources, Supervision, Writing – review & editing.

Funding

The author(s) declare that financial support was received for the research, authorship, and/or publication of this article. This study was partially supported by the Lundbeck Foundation and the Novo Nordisk Foundation.

Acknowledgments

The authors acknowledge the technical assistance of Hans Jørgen Jensen, Bente Dall, Jonni Heberg, and Mette Værum Olesen.

Conflict of interest

AE, AD, and MT are all full-time employees of H. Lundbeck A/S. DanPET AB (100% owned by DP, CEO) commercially offer desmethyl-NS14492, NS14492, and 3H-NS14492 together with Novandi Chemistry AB, Södertälje, Sweden.

The remaining authors declare that the research was conducted in the absence of any commercial or financial relationships that could be construed as a potential conflict of interest.

Publisher's note

All claims expressed in this article are solely those of the authors and do not necessarily represent those of their affiliated organizations, or those of the publisher, the editors and the reviewers. Any product that may be evaluated in this article, or claim that may be made by its manufacturer, is not guaranteed or endorsed by the publisher.

References

Alzforum. (2016). *Rare but Severe Side Effects Sideline Some Phase 3 Encenicline Trials*. Alzforum. Available online at: https://www.alzforum.org/news/research-news/rare-severe-side-effects-sideline-some-phase-3-encenicline-trials (accessed November 10, 2023).

Barbier, A. J., Hilhorst, M., Van Vliet, A., Snyder, P., Palfreyman, M. G., Gawryl, M., et al. (2015). Pharmacodynamics, pharmacokinetics, safety, and tolerability of encenicline, a selective alpha7 nicotinic receptor partial agonist, in single ascending-dose and bioavailability studies. *Clin. Ther.* 37, 311–324. doi: 10.1016/j.clinthera.2014.09.013

Bertrand, D., and Terry, A. V. (2018). The wonderland of neuronal nicotinic acetylcholine receptors. *Biochem. Pharmacol.* 151, 214–225. doi: 10.1016/j.bcp.2017.12.008

Biton, B., Bergis, O. E., Galli, F., Nedelec, A., Lochead, A. W., Jegham, S., et al. (2007). SSR180711, a novel selective alpha7 nicotinic receptor partial agonist: (1) binding and functional profile. *Neuropsychopharmacology* 32, 1–16. doi: 10.1038/sj.npp.1301189

Brannon, S. (2019). Two global phase III trials of encenicline for cognitive impairment in chronic schizophrenia patients: Red flags and lessons learned. *Schizophr. Bull.* 45, 141–142. doi: 10.1093/schbul/sbz022.133

Castner, S. A., Smagin, G. N., Piser, T. M., Wang, Y., Smith, J. S., Christian, E. P., et al. (2011). Immediate and sustained improvements in working memory after selective stimulation of alpha7 nicotinic acetylcholine receptors. *Biol. Psychiatry* 69, 12–18. doi: 10.1016/j.biopsych.2010.08.006

Cunningham, V. J., Rabiner, E. A., Slifstein, M., Laruelle, M., and Gunn, R. N. (2010). Measuring drug occupancy in the absence of a reference region: the Lassen plot re-visited. *J. Cereb. Blood Flow Metab.* 30, 46–50. doi: 10.1038/jcbfm.2009.190

Dani, J. A., and Bertrand, D. (2007). Nicotinic acetylcholine receptors and nicotinic cholinergic mechanisms of the central nervous system. *Annu. Rev. Pharmacol. Toxicol.* 47, 699–729. doi: 10.1146/annurev.pharmtox.47.120505.105214

Deardorff, W. J., Shobassy, A., and Grossberg, G. T. (2015). Safety and clinical effects of EVP-6124 in subjects with Alzheimer's disease currently or previously receiving an acetylcholinesterase inhibitor medication. *Expert. Rev. Neurother.* 15, 7–17. doi: 10.1586/14737175.2015.995639

Deo, A. K., Theil, F. P., and Nicolas, J. M. (2013). Confounding parameters in preclinical assessment of blood-brain barrier permeation: an overview with emphasis on species differences and effect of disease states. *Mol. Pharm.* 10, 1581–1595. doi: 10.1021/mp300570z

Donat, C. K., Hansen, H. H., Hansen, H. D., Mease, R. C., Horti, A. G., Pomper, M. G., et al. (2020). In vitro and in vivo characterization of dibenzothiophene derivatives [(125)I]Iodo-ASEM and [(18)F]ASEM as radiotracers of homo- and heteromeric alpha7 nicotinic acetylcholine receptors. *Molecules* 25:1425. doi: 10.3390/molecules25061425

Ettrup, A., Hansen, M., Santini, M. A., Paine, J., Gillings, N., Palner, M., et al. (2011a). Radiosynthesis and in vivo evaluation of a series of substituted 11C-phenethylamines as 5-HT (2A) agonist PET tracers. *Eur. J. Nucl. Med. Mol. Imaging* 38, 681–693. doi: 10.1007/s00259-010-1686-8

Ettrup, A., Mikkelsen, J. D., Lehel, S., Madsen, J., Nielsen, E. O., Palner, M., et al. (2011b). 11C-NS14492 as a novel PET radioligand for imaging cerebral alpha7 nicotinic acetylcholine receptors: in vivo evaluation and drug occupancy measurements. *J. Nucl. Med.* 52, 1449–1456. doi: 10.2967/jnumed.111.088815

Gillings, N. (2009). A restricted access material for rapid analysis of [(11)C]-labeled radiopharmaceuticals and their metabolites in plasma. *Nucl. Med. Biol.* 36, 961–965. doi: 10.1016/j.nucmedbio.2009.07.004

Gotti, C., Zoli, M., and Clementi, F. (2006). Brain nicotinic acetylcholine receptors: native subtypes and their relevance. *Trends Pharmacol. Sci.* 27, 482–491. doi: 10.1016/j.tips.2006.07.004

Hauser, T. A., Kucinski, A., Jordan, K. G., Gatto, G. J., Wersinger, S. R., Hesse, R. A., et al. (2009). TC-5619: an alpha7 neuronal nicotinic receptor-selective agonist that demonstrates efficacy in animal models of the positive and negative symptoms and cognitive dysfunction of schizophrenia. *Biochem. Pharmacol.* 78, 803–812. doi: 10.1016/j.bcp.2009.05.030

Horti, A. G., Gao, Y., Kuwabara, H., Wang, Y., Abazyan, S., Yasuda, R. P., et al. (2014). 18F-ASEM, a radiolabeled antagonist for imaging the alpha7-nicotinic acetylcholine receptor with PET. *J. Nucl. Med.* 55, 672–677. doi: 10.2967/jnumed.113.132068

Keefe, R. S., Meltzer, H. A., Dgetluck, N., Gawryl, M., Koenig, G., Moebius, H. J., et al. (2015). Randomized, double-blind, placebo-controlled study of encenicline, an alpha7 nicotinic acetylcholine receptor agonist, as a treatment for cognitive impairment in schizophrenia. *Neuropsychopharmacology* 40, 3053–3060. doi: 10.1038/npp.2015.176

Kornum, B. R., Lind, N. M., Gillings, N., Marner, L., Andersen, F., and Knudsen, G. M. (2009). Evaluation of the novel 5-HT4 receptor PET ligand [11C]SB207145 in the Gottingen minipig. *J. Cereb. Blood Flow Metab.* 29, 186–196. doi: 10.1038/jcbfm.2008.110

Lewis, A. S., van Schalkwyk, G. I., and Bloch, M. H. (2017). Alpha-7 nicotinic agonists for cognitive deficits in neuropsychiatric disorders: A translational meta-analysis of rodent and human studies. *Prog. Neuropsychopharmacol. Biol. Psychiatry* 75, 45–53. doi: 10.1016/j.pnpbp.2017.01.001

Li, S. X., Huang, S., Bren, N., Noridomi, K., Dellisanti, C. D., Sine, S. M., et al. (2011). Ligand-binding domain of an alpha7-nicotinic receptor chimera and its complex with agonist. *Nat. Neurosci.* 14, 1253–1259. doi: 10.1038/nn.2908

Lieberman, J. A., Dunbar, G., Segreti, A. C., Girgis, R. R., Seoane, F., Beaver, J. S., et al. (2013). A randomized exploratory trial of an alpha-7 nicotinic receptor agonist (TC-5619) for cognitive enhancement in schizophrenia. *Neuropsychopharmacology* 38, 968–975. doi: 10.1038/npp.2012.259

Logan, J., Fowler, J. S., Volkow, N. D., Wolf, A. P., Dewey, S. L., Schlyer, D. J., et al. (1990). Graphical analysis of reversible radioligand binding from time-activity measurements applied to [N-11C-methyl]-(-)-cocaine PET studies in human subjects. *J. Cereb. Blood Flow Metab.* 10, 740–747. doi: 10.1038/jcbfm.1990.127

Magnussen, J. H., Ettrup, A., Donat, C. K., Peters, D., Pedersen, M. H., Knudsen, G. M., et al. (2015). Radiosynthesis and in vitro validation of (3)H-NS14492 as a novel high affinity alpha7 nicotinic receptor radioligand. *Eur. J. Pharmacol.* 762, 35–41. doi: 10.1016/j.ejphar.2015.04.036

Olincy, A., Harris, J. G., Johnson, L. L., Pender, V., Kongs, S., Allensworth, D., et al. (2006). Proof-of-concept trial of an alpha7 nicotinic agonist in schizophrenia. *Arch. Gen. Psychiat.* 63, 630–638. doi: 10.1001/archpsyc.63.6.630

Pichat, P., Bergis, O. E., Terranova, J. P., Urani, A., Duarte, C., Santucci, V., et al. (2007). SSR180711, a novel selective alpha7 nicotinic receptor partial agonist: (II) efficacy in experimental models predictive of activity against cognitive symptoms of schizophrenia. *Neuropsychopharmacology* 32, 17–34. doi: 10.1038/sj.npp.1301188

Preskorn, S. H., Gawryl, M., Dgetluck, N., Palfreyman, M., Bauer, L. O., and Hilt, D. C. (2014). Normalizing effects of EVP-6124, an alpha-7 nicotinic partial agonist, on event-related potentials and cognition: a proof of concept, randomized trial in patients with schizophrenia. *J. Psychiatr. Pract.* 20, 12–24. doi: 10.1097/01.pra.0000442935.15833.c5

Prickaerts, J., van Goethem, N. P., Chesworth, R., Shapiro, G., Boess, F. G., Methfessel, C., et al. (2012). EVP-6124, a novel and selective alpha7 nicotinic acetylcholine receptor partial agonist, improves memory performance by potentiating the acetylcholine response of alpha7 nicotinic acetylcholine receptors. *Neuropharmacology* 62, 1099–1110. doi: 10.1016/j.neuropharm.2011.10.024

Stanimirovic, D. B., Bani-Yaghoub, M., Perkins, M., and Haqqani, A. S. (2015). Blood-brain barrier models: in vitro to in vivo translation in preclinical development of CNS-targeting biotherapeutics. *Expert. Opin. Drug. Discov.* 10, 141–155. doi: 10.1517/17460441.2015.974545

Syvanen, S., Lindhe, O., Palner, M., Kornum, B. R., Rahman, O., Langstrom, B., et al. (2009). Species differences in blood-brain barrier transport of three positron emission tomography radioligands with emphasis on P-glycoprotein transport. *Drug. Metab. Dispos.* 37, 635–643. doi: 10.1124/dmd.108.024745

Targacept (2013). *Targacept Announces Negative Top-Line Results from Phase 2b Clinical Trial of TC-5619 in Schizophrenia*. Fierce Biotech. Available online at: https://www.fiercebiotech.com/biotech/targacept-announces-negative-top-line-results-from-phase-2b-clinical-trial-of-tc-5619 (accessed July 7, 2023).

Terry, A. V. Jr., and Callahan, P. M. (2020). alpha7 nicotinic acetylcholine receptors as therapeutic targets in schizophrenia: update on animal and clinical studies and strategies for the future. *Neuropharmacology* 170:108053. doi: 10.1016/j.neuropharm.2020.108053

Thomsen, M. S., Hansen, H. H., Timmerman, D. B., and Mikkelsen, J. D. (2010). Cognitive improvement by activation of alpha7 nicotinic acetylcholine receptors: from animal models to human pathophysiology. *Curr. Pharm. Des.* 16, 323–343. doi: 10.2174/138161210790170094

Tribollet, E., Bertrand, D., Marguerat, A., and Raggenbass, M. (2004). Comparative distribution of nicotinic receptor subtypes during development, adulthood and aging: an autoradiographic study in the rat brain. *Neuroscience* 124, 405–420. doi: 10.1016/j.neuroscience.2003.09.028

Wallace, T. L., and Porter, R. H. (2011). Targeting the nicotinic alpha7 acetylcholine receptor to enhance cognition in disease. *Biochem. Pharmacol.* 82, 891–903. doi: 10.1016/j.bcp.2011.06.034

Walling, D., Marder, S. R., Kane, J., Fleischhacker, W. W., Keefe, R. S., Hosford, D. A., et al. (2016). Phase 2 trial of an alpha-7 nicotinic receptor agonist (TC-5619) in negative and cognitive symptoms of schizophrenia. *Schizophr. Bull.* 42, 335–343. doi: 10.1093/schbul/sbv072

Wessler, I., and Kirkpatrick, C. J. (2008). Acetylcholine beyond neurons: the non-neuronal cholinergic system in humans. *Br. J. Pharmacol.* 154, 1558–1571. doi: 10.1038/bjp.2008.185

Wong, D. F., Kuwabara, H., Horti, A. G., Roberts, J. M., Nandi, A., Cascella, N., et al. (2018). Brain PET imaging of alpha7-nAChR with [18F]ASEM: reproducibility, occupancy, receptor density, and changes in schizophrenia. *Int. J. Neuropsychopharmacol.* 21, 656–667. doi: 10.1093/ijnp/pyy021

Wong, D. F., Kuwabara, H., Pomper, M., Holt, D. P., Brasic, J. R., George, N., et al. (2014). Human brain imaging of alpha7 nAChR with [(18)F]ASEM: a new PET radiotracer for neuropsychiatry and determination of drug occupancy. *Mol. Imaging Biol.* 16, 730–738. doi: 10.1007/s11307-014-0779-3

Wu, J., Liu, Q., Tang, P., Mikkelsen, J. D., Shen, J., Whiteaker, P., et al. (2016). Heteromeric alpha7beta2 nicotinic acetylcholine receptors in the brain. *Trends Pharmacol. Sci.* 37, 562–574. doi: 10.1016/j.tips.2016.03.005

Yang, Y., Paspalas, C. D., Jin, L. E., Picciotto, M. R., Arnsten, A. F., and Wang, M. (2013). Nicotinic alpha7 receptors enhance NMDA cognitive circuits in dorsolateral prefrontal cortex. *Proc. Natl. Acad. Sci. U S A* 110, 12078–12083. doi: 10.1073/pnas.1307849110

Thesis references

Abbott, N. J. (2013). Blood-brain barrier structure and function and the challenges for CNS drug delivery. *J Inherit Metab Dis*, *36*(3), 437-449. https://doi.org/10.1007/s10545-013-9608-0

Akaike, H. (1998). Information theory and an extension of the maximum likelihood principle. In *Selected papers of hirotugu akaike* (pp. 199-213). Springer.

Al Aboud, N. M., Tupper, C., & Jialal, I. (2018). Genetics, epigenetic mechanism.

Albuquerque, E. X., Pereira, E. F., Alkondon, M., & Rogers, S. W. (2009). Mammalian nicotinic acetylcholine receptors: from structure to function. *Physiol Rev*, *89*(1), 73-120. https://doi.org/10.1152/physrev.00015.2008

Alexander, G. C., Knopman, D. S., Emerson, S. S., Ovbiagele, B., Kryscio, R. J., Perlmutter, J. S., & Kesselheim, A. S. (2021). Revisiting FDA Approval of Aducanumab. *N Engl J Med*, *385*(9), 769-771. https://doi.org/10.1056/NEJMp2110468

Allfrey, V. G., Faulkner, R., & Mirsky, A. E. (1964). Acetylation and Methylation of Histones and Their Possible Role in the Regulation of Rna Synthesis. *Proc Natl Acad Sci U S A*, *51*(5), 786-794. https://doi.org/10.1073/pnas.51.5.786

Alzforum. (2007). *Memory Pharmaceuticals Announces Positive Phase 2a Results for RG3487 (MEM 3454) in Alzheimer's Disease*. Retrieved 29 January 2024 from https://www.alzforum.org/therapeutics/rg3487

Alzforum. (2015). *Rare but Severe Side Effects Sideline Some Phase 3 Encenicline Trials*. Retrieved 05 June from https://www.alzforum.org/news/research-news/rare-severe-side-effects-sideline-some-phase-3-encenicline-trials

Amemiya, Y., & Miyahara, J. (1988). Imaging plate illuminates many fields. *Nature*, *336*(6194), 89-90. https://doi.org/10.1038/336089a0

Anderson, D. J., Bunnelle, W., Surber, B., Du, J., Surowy, C., Tribollet, E., Marguerat, A., Bertrand, D., & Gopalakrishnan, M. (2008). [3H]A-585539 [(1S,4S)-2,2-dimethyl-5-(6-phenylpyridazin-3-yl)-5-aza-2-azoniabicyclo[2.2.1]heptane], a novel high-affinity alpha7 neuronal nicotinic receptor agonist: radioligand binding characterization to rat and human brain. *J Pharmacol Exp Ther*, *324*(1), 179-187. https://doi.org/10.1124/jpet.107.130062

Aracava, Y., Pereira, E. F., Maelicke, A., & Albuquerque, E. X. (2005). Memantine blocks alpha7* nicotinic acetylcholine receptors more potently than n-methyl-D-aspartate receptors in rat hippocampal neurons. *J Pharmacol Exp Ther*, *312*(3), 1195-1205. https://doi.org/10.1124/jpet.104.077172

Atluri, V. S. R., Tiwari, S., Rodriguez, M., Kaushik, A., Yndart, A., Kolishetti, N., Yatham, M., & Nair, M. (2019). Inhibition of Amyloid-Beta Production, Associated Neuroinflammation, and Histone Deacetylase 2-Mediated Epigenetic Modifications Prevent Neuropathology in

Alzheimer's Disease in vitro Model. *Front Aging Neurosci*, *11*, 342. https://doi.org/10.3389/fnagi.2019.00342

Aubert, I., Araujo, D. M., Cecyre, D., Robitaille, Y., Gauthier, S., & Quirion, R. (1992). Comparative alterations of nicotinic and muscarinic binding sites in Alzheimer's and Parkinson's diseases. *J Neurochem*, *58*(2), 529-541. https://doi.org/10.1111/j.1471-4159.1992.tb09752.x

Azam, L., & McIntosh, J. M. (2009). Alpha-conotoxins as pharmacological probes of nicotinic acetylcholine receptors. *Acta Pharmacol Sin*, *30*(6), 771-783. https://doi.org/10.1038/aps.2009.47

Azam, L., Winzer-Serhan, U., & Leslie, F. M. (2003). Co-expression of alpha7 and beta2 nicotinic acetylcholine receptor subunit mRNAs within rat brain cholinergic neurons. *Neuroscience*, *119*(4), 965-977. https://doi.org/10.1016/s0306-4522(03)00220-3

Bailey, D. L., Maisey, M. N., Townsend, D. W., & Valk, P. E. (2005). *Positron emission tomography* (Vol. 2). Springer.

Bale, T. L., Abel, T., Akil, H., Carlezon, W. A., Jr., Moghaddam, B., Nestler, E. J., Ressler, K. J., & Thompson, S. M. (2019). The critical importance of basic animal research for neuropsychiatric disorders. *Neuropsychopharmacology*, *44*(8), 1349-1353. https://doi.org/10.1038/s41386-019-0405-9

Banerjee, P., Samoriski, G., & Gupta, S. (2005). Comments on "Memantine blocks alpha7* nicotinic acetylcholine receptors more potently than N-methyl-D-aspartate receptors in rat hippocampal neurons". *J Pharmacol Exp Ther*, *313*(2), 928-929; author reply 930-923. https://doi.org/10.1124/jpet.104.081976

Bannister, A. J., & Kouzarides, T. (2011). Regulation of chromatin by histone modifications. *Cell Res*, *21*(3), 381-395. https://doi.org/10.1038/cr.2011.22

Barbier, A. J., Hilhorst, M., Van Vliet, A., Snyder, P., Palfreyman, M. G., Gawryl, M., Dgetluck, N., Massaro, M., Tiessen, R., Timmerman, W., & Hilt, D. C. (2015). Pharmacodynamics, pharmacokinetics, safety, and tolerability of encenicline, a selective alpha7 nicotinic receptor partial agonist, in single ascending-dose and bioavailability studies. *Clin Ther*, *37*(2), 311-324. https://doi.org/10.1016/j.clinthera.2014.09.013

Barch, D. M., Marder, S. R., Harms, M. P., Jarskog, L. F., Buchanan, R. W., Cronenwett, W., Chen, L. S., Weiss, M., Maguire, R. P., Pezous, N., Feuerbach, D., Lopez-Lopez, C., Johns, D. R., Behrje, R. B., & Gomez-Mancilla, B. (2016). Task-related fMRI responses to a nicotinic acetylcholine receptor partial agonist in schizophrenia: A randomized trial. *Prog Neuropsychopharmacol Biol Psychiatry*, *71*, 66-75. https://doi.org/10.1016/j.pnpbp.2016.06.013

Bartus, R. T., Dean, R. L., 3rd, Beer, B., & Lippa, A. S. (1982). The cholinergic hypothesis of geriatric memory dysfunction. *Science*, *217*(4558), 408-414. https://doi.org/10.1126/science.7046051

Bennett, M. R. (2003). Obituary: Sir Bernard Katz (1911-2003). *J Neurocytol*, *32*(5-8), 431-436. https://doi.org/10.1023/B:NEUR.0000020602.24573.9b

Bergstrom, M., Grahnen, A., & Langstrom, B. (2003). Positron emission tomography microdosing: a new concept with application in tracer and early clinical drug development. *Eur J Clin Pharmacol*, *59*(5-6), 357-366. https://doi.org/10.1007/s00228-003-0643-x

Bertrand, D., & Gopalakrishnan, M. (2007). Allosteric modulation of nicotinic acetylcholine receptors. *Biochem Pharmacol*, *74*(8), 1155-1163. https://doi.org/10.1016/j.bcp.2007.07.011

Bertrand, D., Lee, C. H., Flood, D., Marger, F., & Donnelly-Roberts, D. (2015). Therapeutic Potential of alpha7 Nicotinic Acetylcholine Receptors. *Pharmacol Rev*, *67*(4), 1025-1073. https://doi.org/10.1124/pr.113.008581

Betz, H. (1990). Ligand-gated ion channels in the brain: the amino acid receptor superfamily. *Neuron*, *5*(4), 383-392. https://doi.org/10.1016/0896-6273(90)90077-s

Biton, B., Bergis, O. E., Galli, F., Nedelec, A., Lochead, A. W., Jegham, S., Godet, D., Lanneau, C., Santamaria, R., Chesney, F., Leonardon, J., Granger, P., Debono, M. W., Bohme, G. A., Sgard, F., Besnard, F., Graham, D., Coste, A., Oblin, A., . . . Scatton, B. (2007). SSR180711, a novel selective alpha7 nicotinic receptor partial agonist: (1) binding and functional profile. *Neuropsychopharmacology*, *32*(1), 1-16. https://doi.org/10.1038/sj.npp.1301189

Blanchfield, J. T., Gallagher, O. P., Cros, C., Lewis, R. J., Alewood, P. F., & Toth, I. (2007). Oral absorption and in vivo biodistribution of alpha-conotoxin MII and a lipidic analogue. *Biochem Biophys Res Commun*, *361*(1), 97-102. https://doi.org/10.1016/j.bbrc.2007.06.138

Blasberg, R. (2002). PET imaging of gene expression. *Eur J Cancer*, *38*(16), 2137-2146. https://doi.org/10.1016/s0959-8049(02)00390-8

Bloem, B., Poorthuis, R. B., & Mansvelder, H. D. (2014). Cholinergic modulation of the medial prefrontal cortex: the role of nicotinic receptors in attention and regulation of neuronal activity. *Front Neural Circuits*, *8*, 17. https://doi.org/10.3389/fncir.2014.00017

Bocquet, N., Nury, H., Baaden, M., Le Poupon, C., Changeux, J. P., Delarue, M., & Corringer, P. J. (2009). X-ray structure of a pentameric ligand-gated ion channel in an apparently open conformation. *Nature*, *457*(7225), 111-114. https://doi.org/10.1038/nature07462

Bonomi, R., Mukhopadhyay, U., Shavrin, A., Yeh, H. H., Majhi, A., Dewage, S. W., Najjar, A., Lu, X., Cisneros, G. A., Tong, W. P., Alauddin, M. M., Liu, R. S., Mangner, T. J., Turkman, N., & Gelovani, J. G. (2015). Novel Histone Deacetylase Class IIa Selective Substrate Radiotracers for PET Imaging of Epigenetic Regulation in the Brain. *PLoS One*, *10*(8), e0133512. https://doi.org/10.1371/journal.pone.0133512

Bouzat, C., & Sine, S. M. (2018). Nicotinic acetylcholine receptors at the single-channel level. *Br J Pharmacol*, *175*(11), 1789-1804. https://doi.org/10.1111/bph.13770

Brannan, S. (2019). 32.2 Two global phase III trials of encenicline for cognitive impairment in chronic schizophrenia patients: red flags and lessons learned. *Schizophrenia Bulletin*, *45*(Supplement_2), S141-S142.

Buccafusco, J. J., Letchworth, S. R., Bencherif, M., & Lippiello, P. M. (2005). Long-lasting cognitive improvement with nicotinic receptor agonists: mechanisms of pharmacokinetic-

pharmacodynamic discordance. *Trends Pharmacol Sci*, *26*(7), 352-360. https://doi.org/10.1016/j.tips.2005.05.007

Burns, L. H., Pei, Z., & Wang, H. Y. (2023). Targeting alpha7 nicotinic acetylcholine receptors and their protein interactions in Alzheimer's disease drug development. *Drug Dev Res*, *84*(6), 1085-1095. https://doi.org/10.1002/ddr.22085

Burt, T., Young, G., Lee, W., Kusuhara, H., Langer, O., Rowland, M., & Sugiyama, Y. (2020). Phase 0/microdosing approaches: time for mainstream application in drug development? *Nat Rev Drug Discov*, *19*(11), 801-818. https://doi.org/10.1038/s41573-020-0080-x

Cahill, S. (2020). WHO's global action plan on the public health response to dementia: some challenges and opportunities. *Aging Ment Health*, *24*(2), 197-199. https://doi.org/10.1080/13607863.2018.1544213

Cai, C., Wang, L., Li, S., Lou, S., Luo, J. L., Fu, D. Y., & Chen, T. (2022). Ras Inhibitor Lonafarnib Rescues Structural and Functional Impairments of Synapses of Abeta(1-42) Mice via alpha7nAChR-Dependent BDNF Upregulation. *J Neurosci*, *42*(31), 6090-6107. https://doi.org/10.1523/JNEUROSCI.1989-21.2022

Capitanio, J. P., & Emborg, M. E. (2008). Contributions of non-human primates to neuroscience research. *Lancet*, *371*(9618), 1126-1135. https://doi.org/10.1016/S0140-6736(08)60489-4

Carson, R., Toyonaga, T., Badawi, R., Cherry, S., Du, J., Fontaine, K., Gallezot, J.-D., Gravel, P., He, L., & Hillmer, A. (2023). Exceptional PET Images from the First Human Scan on the NeuroEXPLORER, a next-generation ultra-high performance brain PET imager. In: Soc Nuclear Med.

Castner, S. A., Smagin, G. N., Piser, T. M., Wang, Y., Smith, J. S., Christian, E. P., Mrzljak, L., & Williams, G. V. (2011). Immediate and sustained improvements in working memory after selective stimulation of alpha7 nicotinic acetylcholine receptors. *Biol Psychiatry*, *69*(1), 12-18. https://doi.org/10.1016/j.biopsych.2010.08.006

Cedar, H., & Bergman, Y. (2009). Linking DNA methylation and histone modification: patterns and paradigms. *Nat Rev Genet*, *10*(5), 295-304. https://doi.org/10.1038/nrg2540

Chang, C. C. (1999). Looking back on the discovery of alpha-bungarotoxin. *J Biomed Sci*, *6*(6), 368-375. https://doi.org/10.1007/BF02253668

Changeux, J. P., Kasai, M., Huchet, M., & Meunier, J. C. (1970). [Extraction from electric tissue of gymnotus of a protein presenting several typical properties characteristic of the physiological receptor of acetylcholine]. *C R Acad Hebd Seances Acad Sci D*, *270*(23), 2864-2867. https://www.ncbi.nlm.nih.gov/pubmed/4987937 (Extraction a partir du tissu electrique de gymnote d'une proteine presentant plusieurs proprietes caracteristiques du recepteur physiologique de l'acetylcholine.)

Changeux, J. P., Kasai, M., & Lee, C. Y. (1970). Use of a snake venom toxin to characterize the cholinergic receptor protein. *Proc Natl Acad Sci U S A*, *67*(3), 1241-1247. https://doi.org/10.1073/pnas.67.3.1241

Chen, Y. A., Lu, C. H., Ke, C. C., Chiu, S. J., Chang, C. W., Yang, B. H., Gelovani, J. G., & Liu, R. S. (2021). Evaluation of Class IIa Histone Deacetylases Expression and In Vivo Epigenetic

Imaging in a Transgenic Mouse Model of Alzheimer's Disease. *Int J Mol Sci*, *22*(16). https://doi.org/10.3390/ijms22168633

Cheng, Q., & Yakel, J. L. (2015). The effect of alpha7 nicotinic receptor activation on glutamatergic transmission in the hippocampus. *Biochem Pharmacol*, *97*(4), 439-444. https://doi.org/10.1016/j.bcp.2015.07.015

Chiao, P., Bedell, B. J., Avants, B., Zijdenbos, A. P., Grand'Maison, M., O'Neill, P., O'Gorman, J., Chen, T., & Koeppe, R. (2019). Impact of Reference and Target Region Selection on Amyloid PET SUV Ratios in the Phase 1b PRIME Study of Aducanumab. *J Nucl Med*, *60*(1), 100-106. https://doi.org/10.2967/jnumed.118.209130

Chuang, D. M., Leng, Y., Marinova, Z., Kim, H. J., & Chiu, C. T. (2009). Multiple roles of HDAC inhibition in neurodegenerative conditions. *Trends Neurosci*, *32*(11), 591-601. https://doi.org/10.1016/j.tins.2009.06.002

Clarke, P. B., Schwartz, R. D., Paul, S. M., Pert, C. B., & Pert, A. (1985). Nicotinic binding in rat brain: autoradiographic comparison of [3H]acetylcholine, [3H]nicotine, and [125I]-alpha-bungarotoxin. *J Neurosci*, *5*(5), 1307-1315. https://doi.org/10.1523/JNEUROSCI.05-05-01307.1985

Clayden, J. (2019). Fluorinated compounds present opportunities for drug discovery. *Nature*, *573*(7772), 37-38. https://doi.org/10.1038/d41586-019-02611-7

Contestabile, A. (2011). The history of the cholinergic hypothesis. *Behav Brain Res*, *221*(2), 334-340. https://doi.org/10.1016/j.bbr.2009.12.044

Conti, M., & Eriksson, L. (2016). Physics of pure and non-pure positron emitters for PET: a review and a discussion. *EJNMMI Phys*, *3*(1), 8. https://doi.org/10.1186/s40658-016-0144-5

Cook, D., Brown, D., Alexander, R., March, R., Morgan, P., Satterthwaite, G., & Pangalos, M. N. (2014). Lessons learned from the fate of AstraZeneca's drug pipeline: a five-dimensional framework. *Nat Rev Drug Discov*, *13*(6), 419-431. https://doi.org/10.1038/nrd4309

Coughlin, J. M., Du, Y., Crawford, J. L., Rubin, L. H., Behnam Azad, B., Lesniak, W. G., Horti, A. G., Schretlen, D. J., Sawa, A., & Pomper, M. G. (2018). The availability of the alpha7 nicotinic acetylcholine receptor in recent-onset psychosis: a study using (18)F-ASEM PET. *J Nucl Med*. https://doi.org/10.2967/jnumed.118.213686

Coughlin, J. M., Du, Y., Rosenthal, H. B., Slania, S., Min Koo, S., Park, A., Solomon, G., Vranesic, M., Antonsdottir, I., Speck, C. L., Rootes-Murdy, K., Lerner, A., Rowe, S. P., Wang, Y., Lesniak, W. G., Minn, I., Bakker, A., Smith, G. S., Dannals, R. F., . . . Pomper, M. G. (2018). The distribution of the alpha7 nicotinic acetylcholine receptor in healthy aging: An in vivo positron emission tomography study with [(18)F]ASEM. *Neuroimage*, *165*, 118-124. https://doi.org/10.1016/j.neuroimage.2017.10.009

Coughlin, J. M., Rubin, L. H., Du, Y., Rowe, S. P., Crawford, J. L., Rosenthal, H. B., Frey, S. M., Marshall, E. S., Shinehouse, L. K., Chen, A., Speck, C. L., Wang, Y., Lesniak, W. G., Minn, I., Bakker, A., Kamath, V., Smith, G. S., Albert, M. S., Azad, B. B., . . . Pomper, M. G. (2020). High Availability of the alpha7-Nicotinic Acetylcholine Receptor in Brains of Individuals with Mild Cognitive Impairment: A Pilot Study Using (18)F-ASEM PET. *J Nucl Med*, *61*(3), 423-426. https://doi.org/10.2967/jnumed.119.230979

Counts, S. E., He, B., Che, S., Ikonomovic, M. D., DeKosky, S. T., Ginsberg, S. D., & Mufson, E. J. (2007). Alpha7 nicotinic receptor up-regulation in cholinergic basal forebrain neurons in Alzheimer disease. *Arch Neurol*, *64*(12), 1771-1776. https://doi.org/10.1001/archneur.64.12.1771

Court, J., Martin-Ruiz, C., Piggott, M., Spurden, D., Griffiths, M., & Perry, E. (2001). Nicotinic receptor abnormalities in Alzheimer's disease. *Biol Psychiatry*, *49*(3), 175-184. https://doi.org/10.1016/s0006-3223(00)01116-1

Crestini, A., Carbone, E., Rivabene, R., Ancidoni, A., Rosa, P., Tata, A. M., Fabrizi, E., Locuratolo, N., Vanacore, N., Lacorte, E., & Piscopo, P. (2024). A Systematic Review on Drugs Acting as Nicotinic Acetylcholine Receptor Agonists in the Treatment of Dementia. *Cells*, *13*(3). https://doi.org/10.3390/cells13030237

Cunningham, V. J., Rabiner, E. A., Slifstein, M., Laruelle, M., & Gunn, R. N. (2010). Measuring drug occupancy in the absence of a reference region: the Lassen plot re-visited. *J Cereb Blood Flow Metab*, *30*(1), 46-50. https://doi.org/10.1038/jcbfm.2009.190

Dajas-Bailador, F., & Wonnacott, S. (2004). Nicotinic acetylcholine receptors and the regulation of neuronal signalling. *Trends Pharmacol Sci*, *25*(6), 317-324. https://doi.org/10.1016/j.tips.2004.04.006

Dajas-Bailador, F. A., Mogg, A. J., & Wonnacott, S. (2002). Intracellular Ca2+ signals evoked by stimulation of nicotinic acetylcholine receptors in SH-SY5Y cells: contribution of voltage-operated Ca2+ channels and Ca2+ stores. *J Neurochem*, *81*(3), 606-614. https://doi.org/10.1046/j.1471-4159.2002.00846.x

Dani, J. A. (2015). Neuronal Nicotinic Acetylcholine Receptor Structure and Function and Response to Nicotine. *Int Rev Neurobiol*, *124*, 3-19. https://doi.org/10.1016/bs.irn.2015.07.001

Dani, J. A., & Bertrand, D. (2007). Nicotinic acetylcholine receptors and nicotinic cholinergic mechanisms of the central nervous system. *Annu Rev Pharmacol Toxicol*, *47*, 699-729. https://doi.org/10.1146/annurev.pharmtox.47.120505.105214

Datta, M., Staszewski, O., Raschi, E., Frosch, M., Hagemeyer, N., Tay, T. L., Blank, T., Kreutzfeldt, M., Merkler, D., Ziegler-Waldkirch, S., Matthias, P., Meyer-Luehmann, M., & Prinz, M. (2018). Histone Deacetylases 1 and 2 Regulate Microglia Function during Development, Homeostasis, and Neurodegeneration in a Context-Dependent Manner. *Immunity*, *48*(3), 514-529 e516. https://doi.org/10.1016/j.immuni.2018.02.016

Davenport, A. P. (2008). *Receptor binding techniques* (Vol. 306). Springer Science & Business Media.

Davidson, M., Levi, L., Park, J., Nastas, I., Ford, L., Rassnick, S., Canuso, C., Davis, J. M., & Weiser, M. (2021). The effects of JNJ-39393406 a positive allosteric nicotine modulator on mood and cognition in patients with unipolar depression: A double-blind, add-on, placebo-controlled trial. *Eur Neuropsychopharmacol*, *51*, 33-42. https://doi.org/10.1016/j.euroneuro.2021.04.020

de Jong, H. W., van Velden, F. H., Kloet, R. W., Buijs, F. L., Boellaard, R., & Lammertsma, A. A. (2007). Performance evaluation of the ECAT HRRT: an LSO-LYSO double layer high

resolution, high sensitivity scanner. *Phys Med Biol*, *52*(5), 1505-1526. https://doi.org/10.1088/0031-9155/52/5/019

Deardorff, W. J., Shobassy, A., & Grossberg, G. T. (2015). Safety and clinical effects of EVP-6124 in subjects with Alzheimer's disease currently or previously receiving an acetylcholinesterase inhibitor medication. *Expert Rev Neurother*, *15*(1), 7-17. https://doi.org/10.1586/14737175.2015.995639

Deo, A. K., Theil, F. P., & Nicolas, J. M. (2013). Confounding parameters in preclinical assessment of blood-brain barrier permeation: an overview with emphasis on species differences and effect of disease states. *Mol Pharm*, *10*(5), 1581-1595. https://doi.org/10.1021/mp300570z

Deuther-Conrad, W., Fischer, S., Hiller, A., Becker, G., Cumming, P., Xiong, G., Funke, U., Sabri, O., Peters, D., & Brust, P. (2011). Assessment of alpha7 nicotinic acetylcholine receptor availability in juvenile pig brain with [(1)(8)F]NS10743. *Eur J Nucl Med Mol Imaging*, *38*(8), 1541-1549. https://doi.org/10.1007/s00259-011-1808-y

Deuther-Conrad, W., Fischer, S., Hiller, A., Nielsen, E. O., Timmermann, D. B., Steinbach, J., Sabri, O., Peters, D., & Brust, P. (2009). Molecular imaging of alpha7 nicotinic acetylcholine receptors: design and evaluation of the potent radioligand [18F]NS10743. *Eur J Nucl Med Mol Imaging*, *36*(5), 791-800. https://doi.org/10.1007/s00259-008-1031-7

Dhillon, S. (2021). Aducanumab: First Approval. *Drugs*, *81*(12), 1437-1443. https://doi.org/10.1007/s40265-021-01569-z

DiMasi, J. A., Grabowski, H. G., & Hansen, R. W. (2016). Innovation in the pharmaceutical industry: New estimates of R&D costs. *J Health Econ*, *47*, 20-33. https://doi.org/10.1016/j.jhealeco.2016.01.012

Dineley, K. T., Pandya, A. A., & Yakel, J. L. (2015). Nicotinic ACh receptors as therapeutic targets in CNS disorders. *Trends Pharmacol Sci*, *36*(2), 96-108. https://doi.org/10.1016/j.tips.2014.12.002

Ding, M., Ghanekar, S., Elmore, C. S., Zysk, J. R., Werkheiser, J. L., Lee, C. M., Liu, J., Chhajlani, V., & Maier, D. L. (2012). [(3)H]Chiba-1001(methyl-SSR180711) has low in vitro binding affinity and poor in vivo selectivity to nicotinic alpha-7 receptor in rodent brain. *Synapse*, *66*(4), 315-322. https://doi.org/10.1002/syn.21513

Dios, A. M., Babu, S., Granucci, E. J., Mueller, K. A., Mills, A. N., Alshikho, M. J., Zurcher, N. R., Cernasov, P., Gilbert, T. M., Glass, J. D., Berry, J. D., Atassi, N., Hooker, J. M., & Sadri-Vakili, G. (2019). Class I and II histone deacetylase expression is not altered in human amyotrophic lateral sclerosis: Neuropathological and positron emission tomography molecular neuroimaging evidence. *Muscle Nerve*, *60*(4), 443-452. https://doi.org/10.1002/mus.26620

Dolle, F., Valette, H., Hinnen, F., Vaufrey, F., Demphel, S., Coulon, C., Ottaviani, M., Bottlaender, M., & Crouzel, C. (2001). Synthesis and preliminary evaluation of a carbon-11-labelled agonist of the α7 nicotinic acetylcholine receptor. *Journal of Labelled Compounds and Radiopharmaceuticals: The Official Journal of the International Isotope Society*, *44*(11), 785-795.

Dominguez del Toro, E., Juiz, J. M., Peng, X., Lindstrom, J., & Criado, M. (1994). Immunocytochemical localization of the alpha 7 subunit of the nicotinic acetylcholine receptor in the rat central nervous system. *J Comp Neurol*, *349*(3), 325-342. https://doi.org/10.1002/cne.903490302

Donat, C. K., Hansen, H. H., Hansen, H. D., Mease, R. C., Horti, A. G., Pomper, M. G., L'Estrade, E. T., Herth, M. M., Peters, D., Knudsen, G. M., & Mikkelsen, J. D. (2020). In Vitro and In Vivo Characterization of Dibenzothiophene Derivatives [(125)I]Iodo-ASEM and [(18)F]ASEM as Radiotracers of Homo- and Heteromeric alpha7 Nicotinic Acetylcholine Receptors. *Molecules*, *25*(6). https://doi.org/10.3390/molecules25061425

Donde, C., Brunelin, J., Mondino, M., Cellard, C., Rolland, B., & Haesebaert, F. (2020). The effects of acute nicotine administration on cognitive and early sensory processes in schizophrenia: a systematic review. *Neurosci Biobehav Rev*, *118*, 121-133. https://doi.org/10.1016/j.neubiorev.2020.07.035

Donovan, L. L., Magnussen, J. H., Dyssegaard, A., Lehel, S., Hooker, J. M., Knudsen, G. M., & Hansen, H. D. (2020). Imaging HDACs In Vivo: Cross-Validation of the [(11)C]Martinostat Radioligand in the Pig Brain. *Mol Imaging Biol*, *22*(3), 569-577. https://doi.org/10.1007/s11307-019-01403-9

Egger, G., Liang, G., Aparicio, A., & Jones, P. A. (2004). Epigenetics in human disease and prospects for epigenetic therapy. *Nature*, *429*(6990), 457-463. https://doi.org/10.1038/nature02625

Ehman, E. C., Johnson, G. B., Villanueva-Meyer, J. E., Cha, S., Leynes, A. P., Larson, P. E. Z., & Hope, T. A. (2017). PET/MRI: Where might it replace PET/CT? *J Magn Reson Imaging*, *46*(5), 1247-1262. https://doi.org/10.1002/jmri.25711

Ettrup, A., Mikkelsen, J. D., Lehel, S., Madsen, J., Nielsen, E. O., Palner, M., Timmermann, D. B., Peters, D., & Knudsen, G. M. (2011). 11C-NS14492 as a novel PET radioligand for imaging cerebral alpha7 nicotinic acetylcholine receptors: in vivo evaluation and drug occupancy measurements. *J Nucl Med*, *52*(9), 1449-1456. https://doi.org/10.2967/jnumed.111.088815

Fabian-Fine, R., Skehel, P., Errington, M. L., Davies, H. A., Sher, E., Stewart, M. G., & Fine, A. (2001). Ultrastructural distribution of the alpha7 nicotinic acetylcholine receptor subunit in rat hippocampus. *J Neurosci*, *21*(20), 7993-8003. https://doi.org/10.1523/JNEUROSCI.21-20-07993.2001

Falk, L., Nordberg, A., Seiger, A., Kjaeldgaard, A., & Hellstrom-Lindahl, E. (2003). Higher expression of alpha7 nicotinic acetylcholine receptors in human fetal compared to adult brain. *Brain Res Dev Brain Res*, *142*(2), 151-160. https://doi.org/10.1016/s0165-3806(03)00063-4

Fang, H., Disteche, C. M., & Berletch, J. B. (2019). X Inactivation and Escape: Epigenetic and Structural Features. *Front Cell Dev Biol*, *7*, 219. https://doi.org/10.3389/fcell.2019.00219

Florian, H., Meier, A., Gauthier, S., Lipschitz, S., Lin, Y., Tang, Q., Othman, A. A., Robieson, W. Z., & Gault, L. M. (2016). Efficacy and Safety of ABT-126 in Subjects with Mild-to-Moderate Alzheimer's Disease on Stable Doses of Acetylcholinesterase Inhibitors: A Randomized,

Double-Blind, Placebo-Controlled Study. *J Alzheimers Dis*, *51*(4), 1237-1247. https://doi.org/10.3233/JAD-150978

Fontana, I. C., Kumar, A., & Nordberg, A. (2023). The role of astrocytic alpha7 nicotinic acetylcholine receptors in Alzheimer disease. *Nat Rev Neurol*, *19*(5), 278-288. https://doi.org/10.1038/s41582-023-00792-4

Fraga, M. F., Ballestar, E., Paz, M. F., Ropero, S., Setien, F., Ballestar, M. L., Heine-Suner, D., Cigudosa, J. C., Urioste, M., Benitez, J., Boix-Chornet, M., Sanchez-Aguilera, A., Ling, C., Carlsson, E., Poulsen, P., Vaag, A., Stephan, Z., Spector, T. D., Wu, Y. Z., . . . Esteller, M. (2005). Epigenetic differences arise during the lifetime of monozygotic twins. *Proc Natl Acad Sci U S A*, *102*(30), 10604-10609. https://doi.org/10.1073/pnas.0500398102

Frazier, C. J., Rollins, Y. D., Breese, C. R., Leonard, S., Freedman, R., & Dunwiddie, T. V. (1998). Acetylcholine activates an alpha-bungarotoxin-sensitive nicotinic current in rat hippocampal interneurons, but not pyramidal cells. *J Neurosci*, *18*(4), 1187-1195. https://doi.org/10.1523/JNEUROSCI.18-04-01187.1998

Freedman, R., Olincy, A., Buchanan, R. W., Harris, J. G., Gold, J. M., Johnson, L., Allensworth, D., Guzman-Bonilla, A., Clement, B., Ball, M. P., Kutnick, J., Pender, V., Martin, L. F., Stevens, K. E., Wagner, B. D., Zerbe, G. O., Soti, F., & Kem, W. R. (2008). Initial phase 2 trial of a nicotinic agonist in schizophrenia. *Am J Psychiatry*, *165*(8), 1040-1047. https://doi.org/10.1176/appi.ajp.2008.07071135

Gallinari, P., Di Marco, S., Jones, P., Pallaoro, M., & Steinkuhler, C. (2007). HDACs, histone deacetylation and gene transcription: from molecular biology to cancer therapeutics. *Cell Res*, *17*(3), 195-211. https://doi.org/10.1038/sj.cr.7310149

Gault, L. M., Lenz, R. A., Ritchie, C. W., Meier, A., Othman, A. A., Tang, Q., Berry, S., Pritchett, Y., & Robieson, W. Z. (2016). ABT-126 monotherapy in mild-to-moderate Alzheimer's dementia: randomized double-blind, placebo and active controlled adaptive trial and open-label extension. *Alzheimers Res Ther*, *8*(1), 44. https://doi.org/10.1186/s13195-016-0210-1

Gault, L. M., Ritchie, C. W., Robieson, W. Z., Pritchett, Y., Othman, A. A., & Lenz, R. A. (2015). A phase 2 randomized, controlled trial of the alpha7 agonist ABT-126 in mild-to-moderate Alzheimer's dementia. *Alzheimers Dement (N Y)*, *1*(1), 81-90. https://doi.org/10.1016/j.trci.2015.06.001

Ge, S., & Dani, J. A. (2005). Nicotinic acetylcholine receptors at glutamate synapses facilitate long-term depression or potentiation. *J Neurosci*, *25*(26), 6084-6091. https://doi.org/10.1523/JNEUROSCI.0542-05.2005

Gee, K. W., Olincy, A., Kanner, R., Johnson, L., Hogenkamp, D., Harris, J., Tran, M., Edmonds, S. A., Sauer, W., Yoshimura, R., Johnstone, T., & Freedman, R. (2017). First in human trial of a type I positive allosteric modulator of alpha7-nicotinic acetylcholine receptors: Pharmacokinetics, safety, and evidence for neurocognitive effect of AVL-3288. *J Psychopharmacol*, *31*(4), 434-441. https://doi.org/10.1177/0269881117691590

George, N., Gean, E. G., Nandi, A., Frolov, B., Zaidi, E., Lee, H., Brasic, J. R., & Wong, D. F. (2015). Advances in CNS Imaging Agents: Focus on PET and SPECT Tracers in Experimental and Clinical Use. *CNS Drugs*, *29*(4), 313-330. https://doi.org/10.1007/s40263-015-0237-z

Ghosh, K. K., Padmanabhan, P., Yang, C. T., Ng, D. C. E., Palanivel, M., Mishra, S., Halldin, C., & Gulyas, B. (2022). Positron emission tomographic imaging in drug discovery. *Drug Discov Today*, *27*(1), 280-291. https://doi.org/10.1016/j.drudis.2021.07.025

Gilbert, S. F. (2012). Commentary: 'The epigenotype' by C.H. Waddington. *Int J Epidemiol*, *41*(1), 20-23. https://doi.org/10.1093/ije/dyr186

Gilbert, T. M., Zurcher, N. R., Catanese, M. C., Tseng, C. J., Di Biase, M. A., Lyall, A. E., Hightower, B. G., Parmar, A. J., Bhanot, A., Wu, C. J., Hibert, M. L., Kim, M., Mahmood, U., Stufflebeam, S. M., Schroeder, F. A., Wang, C., Roffman, J. L., Holt, D. J., Greve, D. N., . . . Hooker, J. M. (2019). Neuroepigenetic signatures of age and sex in the living human brain. *Nat Commun*, *10*(1), 2945. https://doi.org/10.1038/s41467-019-11031-0

Gilbert, T. M., Zurcher, N. R., Wu, C. J., Bhanot, A., Hightower, B. G., Kim, M., Albrecht, D. S., Wey, H. Y., Schroeder, F. A., Rodriguez-Thompson, A., Morin, T. M., Hart, K. L., Pellegrini, A. M., Riley, M. M., Wang, C., Stufflebeam, S. M., Haggarty, S. J., Holt, D. J., Loggia, M. L., . . . Hooker, J. M. (2019). PET neuroimaging reveals histone deacetylase dysregulation in schizophrenia. *J Clin Invest*, *129*(1), 364-372. https://doi.org/10.1172/JCI123743

Goodheart, A., Yoo, C.-H., Striar, R., Quan, M., Wey, H.-Y., Wang, C., & Gomperts, S. (2023). Imaging regional histone deacetylase expression in dementia with Lewy bodies with [11C] Martinostat (P13-6.008). In: AAN Enterprises.

Gotti, C., Zoli, M., & Clementi, F. (2006). Brain nicotinic acetylcholine receptors: native subtypes and their relevance. *Trends Pharmacol Sci*, *27*(9), 482-491. https://doi.org/10.1016/j.tips.2006.07.004

Graff, J., Rei, D., Guan, J. S., Wang, W. Y., Seo, J., Hennig, K. M., Nieland, T. J., Fass, D. M., Kao, P. F., Kahn, M., Su, S. C., Samiei, A., Joseph, N., Haggarty, S. J., Delalle, I., & Tsai, L. H. (2012). An epigenetic blockade of cognitive functions in the neurodegenerating brain. *Nature*, *483*(7388), 222-226. https://doi.org/10.1038/nature10849

Gray, R., Rajan, A. S., Radcliffe, K. A., Yakehiro, M., & Dani, J. A. (1996). Hippocampal synaptic transmission enhanced by low concentrations of nicotine. *Nature*, *383*(6602), 713-716. https://doi.org/10.1038/383713a0

Gribkoff, V. K., & Kaczmarek, L. K. (2017). The need for new approaches in CNS drug discovery: Why drugs have failed, and what can be done to improve outcomes. *Neuropharmacology*, *120*, 11-19. https://doi.org/10.1016/j.neuropharm.2016.03.021

Griem-Krey, N., Klein, A. B., Herth, M., & Wellendorph, P. (2019). Autoradiography as a simple and powerful method for visualization and characterization of pharmacological targets. *JoVE (Journal of Visualized Experiments)*(145), e58879.

Gu, Z., & Yakel, J. L. (2011). Timing-dependent septal cholinergic induction of dynamic hippocampal synaptic plasticity. *Neuron*, *71*(1), 155-165. https://doi.org/10.1016/j.neuron.2011.04.026

Guan, J. S., Haggarty, S. J., Giacometti, E., Dannenberg, J. H., Joseph, N., Gao, J., Nieland, T. J., Zhou, Y., Wang, X., Mazitschek, R., Bradner, J. E., DePinho, R. A., Jaenisch, R., & Tsai, L. H. (2009). HDAC2 negatively regulates memory formation and synaptic plasticity. *Nature*, *459*(7243), 55-60. https://doi.org/10.1038/nature07925

Guan, Z. Z., Zhang, X., Blennow, K., & Nordberg, A. (1999). Decreased protein level of nicotinic receptor alpha7 subunit in the frontal cortex from schizophrenic brain. *Neuroreport*, *10*(8), 1779-1782. https://doi.org/10.1097/00001756-199906030-00028

Gunn, R. N., & Rabiner, E. A. (2017). Imaging in Central Nervous System Drug Discovery. *Semin Nucl Med*, *47*(1), 89-98. https://doi.org/10.1053/j.semnuclmed.2016.09.001

Haberland, M., Montgomery, R. L., & Olson, E. N. (2009). The many roles of histone deacetylases in development and physiology: implications for disease and therapy. *Nat Rev Genet*, *10*(1), 32-42. https://doi.org/10.1038/nrg2485

Haig, G. M., Bain, E. E., Robieson, W. Z., Baker, J. D., & Othman, A. A. (2016). A Randomized Trial to Assess the Efficacy and Safety of ABT-126, a Selective alpha7 Nicotinic Acetylcholine Receptor Agonist, in the Treatment of Cognitive Impairment in Schizophrenia. *Am J Psychiatry*, *173*(8), 827-835. https://doi.org/10.1176/appi.ajp.2015.15010093

Halldin, C., Gulyas, B., Langer, O., & Farde, L. (2001). Brain radioligands--state of the art and new trends. *Q J Nucl Med*, *45*(2), 139-152. https://www.ncbi.nlm.nih.gov/pubmed/11476163

Hansen, D. V., Hanson, J. E., & Sheng, M. (2018). Microglia in Alzheimer's disease. *J Cell Biol*, *217*(2), 459-472. https://doi.org/10.1083/jcb.201709069

Hansen, H. D., Andersen, V. L., Lehel, S., Magnussen, J. H., Dyssegaard, A., Stroth, N., Kristensen, J. L., Knudsen, G. M., & Herth, M. M. (2015). Labeling and preliminary in vivo evaluation of the 5-HT(7) receptor selective agonist [(11)C]E-55888. *Bioorg Med Chem Lett*, *25*(9), 1901-1904. https://doi.org/10.1016/j.bmcl.2015.03.039

Hansen, H. D., Constantinescu, C. C., Barret, O., Herth, M. M., Magnussen, J. H., Lehel, S., Dyssegaard, A., Colomb, J., Billard, T., Zimmer, L., Tamagnan, G., & Knudsen, G. M. (2019). Evaluation of [(18) F]2FP3 in pigs and non-human primates. *J Labelled Comp Radiopharm*, *62*(1), 34-42. https://doi.org/10.1002/jlcr.3692

Harry, G. J. (2013). Microglia during development and aging. *Pharmacol Ther*, *139*(3), 313-326. https://doi.org/10.1016/j.pharmthera.2013.04.013

Hashimoto, K., Nishiyama, S., Ohba, H., Matsuo, M., Kobashi, T., Takahagi, M., Iyo, M., Kitashoji, T., & Tsukada, H. (2008). [11C]CHIBA-1001 as a novel PET ligand for alpha7 nicotinic receptors in the brain: a PET study in conscious monkeys. *PLoS One*, *3*(9), e3231. https://doi.org/10.1371/journal.pone.0003231

Hasselmo, M. E. (2006). The role of acetylcholine in learning and memory. *Curr Opin Neurobiol*, *16*(6), 710-715. https://doi.org/10.1016/j.conb.2006.09.002

Hauser, T. A., Kucinski, A., Jordan, K. G., Gatto, G. J., Wersinger, S. R., Hesse, R. A., Stachowiak, E. K., Stachowiak, M. K., Papke, R. L., Lippiello, P. M., & Bencherif, M. (2009). TC-5619: an alpha7 neuronal nicotinic receptor-selective agonist that demonstrates efficacy in animal models of the positive and negative symptoms and cognitive dysfunction of

schizophrenia. *Biochem Pharmacol*, *78*(7), 803-812. https://doi.org/10.1016/j.bcp.2009.05.030

Hendricks, J. A., Keliher, E. J., Marinelli, B., Reiner, T., Weissleder, R., & Mazitschek, R. (2011). In vivo PET imaging of histone deacetylases by 18F-suberoylanilide hydroxamic acid (18F-SAHA). *J Med Chem*, *54*(15), 5576-5582. https://doi.org/10.1021/jm200620f

Hernandez, C. M., Kayed, R., Zheng, H., Sweatt, J. D., & Dineley, K. T. (2010). Loss of alpha7 nicotinic receptors enhances beta-amyloid oligomer accumulation, exacerbating early-stage cognitive decline and septohippocampal pathology in a mouse model of Alzheimer's disease. *J Neurosci*, *30*(7), 2442-2453. https://doi.org/10.1523/JNEUROSCI.5038-09.2010

Hilf, R. J., & Dutzler, R. (2008). X-ray structure of a prokaryotic pentameric ligand-gated ion channel. *Nature*, *452*(7185), 375-379. https://doi.org/10.1038/nature06717

Hilf, R. J., & Dutzler, R. (2009). Structure of a potentially open state of a proton-activated pentameric ligand-gated ion channel. *Nature*, *457*(7225), 115-118. https://doi.org/10.1038/nature07461

Hill, S. K., Bishop, J. R., Palumbo, D., & Sweeney, J. A. (2010). Effect of second-generation antipsychotics on cognition: current issues and future challenges. *Expert Rev Neurother*, *10*(1), 43-57. https://doi.org/10.1586/ern.09.143

Hodge, R. D., Bakken, T. E., Miller, J. A., Smith, K. A., Barkan, E. R., Graybuck, L. T., Close, J. L., Long, B., Johansen, N., Penn, O., Yao, Z., Eggermont, J., Hollt, T., Levi, B. P., Shehata, S. I., Aevermann, B., Beller, A., Bertagnolli, D., Brouner, K., . . . Lein, E. S. (2019). Conserved cell types with divergent features in human versus mouse cortex. *Nature*, *573*(7772), 61-68. https://doi.org/10.1038/s41586-019-1506-7

Hoffmeister, P. G., Donat, C. K., Schuhmann, M. U., Voigt, C., Walter, B., Nieber, K., Meixensberger, J., Bauer, R., & Brust, P. (2011). Traumatic brain injury elicits similar alterations in alpha7 nicotinic receptor density in two different experimental models. *Neuromolecular Med*, *13*(1), 44-53. https://doi.org/10.1007/s12017-010-8136-4

Hogg, R. C., Buisson, B., & Bertrand, D. (2005). Allosteric modulation of ligand-gated ion channels. *Biochem Pharmacol*, *70*(9), 1267-1276. https://doi.org/10.1016/j.bcp.2005.06.010

Hoilund-Carlsen, P. F., & Alavi, A. (2021). Aducanumab (Marketed as Aduhelm) Approval Is Likely Based on Misinterpretation of PET Imaging Data. *J Alzheimers Dis*, *84*(4), 1457-1460. https://doi.org/10.3233/JAD-215275

Hoilund-Carlsen, P. F., Revheim, M. E., Alavi, A., Satyamurthy, N., & Barrio, J. R. (2022). Amyloid PET: A Questionable Single Primary Surrogate Efficacy Measure on Alzheimer Immunotherapy Trials. *J Alzheimers Dis*, *90*(4), 1395-1399. https://doi.org/10.3233/JAD-220841

Holland, J. P., Cumming, P., & Vasdev, N. (2013). PET radiopharmaceuticals for probing enzymes in the brain. *Am J Nucl Med Mol Imaging*, *3*(3), 194-216. https://www.ncbi.nlm.nih.gov/pubmed/23638333

Homberg, J. R., Adan, R. A. H., Alenina, N., Asiminas, A., Bader, M., Beckers, T., Begg, D. P., Blokland, A., Burger, M. E., van Dijk, G., Eisel, U. L. M., Elgersma, Y., Englitz, B., Fernandez-Ruiz, A., Fitzsimons, C. P., van Dam, A. M., Gass, P., Grandjean, J., Havekes, R., . . . Genzel, L. (2021). The continued need for animals to advance brain research. *Neuron*, *109*(15), 2374-2379. https://doi.org/10.1016/j.neuron.2021.07.015

Horti, A. G. (2015). Development of [(18)F]ASEM, a specific radiotracer for quantification of the alpha7-nAChR with positron-emission tomography. *Biochem Pharmacol*, *97*(4), 566-575. https://doi.org/10.1016/j.bcp.2015.07.030

Horti, A. G., Gao, Y., Kuwabara, H., Wang, Y., Abazyan, S., Yasuda, R. P., Tran, T., Xiao, Y., Sahibzada, N., Holt, D. P., Kellar, K. J., Pletnikov, M. V., Pomper, M. G., Wong, D. F., & Dannals, R. F. (2014). 18F-ASEM, a radiolabeled antagonist for imaging the alpha7-nicotinic acetylcholine receptor with PET. *J Nucl Med*, *55*(4), 672-677. https://doi.org/10.2967/jnumed.113.132068

Horti, A. G., Ravert, H. T., Gao, Y., Holt, D. P., Bunnelle, W. H., Schrimpf, M. R., Li, T., Ji, J., Valentine, H., Scheffel, U., Kuwabara, H., Wong, D. F., & Dannals, R. F. (2013). Synthesis and evaluation of new radioligands [(11)C]A-833834 and [(11)C]A-752274 for positron-emission tomography of alpha7-nicotinic acetylcholine receptors. *Nucl Med Biol*, *40*(3), 395-402. https://doi.org/10.1016/j.nucmedbio.2012.11.013

Hulme, E. C., & Trevethick, M. A. (2010). Ligand binding assays at equilibrium: validation and interpretation. *Br J Pharmacol*, *161*(6), 1219-1237. https://doi.org/10.1111/j.1476-5381.2009.00604.x

Haake, A., Nguyen, K., Friedman, L., Chakkamparambil, B., & Grossberg, G. T. (2020). An update on the utility and safety of cholinesterase inhibitors for the treatment of Alzheimer's disease. *Expert Opin Drug Saf*, *19*(2), 147-157. https://doi.org/10.1080/14740338.2020.1721456

Ichise, M., Meyer, J. H., & Yonekura, Y. (2001). An introduction to PET and SPECT neuroreceptor quantification models. *J Nucl Med*, *42*(5), 755-763. https://www.ncbi.nlm.nih.gov/pubmed/11337572

Innis, R. B., Cunningham, V. J., Delforge, J., Fujita, M., Gjedde, A., Gunn, R. N., Holden, J., Houle, S., Huang, S. C., Ichise, M., Iida, H., Ito, H., Kimura, Y., Koeppe, R. A., Knudsen, G. M., Knuuti, J., Lammertsma, A. A., Laruelle, M., Logan, J., . . . Carson, R. E. (2007). Consensus nomenclature for in vivo imaging of reversibly binding radioligands. *J Cereb Blood Flow Metab*, *27*(9), 1533-1539. https://doi.org/10.1038/sj.jcbfm.9600493

Ji, D., Lape, R., & Dani, J. A. (2001). Timing and location of nicotinic activity enhances or depresses hippocampal synaptic plasticity. *Neuron*, *31*(1), 131-141. https://doi.org/10.1016/s0896-6273(01)00332-4

Jones, S., Sudweeks, S., & Yakel, J. L. (1999). Nicotinic receptors in the brain: correlating physiology with function. *Trends Neurosci*, *22*(12), 555-561. https://doi.org/10.1016/s0166-2236(99)01471-x

Kaduszkiewicz, H., Zimmermann, T., Beck-Bornholdt, H. P., & van den Bussche, H. (2005). Cholinesterase inhibitors for patients with Alzheimer's disease: systematic review of

randomised clinical trials. *BMJ*, *331*(7512), 321-327. https://doi.org/10.1136/bmj.331.7512.321

Kahn, R. S. (2019). On the Specificity of Continuous Cognitive Decline in Schizophrenia. *Am J Psychiatry*, *176*(10), 774-776. https://doi.org/10.1176/appi.ajp.2019.19080794

Kamal, S. R., Potukutchi, S., Gelovani, D. J., Bonomi, R. E., Kallakuri, S., Cavanaugh, J. M., Mangner, T., Conti, A., Liu, R. S., Pasqualini, R., Arap, W., Sidman, R. L., Perrine, S. A., & Gelovani, J. G. (2022). Spatial and temporal dynamics of HDACs class IIa following mild traumatic brain injury in adult rats. *Mol Psychiatry*, *27*(3), 1683-1693. https://doi.org/10.1038/s41380-021-01369-7

Kantrowitz, J. T., Javitt, D. C., Freedman, R., Sehatpour, P., Kegeles, L. S., Carlson, M., Sobeih, T., Wall, M. M., Choo, T. H., Vail, B., Grinband, J., & Lieberman, J. A. (2020). Double blind, two dose, randomized, placebo-controlled, cross-over clinical trial of the positive allosteric modulator at the alpha7 nicotinic cholinergic receptor AVL-3288 in schizophrenia patients. *Neuropsychopharmacology*, *45*(8), 1339-1345. https://doi.org/10.1038/s41386-020-0628-9

Karisetty, B. C., Bhatnagar, A., Armour, E. M., Beaver, M., Zhang, H., & Elefant, F. (2020). Amyloid-beta Peptide Impact on Synaptic Function and Neuroepigenetic Gene Control Reveal New Therapeutic Strategies for Alzheimer's Disease. *Front Mol Neurosci*, *13*, 577622. https://doi.org/10.3389/fnmol.2020.577622

Kasa, P., Hlavati, I., Dobo, E., Wolff, A., Joo, F., & Wolff, J. R. (1995). Synaptic and non-synaptic cholinergic innervation of the various types of neurons in the main olfactory bulb of adult rat: immunocytochemistry of choline acetyltransferase. *Neuroscience*, *67*(3), 667-677. https://doi.org/10.1016/0306-4522(95)00031-d

Katz, B., & Miledi, R. (1965). Release of acetylcholine from a nerve terminal by electric pulses of variable strength and duration. *Nature*, *207*(5001), 1097-1098. https://doi.org/10.1038/2071097a0

Katz, B., & Miledi, R. (1967). A study of synaptic transmission in the absence of nerve impulses. *J Physiol*, *192*(2), 407-436. https://doi.org/10.1113/jphysiol.1967.sp008307

Katz, B., & Miledi, R. (1968). The role of calcium in neuromuscular facilitation. *J Physiol*, *195*(2), 481-492. https://doi.org/10.1113/jphysiol.1968.sp008469

Kazantsev, A. G., & Thompson, L. M. (2008). Therapeutic application of histone deacetylase inhibitors for central nervous system disorders. *Nat Rev Drug Discov*, *7*(10), 854-868. https://doi.org/10.1038/nrd2681

Keefe, R. S., Meltzer, H. A., Dgetluck, N., Gawryl, M., Koenig, G., Moebius, H. J., Lombardo, I., & Hilt, D. C. (2015). Randomized, Double-Blind, Placebo-Controlled Study of Encenicline, an alpha7 Nicotinic Acetylcholine Receptor Agonist, as a Treatment for Cognitive Impairment in Schizophrenia. *Neuropsychopharmacology*, *40*(13), 3053-3060. https://doi.org/10.1038/npp.2015.176

Kem, W. R. (2000). The brain alpha7 nicotinic receptor may be an important therapeutic target for the treatment of Alzheimer's disease: studies with DMXBA (GTS-21). *Behav Brain Res*, *113*(1-2), 169-181. https://doi.org/10.1016/s0166-4328(00)00211-4

Kendziorra, K., Wolf, H., Meyer, P. M., Barthel, H., Hesse, S., Becker, G. A., Luthardt, J., Schildan, A., Patt, M., Sorger, D., Seese, A., Gertz, H. J., & Sabri, O. (2011). Decreased cerebral alpha4beta2* nicotinic acetylcholine receptor availability in patients with mild cognitive impairment and Alzheimer's disease assessed with positron emission tomography. *Eur J Nucl Med Mol Imaging*, *38*(3), 515-525. https://doi.org/10.1007/s00259-010-1644-5

Kepp, K. P., Robakis, N. K., Hoilund-Carlsen, P. F., Sensi, S. L., & Vissel, B. (2023). The amyloid cascade hypothesis: an updated critical review. *Brain*, *146*(10), 3969-3990. https://doi.org/10.1093/brain/awad159

Keppler, J. S., & Conti, P. S. (2001). A cost analysis of positron emission tomography. *AJR Am J Roentgenol*, *177*(1), 31-40. https://doi.org/10.2214/ajr.177.1.1770031

Kesselheim, A. S., Hwang, T. J., & Franklin, J. M. (2015). Two decades of new drug development for central nervous system disorders. *Nat Rev Drug Discov*, *14*(12), 815-816. https://doi.org/10.1038/nrd4793

Khiroug, L., Giniatullin, R., Klein, R. C., Fayuk, D., & Yakel, J. L. (2003). Functional mapping and Ca2+ regulation of nicotinic acetylcholine receptor channels in rat hippocampal CA1 neurons. *J Neurosci*, *23*(27), 9024-9031. https://doi.org/10.1523/JNEUROSCI.23-27-09024.2003

Khiroug, S. S., Harkness, P. C., Lamb, P. W., Sudweeks, S. N., Khiroug, L., Millar, N. S., & Yakel, J. L. (2002). Rat nicotinic ACh receptor alpha7 and beta2 subunits co-assemble to form functional heteromeric nicotinic receptor channels. *J Physiol*, *540*(Pt 2), 425-434. https://doi.org/10.1113/jphysiol.2001.013847

Kilbourn, M. R. (2021). (11)C- and (18)F-Radiotracers for In Vivo Imaging of the Dopamine System: Past, Present and Future. *Biomedicines*, *9*(2). https://doi.org/10.3390/biomedicines9020108

Kim, S. W., Ding, Y. S., Alexoff, D., Patel, V., Logan, J., Lin, K. S., Shea, C., Muench, L., Xu, Y., Carter, P., King, P., Constanzo, J. R., Ciaccio, J. A., & Fowler, J. S. (2007). Synthesis and positron emission tomography studies of C-11-labeled isotopomers and metabolites of GTS-21, a partial alpha7 nicotinic cholinergic agonist drug. *Nucl Med Biol*, *34*(5), 541-551. https://doi.org/10.1016/j.nucmedbio.2007.04.005

Kim, S. W., Shea, C., Xu, Y., Ding, Y.-S., & Fowler, J. (2008). Synthesis of (R)-5-(6-[18F] fluoropyridin-2-yl)-N-(quinuclidin-3-yl) thiophene-2-carboxamide for evaluation as a selective α7 nAChR PET tracer. In: Soc Nuclear Med.

Kim, Y. I., Lee, S. H., Jung, J. H., Kim, S. Y., Ko, N., Lee, S. J., Oh, S. J., Ryu, J. S., Ko, D., Kim, W., & Kim, K. (2024). (18)F-ASEM PET/MRI targeting alpha7-nicotinic acetylcholine receptor can reveal skeletal muscle denervation. *EJNMMI Res*, *14*(1), 8. https://doi.org/10.1186/s13550-024-01067-9

Kitagawa, H., Takenouchi, T., Azuma, R., Wesnes, K. A., Kramer, W. G., Clody, D. E., & Burnett, A. L. (2003). Safety, pharmacokinetics, and effects on cognitive function of multiple doses of GTS-21 in healthy, male volunteers. *Neuropsychopharmacology*, *28*(3), 542-551. https://doi.org/10.1038/sj.npp.1300028

Klein, R. C., & Yakel, J. L. (2006). Functional somato-dendritic alpha7-containing nicotinic acetylcholine receptors in the rat basolateral amygdala complex. *J Physiol*, *576*(Pt 3), 865-872. https://doi.org/10.1113/jphysiol.2006.118232

Kornum, B. R., Lind, N. M., Gillings, N., Marner, L., Andersen, F., & Knudsen, G. M. (2009). Evaluation of the novel 5-HT4 receptor PET ligand [11C]SB207145 in the Gottingen minipig. *J Cereb Blood Flow Metab*, *29*(1), 186-196. https://doi.org/10.1038/jcbfm.2008.110

Kouzarides, T. (2007). Chromatin modifications and their function. *Cell*, *128*(4), 693-705. https://doi.org/10.1016/j.cell.2007.02.005

Kulak, J. M., Carroll, F. I., & Schneider, J. S. (2006). [125I]Iodomethyllycaconitine binds to alpha7 nicotinic acetylcholine receptors in monkey brain. *Eur J Neurosci*, *23*(10), 2604-2610. https://doi.org/10.1111/j.1460-9568.2006.04804.x

Kwon, H. S., & Koh, S. H. (2020). Neuroinflammation in neurodegenerative disorders: the roles of microglia and astrocytes. *Transl Neurodegener*, *9*(1), 42. https://doi.org/10.1186/s40035-020-00221-2

Laruelle, M. (2000). Imaging synaptic neurotransmission with in vivo binding competition techniques: a critical review. *J Cereb Blood Flow Metab*, *20*(3), 423-451. https://doi.org/10.1097/00004647-200003000-00001

Lassen, N. A., Bartenstein, P. A., Lammertsma, A. A., Prevett, M. C., Turton, D. R., Luthra, S. K., Osman, S., Bloomfield, P. M., Jones, T., Patsalos, P. N., & et al. (1995). Benzodiazepine receptor quantification in vivo in humans using [11C]flumazenil and PET: application of the steady-state principle. *J Cereb Blood Flow Metab*, *15*(1), 152-165. https://doi.org/10.1038/jcbfm.1995.17

Laurell, G. L., Plaven-Sigray, P., Johansen, A., Raval, N. R., Nasser, A., Aabye Madsen, C., Madsen, J., Hansen, H. D., Donovan, L. L., Knudsen, G. M., Lammertsma, A. A., Ogden, R. T., Svarer, C., & Schain, M. (2023). Kinetic models for estimating occupancy from single-scan PET displacement studies. *J Cereb Blood Flow Metab*, *43*(9), 1544-1556. https://doi.org/10.1177/0271678X231168591

Laursen, T. M., Nordentoft, M., & Mortensen, P. B. (2014). Excess early mortality in schizophrenia. *Annu Rev Clin Psychol*, *10*, 425-448. https://doi.org/10.1146/annurev-clinpsy-032813-153657

Laws, M. T., Bonomi, R. E., Kamal, S., Gelovani, D. J., Llaniguez, J., Potukutchi, S., Lu, X., Mangner, T., & Gelovani, J. G. (2019). Molecular imaging HDACs class IIa expression-activity and pharmacologic inhibition in intracerebral glioma models in rats using PET/CT/(MRI) with [(18)F]TFAHA. *Sci Rep*, *9*(1), 3595. https://doi.org/10.1038/s41598-019-40054-2

Leiser, S. C., Bowlby, M. R., Comery, T. A., & Dunlop, J. (2009). A cog in cognition: how the alpha 7 nicotinic acetylcholine receptor is geared towards improving cognitive deficits. *Pharmacol Ther*, *122*(3), 302-311. https://doi.org/10.1016/j.pharmthera.2009.03.009

Leonard, S., Mexal, S., & Freedman, R. (2007). Smoking, Genetics and Schizophrenia: Evidence for Self Medication. *J Dual Diagn*, *3*(3-4), 43-59. https://doi.org/10.1300/J374v03n03_05

Letsinger, A. C., Gu, Z., & Yakel, J. L. (2022). alpha7 nicotinic acetylcholine receptors in the hippocampal circuit: taming complexity. *Trends Neurosci*, *45*(2), 145-157. https://doi.org/10.1016/j.tins.2021.11.006

Levin, E. D. (2013). Complex relationships of nicotinic receptor actions and cognitive functions. *Biochem Pharmacol*, *86*(8), 1145-1152. https://doi.org/10.1016/j.bcp.2013.07.021

Levin, E. D., McClernon, F. J., & Rezvani, A. H. (2006). Nicotinic effects on cognitive function: behavioral characterization, pharmacological specification, and anatomic localization. *Psychopharmacology (Berl)*, *184*(3-4), 523-539. https://doi.org/10.1007/s00213-005-0164-7

Lewis, A. S., van Schalkwyk, G. I., & Bloch, M. H. (2017). Alpha-7 nicotinic agonists for cognitive deficits in neuropsychiatric disorders: A translational meta-analysis of rodent and human studies. *Prog Neuropsychopharmacol Biol Psychiatry*, *75*, 45-53. https://doi.org/10.1016/j.pnpbp.2017.01.001

Lieberman, J. A., Dunbar, G., Segreti, A. C., Girgis, R. R., Seoane, F., Beaver, J. S., Duan, N., & Hosford, D. A. (2013). A randomized exploratory trial of an alpha-7 nicotinic receptor agonist (TC-5619) for cognitive enhancement in schizophrenia. *Neuropsychopharmacology*, *38*(6), 968-975. https://doi.org/10.1038/npp.2012.259

Lind, N. M., Moustgaard, A., Jelsing, J., Vajta, G., Cumming, P., & Hansen, A. K. (2007). The use of pigs in neuroscience: modeling brain disorders. *Neurosci Biobehav Rev*, *31*(5), 728-751. https://doi.org/10.1016/j.neubiorev.2007.02.003

Lisman, J., Buzsaki, G., Eichenbaum, H., Nadel, L., Ranganath, C., & Redish, A. D. (2017). Viewpoints: how the hippocampus contributes to memory, navigation and cognition. *Nat Neurosci*, *20*(11), 1434-1447. https://doi.org/10.1038/nn.4661

Liu, K. Y., & Howard, R. (2021). Can we learn lessons from the FDA's approval of aducanumab? *Nat Rev Neurol*, *17*(11), 715-722. https://doi.org/10.1038/s41582-021-00557-x

Liu, Q., Huang, Y., Xue, F., Simard, A., DeChon, J., Li, G., Zhang, J., Lucero, L., Wang, M., Sierks, M., Hu, G., Chang, Y., Lukas, R. J., & Wu, J. (2009). A novel nicotinic acetylcholine receptor subtype in basal forebrain cholinergic neurons with high sensitivity to amyloid peptides. *J Neurosci*, *29*(4), 918-929. https://doi.org/10.1523/JNEUROSCI.3952-08.2009

Liu, S. S., Wu, F., Jin, Y. M., Chang, W. Q., & Xu, T. M. (2020). HDAC11: a rising star in epigenetics. *Biomed Pharmacother*, *131*, 110607. https://doi.org/10.1016/j.biopha.2020.110607

Loewi, O. (1921). Über humorale Übertragbarkeit der Herznervenwirkung. *Pflügers Arch Ges Physiol*(189), 239-242. https://doi.org/https://doi.org/10.1007/BF01738910

Logan, J., Fowler, J. S., Volkow, N. D., Wolf, A. P., Dewey, S. L., Schlyer, D. J., MacGregor, R. R., Hitzemann, R., Bendriem, B., Gatley, S. J., & et al. (1990). Graphical analysis of reversible radioligand binding from time-activity measurements applied to [N-11C-methyl]-(-)-cocaine PET studies in human subjects. *J Cereb Blood Flow Metab*, *10*(5), 740-747. https://doi.org/10.1038/jcbfm.1990.127

Lunney, J. K., Van Goor, A., Walker, K. E., Hailstock, T., Franklin, J., & Dai, C. (2021). Importance of the pig as a human biomedical model. *Sci Transl Med*, *13*(621), eabd5758. https://doi.org/10.1126/scitranslmed.abd5758

Lyon, M. F. (1961). Gene action in the X-chromosome of the mouse (Mus musculus L.). *Nature*, *190*, 372-373. https://doi.org/10.1038/190372a0

Magnussen, J. H., Ettrup, A., Donat, C. K., Peters, D., Pedersen, M. H., Knudsen, G. M., & Mikkelsen, J. D. (2015). Radiosynthesis and in vitro validation of (3)H-NS14492 as a novel high affinity alpha7 nicotinic receptor radioligand. *Eur J Pharmacol*, *762*, 35-41. https://doi.org/10.1016/j.ejphar.2015.04.036

Magnussen, J. H., Ettrup, A., Lehel, S., Peters, D., Dyssegaard, A., Thomsen, M. S., Mikkelsen, J. D., & Knudsen, G. M. (2024). Characterizing the binding of TC-5619 and encenicline on the alpha7 nicotinic acetylcholine receptor using PET imaging in the pig. *Front Neuroimaging*, *3*, 1358221. https://doi.org/10.3389/fnimg.2024.1358221

Maguire, J. J., Kuc, R. E., & Davenport, A. P. (2012). Radioligand Binding Assays and Their Analysis. In A. P. Davenport (Ed.), *Receptor Binding Techniques* (pp. 31-77). Humana Press. https://doi.org/10.1007/978-1-61779-909-9_3

Mahase, E. (2021). Three FDA advisory panel members resign over approval of Alzheimer's drug. *BMJ*, *373*, n1503. https://doi.org/10.1136/bmj.n1503

Manetti, D., Dei, S., Arias, H. R., Braconi, L., Gabellini, A., Teodori, E., & Romanelli, M. N. (2023). Recent Advances in the Discovery of Nicotinic Acetylcholine Receptor Allosteric Modulators. *Molecules*, *28*(3). https://doi.org/10.3390/molecules28031270

Mansvelder, H. D., & McGehee, D. S. (2000). Long-term potentiation of excitatory inputs to brain reward areas by nicotine. *Neuron*, *27*(2), 349-357. https://doi.org/10.1016/s0896-6273(00)00042-8

Manuel, I., Barreda-Gomez, G., Gonzalez de San Roman, E., Veloso, A., Fernandez, J. A., Giralt, M. T., & Rodriguez-Puertas, R. (2015). Neurotransmitter receptor localization: from autoradiography to imaging mass spectrometry. *ACS Chem Neurosci*, *6*(3), 362-373. https://doi.org/10.1021/cn500281t

Marder, S. R., & Cannon, T. D. (2019). Schizophrenia. *N Engl J Med*, *381*(18), 1753-1761. https://doi.org/10.1056/NEJMra1808803

Markou, A., Chiamulera, C., Geyer, M. A., Tricklebank, M., & Steckler, T. (2009). Removing obstacles in neuroscience drug discovery: the future path for animal models. *Neuropsychopharmacology*, *34*(1), 74-89. https://doi.org/10.1038/npp.2008.173

Marks, P. A., & Breslow, R. (2007). Dimethyl sulfoxide to vorinostat: development of this histone deacetylase inhibitor as an anticancer drug. *Nat Biotechnol*, *25*(1), 84-90. https://doi.org/10.1038/nbt1272

Martin, L. F., & Freedman, R. (2007). Schizophrenia and the alpha7 nicotinic acetylcholine receptor. *Int Rev Neurobiol*, *78*, 225-246. https://doi.org/10.1016/S0074-7742(06)78008-4

Marutle, A., Zhang, X., Court, J., Piggott, M., Johnson, M., Perry, R., Perry, E., & Nordberg, A. (2001). Laminar distribution of nicotinic receptor subtypes in cortical regions in schizophrenia. *J Chem Neuroanat*, *22*(1-2), 115-126. https://doi.org/10.1016/s0891-0618(01)00117-x

Mattick, J. S., & Makunin, I. V. (2006). Non-coding RNA. *Hum Mol Genet*, *15 Spec No 1*, R17-29. https://doi.org/10.1093/hmg/ddl046

Mazurov, A. A., Kombo, D. C., Hauser, T. A., Miao, L., Dull, G., Genus, J. F., Fedorov, N. B., Benson, L., Sidach, S., Xiao, Y., Hammond, P. S., James, J. W., Miller, C. H., & Yohannes, D. (2012). Discovery of (2S,3R)-N-[2-(pyridin-3-ylmethyl)-1-azabicyclo[2.2.2]oct-3-yl]benzo[b]furan-2-carboxamide (TC-5619), a selective alpha7 nicotinic acetylcholine receptor agonist, for the treatment of cognitive disorders. *J Med Chem*, *55*(22), 9793-9809. https://doi.org/10.1021/jm301048a

McCluskey, S. P., Plisson, C., Rabiner, E. A., & Howes, O. (2020). Advances in CNS PET: the state-of-the-art for new imaging targets for pathophysiology and drug development. *Eur J Nucl Med Mol Imaging*, *47*(2), 451-489. https://doi.org/10.1007/s00259-019-04488-0

McCoy, A. N., & Tan, S. Y. (2014). Otto Loewi (1873-1961): Dreamer and Nobel laureate. *Singapore Med J*, *55*(1), 3-4. https://doi.org/10.11622/smedj.2014002

McCutcheon, R. A., Keefe, R. S. E., & McGuire, P. K. (2023). Cognitive impairment in schizophrenia: aetiology, pathophysiology, and treatment. *Mol Psychiatry*, *28*(5), 1902-1918. https://doi.org/10.1038/s41380-023-01949-9

McCutcheon, R. A., Reis Marques, T., & Howes, O. D. (2020). Schizophrenia-An Overview. *JAMA Psychiatry*, *77*(2), 201-210. https://doi.org/10.1001/jamapsychiatry.2019.3360

McQuown, S. C., Barrett, R. M., Matheos, D. P., Post, R. J., Rogge, G. A., Alenghat, T., Mullican, S. E., Jones, S., Rusche, J. R., Lazar, M. A., & Wood, M. A. (2011). HDAC3 is a critical negative regulator of long-term memory formation. *J Neurosci*, *31*(2), 764-774. https://doi.org/10.1523/JNEUROSCI.5052-10.2011

Medeiros, R., Castello, N. A., Cheng, D., Kitazawa, M., Baglietto-Vargas, D., Green, K. N., Esbenshade, T. A., Bitner, R. S., Decker, M. W., & LaFerla, F. M. (2014). alpha7 Nicotinic receptor agonist enhances cognition in aged 3xTg-AD mice with robust plaques and tangles. *Am J Pathol*, *184*(2), 520-529. https://doi.org/10.1016/j.ajpath.2013.10.010

Meyer, E. M., Kuryatov, A., Gerzanich, V., Lindstrom, J., & Papke, R. L. (1998). Analysis of 3-(4-hydroxy, 2-Methoxybenzylidene)anabaseine selectivity and activity at human and rat alpha-7 nicotinic receptors. *J Pharmacol Exp Ther*, *287*(3), 918-925. https://www.ncbi.nlm.nih.gov/pubmed/9864273

Migliore, L., & Coppede, F. (2022). Gene-environment interactions in Alzheimer disease: the emerging role of epigenetics. *Nat Rev Neurol*, *18*(11), 643-660. https://doi.org/10.1038/s41582-022-00714-w

Miledi, R., Molinoff, P., & Potter, L. T. (1971). Isolation of the cholinergic receptor protein of Torpedo electric tissue. *Nature*, *229*(5286), 554-557. https://doi.org/10.1038/229554a0

Mintun, M. A., Raichle, M. E., Kilbourn, M. R., Wooten, G. F., & Welch, M. J. (1984). A quantitative model for the in vivo assessment of drug binding sites with positron emission tomography. *Ann Neurol*, *15*(3), 217-227. https://doi.org/10.1002/ana.410150302

Moretti, M., Zoli, M., George, A. A., Lukas, R. J., Pistillo, F., Maskos, U., Whiteaker, P., & Gotti, C. (2014). The novel alpha7beta2-nicotinic acetylcholine receptor subtype is expressed in mouse and human basal forebrain: biochemical and pharmacological characterization. *Mol Pharmacol*, *86*(3), 306-317. https://doi.org/10.1124/mol.114.093377

Morgan, P., Van Der Graaf, P. H., Arrowsmith, J., Feltner, D. E., Drummond, K. S., Wegner, C. D., & Street, S. D. (2012). Can the flow of medicines be improved? Fundamental pharmacokinetic and pharmacological principles toward improving Phase II survival. *Drug Discov Today*, *17*(9-10), 419-424. https://doi.org/10.1016/j.drudis.2011.12.020

Moses, W. W. (2011). Fundamental Limits of Spatial Resolution in PET. *Nucl Instrum Methods Phys Res A*, *648 Supplement 1*, S236-S240. https://doi.org/10.1016/j.nima.2010.11.092

Mufson, E. J., Counts, S. E., Perez, S. E., & Ginsberg, S. D. (2008). Cholinergic system during the progression of Alzheimer's disease: therapeutic implications. *Expert Rev Neurother*, *8*(11), 1703-1718. https://doi.org/10.1586/14737175.8.11.1703

Mukhopadhyay, U., Tong, W. P., Gelovani, J. G., & Alauddin, M. M. (2006). Radiosynthesis of 6-([18F] fluoroacetamido)-1-hexanoicanilide ([18F] FAHA) for PET imaging of histone deacetylase (HDAC). *Journal of Labelled Compounds and Radiopharmaceuticals: The Official Journal of the International Isotope Society*, *49*(11), 997-1006.

Mullard, A. (2021). FDA approval for Biogen's aducanumab sparks Alzheimer disease firestorm. *Nat Rev Drug Discov*, *20*(7), 496. https://doi.org/10.1038/d41573-021-00099-3

Mulle, C., Choquet, D., Korn, H., & Changeux, J. P. (1992). Calcium influx through nicotinic receptor in rat central neurons: its relevance to cellular regulation. *Neuron*, *8*(1), 135-143. https://doi.org/10.1016/0896-6273(92)90115-t

Murray, K. O., Clanton, T. L., & Horowitz, M. (2022). Epigenetic responses to heat: From adaptation to maladaptation. *Exp Physiol*, *107*(10), 1144-1158. https://doi.org/10.1113/EP090143

Nachmansohn, D. (1964). Chemical Control of Bioelectric Currents in Membranes of Conducting Cells. *J Mt Sinai Hosp N Y*, *31*, 549-583. https://www.ncbi.nlm.nih.gov/pubmed/14232382

Nachmansohn, D. (1966). Role of acetylcholine in neuromuscular transmission. *Ann N Y Acad Sci*, *135*(1), 136-149. https://doi.org/10.1111/j.1749-6632.1966.tb45468.x

Nachmansohn, D. (1972). Biochemistry as part of my life. *Annu Rev Biochem*, *41*, 1-28. https://doi.org/10.1146/annurev.bi.41.070172.000245

Nag, S., Miranda-Azpiazu, P., Jia, Z., Datta, P., Arakawa, R., Moein, M. M., Yang, Z., Tu, Y., Lemoine, L., Agren, H., Nordberg, A., Langstrom, B., & Halldin, C. (2022). Development of (11)C-Labeled ASEM Analogues for the Detection of Neuronal Nicotinic Acetylcholine Receptors (alpha7-nAChR). *ACS Chem Neurosci*, *13*(3), 352-362. https://doi.org/10.1021/acschemneuro.1c00730

Nakaizumi, K., Ouchi, Y., Terada, T., Yoshikawa, E., Kakimoto, A., Isobe, T., Bunai, T., Yokokura, M., Suzuki, K., & Magata, Y. (2018). In vivo Depiction of alpha7 Nicotinic Receptor Loss for Cognitive Decline in Alzheimer's Disease. *J Alzheimers Dis*, *61*(4), 1355-1365. https://doi.org/10.3233/JAD-170591

Nestler, E. J., & Hyman, S. E. (2010). Animal models of neuropsychiatric disorders. *Nat Neurosci*, *13*(10), 1161-1169. https://doi.org/10.1038/nn.2647

Netzley, A. H., & Pelled, G. (2023). The Pig as a Translational Animal Model for Biobehavioral and Neurotrauma Research. *Biomedicines*, *11*(8), 2165.

Nikolac Perkovic, M., Videtic Paska, A., Konjevod, M., Kouter, K., Svob Strac, D., Nedic Erjavec, G., & Pivac, N. (2021). Epigenetics of Alzheimer's Disease. *Biomolecules*, *11*(2). https://doi.org/10.3390/biom11020195

Nordberg, A., & Winblad, B. (1986). Reduced number of [3H]nicotine and [3H]acetylcholine binding sites in the frontal cortex of Alzheimer brains. *Neurosci Lett*, *72*(1), 115-119. https://doi.org/10.1016/0304-3940(86)90629-4

Ogawa, M., Nishiyama, S., Tsukada, H., Hatano, K., Fuchigami, T., Yamaguchi, H., Matsushima, Y., Ito, K., & Magata, Y. (2010). Synthesis and evaluation of new imaging agent for central nicotinic acetylcholine receptor alpha7 subtype. *Nucl Med Biol*, *37*(3), 347-355. https://doi.org/10.1016/j.nucmedbio.2009.11.007

Olincy, A., Harris, J. G., Johnson, L. L., Pender, V., Kongs, S., Allensworth, D., Ellis, J., Zerbe, G. O., Leonard, S., Stevens, K. E., Stevens, J. O., Martin, L., Adler, L. E., Soti, F., Kem, W. R., & Freedman, R. (2006). Proof-of-concept trial of an alpha7 nicotinic agonist in schizophrenia. *Arch Gen Psychiatry*, *63*(6), 630-638. https://doi.org/10.1001/archpsyc.63.6.630

Owens, P. K., Raddad, E., Miller, J. W., Stille, J. R., Olovich, K. G., Smith, N. V., Jones, R. S., & Scherer, J. C. (2015). A decade of innovation in pharmaceutical R&D: the Chorus model. *Nat Rev Drug Discov*, *14*(1), 17-28. https://doi.org/10.1038/nrd4497

Pangalos, M. N., Schechter, L. E., & Hurko, O. (2007). Drug development for CNS disorders: strategies for balancing risk and reducing attrition. *Nat Rev Drug Discov*, *6*(7), 521-532. https://doi.org/10.1038/nrd2094

Panikker, P., Xu, S. J., Zhang, H., Sarthi, J., Beaver, M., Sheth, A., Akhter, S., & Elefant, F. (2018). Restoring Tip60 HAT/HDAC2 Balance in the Neurodegenerative Brain Relieves Epigenetic Transcriptional Repression and Reinstates Cognition. *J Neurosci*, *38*(19), 4569-4583. https://doi.org/10.1523/JNEUROSCI.2840-17.2018

Papke, R. L., & Horenstein, N. A. (2021). Therapeutic Targeting of alpha7 Nicotinic Acetylcholine Receptors. *Pharmacol Rev*, *73*(3), 1118-1149. https://doi.org/10.1124/pharmrev.120.000097

Papke, R. L., & Lindstrom, J. M. (2020). Nicotinic acetylcholine receptors: Conventional and unconventional ligands and signaling. *Neuropharmacology*, *168*, 108021. https://doi.org/10.1016/j.neuropharm.2020.108021

Park, S. Y., & Kim, J. S. (2020). A short guide to histone deacetylases including recent progress on class II enzymes. *Exp Mol Med*, *52*(2), 204-212. https://doi.org/10.1038/s12276-020-0382-4

Parri, H. R., Hernandez, C. M., & Dineley, K. T. (2011). Research update: Alpha7 nicotinic acetylcholine receptor mechanisms in Alzheimer's disease. *Biochem Pharmacol*, *82*(8), 931-942. https://doi.org/10.1016/j.bcp.2011.06.039

Pascoal, T. A., Chamoun, M., Lax, E., Wey, H. Y., Shin, M., Ng, K. P., Kang, M. S., Mathotaarachchi, S., Benedet, A. L., Therriault, J., Lussier, F. Z., Schroeder, F. A., DuBois, J. M., Hightower, B. G., Gilbert, T. M., Zurcher, N. R., Wang, C., Hopewell, R., Chakravarty, M., . . . Rosa-Neto, P. (2022). [(11)C]Martinostat PET analysis reveals reduced HDAC I availability in Alzheimer's disease. *Nat Commun*, *13*(1), 4171. https://doi.org/10.1038/s41467-022-30653-5

Passchier, J., Gee, A., Willemsen, A., Vaalburg, W., & van Waarde, A. (2002). Measuring drug-related receptor occupancy with positron emission tomography. *Methods*, *27*(3), 278-286. https://doi.org/10.1016/s1046-2023(02)00084-1

Pastor, V., & Medina, J. H. (2024). alpha7 nicotinic acetylcholine receptor in memory processing. *Eur J Neurosci*, *59*(9), 2138-2154. https://doi.org/10.1111/ejn.15913

Pereira, M., Cruz, M. T., Fortuna, A., & Bicker, J. (2024). Restoring the epigenome in Alzheimer's disease: advancing HDAC inhibitors as therapeutic agents. *Drug Discov Today*, 104052. https://doi.org/10.1016/j.drudis.2024.104052

Perkins, K. A., Roy Chengappa, K. N., Karelitz, J. L., Boldry, M. C., Michael, V., Herb, T., Gannon, J., Brar, J., Ford, L., Rassnick, S., & Brunzell, D. H. (2018). Initial Cross-Over Test of A Positive Allosteric Modulator of Alpha-7 Nicotinic Receptors to Aid Cessation in Smokers With Or Without Schizophrenia. *Neuropsychopharmacology*, *43*(6), 1334-1342. https://doi.org/10.1038/npp.2017.292

Perrine, S. A., Alsharif, W. F., Harutyunyan, A., Kamal, S., Viola, N. T., & Gelovani, J. G. (2022). Low- and high-cocaine intake affects the spatial and temporal dynamics of class IIa HDAC expression-activity in the nucleus accumbens and hippocampus of male rats as measured by [18F]TFAHA PET/CT neuroimaging. *Addict Neurosci*, *4*. https://doi.org/10.1016/j.addicn.2022.100046

Petronis, A. (2010). Epigenetics as a unifying principle in the aetiology of complex traits and diseases. *Nature*, *465*(7299), 721-727. https://doi.org/10.1038/nature09230

Phelps, M. E. (2000). Positron emission tomography provides molecular imaging of biological processes. *Proc Natl Acad Sci U S A*, *97*(16), 9226-9233. https://doi.org/10.1073/pnas.97.16.9226

Phelps, M. E., Hoffman, E. J., Huang, S. C., & Ter-Pogossian, M. M. (1975). Effect of positron range on spatial resolution. *J Nucl Med*, *16*(7), 649-652. https://www.ncbi.nlm.nih.gov/pubmed/1151485

Phelps, M. E., Hoffman, E. J., Mullani, N. A., & Ter-Pogossian, M. M. (1975). Application of annihilation coincidence detection to transaxial reconstruction tomography. *J Nucl Med*, *16*(3), 210-224. https://www.ncbi.nlm.nih.gov/pubmed/1113170

Picciotto, M. R., Caldarone, B. J., King, S. L., & Zachariou, V. (2000). Nicotinic receptors in the brain. Links between molecular biology and behavior. *Neuropsychopharmacology*, *22*(5), 451-465. https://doi.org/10.1016/S0893-133X(99)00146-3

Pichler, B. J., Judenhofer, M. S., & Pfannenberg, C. (2008). Multimodal imaging approaches: PET/CT and PET/MRI. *Handb Exp Pharmacol*(185 Pt 1), 109-132. https://doi.org/10.1007/978-3-540-72718-7_6

Pidoplichko, V. I., Prager, E. M., Aroniadou-Anderjaska, V., & Braga, M. F. (2013). alpha7-Containing nicotinic acetylcholine receptors on interneurons of the basolateral amygdala and their role in the regulation of the network excitability. *J Neurophysiol*, *110*(10), 2358-2369. https://doi.org/10.1152/jn.01030.2012

Pin, F., Vercouillie, J., Ouach, A., Mavel, S., Gulhan, Z., Chicheri, G., Jarry, C., Massip, S., Deloye, J. B., Guilloteau, D., Suzenet, F., Chalon, S., & Routier, S. (2014). Design of alpha7 nicotinic acetylcholine receptor ligands in quinuclidine, tropane and quinazoline series. Chemistry, molecular modeling, radiochemistry, in vitro and in rats evaluations of a [(18)F] quinuclidine derivative. *Eur J Med Chem*, *82*, 214-224. https://doi.org/10.1016/j.ejmech.2014.04.057

Platt, S. R., Holmes, S. P., Howerth, E. W., Duberstein, K. J. J., Dove, C. R., Kinder, H. A., Wyatt, E. L., Linville, A. V., Lau, V. W., Stice, S. L., Hill, W. D., Hess, D. C., & West, F. D. (2014). Development and characterization of a Yucatan miniature biomedical pig permanent middle cerebral artery occlusion stroke model. *Exp Transl Stroke Med*, *6*(1), 5. https://doi.org/10.1186/2040-7378-6-5

Pomper, M. G., Phillips, E., Fan, H., McCarthy, D. J., Keith, R. A., Gordon, J. C., Scheffel, U., Dannals, R. F., & Musachio, J. L. (2005). Synthesis and biodistribution of radiolabeled alpha 7 nicotinic acetylcholine receptor ligands. *J Nucl Med*, *46*(2), 326-334. https://www.ncbi.nlm.nih.gov/pubmed/15695794

Preskorn, S. H., Gawryl, M., Dgetluck, N., Palfreyman, M., Bauer, L. O., & Hilt, D. C. (2014). Normalizing effects of EVP-6124, an alpha-7 nicotinic partial agonist, on event-related potentials and cognition: a proof of concept, randomized trial in patients with schizophrenia. *J Psychiatr Pract*, *20*(1), 12-24. https://doi.org/10.1097/01.pra.0000442935.15833.c5

Prevost, M. S., Barilone, N., Dejean de la Batie, G., Pons, S., Ayme, G., England, P., Gielen, M., Bontems, F., Pehau-Arnaudet, G., Maskos, U., Lafaye, P., & Corringer, P. J. (2023). An original potentiating mechanism revealed by the cryo-EM structures of the human alpha7 nicotinic receptor in complex with nanobodies. *Nat Commun*, *14*(1), 5964. https://doi.org/10.1038/s41467-023-41734-4

Prickaerts, J., van Goethem, N. P., Chesworth, R., Shapiro, G., Boess, F. G., Methfessel, C., Reneerkens, O. A., Flood, D. G., Hilt, D., Gawryl, M., Bertrand, S., Bertrand, D., & Konig, G. (2012). EVP-6124, a novel and selective alpha7 nicotinic acetylcholine receptor partial agonist, improves memory performance by potentiating the acetylcholine response of alpha7 nicotinic acetylcholine receptors. *Neuropharmacology*, *62*(2), 1099-1110. https://doi.org/10.1016/j.neuropharm.2011.10.024

Quick, M. W., & Lester, R. A. (2002). Desensitization of neuronal nicotinic receptors. *J Neurobiol*, *53*(4), 457-478. https://doi.org/10.1002/neu.10109

Radcliffe, K. A., Fisher, J. L., Gray, R., & Dani, J. A. (1999). Nicotinic modulation of glutamate and GABA synaptic transmission of hippocampal neurons. *Ann N Y Acad Sci*, *868*, 591-610. https://doi.org/10.1111/j.1749-6632.1999.tb11332.x

Rakyan, V. K., Down, T. A., Balding, D. J., & Beck, S. (2011). Epigenome-wide association studies for common human diseases. *Nat Rev Genet*, *12*(8), 529-541. https://doi.org/10.1038/nrg3000

Rastan, S. (2015). Mary F. Lyon (1925-2014). *Nature*, *518*(7537), 36. https://doi.org/10.1038/518036a

Ravert, H. T., Dorff, P., Foss, C. A., Mease, R. C., Fan, H., Holmquist, C. R., Phillips, E., McCarthy, D. J., Heys, J. R., Holt, D. P., Wang, Y., Endres, C. J., Dannals, R. F., & Pomper, M. G. (2013). Radiochemical synthesis and in vivo evaluation of [18F]AZ11637326: an agonist probe for the alpha7 nicotinic acetylcholine receptor. *Nucl Med Biol*, *40*(6), 731-739. https://doi.org/10.1016/j.nucmedbio.2013.04.005

Reid, A. E., Hooker, J., Shumay, E., Logan, J., Shea, C., Kim, S. W., Collins, S., Xu, Y., Volkow, N., & Fowler, J. S. (2009). Evaluation of 6-([(18)F]fluoroacetamido)-1-hexanoicanilide for PET imaging of histone deacetylase in the baboon brain. *Nucl Med Biol*, *36*(3), 247-258. https://doi.org/10.1016/j.nucmedbio.2008.12.005

Reid, V., Iškauskienė, M., Sackus, A., Marti, J., Kurian, D., Wishart, T., Lucatelli, C., Peters, D., Baker, A., Newby, D., Hadoke, P., Gray, G., Tavares, A., & MacAskill, M. (2023). 15 Investigation of alpha-7 nicotinic acetylcholine receptor as an imaging target for myocardial infarct healing. *Heart*, *109*(Suppl 2), A5-A5. https://doi.org/10.1136/heartjnl-SCF-2023.15

Rezvani, A. H., Kholdebarin, E., Brucato, F. H., Callahan, P. M., Lowe, D. A., & Levin, E. D. (2009). Effect of R3487/MEM3454, a novel nicotinic alpha7 receptor partial agonist and 5-HT3 antagonist on sustained attention in rats. *Prog Neuropsychopharmacol Biol Psychiatry*, *33*(2), 269-275. https://doi.org/10.1016/j.pnpbp.2008.11.018

Rich, D. A. (1997). A brief history of positron emission tomography. *J Nucl Med Technol*, *25*(1), 4-11. https://www.ncbi.nlm.nih.gov/pubmed/9239597

Rotering, S., Scheunemann, M., Fischer, S., Hiller, A., Peters, D., Deuther-Conrad, W., & Brust, P. (2013). Radiosynthesis and first evaluation in mice of [(18)F]NS14490 for molecular imaging of alpha7 nicotinic acetylcholine receptors. *Bioorg Med Chem*, *21*(9), 2635-2642. https://doi.org/10.1016/j.bmc.2013.02.018

Sabri, O., Sabbagh, M. N., Seibyl, J., Barthel, H., Akatsu, H., Ouchi, Y., Senda, K., Murayama, S., Ishii, K., Takao, M., Beach, T. G., Rowe, C. C., Leverenz, J. B., Ghetti, B., Ironside, J. W., Catafau, A. M., Stephens, A. W., Mueller, A., Koglin, N., . . . Florbetaben Phase 3 Study, G. (2015). Florbetaben PET imaging to detect amyloid beta plaques in Alzheimer's disease: phase 3 study. *Alzheimers Dement*, *11*(8), 964-974. https://doi.org/10.1016/j.jalz.2015.02.004

Sanders, V. R., & Millar, N. S. (2023). Potentiation and allosteric agonist activation of alpha7 nicotinic acetylcholine receptors: binding sites and hypotheses. *Pharmacol Res*, *191*, 106759. https://doi.org/10.1016/j.phrs.2023.106759

Scheltens, P., Blennow, K., Breteler, M. M., de Strooper, B., Frisoni, G. B., Salloway, S., & Van der Flier, W. M. (2016). Alzheimer's disease. *Lancet*, *388*(10043), 505-517. https://doi.org/10.1016/S0140-6736(15)01124-1

Schneider, L. S. (2022). Editorial: Aducanumab Trials EMERGE But Don't ENGAGE. *J Prev Alzheimers Dis*, *9*(2), 193-196. https://doi.org/10.14283/jpad.2022.37

Schroeder, F. A., Wang, C., Van de Bittner, G. C., Neelamegam, R., Takakura, W. R., Karunakaran, A., Wey, H. Y., Reis, S. A., Gale, J., Zhang, Y. L., Holson, E. B., Haggarty, S. J., & Hooker, J. M. (2014). PET imaging demonstrates histone deacetylase target engagement and clarifies brain penetrance of known and novel small molecule inhibitors in rat. *ACS Chem Neurosci*, *5*(10), 1055-1062. https://doi.org/10.1021/cn500162j

Seguela, P., Wadiche, J., Dineley-Miller, K., Dani, J. A., & Patrick, J. W. (1993). Molecular cloning, functional properties, and distribution of rat brain alpha 7: a nicotinic cation channel highly permeable to calcium. *J Neurosci*, *13*(2), 596-604. https://doi.org/10.1523/JNEUROSCI.13-02-00596.1993

Seo, Y. J., Muench, L., Reid, A., Chen, J., Kang, Y., Hooker, J. M., Volkow, N. D., Fowler, J. S., & Kim, S. W. (2013). Radionuclide labeling and evaluation of candidate radioligands for PET imaging of histone deacetylase in the brain. *Bioorg Med Chem Lett*, *23*(24), 6700-6705. https://doi.org/10.1016/j.bmcl.2013.10.038

Seto, E., & Yoshida, M. (2014). Erasers of histone acetylation: the histone deacetylase enzymes. *Cold Spring Harb Perspect Biol*, *6*(4), a018713. https://doi.org/10.1101/cshperspect.a018713

Sevigny, J., Chiao, P., Bussiere, T., Weinreb, P. H., Williams, L., Maier, M., Dunstan, R., Salloway, S., Chen, T., Ling, Y., O'Gorman, J., Qian, F., Arastu, M., Li, M., Chollate, S., Brennan, M. S., Quintero-Monzon, O., Scannevin, R. H., Arnold, H. M., . . . Sandrock, A. (2016). The antibody aducanumab reduces Abeta plaques in Alzheimer's disease. *Nature*, *537*(7618), 50-56. https://doi.org/10.1038/nature19323

Shah, P., & Westwell, A. D. (2007). The role of fluorine in medicinal chemistry. *J Enzyme Inhib Med Chem*, *22*(5), 527-540. https://doi.org/10.1080/14756360701425014

Shen, J. X., & Yakel, J. L. (2009). Nicotinic acetylcholine receptor-mediated calcium signaling in the nervous system. *Acta Pharmacol Sin*, *30*(6), 673-680. https://doi.org/10.1038/aps.2009.64

Shytle, R. D., Mori, T., Townsend, K., Vendrame, M., Sun, N., Zeng, J., Ehrhart, J., Silver, A. A., Sanberg, P. R., & Tan, J. (2004). Cholinergic modulation of microglial activation by alpha 7 nicotinic receptors. *J Neurochem*, *89*(2), 337-343. https://doi.org/10.1046/j.1471-4159.2004.02347.x

Simchick, G., Shen, A., Campbell, B., Park, H. J., West, F. D., & Zhao, Q. (2019). Pig Brains Have Homologous Resting-State Networks with Human Brains. *Brain Connect*, *9*(7), 566-579. https://doi.org/10.1089/brain.2019.0673

Sinkus, M. L., Graw, S., Freedman, R., Ross, R. G., Lester, H. A., & Leonard, S. (2015). The human CHRNA7 and CHRFAM7A genes: A review of the genetics, regulation, and function. *Neuropharmacology*, *96*(Pt B), 274-288. https://doi.org/10.1016/j.neuropharm.2015.02.006

Smith, Z. D., & Meissner, A. (2013). DNA methylation: roles in mammalian development. *Nat Rev Genet*, *14*(3), 204-220. https://doi.org/10.1038/nrg3354

Solon, E. G. (2007). Autoradiography: high-resolution molecular imaging in pharmaceutical discovery and development. *Expert Opin Drug Discov*, *2*(4), 503-514. https://doi.org/10.1517/17460441.2.4.503

Stanimirovic, D. B., Bani-Yaghoub, M., Perkins, M., & Haqqani, A. S. (2015). Blood-brain barrier models: in vitro to in vivo translation in preclinical development of CNS-targeting biotherapeutics. *Expert Opin Drug Discov*, *10*(2), 141-155. https://doi.org/10.1517/17460441.2015.974545

Statello, L., Guo, C. J., Chen, L. L., & Huarte, M. (2021). Gene regulation by long non-coding RNAs and its biological functions. *Nat Rev Mol Cell Biol*, *22*(2), 96-118. https://doi.org/10.1038/s41580-020-00315-9

Steeds, H., Carhart-Harris, R. L., & Stone, J. M. (2015). Drug models of schizophrenia. *Ther Adv Psychopharmacol*, *5*(1), 43-58. https://doi.org/10.1177/2045125314557797

Strahl, B. D., & Allis, C. D. (2000). The language of covalent histone modifications. *Nature*, *403*(6765), 41-45. https://doi.org/10.1038/47412

Sureau, F. C., Reader, A. J., Comtat, C., Leroy, C., Ribeiro, M. J., Buvat, I., & Trebossen, R. (2008). Impact of image-space resolution modeling for studies with the high-resolution research tomograph. *J Nucl Med*, *49*(6), 1000-1008. https://doi.org/10.2967/jnumed.107.045351

Sydserff, S., Sutton, E. J., Song, D., Quirk, M. C., Maciag, C., Li, C., Jonak, G., Gurley, D., Gordon, J. C., Christian, E. P., Doherty, J. J., Hudzik, T., Johnson, E., Mrzljak, L., Piser, T., Smagin, G. N., Wang, Y., Widzowski, D., & Smith, J. S. (2009). Selective alpha7 nicotinic receptor activation by AZD0328 enhances cortical dopamine release and improves learning and attentional processes. *Biochem Pharmacol*, *78*(7), 880-888. https://doi.org/10.1016/j.bcp.2009.07.005

Syvanen, S., Lindhe, O., Palner, M., Kornum, B. R., Rahman, O., Langstrom, B., Knudsen, G. M., & Hammarlund-Udenaes, M. (2009). Species differences in blood-brain barrier transport of three positron emission tomography radioligands with emphasis on P-glycoprotein transport. *Drug Metab Dispos*, *37*(3), 635-643. https://doi.org/10.1124/dmd.108.024745

Szabo, A. K., Pesti, K., Mike, A., & Vizi, E. S. (2014). Mode of action of the positive modulator PNU-120596 on alpha7 nicotinic acetylcholine receptors. *Neuropharmacology*, *81*, 42-54. https://doi.org/10.1016/j.neuropharm.2014.01.033

Tago, T., Sakata, M., Kanazawa, M., Yamamoto, S., Ishii, K., & Toyohara, J. (2024). Preclinical validation of a novel brain-penetrant PET ligand for visualization of histone deacetylase 6: a potential imaging target for neurodegenerative diseases. *European Journal of Nuclear Medicine and Molecular Imaging*, 1-11.

Tago, T., Toyohara, J., & Ishii, K. (2021). Preclinical evaluation of an 18F-labeled SW-100 derivative for PET imaging of histone deacetylase 6 in the brain. *ACS Chemical Neuroscience*, *12*(4), 746-755.

Tahami Monfared, A. A., Byrnes, M. J., White, L. A., & Zhang, Q. (2022). The Humanistic and Economic Burden of Alzheimer's Disease. *Neurol Ther*, *11*(2), 525-551. https://doi.org/10.1007/s40120-022-00335-x

Takano, A., Varrone, A., Gulyas, B., Salvadori, P., Gee, A., Windhorst, A., Vercouillie, J., Bormans, G., Lammertsma, A. A., & Halldin, C. (2016). Guidelines to PET measurements of the target occupancy in the brain for drug development. *Eur J Nucl Med Mol Imaging*, *43*(12), 2255-2262. https://doi.org/10.1007/s00259-016-3476-4

Takata, K., Kitamura, Y., Saeki, M., Terada, M., Kagitani, S., Kitamura, R., Fujikawa, Y., Maelicke, A., Tomimoto, H., Taniguchi, T., & Shimohama, S. (2010). Galantamine-induced amyloid-beta clearance mediated via stimulation of microglial nicotinic acetylcholine receptors. *J Biol Chem*, *285*(51), 40180-40191. https://doi.org/10.1074/jbc.M110.142356

Taly, A., Corringer, P. J., Guedin, D., Lestage, P., & Changeux, J. P. (2009). Nicotinic receptors: allosteric transitions and therapeutic targets in the nervous system. *Nat Rev Drug Discov*, *8*(9), 733-750. https://doi.org/10.1038/nrd2927

Tansey, E. M. (2006). Henry Dale and the discovery of acetylcholine. *C R Biol*, *329*(5-6), 419-425. https://doi.org/10.1016/j.crvi.2006.03.012

Teaktong, T., Graham, A. J., Court, J. A., Perry, R. H., Jaros, E., Johnson, M., Hall, R., & Perry, E. K. (2004). Nicotinic acetylcholine receptor immunohistochemistry in Alzheimer's disease and dementia with Lewy bodies: differential neuronal and astroglial pathology. *J Neurol Sci*, *225*(1-2), 39-49. https://doi.org/10.1016/j.jns.2004.06.015

Ter-Pogossian, M. M., Phelps, M. E., Hoffman, E. J., & Mullani, N. A. (1975). A positron-emission transaxial tomograph for nuclear imaging (PETT). *Radiology*, *114*(1), 89-98. https://doi.org/10.1148/114.1.89

Terry, A. V., Jr., Jones, K., & Bertrand, D. (2023). Nicotinic acetylcholine receptors in neurological and psychiatric diseases. *Pharmacol Res*, *191*, 106764. https://doi.org/10.1016/j.phrs.2023.106764

Thomsen, M. S., Hansen, H. H., Timmerman, D. B., & Mikkelsen, J. D. (2010). Cognitive improvement by activation of alpha7 nicotinic acetylcholine receptors: from animal models to human pathophysiology. *Curr Pharm Des*, *16*(3), 323-343. https://doi.org/10.2174/138161210790170094

Thomsen, M. S., Zwart, R., Ursu, D., Jensen, M. M., Pinborg, L. H., Gilmour, G., Wu, J., Sher, E., & Mikkelsen, J. D. (2015). alpha7 and beta2 Nicotinic Acetylcholine Receptor Subunits Form Heteromeric Receptor Complexes that Are Expressed in the Human Cortex and Display Distinct Pharmacological Properties. *PLoS One*, *10*(6), e0130572. https://doi.org/10.1371/journal.pone.0130572

Toyohara, J., Ishiwata, K., Sakata, M., Wu, J., Nishiyama, S., Tsukada, H., & Hashimoto, K. (2010). In vivo evaluation of alpha7 nicotinic acetylcholine receptor agonists [11C]A-582941 and

[11C]A-844606 in mice and conscious monkeys. *PLoS One*, *5*(2), e8961. https://doi.org/10.1371/journal.pone.0008961

Toyohara, J., Sakata, M., Wu, J., Ishikawa, M., Oda, K., Ishii, K., Iyo, M., Hashimoto, K., & Ishiwata, K. (2009). Preclinical and the first clinical studies on [11C]CHIBA-1001 for mapping alpha7 nicotinic receptors by positron emission tomography. *Ann Nucl Med*, *23*(3), 301-309. https://doi.org/10.1007/s12149-009-0240-x

Tregellas, J. R., & Wylie, K. P. (2019). Alpha7 Nicotinic Receptors as Therapeutic Targets in Schizophrenia. *Nicotine Tob Res*, *21*(3), 349-356. https://doi.org/10.1093/ntr/nty034

Trenkwalder, C., Berg, D., Rascol, O., Eggert, K., Ceballos-Baumann, A., Corvol, J. C., Storch, A., Zhang, L., Azulay, J. P., Broussolle, E., Defebvre, L., Geny, C., Gostkowski, M., Stocchi, F., Tranchant, C., Derkinderen, P., Durif, F., Espay, A. J., Feigin, A., . . . Gomez-Mancilla, B. (2016). A Placebo-Controlled Trial of AQW051 in Patients With Moderate to Severe Levodopa-Induced Dyskinesia. *Mov Disord*, *31*(7), 1049-1054. https://doi.org/10.1002/mds.26569

Tribollet, E., Bertrand, D., Marguerat, A., & Raggenbass, M. (2004). Comparative distribution of nicotinic receptor subtypes during development, adulthood and aging: an autoradiographic study in the rat brain. *Neuroscience*, *124*(2), 405-420. https://doi.org/10.1016/j.neuroscience.2003.09.028

Tseng, C. J., Gilbert, T. M., Catanese, M. C., Hightower, B. G., Peters, A. T., Parmar, A. J., Kim, M., Wang, C., Roffman, J. L., Brown, H. E., Perlis, R. H., Zurcher, N. R., & Hooker, J. M. (2020). In vivo human brain expression of histone deacetylases in bipolar disorder. *Transl Psychiatry*, *10*(1), 224. https://doi.org/10.1038/s41398-020-00911-5

Umbricht, D., Keefe, R. S., Murray, S., Lowe, D. A., Porter, R., Garibaldi, G., & Santarelli, L. (2014). A randomized, placebo-controlled study investigating the nicotinic alpha7 agonist, RG3487, for cognitive deficits in schizophrenia. *Neuropsychopharmacology*, *39*(7), 1568-1577. https://doi.org/10.1038/npp.2014.17

Valenstein, E. S. (2002). The discovery of chemical neurotransmitters. *Brain Cogn*, *49*(1), 73-95. https://doi.org/10.1006/brcg.2001.1487

van Waarde, A., Marcolini, S., de Deyn, P. P., & Dierckx, R. (2021). PET Agents in Dementia: An Overview. *Semin Nucl Med*, *51*(3), 196-229. https://doi.org/10.1053/j.semnuclmed.2020.12.008

Vaquero, J. J., & Kinahan, P. (2015). Positron Emission Tomography: Current Challenges and Opportunities for Technological Advances in Clinical and Preclinical Imaging Systems. *Annu Rev Biomed Eng*, *17*, 385-414. https://doi.org/10.1146/annurev-bioeng-071114-040723

Vetel, S., Vercouillie, J., Buron, F., Vergote, J., Tauber, C., Busson, J., Chicheri, G., Routier, S., Serriere, S., & Chalon, S. (2020). Longitudinal PET Imaging of alpha7 Nicotinic Acetylcholine Receptors with [(18)F]ASEM in a Rat Model of Parkinson's Disease. *Mol Imaging Biol*, *22*(2), 348-357. https://doi.org/10.1007/s11307-019-01400-y

Villadsen, J., Hansen, H. D., Jorgensen, L. M., Keller, S. H., Andersen, F. L., Petersen, I. N., Knudsen, G. M., & Svarer, C. (2018). Automatic delineation of brain regions on MRI and PET images

from the pig. *J Neurosci Methods*, *294*, 51-58. https://doi.org/10.1016/j.jneumeth.2017.11.008

Volpi, T., Maccioni, L., Colpo, M., Debiasi, G., Capotosti, A., Ciceri, T., Carson, R. E., DeLorenzo, C., Hahn, A., Knudsen, G. M., Lammertsma, A. A., Price, J. C., Sossi, V., Wang, G., Zanotti-Fregonara, P., Bertoldo, A., & Veronese, M. (2023). An update on the use of image-derived input functions for human PET studies: new hopes or old illusions? *EJNMMI Res*, *13*(1), 97. https://doi.org/10.1186/s13550-023-01050-w

Vos, T., Abajobir, A. A., Abate, K. H., Abbafati, C., Abbas, K. M., Abd-Allah, F., Abdulkader, R. S., Abdulle, A. M., Abebo, T. A., & Abera, S. F. (2017). Global, regional, and national incidence, prevalence, and years lived with disability for 328 diseases and injuries for 195 countries, 1990–2016: a systematic analysis for the Global Burden of Disease Study 2016. *The Lancet*, *390*(10100), 1211-1259.

Waddington, C. H. (2012). The epigenotype. 1942. *Int J Epidemiol*, *41*(1), 10-13. https://doi.org/10.1093/ije/dyr184

Wakuda, T., Yokokura, M., Nakaizumi, K., Kato, Y., Kameno, Y., Futatsubashi, M., Yoshikawa, E., Magata, Y., Ouchi, Y., & Yamasue, H. (2018). F148. A Pilot Study of [11C](R)-MEQAA PET Brain Imaging Analysis of Alpha 7 Nicotinic Acetylcholine Receptors Availability in Schizophrenia. *Schizophrenia Bulletin*, *44*(suppl_1), S277-S278.

Wallace, T. L., & Bertrand, D. (2013). Importance of the nicotinic acetylcholine receptor system in the prefrontal cortex. *Biochem Pharmacol*, *85*(12), 1713-1720. https://doi.org/10.1016/j.bcp.2013.04.001

Walling, D., Marder, S. R., Kane, J., Fleischhacker, W. W., Keefe, R. S., Hosford, D. A., Dvergsten, C., Segreti, A. C., Beaver, J. S., Toler, S. M., Jett, J. E., & Dunbar, G. C. (2016). Phase 2 Trial of an Alpha-7 Nicotinic Receptor Agonist (TC-5619) in Negative and Cognitive Symptoms of Schizophrenia. *Schizophr Bull*, *42*(2), 335-343. https://doi.org/10.1093/schbul/sbv072

Wang, C., Schroeder, F. A., & Hooker, J. M. (2014). Visualizing epigenetics: current advances and advantages in HDAC PET imaging techniques. *Neuroscience*, *264*, 186-197. https://doi.org/10.1016/j.neuroscience.2013.09.018

Wang, C., Schroeder, F. A., Wey, H. Y., Borra, R., Wagner, F. F., Reis, S., Kim, S. W., Holson, E. B., Haggarty, S. J., & Hooker, J. M. (2014). In vivo imaging of histone deacetylases (HDACs) in the central nervous system and major peripheral organs. *J Med Chem*, *57*(19), 7999-8009. https://doi.org/10.1021/jm500872p

Wang, D., Yao, Y., Wang, S., Zhang, H., & He, Z. X. (2021). The Availability of the alpha7-Nicotinic Acetylcholine Receptor in Early Identification of Vulnerable Atherosclerotic Plaques: A Study Using a Novel (18)F-Label Radioligand PET. *Front Bioeng Biotechnol*, *9*, 640037. https://doi.org/10.3389/fbioe.2021.640037

Wang, H., Yu, M., Ochani, M., Amella, C. A., Tanovic, M., Susarla, S., Li, J. H., Wang, H., Yang, H., Ulloa, L., Al-Abed, Y., Czura, C. J., & Tracey, K. J. (2003). Nicotinic acetylcholine receptor alpha7 subunit is an essential regulator of inflammation. *Nature*, *421*(6921), 384-388. https://doi.org/10.1038/nature01339

Wang, S., Fang, Y., Wang, H., Gao, H., Jiang, G., Liu, J., Xue, Q., Qi, Y., Cao, M., Qiang, B., & Zhang, H. (2018). Design, synthesis and biological evaluation of 1,4-Diazobicylco[3.2.2]nonane derivatives as alpha7-Nicotinic acetylcholine receptor PET/CT imaging agents and agonists for Alzheimer's disease. *Eur J Med Chem*, *159*, 255-266. https://doi.org/10.1016/j.ejmech.2018.09.064

Wanka, L., Iqbal, K., & Schreiner, P. R. (2013). The lipophilic bullet hits the targets: medicinal chemistry of adamantane derivatives. *Chem Rev*, *113*(5), 3516-3604. https://doi.org/10.1021/cr100264t

Watabe, H., Ikoma, Y., Kimura, Y., Naganawa, M., & Shidahara, M. (2006). PET kinetic analysis--compartmental model. *Ann Nucl Med*, *20*(9), 583-588. https://doi.org/10.1007/BF02984655

Webster, A. L., Yan, M. S., & Marsden, P. A. (2013). Epigenetics and cardiovascular disease. *Can J Cardiol*, *29*(1), 46-57. https://doi.org/10.1016/j.cjca.2012.10.023

Wei, P., Lyu, W., Xu, L., Feng, H., Zhou, H., & Li, J. (2022). alpha7 Nicotinic Acetylcholine Receptor May Be a Pharmacological Target for Perioperative Neurocognitive Disorders. *Front Pharmacol*, *13*, 907713. https://doi.org/10.3389/fphar.2022.907713

West, A. C., & Johnstone, R. W. (2014). New and emerging HDAC inhibitors for cancer treatment. *J Clin Invest*, *124*(1), 30-39. https://doi.org/10.1172/JCI69738

Wey, H. Y., Gilbert, T. M., Zurcher, N. R., She, A., Bhanot, A., Taillon, B. D., Schroeder, F. A., Wang, C., Haggarty, S. J., & Hooker, J. M. (2016). Insights into neuroepigenetics through human histone deacetylase PET imaging. *Sci Transl Med*, *8*(351), 351ra106. https://doi.org/10.1126/scitranslmed.aaf7551

Wey, H. Y., Wang, C., Schroeder, F. A., Logan, J., Price, J. C., & Hooker, J. M. (2015). Kinetic Analysis and Quantification of [(1)(1)C]Martinostat for in Vivo HDAC Imaging of the Brain. *ACS Chem Neurosci*, *6*(5), 708-715. https://doi.org/10.1021/acschemneuro.5b00066

Williams, D. K., Wang, J., & Papke, R. L. (2011). Positive allosteric modulators as an approach to nicotinic acetylcholine receptor-targeted therapeutics: advantages and limitations. *Biochem Pharmacol*, *82*(8), 915-930. https://doi.org/10.1016/j.bcp.2011.05.001

Wilson, A. J., Byun, D. S., Nasser, S., Murray, L. B., Ayyanar, K., Arango, D., Figueroa, M., Melnick, A., Kao, G. D., Augenlicht, L. H., & Mariadason, J. M. (2008). HDAC4 promotes growth of colon cancer cells via repression of p21. *Mol Biol Cell*, *19*(10), 4062-4075. https://doi.org/10.1091/mbc.e08-02-0139

Winblad, B., Amouyel, P., Andrieu, S., Ballard, C., Brayne, C., Brodaty, H., Cedazo-Minguez, A., Dubois, B., Edvardsson, D., Feldman, H., Fratiglioni, L., Frisoni, G. B., Gauthier, S., Georges, J., Graff, C., Iqbal, K., Jessen, F., Johansson, G., Jonsson, L., . . . Zetterberg, H. (2016). Defeating Alzheimer's disease and other dementias: a priority for European science and society. *Lancet Neurol*, *15*(5), 455-532. https://doi.org/10.1016/S1474-4422(16)00062-4

Winterer, G., Gallinat, J., Brinkmeyer, J., Musso, F., Kornhuber, J., Thuerauf, N., Rujescu, D., Favis, R., Sun, Y., Franc, M. A., Ouwerkerk-Mahadevan, S., Janssens, L., Timmers, M., & Streffer, J. R. (2013). Allosteric alpha-7 nicotinic receptor modulation and P50 sensory gating in

schizophrenia: a proof-of-mechanism study. *Neuropharmacology*, *64*, 197-204. https://doi.org/10.1016/j.neuropharm.2012.06.040

Wittenberg, R. E., Wolfman, S. L., De Biasi, M., & Dani, J. A. (2020). Nicotinic acetylcholine receptors and nicotine addiction: A brief introduction. *Neuropharmacology*, *177*, 108256. https://doi.org/10.1016/j.neuropharm.2020.108256

Wong, D. F., Kuwabara, H., Pomper, M., Holt, D. P., Brasic, J. R., George, N., Frolov, B., Willis, W., Gao, Y., Valentine, H., Nandi, A., Gapasin, L., Dannals, R. F., & Horti, A. G. (2014). Human brain imaging of alpha7 nAChR with [(18)F]ASEM: a new PET radiotracer for neuropsychiatry and determination of drug occupancy. *Mol Imaging Biol*, *16*(5), 730-738. https://doi.org/10.1007/s11307-014-0779-3

Wong, N., Harrington, C., Jenkins, K., Yoon, M., Soule, A., Du, Y., Horti, A., Pomper, M., Kamath, V., & Rubin, L. (2024). 407. The Low Availability of the α7-NAChR in Recent-Onset Psychosis and its Link to Cognitive and Psychotic Symptom Burden. *Biological Psychiatry*, *95*(10), S266.

Woolsey, A., Jenkins, K. R., Harrington, C. K., Miller, H. M., Soule, A. R., Du, Y., Horti, A. G., Pomper, M. G., Bakker, A., & Rubin, L. H. (2024). 491. Higher Availability of the α7 Nicotinic Acetylcholine Receptor in the Brains of Older, Cognitively Normal Individuals. *Biological Psychiatry*, *95*(10), S300.

Wu, J., Liu, Q., Tang, P., Mikkelsen, J. D., Shen, J., Whiteaker, P., & Yakel, J. L. (2016). Heteromeric alpha7beta2 Nicotinic Acetylcholine Receptors in the Brain. *Trends Pharmacol Sci*, *37*(7), 562-574. https://doi.org/10.1016/j.tips.2016.03.005

Xu, W. S., Parmigiani, R. B., & Marks, P. A. (2007). Histone deacetylase inhibitors: molecular mechanisms of action. *Oncogene*, *26*(37), 5541-5552. https://doi.org/10.1038/sj.onc.1210620

Yan, M. S., Matouk, C. C., & Marsden, P. A. (2010). Epigenetics of the vascular endothelium. *J Appl Physiol (1985)*, *109*(3), 916-926. https://doi.org/10.1152/japplphysiol.00131.2010

Yang, T., Wang, D., Chen, X., Liang, Y., Guo, F., Wu, C., Jia, L., Hou, Z., Li, W., He, Z., & Wang, X. (2021). (18)F-ASEM Imaging for Evaluating Atherosclerotic Plaques Linked to alpha7-Nicotinic Acetylcholine Receptor. *Front Bioeng Biotechnol*, *9*, 684221. https://doi.org/10.3389/fbioe.2021.684221

Yang, Y., Paspalas, C. D., Jin, L. E., Picciotto, M. R., Arnsten, A. F., & Wang, M. (2013). Nicotinic alpha7 receptors enhance NMDA cognitive circuits in dorsolateral prefrontal cortex. *Proc Natl Acad Sci U S A*, *110*(29), 12078-12083. https://doi.org/10.1073/pnas.1307849110

Yeh, H. H., Tian, M., Hinz, R., Young, D., Shavrin, A., Mukhapadhyay, U., Flores, L. G., Balatoni, J., Soghomonyan, S., Jeong, H. J., Pal, A., Uthamanthil, R., Jackson, J. N., Nishii, R., Mizuma, H., Onoe, H., Kagawa, S., Higashi, T., Fukumitsu, N., . . . Gelovani, J. G. (2013). Imaging epigenetic regulation by histone deacetylases in the brain using PET/MRI with (1)(8)F-FAHA. *Neuroimage*, *64*, 630-639. https://doi.org/10.1016/j.neuroimage.2012.09.019

Yin, J., Chen, W., Yang, H., Xue, M., & Schaaf, C. P. (2017). Chrna7 deficient mice manifest no consistent neuropsychiatric and behavioral phenotypes. *Sci Rep*, *7*, 39941. https://doi.org/10.1038/srep39941

Young, H. S., Herbette, L. G., & Skita, V. (2003). Alpha-bungarotoxin binding to acetylcholine receptor membranes studied by low angle X-ray diffraction. *Biophys J*, *85*(2), 943-953. https://doi.org/10.1016/S0006-3495(03)74533-0

Yu, Y., Annala, A. J., Barrio, J. R., Toyokuni, T., Satyamurthy, N., Namavari, M., Cherry, S. R., Phelps, M. E., Herschman, H. R., & Gambhir, S. S. (2000). Quantification of target gene expression by imaging reporter gene expression in living animals. *Nat Med*, *6*(8), 933-937. https://doi.org/10.1038/78704

Zanzonico, P. (2004). Positron emission tomography: a review of basic principles, scanner design and performance, and current systems. *Semin Nucl Med*, *34*(2), 87-111. https://doi.org/10.1053/j.semnuclmed.2003.12.002

Zeglis, B. M., Pillarsetty, N., Divilov, V., Blasberg, R. A., & Lewis, J. S. (2011). The synthesis and evaluation of N1-(4-(2-[18F]-fluoroethyl)phenyl)-N8-hydroxyoctanediamide ([18F]-FESAHA), a PET radiotracer designed for the delineation of histone deacetylase expression in cancer. *Nucl Med Biol*, *38*(5), 683-696. https://doi.org/10.1016/j.nucmedbio.2010.12.008

Zhang, J. J., Fu, H., Lin, R., Zhou, J., Haider, A., Fang, W., Elghazawy, N. H., Rong, J., Chen, J., Li, Y., Ran, C., Collier, T. L., Chen, Z., & Liang, S. H. (2023). Imaging Cholinergic Receptors in the Brain by Positron Emission Tomography. *J Med Chem*, *66*(16), 10889-10916. https://doi.org/10.1021/acs.jmedchem.3c00573

Zhong, G., Wang, Y., Zhang, Y., Guo, J. J., & Zhao, Y. (2015). Smoking is associated with an increased risk of dementia: a meta-analysis of prospective cohort studies with investigation of potential effect modifiers. *PLoS One*, *10*(3), e0118333. https://doi.org/10.1371/journal.pone.0118333

Ziedonis, D., Hitsman, B., Beckham, J. C., Zvolensky, M., Adler, L. E., Audrain-McGovern, J., Breslau, N., Brown, R. A., George, T. P., Williams, J., Calhoun, P. S., & Riley, W. T. (2008). Tobacco use and cessation in psychiatric disorders: National Institute of Mental Health report. *Nicotine Tob Res*, *10*(12), 1691-1715. https://doi.org/10.1080/14622200802443569

Zoli, M., Pistillo, F., & Gotti, C. (2015). Diversity of native nicotinic receptor subtypes in mammalian brain. *Neuropharmacology*, *96*(Pt B), 302-311. https://doi.org/10.1016/j.neuropharm.2014.11.003

“*You can't stay in your corner of the Forest waiting for others to come to you. You have to go to them sometimes*.”
— Winnie-the-Pooh, in A.A. Milne's *Winnie-the-Pooh*

UNIVERSITY OF
COPENHAGEN